LOW TEMPERATURE CLAUS REACTOR STUDIES

By

ELMARGHANI M. BESHER

B.Sc. University of Tripoli

M.Sc. University of Southern California

A THESIS SUBMITTED IN PARTIAL FULFILLMENT OF

THE REQUIREMENTS FOR THE DEGREE OF

DOCTOR OF PHILOSOPHY

in

THE FACULTY OF GRADUATE STUDIES

CHEMICAL ENGINEERING

We accept this thesis as conforming

to the required standard

THE UNIVERSITY OF BRITISH COLUMBIA

September 1990

15 1

In presenting this thesis in partial fulfilment of the requirements for an advanced degree at the University of British Columbia, I agree that the Library shall make it freely available for reference and study. I further agree that permission for extensive copying of this thesis for scholarly purposes may be granted by the head of my department or by his or her representatives. It is understood that copying or publication of this thesis for financial gain shall not be allowed without my written permission.

Department of CHEMICAL ENGINEERING

The University of British Columbia
Vancouver, Canada

Date SEPT 21/1990

Abstract

A small-scale fluidized bed reactor (0.1m ID, 0.86m high) was used to carry out the Claus reaction

$$2H_2S + SO_2 \rightleftharpoons \frac{3}{x}S_x + 2H_2O$$

at low temperatures (100 to 150°C) where elemental sulphur condensed on the catalyst particles (Kaiser alumina S-501, 195μm mean particle size). The experimental apparatus was similar to that described by Bonsu and Meisen (1985). The feed gas consisted of pure nitrogen mixed with H_2S and SO_2 in the ratio of 2 to 1. The H_2S concentration was varied from 200 to 1300 ppm. The feed gas flow rate ranged from approximately 1.4 to 5.6 m^3/h. The corresponding U/U_{mf} ranges were approximately 2.2 to 8.8. The bed heights varied from 0.12 to 0.38m.

It was found that the experimental conversion efficiencies ranged from 60 to 96% and that they were less than those predicted thermodynamically. The conversion efficiency was found to increase with H_2S concentration and catalyst bed height; it decreased with gas flow rate. Contrary to thermodynamic predictions, the conversion efficiency increased with temperature. These results suggest that thermodynamic equilibrium was not achieved in the reactor. The decline in conversion due to catalyst fouling was measured as a function of catalyst sulphur content.

The experimental results could be interpreted by means of a bubbling bed model. New analytical expressions for predicting the overall conversion and the concentration profiles were developed for reactions of order n. For the Claus reaction, where n=1.5, good agreement was found between the model predictions and experimental values. The model

properly discribed the observed behavior resulting from changes in feed concentration, bed temperature, U/U_{mf} and static bed height.

The bubbling bed model was used to predict the effect of particle size on conversion for various operating gas velocities and bed dimensions. The model predictions showed that the canversion improved with decreasing particle size and that the improvement depended on U/U_{mf}.

The bubbling bed model was modified for conditions where condensed sulphur fouled the catalyst. A catalyst deactivation function, derived from first principles and based on catalyst sulphur content, was incorporated into the rate expression. The modified model predicted the the experimental measurements well and conclusions are drawn regarding the continuous operation of fluidized bed Claus reactor operating under sulphur condensing conditions.

A general procedure is presented to demonstrate the applicability of the bubbling bed model in the design of large scale reactors; examples for specific conditions are given.

Attrition tests were performed on the catalyst at U/U_{mf}=5.1 and room temperatures. It was found that most of the attrition occurred in the first few hours when the catalyst particles were rough. The overall test results indicated that attrition of the catalyst was negligibly small thereby suggesting the suitability of the Kaiser S-501 catalyst for long term use in fluidized bed Claus reactors.

Table of Contents

List of Figures

List of Tables

Acknowledgement

This work would not have been completed without the great help and support of various people. I would like to take this opportunity to thank all of them for the time and effort they gave to help bring this thesis into being.

Firstly, my deep gratitude and appreciation go to my supervisor Dr. Axel Meisen, who was my first syntax teacher when I started my Ph.D. degree program at the University of British Columbia, and who, since the beginning, gave generously of his time and effort toward the creation and correction of this work. Many thanks go also to my professors, whose contribution to my background in research, reaction engineering, fluidization engineering and mathematical operations I will remember and appreciate for the rest of my life.

Secondly, I would like to thank the Libyan people represented by Elfateh University in Tripoli, Libya, and The People's Committee for Students of the Socialist People's Libyan Arab Jamahiriya (PCSSPLAJ) in the United States and Canada for their financial support in offering me a scholarship for the period of January 1984 to June 1988. Thanks are also deserved by the personnel of the PCSSPLAJ for their tolerance and patience during the period of my sponsorship.

Thirdly, thanks go to the personnel of the Chemical Engineering Workshop, Stores and the staff of the Chemical Engineering main office for their cooperation and kindness during my stay at the department.

Last but not least, with the help of numerous friends and colleagues in the department and in the university a lot of work was made easier and more enjoyable. I would like to express my appreciation and thanks to Mr. Van Le for assisting me in writing the data logging program. Thanks also go to the personnel in the Mineral Processing Laboratory for use of their grinding facilities.

I would like to thank all my other friends for creating a suitable atmosphere in which to work toward the completion of this thesis.

Chapter 1

INTRODUCTION

Large quantities of sulphur compounds such as hydrogen sulphide are present in gas streams arising in refineries and natural gas plants. Removal of sulphur compounds is necessitated by the high demands for clean energy sources, by the value of sulphur (which furnishes the basis for a broad range of chemical industries) and by the need to meet air pollution control regulations. To achieve these goals, sulphur compounds are stripped from sour gas streams by means of selective absorption processes to produce acid gases typically rich in H_2S.

The objective of the Claus process is the recovery of elemental sulphur from these acid gas streams. In its original version, as developed by Claus in 1883, elemental sulphur is produced by oxidizing hydrogen sulphide with a stoichiometric amount of air over hot iron oxide according to the overall chemical reaction:

$$H_2S + \frac{1}{2}O_2 \rightleftharpoons \frac{1}{\times}S_\times + H_2O \tag{1.1}$$

The subscript $\times$ denotes the number of atoms per molecule of sulphur and depends on the temperature. At temperatures less than $150°C$, $\times \approx 8$ whereas above $800°C$, $\times \approx 2$. For temperatures between 150 and $800°C$, $\times$ ranges from 8 to 2. The above reaction is exothermic in nature ($\Delta H = -145$ to -173 kcal/mole H_2S) and, at elevated temperatures, the conversion efficiencies are usually less than 80%.

To overcome the restrictions imposed by the exothermic nature of the reaction, several modified Claus processes have evolved. Two variations used world wide were developed by I.G. Farbenindustrie (Gamson and Elkins, 1953).

In the first modification, known as the "Split-Stream Process", hydrogen sulphide is split into two streams (see Figure 1.1). One third of the H_2S is completely burned to SO_2 in a free flame combustion chamber at about 1100 to 1200°C:

$$H_2S + \frac{3}{2}O_2 \rightleftharpoons H_2O + SO_2 \tag{1.2}$$

($\Delta H = -124$ to -138 kcal/mole H_2S, T=1100 to 1200°C, P=1 atm)

The sulphur dioxide is then used to oxidize the remaining two thirds of H_2S to elemental sulphur in catalytic reactors:

$$H_2S + \frac{1}{2}SO_2 \rightleftharpoons H_2O + \frac{3}{2x}S_x \tag{1.3}$$

($\Delta H = -21$ to -35 kcal/mole H_2S, T=220 to 300°C, P=1 atm.)

A significant improvement in this modification can be deduced by comparing the heats of reaction of equations 1.1, 1.2, and 1.3. Over 80% of the total heat from reaction 1.1 may be recovered at the exit of the combustion furnace and upstream of the catalytic reactors. Since reaction 1.3 represents the catalytic stage, it is seen that the operating temperature can be maintained at sufficiently low levels with greatly increased space velocity, and consequently the attainment of high conversion.

In the second modification, known as the "Straight-Through Process", all H_2S is burned with stoichiometric amounts of air in a free flame combustion furnace at about 1100°C to produce a mixture of sulphur vapour, sulphur dioxide, hydrogen sulphide, water vapour, and nitrogen:

$$2H_2S + 2O_2 \rightleftharpoons 2H_2O + SO_2 + 1/\times S_x \tag{1.4}$$

H_2S	STRAIGHT THROUGH	SPLIT FLOW	DIRECT OXIDATION
	50-100%	15-50%	2-15%
HYDROCARBON	<2%	<5%	>5%

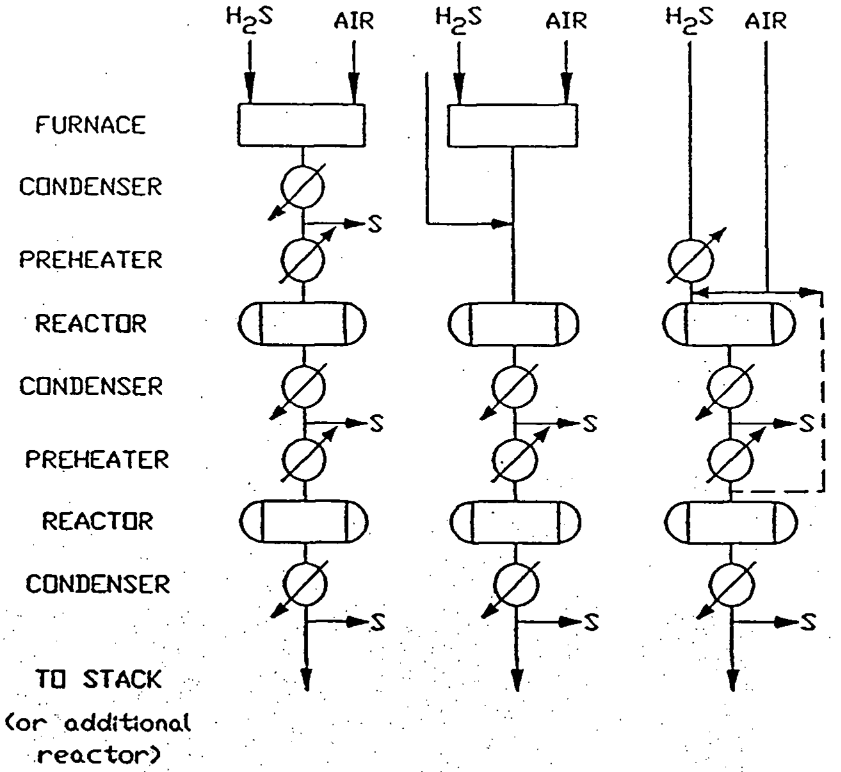

Figure 1.1: Modified Claus processes

The unconverted H_2S is then oxidized, according to reaction 1.3, with SO_2 in two or more catalytic converters. The elemental sulphur is removed by condensation which shifts the equilibrium to the product side and lowers the sulphur dew point temperature in each converter.

The straight-through process has two advantages over the split-stream process. First, about 90 to 95% of the total heat of reaction is recovered in the high temperature, free flame combustion furnace and, second, almost 70% sulphur is recovered prior to the first catalytic stage.

The choice of Claus process depends primarily on the concentration of H_2S in the feed gas. Well-operated Claus plants using a furnace and two catalytic reactors in series are capable of achieving approximately 95% total sulphur recovery provided the H_2S concentration in the feed exceeds 30%. The unconverted H_2S is normally incinerated to SO_2 and discharged into the atmospher. However, severe damage of animals and plants may occur upon exposure to even low levels of SO_2 (see Tables 1.1 and 1.2). To protect the environment, most industrialized nations have passed regulations restricting SO_2 emissions to the atmospher. Air pollution control laws, such as those in effect in Brithish Columbia (see Table 1.3) and other provinces, often necessitate the improvement of Claus plant performance to achieve conversion efficiencies higher than 99%.

Table 1.1: Maximum permissible atmospheric SO_2 levels (Goar, 1977).

Exposure time	Approximate SO_2 concentrations hazardous to human health ppmv	Approximate SO_2 concentrations hazardous to vegetation ppmv
1 hour	0.5	0.8
1 day	0.2	0.3
4 days	0.15	0.2
1 month	0.07	0.09
1 year	0.01	0.01

Table 1.2: Toxicity effect of H_2S on the human body (Archibald, 1977).

H_2S concentration in air (ppm)	Period of exposure
10	Maximum allowable concentration for 8 hours.
70-150	Slight symptoms after exposure of several hours.
150-300	Maximum concentration that can be inhaled for 1 hour.
400-500	Dangerous upon exposure for 30 minutes to 1 hour.
600-800	Fatal after exposure of 30 minutes or less.

Table 1.3: Ambient air-quality guidelines for the petroleum and chemical industries in British Columbia (Venables, 1989)
(Dry basis, 20°C, 760 mm Hg)

	Level A (ppmv)	Level B (ppmv)	Level C (ppmv)
SO_2			
1 hour maximum	0.17	0.34	0.5
24 hour maximum	0.06	0.10	0.14
Annual arithmetic mean	0.01	0.02	0.03
H_2S			
1 hour maximum	0.005	0.03	0.03
24 hour maximum	–	0.005	0.005

New operations are required to meet level A emissions;
Existing operations are required to meet level C;
Existing operations are required to upgrade emissions to level B and ultimately to level A.

Although such high conversions are thermodynamically attainable at temperatures below the sulphur dew point, sulphur condensation leads to catalyst deactivation. To recover deposited sulphur by vaporization, traditional fixed bed reactors cannot be operated continuously. Fluidized bed reactors, on the other hand, can be operated with continuous catalyst regeneration and have been proposed for the Claus process operating at low temperatures (Meisen, 1977, see Figure 1.2).

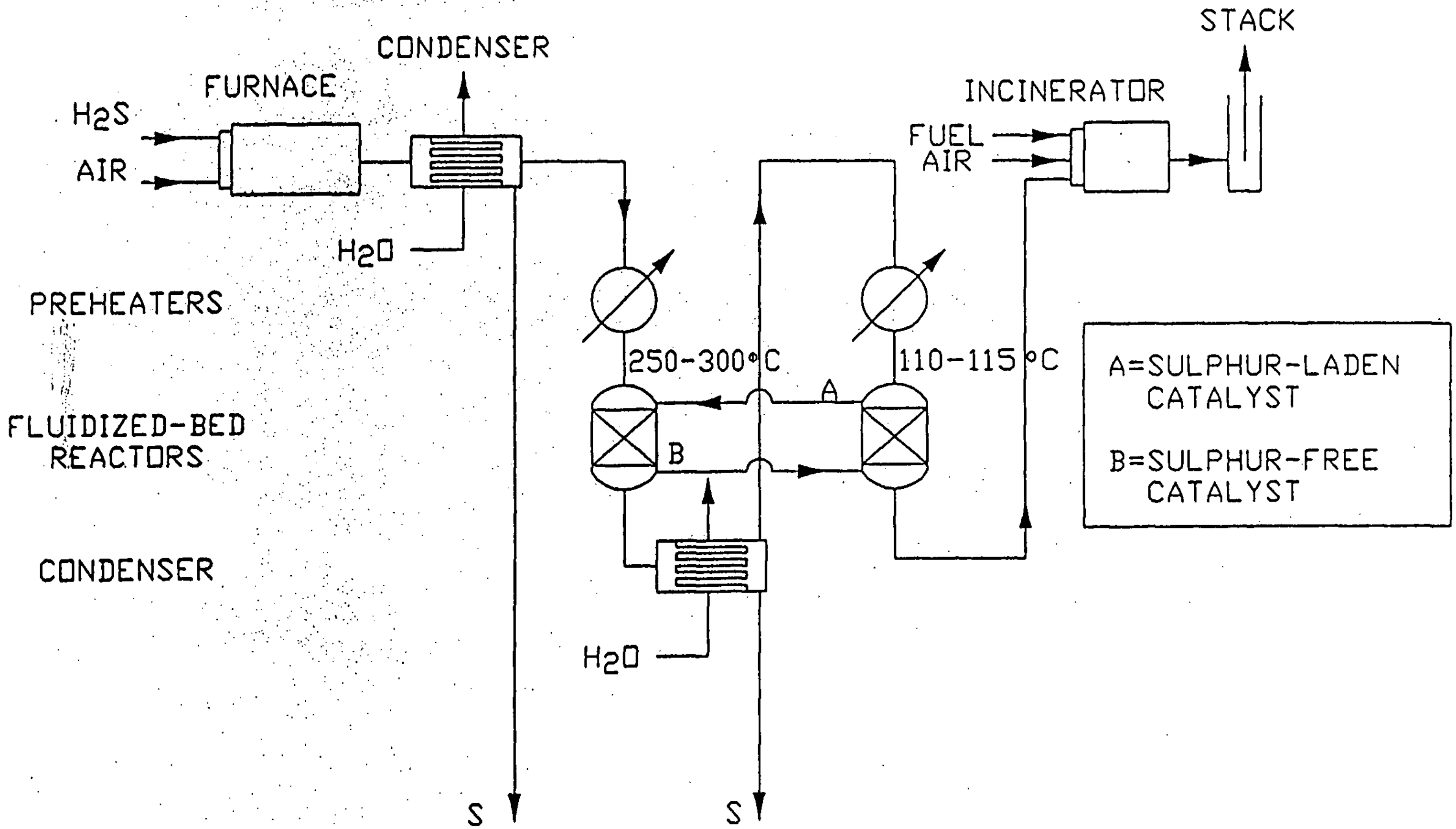

Figure 1.2: Fluidized bed Claus process (Meisen, 1977)

A fluidized bed is formed by passing a gas upward through a bed of a finely divided particles supported by a distributor or grid. The superficial gas velocity at which the fine particles of a fixed bed start to move is known as the minimum fluidization velocity, U_{mf}, and its value depends on the physical properties of the gas and solid particles. At gas velocities above U_{mf}, the bed expands and small gas bubbles form at the distributor and ascend to the surface of the bed where they burst causing splashing of particles into the space known as the freeboard region. During their rise, bubbles may grow by coalescence and may shrink due to splitting. The bed may be notionally divided into a dense and dilute phase. Part of the gas percolates through the dense phase and the remainder passes through the bed in the form of gas bubbles.

The main advantages of fluidized beds over the fixed beds for the Claus reactions were summarized by Bonsu (1981):

1. The bed temperature is uniform due to the intense agitation of the catalyst particles by the rapidly rising gas bubbles.

2. Operation at temperatures below the sulphur dewpoint (where thermodynamic yields are high) is possible. Operation even below the sulphur melting point is, in principle, attainable. Catalyst fouling caused by condensed sulphur can be controlled by continuously circulating the catalyst through a regenerator.

3. Catalyst deactivation from sulphation and deposition of impurities such as carbon can also be controlled by means of a regenerator.

4. The catalyst activity is enhanced by the large specific surface area of the fine particles.

5. The pressure drop across fluidized beds is moderate.

6. Pelletizing, which is an important cost item in the production of Claus catalysts, may not be required for fluidized bed catalysts.

However, fluidized beds also have some basic disadvantages such as:

1. Lowering of conversion efficiency due to the fact that some gas by-passes the catalyst in the form of bubbles.

2. Reduction of conversion due to backmixing.

3. Attrition of catalyst particles and erosion of the reactor walls due to the intense catalyst agitation.

4. Elutriation of catalyst fines from the bed.

Detailed literature reviews of Claus reactions and fluidized bed reactors are included in chapter 2. Models for fluidized bed Claus reactors are developed in chapter 3. Description of a small-scale fluidized bed reactor and auxiliary components are summarized in chapter 4. In chapter 5, experimental procedures and calibration of instruments are outlined. The performance of a small scale fluidized bed reactor at low temperature is compared with model predictions and practical implications are discussed in chapter 6. Conclusions are drawn and recommendations for future work are itemized in chapter 7.

The final part of this thesis is presented in the form of appendices. The appendices contain statistical analyses of the experimental results, computer programmes, and calibration tables.

Chapter 2

LITERATURE REVIEW

2.1 CLAUS REACTIONS

2.1.1 Theoretical Studies

The first fundamental investigation of the Claus process was published by Gamson and Elkins (1953). Using the thermodynamic data of Kelly (1937), they employed the equilibrium constant method to predict sulphur yields and equilibrium composition for an idealized Claus process. McGregor (1971) used more accurate data compiled by McBride et al. (1963) to calculate Claus conversions. He utilized the free energy minimization approach developed by White et al. (1958). Bennett and Meisen (1973) employed the key component method proposed by Kellogg (1971) and considered up to 44 compounds to be present under equilibrium conditions. Their results agree quite well with those reported by Kellogg but only 25 species were found to have concentrations in excess of 0.1 ppm. The slight discrepancies in the results (see Figure 2.1) are likely caused by the different free energy data used by the various authors (Bennett and Meisen, 1973).

Results from the above studies provide basic information for understanding the nature of Claus reactions and serve as a guide for the design and prediction of maximum yields of Claus plants. Despite the differences in the methods employed and the system complexity, there is basic agreement that the theoretical conversion efficiencies are high at low temperatures, fall rapidly with increasing temperature and pass through a minimum before increasing again at elevated temperatures. These studies also showed that, at

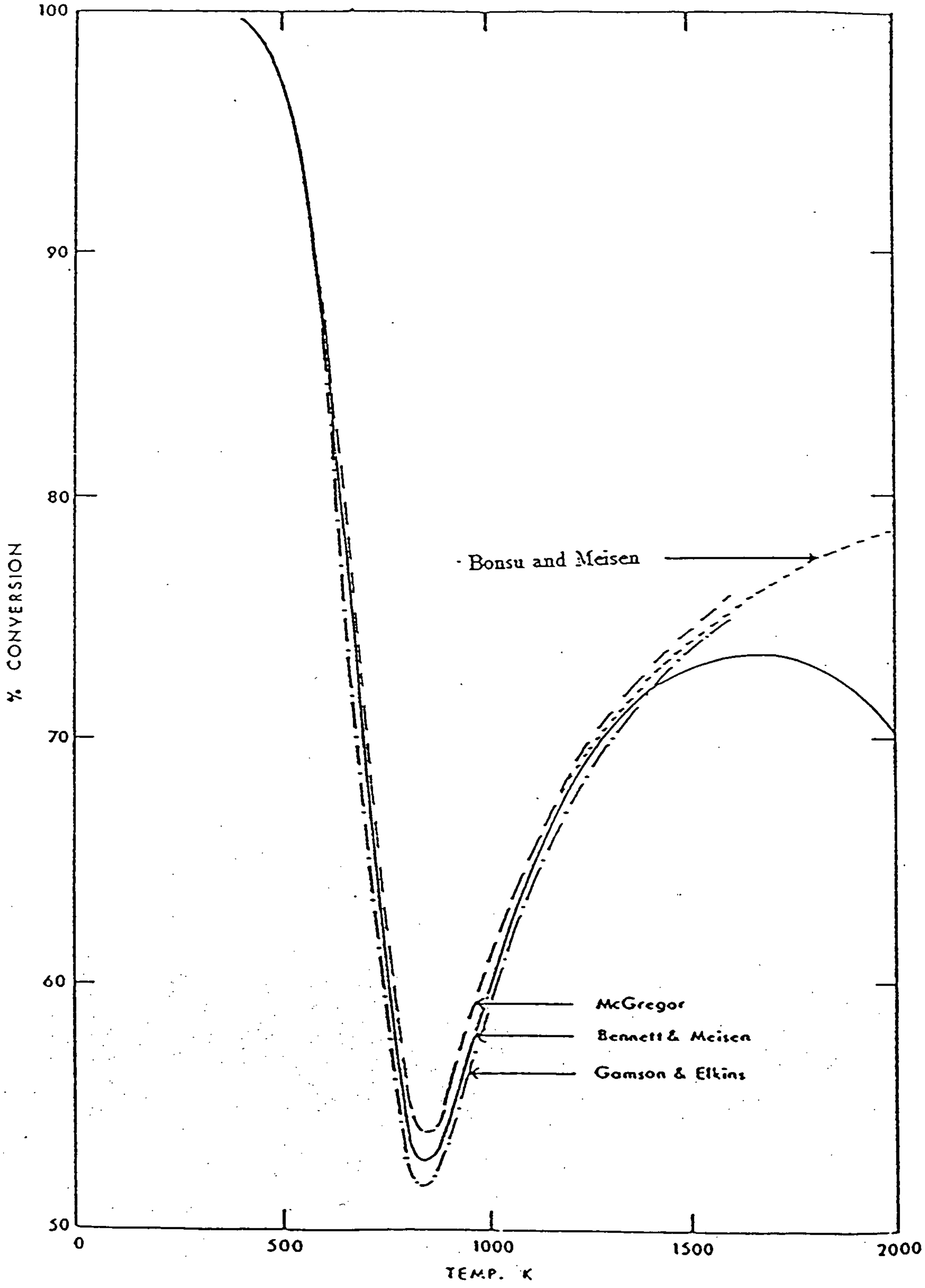

Figure 2.1: Claus reaction equilibrium conversion versus temperature (basis: 1 mole H_2S with stoichiometric air)

temperatures below 300°C, the dominant sulphur species is S_8 whereas at temperatures higher than 1000°K, sulphur occurs essentially in the di- and monoatomic forms (S_2 and S). This change in the degree of polymerization is due to the endothermic dissociation reactions of S_8 and S_6. Hence the overall reaction becomes progressively less exothermic and leads to increased sulphur yields at elevated temperatures.

Considering the presence of feed impurities such as ammonia, hydrocarbons, and carbon dioxide and accounting for a large number of chemical reactions, Maadah and Maddox (1978) concluded that large amounts of such impurities in the furnace feed decrease the conversion. The primary reason for this effect appeared to be the decreased H_2S concentration in the sour gas. They also found that including sulphur polymers with an odd number of atoms does not significantly affect the equilibrium conversions predicted for Claus processes. However, they observed a notable decrease in the combined H_2S and SO_2 concentration in the tail-gas stream when all sulphur polymers were considered to be present under equilibrium conditions. Bragg (1976) has developed a computer program to predict the performance of Claus plants under both equilibrium and non-equilibrium conditions. His predictions agreed quite well with measured plant performance.

In practice, sulphur plants use, whenever possible, a furnace operating in the high temperature region ($\sim$ 1000°C) where sulphur yields are about 70%. The thermal stage is followed by a waste heat boiler where most of the heat of reaction is removed. The gases leaving the furnace are passed through a condenser to recover the elemental sulphur before they enter the catalytic stage. Two or three catalytic converters are often used to maximize sulphur recovery and minimize sour gas emissions into the atmosphere. The temperature of the first reactor is normally set in response to the concentration of carbon disulphide and carbonyl sulphide (which may be formed in the furnace) since conversion of these compounds is high at temperatures above 300°C (Pearson, 1973; George, 1975; Grancher, 1978). The downstream reactors are operated at lower temperatures to take advantage of the high conversion of H_2S and SO_2 favoured by thermodynamics. However, at low temperatures, the reactions become kinetically controlled. Moreover, at very low temperatures, condensation of sulphur occurs and causes catalyst fouling. Most catalytic Claus reactors are therefore operated above the sulphur dew point.

2.1.2 Fluidized Bed Claus Process

A two stage fluidized bed Claus process (FBCP) was proposed by Meisen (1977) as an alternative to three fixed bed reactors in series used in many conventional Claus plants. The downstream reactor in the FBCP is kept at a temperature below the sulphur dew point. Under such conditions, the catalyst collects the condensed sulphur formed in the reaction. The sulphur laden catalyst is recycled to the upstream reactor, which is operated at an elevated temperature, where vaporization of sulphur occurs and regeneration of the catalyst takes place. The sulphur free catalyst is then recycled back to the second reactor. This novel process represents a sub-dew point process which is truly continuous (see Fig. 1.2).

In assessing fluidized bed Claus technology, Bonsu and Meisen (1985) used the equilibrium constant method to simulate various idealized FBCP's. Their results indicated that, for a pure H_2S feed, an overall sulphur conversion of 99% was attainable by using a Claus furnace and two fluidized bed reactors in series. Such high conversions were independent of the first reactor temperature which varied from 400 to $800°K$. The temperature in the downstream reactor was kept constant at $383°K$ thereby always compensating for incomplete conversion in the first reactor. In addition, they reported sulphur conversions for an experimental fluidized bed Claus reactor which exceeded equilibrium conversions predicted from thermodynamic principles.

Using the bubble assemblage model developed by Kato and Wen (1969) and a kinetic rate expression referred to as the LIU Model II, Birkholz et al. (1987) simulated the

FBCP. They found that the overall recovery efficiency is the same as that achieved in a Claus plant containing three fixed beds. Furthermore, only 50% of the catalyst was required compared with the conventional fixed bed process; the pressure drop was 25% less. It is therefore clear that the FBCP should be capable of achieving sulphur recoveries comparable to those obtained in Claus plants having three fixed bed reactors.

2.1.3 Experimental Studies

The first experimental studies of the Claus reactions in fluidized bed reactors were undertaken by Bonsu and Meisen (1985). Using an activated alumina catalyst, they reported that at elevated temperatures experimental conversions are in good agreement with those obtained from fixed bed studies by Gamson and Elkins (1953) and Dalla Lana (1978). For dry feed mixtures consisting of H_2S, SO_2 and N_2, and temperatures ranging from 150 to 300°C, Bonsu and Meisen observed that, for some experiments, sulphur conversions were reduced at low temperatures and high H_2S feed concentrations. They also found a weak relationship between sulphur conversion and the ratio U/U_{mf}. They concluded that the performance of fluidized bed Claus reactors is only slightly affected by gas by-passing the catalyst particles in the form of bubbles. Furthermore, they reported that experimental conversions are independent of bed height above 0.12m. These observations were attributed to the fact that the Claus reaction is very fast and almost complete conversion occurs near the gas distributor.

With the exception of the work by Bonsu and Meisen, all reported Claus reaction studies were performed with fixed bed reactors. Fixed bed reactor studies are discussed in the following paragraphs.

Claus catalysts and reaction kinetics have been the subject of experimental investigation since Tayler and Wesley (1927) recognized that the reaction between H_2S and SO_2 proceeds entirely on solid surfaces. They noted that the reaction rate was proportional to the surface area of their glass reactor and that the reaction order was 1.5 and 1.0 for H_2S and SO_2, respectively.

Using cobalt thiomolybdate catalyst, Murthy and Roa (1951) observed that no reaction occurred at temperatures of $25°C$ or less in the absence of water. They reported an overall reaction order of 2.

McGregor (1971) studied, in detail, the kinetics of the Claus reaction using commercial bauxite catalyst and proposed the following rate expression for the disappearance of H_2S (gmole/h-g cat):

$$r_{H_2S} = k_0 exp(-E/RT) P^a_{H_2S} P^b_{SO_2} \tag{2.1}$$

where:

$k_0 = 2.198 \pm 0.564\ h^{-1}$

E=7589±451 $cal/mole$

a=0.963±0.0448

b=0.359±0.135

R=1.987 $cal/mole/K$.

P_{H_2S} and P_{SO_2} denote the partial pressures (in mm Hg) of H_2S and SO_2, respectively. T denotes the absolute temperature (in K). It should be noted that the equation proposed by McGregor is not dimensionally consistent. McGregor observed that, while low partial pressures of water vapour had an autocatalytic effect on the reaction, high partial pressures caused marked retardation.

The effect of water vapour on the kinetics of the Claus reaction was further investigated by Dalla Lana et al. (1972) using commercial bauxite catalyst. They proposed the following rate expression:

$$r_{H_2S} = 1.121 exp(-7441/RT) \frac{P^{1.0}_{H_2S} P^{0.5}_{SO_2}}{1 + 0.00423 P_{H_2O}} \tag{2.2}$$

The retarding effect of water vapour is reflected by the denominator of the rate expression.

Dalla Lana et al. (1972) concluded that water vapour competes with either H_2S or SO_2 molecules for adsorption sites on the catalyst surface. A similar rate expression was proposed by Dalla Lana (1976) who studied alumina catalysts:

$$r_{H_2S} = 0.92exp(-7350/RT)\frac{P_{H_2S}^{1.0}P_{SO_2}^{0.5}}{(1 + 0.006P_{H_2O})^2} \tag{2.3}$$

Water inhibition was also confirmed by George (1974). He reported 1.0 and 0 as the reaction orders for H_2S and SO_2, respectively, and found the activation energy to be 5.5 kcal/mole of H_2S. Due to the low value of E, George concluded that the Claus reaction is controlled by pore diffusion. Similar conclusions were reached by Grancher (1978) who recommended the use of small catalyst particles. Using activated alumina catalyst, he obtained reaction orders of 1 and 0.5 for H_2S and SO_2, respectively.

The control of the Claus reaction by pore diffusion has also been reported by Landau et al. (1968). They based their conclusions on the fact that the activity of bauxite catalyst increased with decreasing particle size.

Pearson (1973) examined the activity of various Claus catalysts. He found that Kaiser S-501 activated alumina and cobalt-molbydenum had the highest resistance to catalyst poisoning. George (1975) studied the catalytic activities of acids and bases for the Claus reactions. He found that, while acidity did not have any effect, basicity considerably improved the catalyst activity for the reactions.

2.1.4 Catalyst Deactivation By Fouling

Operating Claus reactors below the sulphur dew point leads to the deposition of sulphur on the external and internal surfaces of the catalyst. This deposit causes a decrease in catalyst activity (termed fouling) and leads to reduced conversions. Pearson (1977) tested the performance of the activated alumina under fouling conditions. His study showed that the alumina S-501 retains its activity (conversion was higher than 98%) even when loaded up to 50 wt% with condensed sulphur. At a sulphur loading of 80 wt% the sulphur conversion dropped from 80% to 31%.

To model reactors with fouling, it is clear that the reaction rate expression must include a deactivation term. There are basically two different procedures for introducing such a term into the rate expression. One procedure is based on the so called "time on stream theory" which envisions the catalyst decay to be a function of the length of time for which the process has been in operation (Pachovsky et al., 1973; Sadana et al., 1971). A second group of workers suggested that the amount of deposit retards the reactants from reaching the active surface of the catalyst and therefore reduces the activity (Froment and Bischoff, 1961; Masamune and Smith, 1966). Froment and Bischoff alluded to the fact that treating the deactivation function in terms of the foulant concentration in solids would allow comparisons between different systems, whereas a correlation with respect to "time on stream" is specific for the conditions and operations under consideration.

The accumulation of sulphur in pores of the Claus catalyst such as activated alumina and bauxite may arise from two mechanisms: adsorption of elemental sulphur on the surface since the sulphur is actually produced on the surface or condensation when the temperature is below the dew point. The concentration of the feed gas and the type of reactor are also important. For a dilute feed gas, it takes longer for sulphur to collect in appreciable amounts and catalyst deactivation due to fouling is slow relative to the gas residence time in the reactor. Under such conditions, all catalyst particles in a fluidized bed are exposed to the same extent of fouling. On the other hand, a concentrated feed gas entering a fixed bed reactor creates a fouling front travelling along the axis of the reactor. Hence a transient model is required to describe this situation. Razzaghi and Dalla Lana (1984) showed that fouling of fixed bed Claus reactors is a relatively slow process. They assumed that pseudo-steady state prevailed in order to study cold-bed sulphur recovery processes.

2.1.5 Low Temperature Industrial Processes

The first commercial recovery of sulphur from tail gases leaving Claus process was achieved by the Sulfreen process (Martin and Guyot, 1971; Cameron, 1974). This process is, in essence, an extension of the Claus process described in section 1.1. In the original Sulfreen plants, reaction 1.3 is carried out at temperatures below the sulphur dew point over a fixed bed of activated carbon. As in the Claus process, the ratio of H_2S to SO_2 is set to 2. At the operating temperature (125-135$°C$), the condensed sulphur remains on the carbon catalyst. Although highly efficient, carbon requires high temperatures (500 - 600$°C$) to vapourize the sulphur during regeneration. In the process developed jointly by Lurgi Gesellschaft füs Wärme und Chemotechnik of West Germany and Société National des Petroles d'Aquitaine (recently Société Elf Aquitaine) of France, four reactors in parallel are used for adsorption while a fifth reactor is in desorption mode and a sixth reactor is cooled to the required reaction temperature.

A loop of hot inert gas is used to desorb the sulphur from the saturated carbon bed. Sulphur is recovered from this hot gas in a sulphur condenser. The gas is then passed to a tower where it is further cooled by washing with liquid sulphur and additional sulphur is recovered. Because of the high regeneration temperature, stainless steel is used throughout the plant.

Modern Sulfreen plants use activated alumina catalyst which requires a regeneration temperature of about 300$°C$. In addition, the number and size of the reactors are smaller. The wash tower in the old process is replaced by a sulphur condenser. Another aspect of the modern Sulfreen process is that the activity of the alumina catalyst is restored by introducing a stream of H_2S into the regeneration loop when the bed temperature reaches 300$°C$

A similar process was developed by AMOCO Canada Company designated as the

CBA (Cold Bed Adsorption) process (Goddin et al. 1974). An alumina catalyst is used for the recovery of sulphur from Claus tail gases at $130°C$. This process also requires H_2S/SO_2 ratios of 2 for optimum conversion. However, the regeneration step is different from that of the Sulfureen process. Part of the feed to the first Claus reactor is passed to the saturated CBA reactor where, in addition to the release of sensible heat, heat is generated due to the reaction between H_2S and SO_2. As a result, the bed temperature rises to about $300°C$ which corresponds to the outlet temperature of the first Claus reactor. The rise in temperature causes gradual vaporization of sulphur. The regeneration gas is then returned to the first Claus reactor after passing through a sulphur condenser. Once the regeneration cycle is complete, the gas stream from the last Claus reactor is passed through a sulphur condenser and then to the hot CBA reactor to lower its temperature to about $130°C$.

Other low temperature processes such as JLSC and MCRC use basically the same principles and are described by Kohl and Riesenfeld (1985).

All of the above processes use fixed bed reactors and have to be operated in cyclic mode. Catalyst regeneration may be performed by taking the reactor out of operation when the catalyst sulphur loading has reached a certain value. To achieve the changes in operations, quite sophisticated process control schemes are needed.

2.2 FLUIDIZED BED REACTOR MODELLING

Early fluidized bed models were based on the assumption that the gas and catalyst are in intimate contact and well mixed without segregation into dilute and dense phases. Most fluidized bed models postulated in the 1950's assume that fluidized bed reactors consist of two parallel, single-phase reactors with cross-flow between them. In reality, however, the hydrodynamics of fluidized bed reactors are far more complex; some of the gas flows through the bed in the form of bubbles, thus forming a dilute phase, whereas the remainder percolates through a region of high particle density called the "dense phase". The fact that the gas in the bubbles is in poor contact with the catalyst particles and the gas contact in the dense phase is intimate, has led researchers in the 1960's to the development of fluidized bed reactor models which focus on the properties of the rising bubbles.

The complexity of fluidized bed models depends on the assumptions underlying their formulation (see Table 2.1 and 2.2 for common assumptions). Furthermore, model predictions are sensitive to certain assumptions. In the 1970's, experimental evaluations of these models were undertaken to discriminate between the various model parameters and the degree of importance of individual assumptions. Although more than a dozen assumptions (related to bubbling bed reactors) have been invoked to describe mathematically the behavior of the gas and solids in fluidized beds, only the principal ones are discussed in the following sections. A number of reviews and model evaluations have been published (Grace, 1971; Pyle, 1972; Chavarie and Grace, 1975; Yates,1975; Horio and Wen, 1977)

2.2.1 Number Of Phases

The majority of bubbling bed models are based on the assumption that a fluidized bed may be envisioned to consist of a dilute and dense phase (e.g. Kato and Wen, 1969; Grace, 1984). In some models, the clouds surrounding the bubbles are lumped together with the emulsion phase (Orcutt et al., 1962) whereas in others they are included in the bubble phase (Partridge and Rowe, 1966). Very few models account for the presence of a cloud phase between the bubble and emulsion phases (Kunii and Levenspiel, 1969; Fryer and Potter, 1972).

The main advantage of the two phase theory is that it leads to simpler equations and

Table 2.1: Typical assumptions for two- and three-phase reactor models (Grace, 1987)

A.		Nature of dilute phase:
	1.	Bubble phase completely free of particles.
	2.	Bubbles containing some widely dispersed solids.
	3.	Bubble-clouds are included.
B.		Division of gas between phases:
	1.	Governed by two-phase theory.
	2.	All gas carried by bubbles.
	3.	Some downflow of gas in the dense phase is permitted.
	4.	Other or fitted parameter.
C		Axial dispersion in dilute phase:
	1.	Plug flow.
	2.	Disperse plug flow.
D.		Axial dispersion in dense phase:
	1.	Plug flow.
	2.	Disperse plug flow.
	3.	Stagnant.
	4.	Well-mixed tanks in series.
	5.	Perfect mixing.
	6.	Downflow.
	7.	Bubble-induced turbulent fluctuations.
E.		Mass transfer between phases:
	1.	Obtained from independent gas mixing or mass transfer studies.
	2.	Fitted parameter for case under study.
	3.	Empirical correlation from previous or pilot plant data.
	4.	Bubble to dense phase transfer obtained from experimental or theoretical single bubble studies.
	5.	Transfer across cloud/emulsion boundary due to diffusion.
	6.	Enhancement due to bubble interaction included.
F.		Cloud size:
	1.	Davidson theory.
	2.	Murray or modified Murray analysis.
	3.	Wake not specifically included or assumed negligible.
	4.	Wake added to cloud.
	5.	Recognized but assumed negligible.
G.		Bubble size:
	1.	Not specifically included.
	2.	One size for entire bed.
	3.	Increases with height.
	4.	Obtained from separate measurement, correlation, or estimated.
	5.	Kept as fitting parameter.

Table 2.2: Assumption or approaches embodied in some of the principal two- and three phase reactor models

Authors	Assumptions						
	A	B	C	D	E	F	G
(a) Two-phase models:							
Shen and Johnstone (1955)	1	1	1	1 or 5	3	NA	1
Lewis, Gilliland, and Glass (1959)	2	2	1	1 or 5	3	NA	1
May (1959)	1	1	1	2	1	NA	1
Van Deemter (1961)	1	4	1	2	1	NA	1
Orcutt, Davidson, and Pigford(1962)	1	1	1	1 or 5	4	NA	2,5
Partridge and Rowe (1966)	3	1	1	1	5	2,4	4
Mireur and Bischoff (1967)	1	1	1	2	1,3	NA	1
Kato and Wen (1969)	3	2	1	4	1	1,3	3,4
Bywater (1978)	1	4	1	7	5	5	2,4
Darton (1979)	1	1	1	5	4,5	5	3,4
Werther (1980)	1	1	1	1	3	NA	3,4
Grace (1984)	2	2	1	3	4,6	NA	2,4
(b) Three phase models:							
Kunii and Levenspiel (1969)	2,1	1 or 2	1	3	4,5	1,4	2,4
Fryer and Potter (1972)	1	3	1	6	4,5	4,5	2,4
Fan, Fan, and Miyanami (1977)	2	1	2	2	4,5	2,3	3,4

Letters and numbers in the table refer to Table 2.1

less computation than the three phase theory. However, the number of phases could be considered as an integral part of other assumptions such as interphase transfer coefficients and the presence of solids in some or all phases.

The concept of the cloud phase was based on Davidson's treatment of a rising bubble through a dense phase (Davidson and Harrison, 1963). This model showed that cloud formation depends solely on the relative velocity of the rising bubble to that of the percolating gas [i.e $u_b/(U_{mf}/\epsilon_{mf})$]. The model assumes that the bubbles are spherical and it leads to the prediction of spherical, concentric clouds with radius:

$$(\frac{r_c}{r_b})^3 = \frac{\bar{\alpha}+2}{\bar{\alpha}-1} \tag{2.4}$$

where $\bar{\alpha} = u_b/(U_{mf}/\epsilon_{mf})$.

The model also predicts the through flow (i.e. the volumetric gas flow rate that enters and leaves a bubble during its rise):

$$q = 3\pi U_{mf} r_b^2 \tag{2.5}$$

A more sophisticated mathematical analysis by Murray (1965, 1966) led to smaller and non-spherical clouds with centroids above the centre of the "assumed" spherical bubble (see Figure 2.2). The Murray model predicts that the ratio of the cloud to bubble radius and the through flow are given by:

$$(\bar{\alpha}-1)(\frac{r_c}{r_b})^4 - \bar{\alpha}(\frac{r_c}{r_b}) - 4\cos\theta = 0 \tag{2.6}$$

$$q = 1.185\pi U_{mf} r_b^2 \tag{2.7}$$

where θ denotes the angle (in spherical coordinates) measured from the bubble nose. Experimental results by Rowe et al.(1964) indicate that Murray's model gives more accurate predictions than Davidson's model. The above equations suggest three situations:

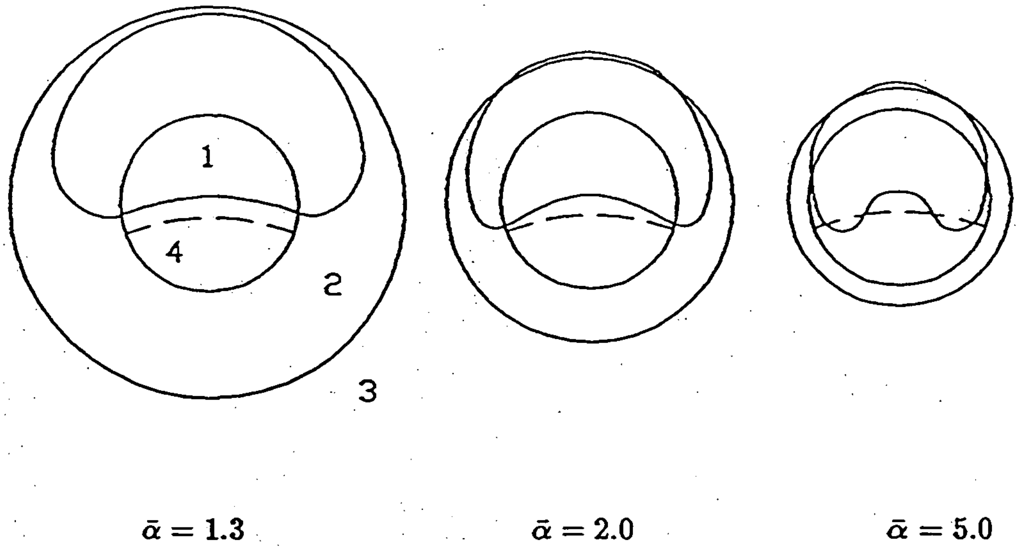

1 Bubble boundary

2 Cloud according to Murray's model (1965,1966)

3 Cloud according to Davidson's model (1963)

4 Typical position of wake according to Rowe et al. (1964)

Figure 2.2: Schematic representation of Davidson and Murray models

For $\bar{\alpha} < 1$, often referred to as " slow bubble regime", the bubbles are cloudless and the quickly rising gas uses the bubble as a short cut on its way through the bed. The gas enters the bottom of the bubble and leaves the top with a velocity of the order of U_{mf}. As the gas leaves the top of the bubble, it encounters particles moving tangentially to the bubble with a velocity of order u_b. The gas experiences a slight change in direction due to the drag force of the particles but, since the gas velocity is high, the inertial force results in deep gas penetration into the dense phase. Clouds can therefore not form. Hence a bed consisting of only two phases is a more realistic assumption for $\bar{\alpha} < 1$.

As the bubble velocity approaches the interstitial gas velocity, the drag force on the gas increases and becomes comparable to the inertial force. Hence the gas penetration into the dense phase becomes smaller and leads to gas circulation. Thus the gas emerging from the roof of a bubble is swept back to re-enter it at the bottom. Inspection of the above equations show that for $\bar{\alpha} = 1$, the cloud is infinite in size (i.e. the cloud covers the entire emulsion phase). This overlap suggests that a simple two phase model is more appropriate to apply provided other parameters such as interphase transport are properly determined.

When $\bar{\alpha} > 2$, commonly referred to as "the fast bubbles regime", the clouds become very thin and the emulsion phase occupies practically the entire bed except for the fraction occupied by the bubble phase.

2.2.2 Mass Transfer Between Phases

The success of a fluidized bed reactor model in predicting reactor performance depends primarily on the proper determination of interphase mass transfer coefficients. Numerous mass transfer models have been proposed in the literature for predicting the overall mass transfer coefficient (see Table 2.1). The majority of these models is based on the single isolated bubble theory. According to this theory, transfer coefficients derived from the

Table 2.3: Interphase mass transfer models

	Model	Overall mass transfer coefficient	Description
1	Partridge and Rowe (1966)	$k_q d_c/D_g = 2 + 0.69 Sc^{1/3} Re_c^{1/2}$ $Re_c = \rho_g u_b d_c/\mu_g$	Pure diffusion at cloud boundary.
2	Chiba and Kobayashi (1970)	$k_q = 1.128\sqrt{\epsilon_{mf}^2 D_g u_b/d_b}[(\bar{\alpha}-1)/\bar{\alpha}]^{2/3}$	Same as in (1).
3	Kunii and Levenspiel (1969)	$k_q = 1/[1/k_b + 1/k_e]$ $k_b = 0.75U_{mf} + 0.975\sqrt[4]{D_g^2 g/d_b}$ $k_e = 1.128\sqrt{\epsilon_{mf} D_g u_b/d_b^3}$	Three mass transfer resistances, diffusion resistance at cloud boundary is dominant.
4	Davidson and Harrison (1963)	$k_q = 0.75U_{mf} + 0.975\sqrt[4]{D_g^2 g/d_b}$	Additive convection and diffusion terms at bubble interface.
5	Calderbank et al. (1975)	$k_q = 0.75U_{mf} + 1.228\sqrt{D_g u_b/L_b}$	Same as (4), L_b is the vertical dimension of the bubble.
6	Chavarie and Grace (1976)	$k_q = U_{mf}/4$	Murray's through flow for spherical bubble, no diffusion.
7	Sit and Grace (1978)	$k_q = U_{mf}/4 + 1.128\sqrt{D_g \epsilon_{mf} u_b/d_b}$	Through flow as in (6), diffusion from penetration theory.
8	Sit and Grace (1978)	$k_q = 0.39U_{mf} + \sqrt{1.8 D_g \epsilon_{mf} u_b/d_b}$	As in (7) for spherical cap bubble
9	Hovmand and Davidson (1968)	$[1.19F_b/(F_b + \epsilon_{mf}F_p)][U_{mf}+$ $0.764F_p\epsilon_{mf}\sqrt[4]{D_g g/d_b}]$, $F_b = exp(-B^2/4D_g)/[1 - erf(B/2D_g^{1/4})]$, $F_p = exp(-B^2/4D_g)/[1 + erf(B/2D_g^{1/4})]$, $B = U_{mf}(3.738 d_b/u_b)^{1/4}$,	Interacton of diffusion and convection terms, F_b and F_p are interaction factors; through flow from Davidson model.
10	Walker (1975)	$k_q = [0.472F_b/(F_b + \epsilon_{mf}F_p)][U_{mf}+$ $+1.93F_p\epsilon_{mf}\sqrt[4]{D_g g/d_b}]$, $B = U_{mf}\sqrt[4]{1.115 d_b/u_b}$	Interaction as in (9) with through flow based on Murray's analysis.

properties of a single rising bubble and are assumed to apply accurately to freely bubbling beds. There are at least three approaches in modelling single bubble mass transfer (for reviews see Drinkenburg and Rietema, 1972; Walker, 1975; Sit and Grace, 1978):

1. Pure diffusion approach: In this type of model, three principal assumptions are made: (i) A cloud surrounds each bubble, (ii) The cloud is closed with no shedding of particles from the wake behind the bubble, (iii) The resistance to mass transfer resides at the cloud-emulsion interface. Ciné photographs by Rowe et al. (1964) and Toei et al. (1969) showed the shedding of gas from the wake to the surrounding continuous phase with the shedded gas elements becoming part of the interstitial gas. Walker (1975) pointed out that the contribution to bulk flow due to the shedding phenomenon is significant and cannot be ignored. Grace (1981) argued that this type does not account for at least three important mechanisms: (i) The shedding mechanism as indicated by the previously mentioned photographs, (ii) Distortion and volume changes of bubbles and their clouds during bubble coalescence and interaction, (iii) The cloud boundary is a streamline for the gas but not for the solid particles; hence particles entering and leaving the cloud contribute to the transfer of gas. Chavarie and Grace (1976) injected ozone tracer bubbles and measured concentration profiles near single rising bubbles in a two dimensional bed. They allowed for bubble growth and evaluated published mass transfer models. This technique was also used by Sit and Grace (1978) to measure the overall mass transfer (bubble to dense phase) for different particle sizes ranging from 90 to $390\mu m$. Their results indicate that diffusion controlled models consistently underestimate the overall mass transfer coefficient by at least one order of magnitude.

2. Convection and diffusion approach: In this approach, transfer models are based on three common assumptions: (i) The principal resistance to mass transfer resides at the bubble boundary, (ii) Mass transfer occurs by diffusive and convective mechanisms, (iii) The overall mass transfer is the sum of the diffusive and convective components. Other

assumptions varied among models. In some models, the diffusion term was obtained from the Davidson and Harrison (1963) analysis, whereas in others it was derived from the penetration theory. Assumptions regarding the convective term ranged from those based on the Davidson model for throughflow to Murray's analysis for either spherical or hemispherical bubbles. The experimental results by Chavarie and Grace (1976) suggest that models which are based on the concept of additive diffusive and convective transport at the bubble interface overpredict the transfer rate. This conclusion was confirmed later by Sit and Grace (1978). The latter also reported that models with the diffusive component calculated from the penetration theory and the convective component determined by the Murray model showed better agreement with experiments.

3. Interactive diffusion and convective approach: This type of model is similar to the previous ones since the mass transfer is thought to be controlled by diffusion and convection at the bubble boundary. However, unlike the previous models, the diffusion and convection terms are assumed to interact (Hovmand et al., 1971; Walker, 1975). As a result, the overall transfer is less than the sum of the individual components. Although the agreement between predictions from these models and experimental results (see Sit and Grace, 1978) was quite good for some particle sizes, none of these models was accurate over a wide range of particles sizes.

In a freely bubbling bed, the shape, size and velocity of a rising bubble is affected by the presence of neighbouring bubbles. Coalescence of bubbles has been described by Toei and Matsuno (1967), Clift and Grace (1970), Grace (1971) and Darton et al. (1977). They found that a trailing bubble elongates and its velocity increases as it is drawn into a leading bubble. Experimental measurements (in two dimentional beds) by Sit and Grace (1981) on pairs of obliquely aligned bubbles indicate that the leading bubble grew 2.5 times as quickly as an isolated bubble, while the trailing bubble increased its area 3.5 times as quickly. They obtained similar results for pairs of bubbles in vertical alignment where the overtaking bubble grew 20-80% more quickly than the leading bubble. This bubble interaction was found to significantly enhance interphase transfer. For example Sit and Grace (1981) reported overall mass transfer coefficients for interacting pairs of bubbles (9.6 and 8.5 cm/s for vertical and oblique alignments) to be 2 to 3 times higher than those obtained by Sit and Grace (1978) from isolated bubble measurements (3.4 cm/s).

Based on their experimental results and those obtained by Toei et al. (1969) for interacting bubbles in two dimensional beds as well as the results obtained by Pereira (1977) in three dimensional beds, Sit and Grace (1981) modified their original equation (Sit and Grace, 1978) to account for bubble interaction:

$$k_q = \frac{U_{mf}}{3} + \sqrt{\frac{4D_g \epsilon_{mf} u_b}{\pi d_b}} \tag{2.8}$$

The first term in the above equation represents the throughflow from Murray's analysis corrected to account for enhancement due to bubble interaction. The second term represents the flow due to diffusion based on the penetration theory.

2.2.3 Division Of Flow Between Phases

Most models rely on the two phase theory (Toomey and Johnstone, 1952), which states that all gas in excess of that required for minimum fluidization flows through the bubble phase and the local emulsion velocity, U_e, is equal to U_{mf}/ϵ_{mf} i.e:

$$Q_b = A(U - U_{mf}) \tag{2.9}$$

$$U_e = U_{mf}/\epsilon_{mf} \tag{2.10}$$

The minimum fluidizing velocity can be measured by plotting the pressure drop across the bed ($\Delta p/l$) versus the superficial gas velocity U. It can also be estimated from a number of correlations, e.g the equation recommended by Grace (1982):

$$Re_{mf} = \sqrt{(27.2)^2 + 0.0408Ar} - 0.0408 \tag{2.11}$$

where $Re_{mf} = d_p U_{mf} \rho_g / \mu_g$ and $Ar = \rho_g(\rho_p - \rho_g) g d_p^3 / \mu_g^2$.

The voidage at minimum fluidization may be estimated from the Broadhurst and Becker(1975) correlation:

$$\epsilon_{mf} = 0.586\psi^{-0.72} Ar^{-0.029} (\frac{\rho_g}{\rho_p})^{0.021} \tag{2.12}$$

(2.13)

It has been reported, however, that the two phase theory overestimates the flow, Q_b, and is only valid in shallow beds and near the top of deep beds (Grace and Clift, 1974). The popularity of this theory continues to be the means for flow division between phases for two reasons (Grace, 1981): (i) Lack of a suitable alternative and (ii) Confusion between the flow in the voids (visible flow) and flow resulting from gas exchange with the clouds (invisible or throughflow).

The visible flow, Q_b, is needed to calculate the hydrodynamic parameters such as bed expansion, bubble diameter and bubble velocity. The total bubble flow is needed for writing the material balances for each phase. The total flow in the dilute phase equals the visible flow plus the flow due to gas short-circuiting through each bubble (i.e the throughflow). When $(U - U_{mf})$ is small, the throughflow is of order $U_{mf}\epsilon_b A$ but there is evidence that this value may be exceeded considerably when $(U - U_{mf})$ is large (Valenzuela and Glicksman, 1985). Since the visible flow is agumented by the through flow, it is reasonable to make the simplifying assumption of zero vertical flow in the dense phase (i.e. all gas flows through the dilute phase).

The rising bubbles induce circulation of solids in the dense phase which, in turn, modifies the flow pattern of the percolating gas. Analysis by Calderbank et al.(1975)

suggests that local circulation of solids occurs in different regions in the bed. They found that particles, just above the distributor, tend to move upward at the centre and downward near the walls. They noticed that bubbles grew during their rise and tended to drift towards the centre of the bed causing solids to move down at the wall. They reported interstitial upward emulsion velocities of about 0.1m/s at the center of the bed and about 0.05m/s downward near the walls (U=0.031m/s; U_{mf} = 0.011 m/s; static height=0.48m; $d_p = 90\mu m$)

Rowe and Partridge (1962) have pointed out that, since particles are carried upward in the wake of rising bubbles, they must move down with the same rate. More work by Rowe and Partridge (1965) indicates that wakes occupy about 30% of the bubble phase. As the bubble velocity increases, solids must move down faster. Sufficiently high solid velocity causes reversal in the direction of the dense phase gas as confirmed by the tracer studies of Kunii et al. (1967). According to Kunii and Levenspiel (1969), the dense phase gas velocity is given by:

$$\frac{U_e}{(U_{mf}/\epsilon_{mf})} = (1 - \epsilon_{mf} V_w/V_b) - \left[\frac{\epsilon_{mf} V_w/V_b}{1 - \epsilon_b - \epsilon_b V_w/V_b}\right] \frac{U}{U_{mf}} \tag{2.14}$$

where V_w/V_b is the ratio of the wake to bubble volume. A similar expression was derived by Fryer and Potter (1972). For typical values of $V_w/V_b \sim$ 0.2 - 0.4 (Rowe and Partridge, 1965), $\epsilon_{mf} \sim$ 0.5 - 0.7 (Kunii and Levenspiel 1969), $\epsilon_b \leq$ 0.4 (Grace, 1984), it is reasonable to assume that $U_e = 0$ for U/U_{mf} = 4.5 - 8.5. The accuracy of models is hardly affected by this assumption (Grace, 1984) and few models were based on the above concept (Lewis et al, 1959; Kunii and Levenspiel, 1969; Kato and Wen, 1969; Grace, 1984).

2.2.4 Gas Mixing In The Dense Phase

Several alternatives have been employed to represent the gas flow pattern in the dense phase. Assumptions ranged from upward plug flow (Orcutt et al., 1962; Partridge and

Rowe, 1966) to perfect mixing (Davidson and Harrison, 1963) and stagnant gas (Kunii and Levenspiel, 1969; Grace, 1984) to down flow (Fryer and Potter, 1972). Some authors used a dispersed plug flow representation (May 1959) while others assumed well mixed compartments in series (Kato and Wen, 1969). The overall reactor performance is affected by dense phase gas mixing if conversions higher than 90% are sought; it is insensitive to the dense phase flow pattern for lower conversions Grace (1981).

2.2.5 Fraction Of Bed Occupied By Bubbles

The bubble volume fraction, ϵ_b, depends on the hydrodynamics prevailing in the bed. The bubble size and velocity are essential factors for the predictions of ϵ_b. The bubble velocity, u_b, can be calculated from the equation:

$$u_b = 0.711\sqrt{gd_b} + (U - U_{mf}) \tag{2.15}$$

Several expressions were proposed for the estimation of d_b as function of bed height (Mori and Wen, 1975; Darton et al., 1977). An iterative procedure is required for estimating ϵ_b (Grace, 1982). Using a first guess of ϵ_b, the bed height, H, can be calculated from the relation:

$$H = H_{mf}/(1 - \epsilon_b) \tag{2.16}$$

The bubble diameter is then calculated at 0.4H from Mori and Wen (1975) or the Darton et al. (1977) equations. The Mori and Wen (1975) correlation is widely used for calculating the bubble diameter at any bed height z:

$$\frac{d_b - d_{bm}}{d_{bo} - d_{bm}} = exp\{-0.3z/D\} \tag{2.17}$$

where the maximum bubble diameter is given by:

$$d_{bm} = 1.64\{A(U - U_{mf})\}^{0.4} \tag{2.18}$$

and the initial bubble diameter is given by (Miwa et al., 1972):

$$d_{bo} = 0.376(U - U_{mf})^2 \tag{2.19}$$

Finally, ϵ_b is calculated from:

$$\epsilon_b = Q_b / A u_b \tag{2.20}$$

2.2.6 Reaction In Dilute Phase

Very few models account for chemical reaction that might take place in the bubble phase (Kato and Wen, 1969; Grace 1984). This is particularly important for fast chemical reactions. Catalytic chemical reactions in the bubble phase may be simulated by introducing the volume fraction of bubbles occupied by solid particles, ϕ_b, as a model parameter. Based on experimental findings, Kunii and Levenspiel (1969) reported that 0.2 to 1% solids are present in the bubbles. The value of ϕ_b in the Grace model was recommended as

$$0.001\epsilon_b \leq \phi_b \leq 0.01\epsilon_b. \tag{2.21}$$

For slow reactions ϕ_b may be set equal to zero.

The recommended expression for the solid fraction in the dense phase, ϕ_d, is given by:

$$\phi_d = (1 - \epsilon_b)(1 - \epsilon_{mf}). \tag{2.22}$$

2.3 CATALYST ATTRITION

Catalyst particles in fluidized bed reactors usually collide and rub against each other. They also suffer wall abrasion. These actions cause larger particles to break into finer ones which may then elutriate. It has been reported that the rate of attrition decreases with time (Forsythe and Hertwig, 1949; Vaux and Schruben, 1983) because the attrition resistance increases as the rough edges of the particles are smoothed off and the weaker particles are eliminated (Forsythe and Hertwig, 1949).

There is no universally accepted procedure for measuring attrition because there is not a single mechanism of attrition. Various attrition phenomena and attrition tests have been summarized by Zenz (1979) and Vaux and Keairns (1980). Kono determined the attrition rate of relatively coarse alumina-silica particles by measuring the decrease in weight for a certain period of fluidization. He observed that the attrition rate is constant and concluded that attrition rates are influenced mainly by the superficial gas velocity and the ratio of the bed height at minimum fluidization to the bed diameter. He also found that the effect of particle size on attrition is small. Vaux and Fellers (1981) determined the degree of attrition of granular solid particles in fluidized beds by measuring the changes in particle specific surface area and increase in fines fraction. They concluded that sieve analysis of particles before and after fluidization of solids for one hour discriminates clearly between the attrition tendencies of different bed materials.

A number of standard attrition tests have been developed by various manufacturers and users of catalysts. These tests include shaker tests, spouting jets, submerged jets, and Chevron impingement tests. The standard apparatus and procedure for such tests varies among its users. The submerged jet test is used to simulate attrition which can occur in the grid region of deep fluidized beds. The original apparatus consisted of a 0.038m I.D. tube, 0.686 m long fitted with a grid plate having three 0.0004m diameter holes. At its upper end, the tube expands to a diameter of 0.127m. High pressure air is admitted to yield near sonic velocities (274.3 m/s) through the 0.0004m diameter holes. Typically, 0.1 kg samples are used. In the expanded section, the velocity is reduced to about 0.006 m/s which just exceeds the terminal velocity of 16 to 20 micron particles. The weight of particles smaller than 20 microns (including those originally present) is collected over a period of 5 to 45 hours and is expressed as a percentage of the original charge. This percentage, which is called the attrition index, is used to compare different catalysts.

In contrast to the submerged jet test, the spouting jet test is used to simulate the attrition under acceleration and impact conditions. In this test, the particles are subjected to a high velocity and impacted on a solid surface. The test procedure consists of placing a 0.3 Kg sample in an inverted Erlenmeyer flask having a 0.0254 m diameter hole in its bottom. The hole is covered with a 10 mesh screen. Bone dry air is admitted through a 0.0063m diameter stopper connected to the mouth of the flask. The air enters the flask at a velocity of 91.4 m/s and penetrates the entire catalyst sample as a spout thereby picking up catalyst particles and throwing them up against the base of the flask. The air leaves through the covered 0.0254m diameter hole. After one hour of operation, the material in the flask is screened through a number 10 mesh screen. The catalyst loss during the spouting plus that passing through a 10 mesh grid in the final sieving is reported as the attrition loss.

Chapter 3

MODEL FOR FLUIDIZED BED CLAUS REACTOR

Based on fundamental hydrodynamic considerations as well as experimental observations, Grace(1984) has proposed a general two phase model to predict the performance of fluidized bed reactors operating in the bubbling regime. This model is used as a basis for simulating fluidized bed Claus reactors.

3.1 MODEL ASSUMPTIONS

The basic assumptions underlying this model are:

- The bed consists of a dilute phase and a dense phase;
- All gas enters and flows through the dilute phase and there is no net flow in the dense phase;
- Catalyst particles are present in both phases and are well mixed;
- Mass exchange takes place between the two phases;
- The voidage in the dense phase is the same as that at minimum fluidization;
- Chemical reactions take place in both phases.

A schematic diagram of the model is shown in Figure 3.1. In addition, the following assumptions are invoked in this work:

- Isothermal conditions prevail throughout the bed;

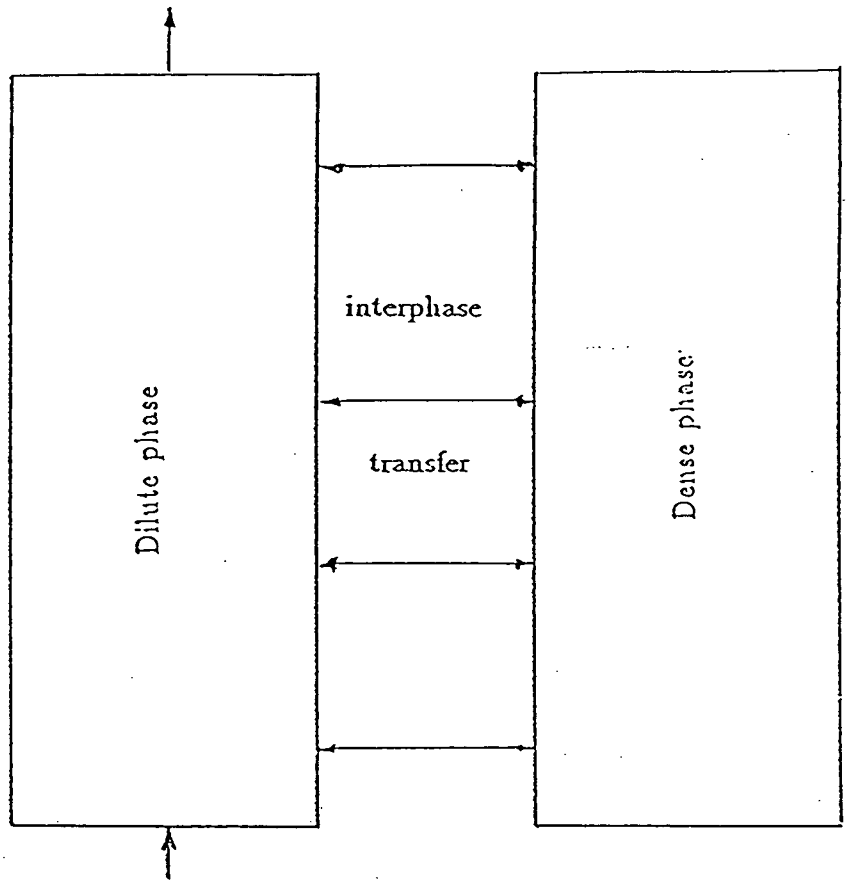

	Dilute phase	Dense phase
Concentration at z=0	C_0	$C_{2,0}$
Gas flow rate	UA	0
Fraction of bed accupied by phase	ϵ_b	$1-\epsilon_b$
Solids associated with phase	$\phi_b = 0.01\epsilon_b$	$\phi_d = (1-\epsilon_b)(1-\epsilon_{mf})$
Voidage		ϵ_{mf}

Figure 3.1: Schematic diagram for the two phase bubbling model

- Quasi-steady state prevails;
- The hydrogen sulphide/sulphur dioxide ratio is 2/1.

Based on the notion that fouling merely reduces the active catalyst surface, a fouling term is introduced as a multiplying factor in the numerator of the rate equation. The rate of disappearance of H_2S for the reversible Claus reaction can then be expressed as the difference of two terms, one pertaining to the forward reaction and the other to the reverse reaction, i.e.

$$r_{H_2S} = k'_w \Psi \left[P_{H_2S} P_{SO_2}^{0.5} - \frac{1}{K_e} P_{H_2O} P_{s_x}^{3/2x} \right] \tag{3.1}$$

where k'_w, K_e and Ψ denote the rate constant, the equilibrium constant and deactivation function, respectively.

The present study was confined to the temperature and H_2S concentration ranges of 100 to 150°C and 200 to 1300 ppm, respectively. It will be shown subsequently that, under these conditions, the second term in Equation 3.1 is negligible. For a gas mixture containing 1300 ppm H_2S and 650 ppm SO_2, the first term in the parenthetical expression in Equation 3.1 is

$$\begin{aligned} P_{H_2S} P_{SO_2}^{0.5} &= (1300 \times 10^{-6} \times 760)(650 \times 10^{-6} \times 760)^{0.5} \\ &= 0.694 \text{ (mm Hg)}^{1.5}. \end{aligned}$$

If it is assumed that the reaction goes to completion, then $P_{H_2O} = P_{H_2S} = 1300 \times 10^{-6} \times 760$ or 0.988 mm Hg. The partial pressure of sulphur cannot exceed the sulphur vapour pressure. At 150°C, the latter is 0.196 mm Hg according to the equation given by Meisen and Bennett (1979). The equilibrium constant, K_e, can be estimated from the free energy data compiled by McBride et al. (1963). At 150°C, $K_e = 1.66 \times 10^7$ and the second term in the parenthetical expression in Equation 3.1 therefore becomes:

$$\begin{aligned}\frac{1}{K_e}P_{H_2O}P_{S_8}^{3/16} &= (\frac{1}{1.667 \times 10^7})(0.988)(0.196)^{0.1875}\\ &= 4.38 \times 10^{-8}\ (\text{mm Hg})^{1.5}.\end{aligned}$$

The reverse Claus reaction is therefore negligible under the conditions examined in the present study. The rate expression may therefore be rewritten as:

$$r_{H_2S} = k'_w \Psi P_{H_2S} P_{SO_2}^{0.5} \tag{3.2}$$

For $P_{SO_2} = 0.5P_{H_2S}$ and assuming ideal gas behavior, the rate expression takes the form:

$$r_{H_2S} = k_w \Psi C_{H_2S}^{1.5} \tag{3.3}$$

where $k_w = k'_w(RT)^{1.5}/\sqrt{2}$.

3.2 GOVERNING EQUATIONS

An H_2S mass balance over differential volumes leads to the following equations for a fresh catalyst for which $\Psi = 1$.

Dilute phase:

$$U\frac{dC_{Ab}}{dz} + k_q \epsilon_b a_b (C_{Ab} - C_{Ad}) + k_v \phi_b C_{Ab}^{1.5} = 0 \tag{3.4}$$

Dense phase:

$$k_q a_b \epsilon_b (C_{Ab} - C_{Ad}) = k_v \phi_d C_{Ad}^{1.5} \tag{3.5}$$

These equations must be solved simultaneously subject to boundary conditions at z= 0. In this work, the following boundary conditions are used.

Dilute phase:

$$C_{Ab,0} = C_0 \tag{3.6}$$

Dense phase:

$$k_v \phi_d C_{Ad,0}^{1.5} + k_q a_b \epsilon_b (C_{Ad,0} - C_0) = 0 \tag{3.7}$$

These conditions imply that, at $z = 0$, the dense phase concentration is established by mass transfer from the dilute phase and chemical reaction in the dense phase. It is less than the dilute phase concentration. This assumption is based on the premise that all gas enters the reactor as the dilute phase and that there is no net flow of gas in the dense phase.

3.3 SOLUTION OF EQUATIONS

The above equations can be made dimensionless by introducing the following variables:

$$C_1 = C_{Ab}/C_0, \qquad C_2 = C_{Ad}/C_0, \qquad \text{and} \qquad \xi = z/H. \tag{3.8}$$

Equations 3.4 to 3.7 therefore become:

$$\frac{dC_1}{d\xi} = \alpha(C_2 - C_1) - \beta_1 C_1^{1.5} \tag{3.9}$$

$$\alpha(C_1 - C_2) = \beta_2 C_2^{1.5} \tag{3.10}$$

with the boundary conditions at $\xi = 0$:

$$C_1 = 1 \tag{3.11}$$

$$\beta_2 C_2^{1.5} + \alpha(C_2 - 1) = 0 \tag{3.12}$$

where:

$$\alpha = \frac{k_q a_b \epsilon_b H}{U}; \tag{3.13}$$

$$\beta_1 = \frac{k_v \phi_b H \sqrt{C_0}}{U}; \tag{3.14}$$

$$\beta_2 = \frac{k_v \phi_d H \sqrt{C_0}}{U}. \tag{3.15}$$

If $C_{2,0}$ denotes the value of C_2 at $\xi = 0$, then equation 3.12 may be rewritten in the form:

$$(\sqrt{C_{2,0}})^3 + \frac{\alpha}{\beta_2}(\sqrt{C_{2,0}})^2 - \frac{\alpha}{\beta_2} = 0 \tag{3.16}$$

It may be shown that the positive real root of the above cubic equation (for $\sigma > 0$) is given by

$$\sqrt{C_{2,0}} = (\frac{\alpha}{2\beta_2})^{1/3}[(\sigma + \sqrt{\sigma})^{1/3} + (\sigma - \sqrt{\sigma})^{1/3}] - \frac{\alpha}{3\beta_2} \tag{3.17}$$

where $\sigma = 1 - 2(\alpha/\beta_2)/27$.

Equations 3.9 and 3.10 can be combined by introducing the transformation

$$x = \sqrt{(1 + \frac{\beta_2}{\alpha}\sqrt{C_2})}$$

$$C_2 = \{\frac{\alpha}{\beta_2}(x^2 - 1)\}^2$$

$$C_1 = (\frac{\alpha}{\beta_2})^2 x^2 (x^2 - 1)^2. \tag{3.18}$$

Differentiating equation 3.18 yields:

$$\frac{dC_1}{d\xi} = 2(\frac{\alpha}{\beta_2})^2 x (x^2 - 1)(3x^2 - 1)\frac{dx}{d\xi}. \tag{3.19}$$

It is clear that equation 3.10 is automatically satisfied. Substituting the expressions for C_1, C_2 and $dC_1/d\xi$ into equation 3.9 and simplifying gives:

$$\frac{dx}{d\xi} = -\frac{\alpha}{2\gamma^3}\{\frac{(1 - x^2)^2(\gamma^3 + x^3)}{(3x^2 - 1)x}\} \tag{3.20}$$

where $\gamma^3 = \beta_2/\beta_1$.

If x_0 denotes the value of x at $\xi = 0$ and x_1 the corresponding value at $\xi = 1$, then x_0 can be calculated from the value of C_2 at the bottom of the reactor (i.e. $C_{2,0}$):

$$x_0 = \sqrt{1 + \frac{\beta_2}{\alpha}\sqrt{C_{2,0}}} \tag{3.21}$$

where $C_{2,0}$ is given by equation 3.17.

To find x_1, equation 3.20 is integrated (by partial fractions) between the limits x_0 and x_1 to give:

$$\frac{\alpha}{2\gamma^3} + f(x_1, x_0) = 0 \tag{3.22}$$

where $f(x_1, x_0)$ is the function whose root gives x_1 at $\xi = 1$. Once x_1 is found, C_1 and C_2 can be calculated at the top of the reactor.

The function $f(x_1, x_0)$ at $\xi = 1$ is given by:

$$f(x_0, x_1) = \int_{x_0}^{x_1} \{\frac{(3x^2 - 1)x}{(1 - x^2)^2(\gamma^3 + x^3)}\} dx. \tag{3.23}$$

The kernel in the above integral may be rearranged into:

$$\frac{(3x^2 - 1)x}{(1 - x^2)^2(\gamma^3 + x^3)} = \frac{(3x^2 - 1)x}{(1 + x)^2(1 - x)^2(\gamma + x)(x^2 - \gamma x + \gamma^2)}. \tag{3.24}$$

The right hand side may then be rewritten in terms of partial fractions as:

$$\frac{(3x^2 - 1)x}{(1 - x^2)^2(\gamma^3 + x^3)} = \frac{A_1}{1 + x} + \frac{A_2}{(1 + x)^2} + \frac{A_3}{1 - x} + \frac{A_4}{(1 - x)^2} + \frac{A_5}{\gamma + x} + \frac{A_6 x + A_7}{x^2 - \gamma x + \gamma^2} \tag{3.25}$$

The constants A_1 to A_7 are evaluated as follow:

$$\begin{aligned} A_1 &= \lim_{x \to -1} \frac{d}{dx} \{\frac{x(3x^2 - 1)}{(1 + x)^2(x - 1)^2(\gamma^3 + x^3)}\}(x + 1)^2 \\ &= \frac{3}{2} \frac{\gamma^3}{(\gamma^3 - 1)^2} \end{aligned} \tag{3.26}$$

and A_2 is given by:

$$\begin{aligned} A_2 &= \lim_{x \to -1} \{\frac{x(3x^2 - 1)}{(1 + x)^2(1 - x)^2(\gamma^3 + x^3)}\}(1 + x)^2 \\ &= \frac{-1}{2(\gamma^3 - 1)} \end{aligned} \tag{3.27}$$

$$\begin{aligned} A_3 &= \lim_{x \to 1} \frac{d}{dx} \{\frac{(3x^2 - 1)x}{(1 + x)^2(1 - x)^2(\gamma^3 + x^3)}\}(1 - x)^2 \\ &= \frac{3}{2} \frac{\gamma^3}{(\gamma^3 + 1)^2} \end{aligned} \tag{3.28}$$

$$\begin{aligned} A_4 &= \lim_{x\to 1}\{\frac{(3x-1)x}{(1+x)^2(1-x)^2(\gamma^3+x^3)}\}(1-x)^2 \\ &= \frac{1}{2(\gamma^3+1)} \end{aligned} \tag{3.29}$$

$$\begin{aligned} A_5 &= \lim_{x\to -\gamma}\{\frac{(3x^2-1)x}{(x^2-1)(x+\gamma)(x^2-\gamma x+\gamma^2)}\}(x+\gamma) \\ &= -\frac{1}{3\gamma}\frac{3\gamma^3-1}{(\gamma^2-1)^2}. \end{aligned} \tag{3.30}$$

To find A_6 and A_7, the function $\Lambda(x)$ is introduced to simplify the notation. The kernel may be rewritten as

$$\frac{x(3x^2-1)}{(1-x^2)^2(\gamma+x)(x^2-\gamma x+\gamma^2)} = \frac{\Lambda(x)}{x^2-\gamma x+\gamma^2} \tag{3.31}$$

where

$$\Lambda(x) = \frac{x(3x^2-1)}{(1-x^2)^2(\gamma+x)} \tag{3.32}$$

By inspection of equation 3.25, $\Lambda(x)$ is also given by:

$$\Lambda(x) = A_6 x + A_7 + (x^2-\gamma x+\gamma^2)G(x) \tag{3.33}$$

and $G(x)$ denotes the first five terms on the right hand side of equation 3.25. The roots of the expression $x^2-\gamma x+\gamma^2$ are $x=\gamma(1\pm\imath\sqrt{3})/2$, where $\imath=\sqrt{-1}$. Substituting for $x=\gamma(1+\imath\sqrt{3})/2$ in equation 3.33 gives:

$$\begin{aligned} \Lambda(\frac{\gamma}{2}+\imath\frac{\gamma\sqrt{3}}{2}) &= \gamma A_6(1+\imath\sqrt{3})/2+A_7 \\ &= \Lambda_r+\imath\Lambda_\imath \end{aligned} \tag{3.34}$$

where $\Lambda_\imath$ and Λ_r denote the imaginary and real parts of Λ. Equating the imaginary terms in equation 3.34 gives:

$$A_6 = \Lambda_\imath/(\gamma\sqrt{3}/2). \tag{3.35}$$

Similarly, A_7 is determined by equating the real term in equation 3.34:

$$A_7 = \Lambda_r - \Lambda_\imath/\sqrt{3}. \tag{3.36}$$

It is easy to show (after some algebraic manipulation) that

$$\Lambda(\frac{\gamma}{2} + \imath\frac{\gamma\sqrt{3}}{2}) = -\frac{1}{2}\frac{5\gamma^4+3\gamma^2+1}{(\gamma^4+\gamma^2+1)^2} + \imath\frac{\sqrt{3}}{6}\frac{6\gamma^6+7\gamma^7+\gamma^2+1}{(\gamma^4+\gamma^2+1)^2}. \tag{3.37}$$

Hence:

$$\Lambda_r = -\frac{1}{2}\frac{5\gamma^4+3\gamma^2+1}{(\gamma^4+\gamma^2+1)^2} \tag{3.38}$$

and

$$\Lambda_\imath = \frac{\sqrt{3}}{6}\frac{6\gamma^6+7\gamma^7+\gamma^2+1}{(\gamma^4+\gamma^2+1)^2}. \tag{3.39}$$

Thus the constants A_6 and A_7 are given by:

$$A_6 = -\frac{1}{3\gamma}\{\frac{6\gamma^6+7\gamma^4+\gamma^2+1}{(\gamma^4+\gamma^2+1)^2}\} \tag{3.40}$$

and

$$A_7 = \frac{1}{3}\{\frac{3\gamma^6-4\gamma^4-4\gamma^2-1}{(\gamma^4+\gamma^2+1)^2}\}. \tag{3.41}$$

Substituting the constants A_1 to A_7 into equation 3.25 and integrating term by term gives:

$$\begin{aligned} f(x_1,x_0) &= A_1\ln(\frac{1+x_1}{1+x_0}) + A_3\ln(\frac{1-x_1}{1-x_0}) + A_5\ln(\frac{\gamma+x_1}{\gamma+x_0}) \\ &- A_2(\frac{1}{1+x_1} - \frac{1}{1+x_0}) + A_4(\frac{1}{1-x_1} - \frac{1}{1-x_0}) \\ &+ \frac{2A_7-\gamma A_6}{\sqrt{3}\gamma}\left[\arctan(\frac{2x_1-\gamma}{\sqrt{3}\gamma}) - \arctan(\frac{2x_0-\gamma}{\sqrt{3}\gamma})\right] \\ &+ A_6\ln(\frac{x_1^2-\gamma x_1+\gamma^2}{x_0^2-\gamma x_0+\gamma^2}). \end{aligned} \tag{3.42}$$

Although this expression is not an explicit function of x_1, it is well behaved except at $x_1 \pm 1$ (see Figure 3.2). The singularity at $x_1 = 1$, arises when C_1 and $C_2 \to 0$ (the

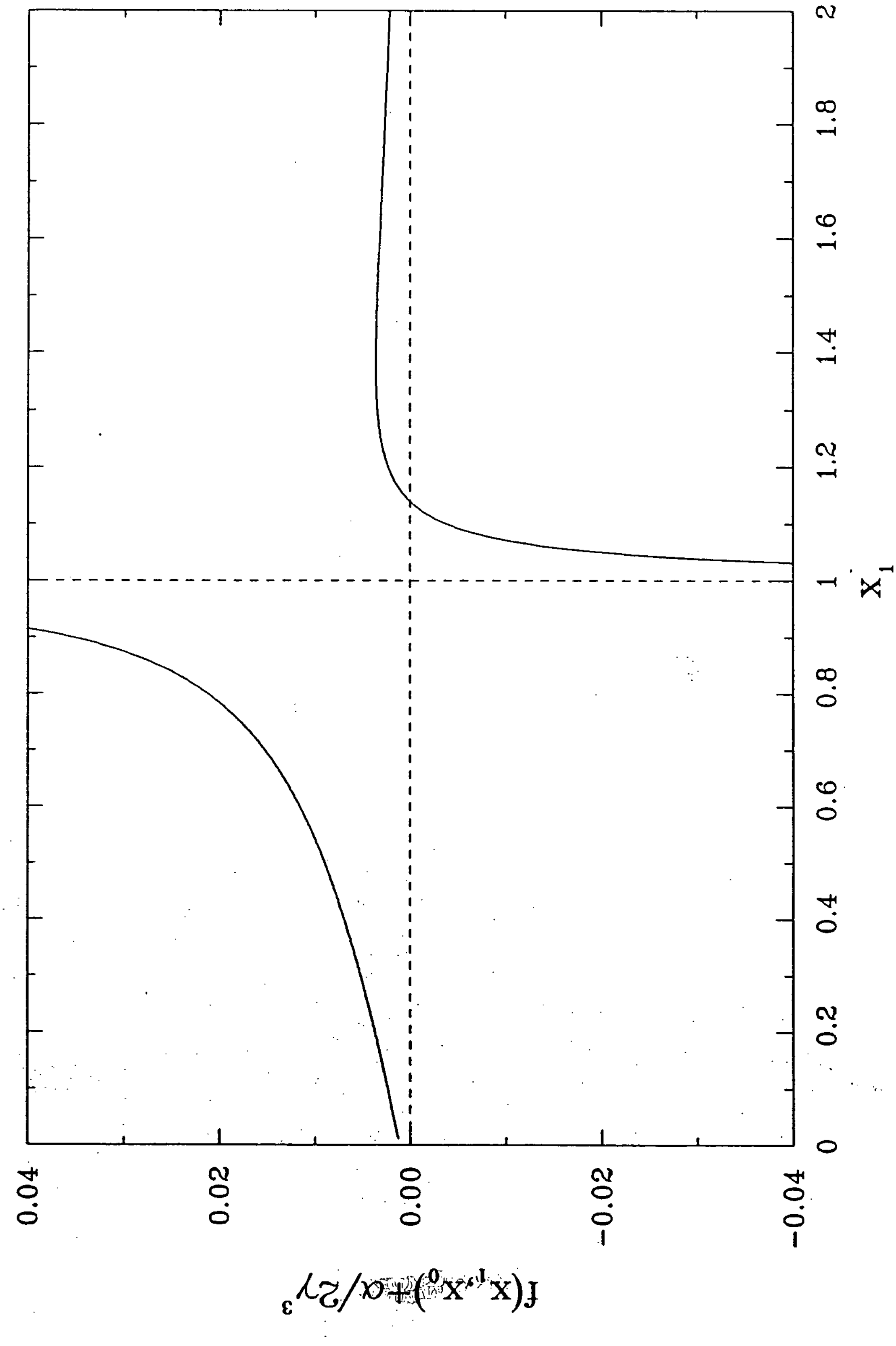

Figure 3.2: Solution of equation 3.40 (α=1.701, β_2=1.387, γ=6.36, x_0=1.307)

ratio C_1/C_2 approaches 1) and hence both the rate of reaction and mass transfer are zero. The root, x_1, of equation 3.22 can be found within a few iterations provided that $1 < x_1 < x_0$ (see Figure 3.2). A root finding subroutine, which uses the bisection method to calculate any specified number of roots in a given interval and avoids discontinuities, was developed to find x_1 (see Appendix B). Values of C_2 and C_1 at $\xi = 1$ are calculated from the relations:

$$C_2 = \{\frac{\alpha}{\beta_2}(x_1^2 - 1)\}^2 \tag{3.43}$$

$$C_1 = (\frac{\alpha}{\beta_2})^2 x_1^2 (x_1^2 - 1)^2. \tag{3.44}$$

The theoretical conversion is then given by:

$$\chi = 1 - C_1. \tag{3.45}$$

The above equations were formulated for the calculation of the overall conversion and the concentration at the top of the reactor. Concentration profiles for the dilute and dense phases can be predicted by replacing x_1 by $x(\xi)$ in equations 3.42, 3.43, 3.44, and by multiplying the term $\alpha/2\gamma^3$ in equation 3.22 by ξ i.e:

$$\frac{\alpha}{2\gamma^3}\xi + A_1 \ln\left[\frac{1+x(\xi)}{1+x_0}\right] + A_3 \ln\left[\frac{1-x(\xi)}{1-x_0}\right] + A_5 \ln\left[\frac{\gamma+x(\xi)}{\gamma+x_0}\right]$$

$$+A_6 \ln\left[\frac{x^2(\xi)-\gamma x(\xi)+\gamma^2}{x_0^2-\gamma x_0+\gamma^2}\right] + A_2\left[\frac{1}{1+x_0} - \frac{1}{1+x(\xi)}\right] + A_4\{\frac{1}{1-x(\xi)}$$

$$-\frac{1}{1-x_0}\} + \frac{2A_7-\gamma A_6}{\sqrt{3}\gamma}\left[\arctan(\frac{2x(\xi)-\gamma}{\sqrt{3}\gamma}) - \arctan(\frac{2x_0-\gamma}{\sqrt{3}\gamma})\right] = 0 \tag{3.46}$$

Similarly the dimensionless concentrations as a function of ξ are given by:

$$C_2(\xi) = \left[\frac{\alpha}{\beta_2}(x^2(\xi)-1)\right]^2 \tag{3.47}$$

$$C_1(\xi) = (\frac{\alpha}{\beta_2})^2 x^2(\xi)\left[x^2(\xi)-1\right]^2. \tag{3.48}$$

Concentration profiles generated from the above equation are shown in Figure 3.3 for the case where $\alpha = 1.701$, $\beta_2 = 1.387$, $\gamma = 6.36$ and $x_0 = 1.307$ which were calculated in Appendix B for the conditions $U/U_{mf} = 4.44$, $H_s = 0.19$m and T=150°C. The above procedure can be extended to any reaction of order $n(= p/q \neq 1)$ by choosing $x = (C_1/C_2)^{1/q}$ to combine the equations for the dilute and dense phases. The resulting equations will be:

$$C_1 = (\frac{\alpha}{\beta_2})^{q/(p-q)} x^q (x^q - 1)^{q/(p-q)} \tag{3.49}$$

$$C_2 = (\frac{\alpha}{\beta_2})^{q/(p-q)} (x^q - 1)^{q/(p-q)} \tag{3.50}$$

$$\left[\frac{x^{q-1}(px^q + q - p)}{(x^2 - 1)^2(\gamma^p + x^p)}\right] dx = \frac{-\alpha}{q(p-q)\gamma^p} d\xi \tag{3.51}$$

subjected to the boundary condition at $\xi = 0$

$$x_0^p - x_0^{p-q} - \frac{\beta_2}{\alpha} = 0 \tag{3.52}$$

where $\gamma^p = \beta_1/\beta_2$. Partial fractions may be used, in principle, to integrate equation 3.51. The result of the integration of equation 3.51 is a function of x_1, x_0, γ, and α. The solution may expressed as:

$$\mathcal{F}(x_1, x_0, \gamma, \alpha) = 0. \tag{3.53}$$

Table 3.1 presents expressions for $\mathcal{F}$ for reactions of order n.

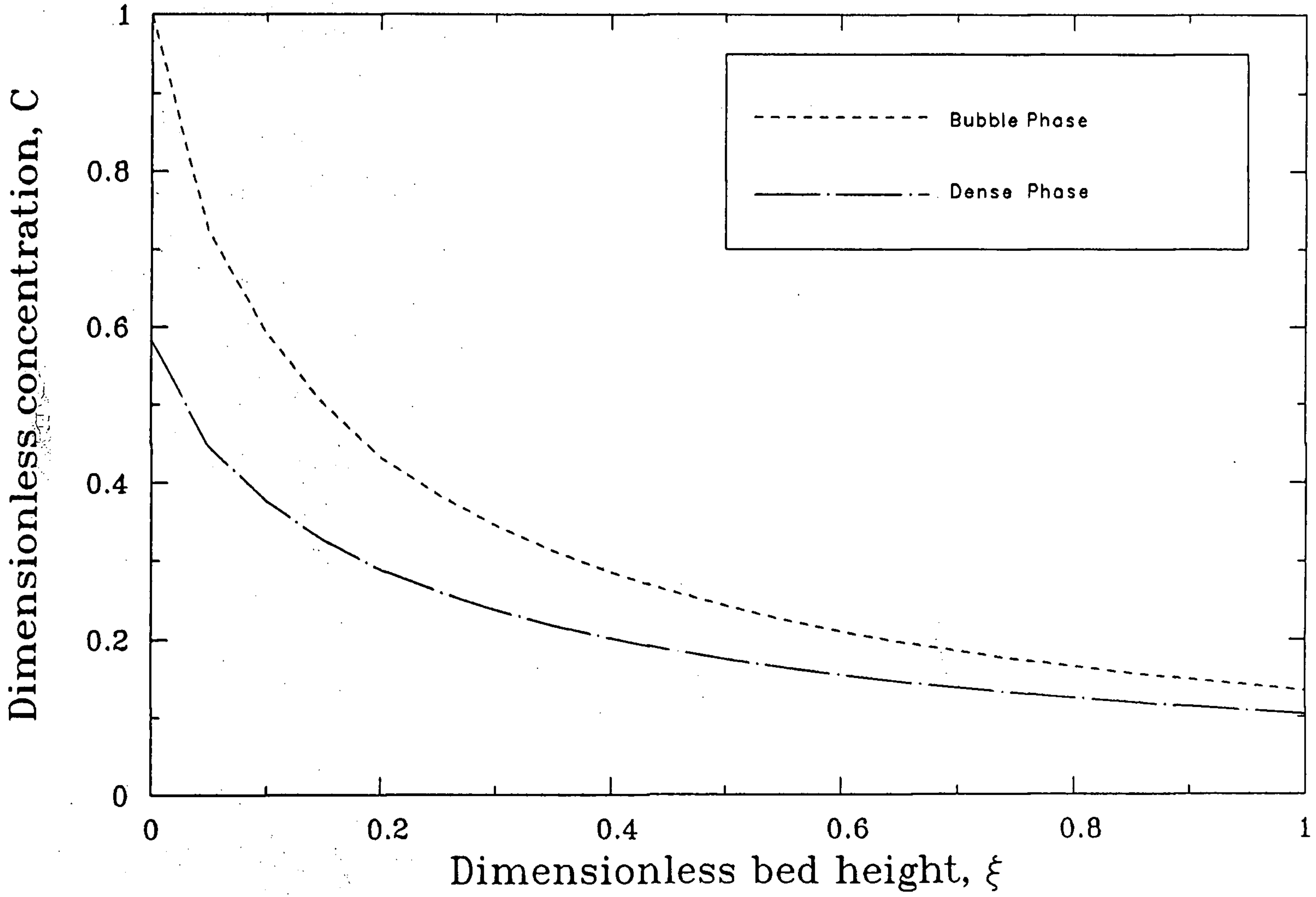

Figure 3.3: Predicted concentration profiles (α=1.701, β_2=1.387, γ=6.36, x_*=1.307)

Table 3.1: Solutions for equation 3.51 at the top of the bed for selected reaction orders

n	$\frac{dx}{d\xi}$	$\mathcal{F}(x_1, x_0, \gamma, \alpha)$
$\frac{1}{2}$	$\frac{\alpha}{2\gamma^3}\frac{(1-x^2)^2(\gamma+x)}{x(x^2+1)}$	$A_1\ln(\frac{1+x_1}{1+x_0}) + A_3\ln(\frac{1-x_1}{1-x_0}) + \frac{A_5}{\gamma}[\arctan(x_1/\gamma) - \arctan(x_0/\gamma)]$ $-A2(\frac{1}{1+x_1} - \frac{1}{1+x_0}) + A_4(\frac{1}{1-x_1} - \frac{1}{x_0}) - \frac{\alpha}{2\gamma}$
2	$-\frac{\alpha}{\gamma^2}\frac{(1-x^2)^2(\gamma^2+x^2)}{(2x-1)}$	$A_1\ln(\frac{1+x_1}{1+x_0}) + A_3\ln(\frac{1-x_1}{1-x_0}) - A_2(\frac{1}{1+x_1} - \frac{1}{1+x_0}) + A_4(\frac{1}{1-x_1} - \frac{1}{1-x_0})$ $+\frac{A_5}{\gamma}\ln(\frac{x_1^2+\gamma^2}{x_0^2+\gamma^2}) + \frac{A_6}{\gamma}[\arctan(x_1/\gamma) - \arctan(x_0/\gamma)] + \frac{\alpha}{\gamma^2}$
3	$-\frac{\alpha}{2\gamma^3}\frac{(1-x^2)^2(\gamma^3+x^3)}{(3x-2)}$	$A_1\ln(\frac{1+x_1}{1+x_0}) + A_3\ln(\frac{1-x_1}{1-x_0}) + A_5\ln(\frac{\gamma+x_1}{\gamma+x_0}) + A_6\ln(\frac{x_1^2-\gamma x_1+\gamma^2}{x_0^2-\gamma x_0+\gamma^2})$ $-A_2(\frac{1}{1+x_1} - \frac{1}{1+x_0}) + A_4(\frac{1}{1-x_1} - \frac{1}{1-x_0}) + \frac{2A_7-\gamma A_6}{\gamma\sqrt{3}}[\arctan(\frac{2x_1-\gamma}{\gamma\sqrt{3}})$ $-\arctan(\frac{2x_0-\gamma}{\gamma\sqrt{3}})] + \frac{\alpha}{2\gamma^3}$

n	A_1	A_2	A_3	A_4	A_5	A_6	A_7
$\frac{1}{2}$	$\frac{\gamma}{2(\gamma-1)^2}$	$\frac{-1}{2(\gamma-1)}$	$\frac{\gamma}{2(\gamma+1)^2}$	$\frac{1}{2(\gamma+1)}$	NA	NA	NA
2	$\frac{-\gamma^2-3}{4(\gamma^2+1)^2}$	$\frac{-3}{4(\gamma^2-1)}$	$\frac{\gamma^2-1}{4(\gamma^2+1)^2}$	$\frac{1}{4(\gamma^2+1)}$	$\frac{-1}{\gamma(\gamma^2+1)^2}$	$\frac{-2\gamma^3}{(\gamma^2+1)^2}$	NA
3	$\frac{-2\gamma^3+17}{4(\gamma^3-1)^2}$	$\frac{-5}{4(\gamma^3-1)}$	$\frac{2\gamma^3-1}{4(\gamma^3+1)^2}$	$\frac{1}{4(\gamma^3+1)}$	$\frac{-3\gamma-2}{3\gamma(\gamma^2-1)^2}$	$\frac{-6\gamma^5+2\gamma^4-6\gamma^3-4\gamma^2+3\gamma-2}{3\gamma(\gamma^4+\gamma^2+1)^2}$	$\frac{3\gamma^5-4\gamma^4+12\gamma^3-4\gamma^2+3\gamma+2}{3\gamma^2(\gamma^4+\gamma^2+1)^2}$

3.4 DETERMINATION OF THE RATE CONSTANT

The reaction rate constant used in the bubbling bed model was determined from fixed bed studies. This constant is a function of temperature and catalyst characteristics. Although rate expressions for the Claus reaction over various catalysts have been published (see Section 2.1.3), the rate constant for the catalyst used in this study (known as Kaiser S-501 alumina) has not been reported in the literature. Furthermore, the rate expressions cited in section 2.1.3 were developed under temperature conditions ranging from 200 to 325°C (Dalla Lana et al., 1972, 1976). Therefore, the decision was made to carry out experiments within the temperature range shown in Table 5.1 and at gas velocities lower than the minimum fluidizing velocity. During these experiments, the catalyst weight, W_{cat}, and the H_2S concentration in the feed were kept constant at 1.2 kg and 600 ppm, respectively. The bed diameter was 0.1 m and its depth was 0.19 m. The ratio of H_2S to SO_2 in the feed was fixed at 2. The experiments were performed according to the procedure described in section 5.1.2.

Three basic assumptions are invoked in the following analysis:

- Constant temperature throughout the bed.
- Plug flow of gas through the bed.
- Reaction orders are 1 and 0.5 for H_2S and SO_2, respectively.

The axial and radial dispersions arising in the fixed bed experiments may be tested by means of the Peclet numbers, Pe_L and Pe_r, defined as:

$$Pe_L = \frac{\text{axial convection}}{\text{axial dispersion}} = \frac{DU}{D_L} \tag{3.54}$$

and

$$Pe_r = \frac{\text{axial convection}}{\text{radial dispersion}} = \frac{DU}{D_r} \tag{3.55}$$

where D_L and D_r denote the axial and radial dispersion coefficients, respectively. Dispersion coefficients in packed beds were reported by Bischoff and Levenspiel (1962). The estimated values of D_L and D_r were taken as 9.12×10^{-6} and 5.58×10^{-6} $m^2/s./$, respectively, and the corresponding values of Pe_L and Pe_r were 219 and 358. According to Levenspiel (1972), deviation from plug flow occurs when $Pe < 100$. The assumption of plug flow in the present fixed bed reactor was therefore justified.

The material balance equation for the plug flow reactor is given by:

$$\frac{W_{cat}}{UAC_{H_2S,0}} = \int_0^{\chi} \frac{d\chi}{-r_{H_2S}}. \tag{3.56}$$

Substituting equation 3.3 into equation 3.56 and rearranging gives (for $\Psi = 1$):

$$\begin{aligned} k_w &= \frac{UA}{W_{cat}\sqrt{C_{H_2S}}} \int_0^{\chi} \frac{d\chi}{(1-\chi)^{1.5}} \\ &= \frac{UA}{W_{cat}\sqrt{C_{H_2S,0}}} \left[\frac{1}{\sqrt{1-\chi}} - 1\right] \end{aligned} \tag{3.57}$$

where k_w denotes the rate constant per unit catalyst mass. Values for k_w were found to be 0.1834, 0.202, 0.239 $(\text{kmole/m}^3)^{-0.5}/\text{s.kgcat}$ at 100, 124, 150°C, respectively.

Rate constants for other catalysts could be obtained from expressions reported by Dalla Lana et al.(1972, 1976) and by McGregor(1971). For instance when equation 2.2 is evaluated at 373 K and $P_{SO_2} = P_{H_2S}/2$,

$$\begin{aligned} r_{H_2S} &= \frac{1.12}{3600}\frac{(62.4 \times 373)^{1.5}}{\sqrt{2}} \exp\left(\frac{-7440}{1.987 \times 373}\right) C_{H_2S}^{1.5} \\ &= 0.034 C_{H_2S}^{1.5} \qquad \frac{(\text{kmole/m}^3)}{\text{s.kg bauxite}}) \end{aligned} \tag{3.58}$$

The k_w values are summarized in Table 3.2. It should be noted that equation 2.2 was developed for the temperature range of 481 to 560 K, the reported temperature range for equation 2.3 was 473 to 596 K. Table 3.2 shows that the values of k_w determined in

Table 3.2: Values of rate constant, k_w

Temperature (K)	Rate constant, k_w $\frac{(\mathrm{kmol/m^3})^{-0.5}}{\mathrm{s.kg\ cat}}$			
	a	b	c	d
373	0.031	0.034	0.055	0.183
397	0.063	0.069	0.112	0.202
423	0.135	0.124	0.222	0.239

a) Dalla Lana et al.(1976); b) Dalla Lana et al.(1972); c) McGregor (1971); d) This work.

this study are significantly higher than those obtained from equations 2.2 and 2.3 thus indicating that the activity of the promoted alumina S-501 exceeds that of bauxite and γ-alumina. This is consistent with the findings of Pearson (1973) who reported that the S-501 catalyst had led to higher conversions than those obtained with bauxite and an S-201 alumina catalyst.

Figure 3.4 shows the Arrhenius plots for various catalysts. Curves 2 to 5 are based on the results of previous studies which were conducted at temperatures greater than $200°C$. Extrapolation of these expressions to the lower temperatures used in the present study is not reliable and is provided for comparision purposes only. The corresponding activation energies and frequency factors are listed in Table 3.3. The low value of E determined in this study is associated with a low value of A_f thus indicating a compensating behavior.

To elucidate these results, the effects of external mass transfer and pore diffusion were calculated. The influence of the external mass transfer effects may be determined from the effectiveness factor, η, defined by:

$$\eta = \frac{\text{Reaction rate with mass transfer resistance}}{\text{Reaction rate without mass transfer resistance}} \tag{3.59}$$

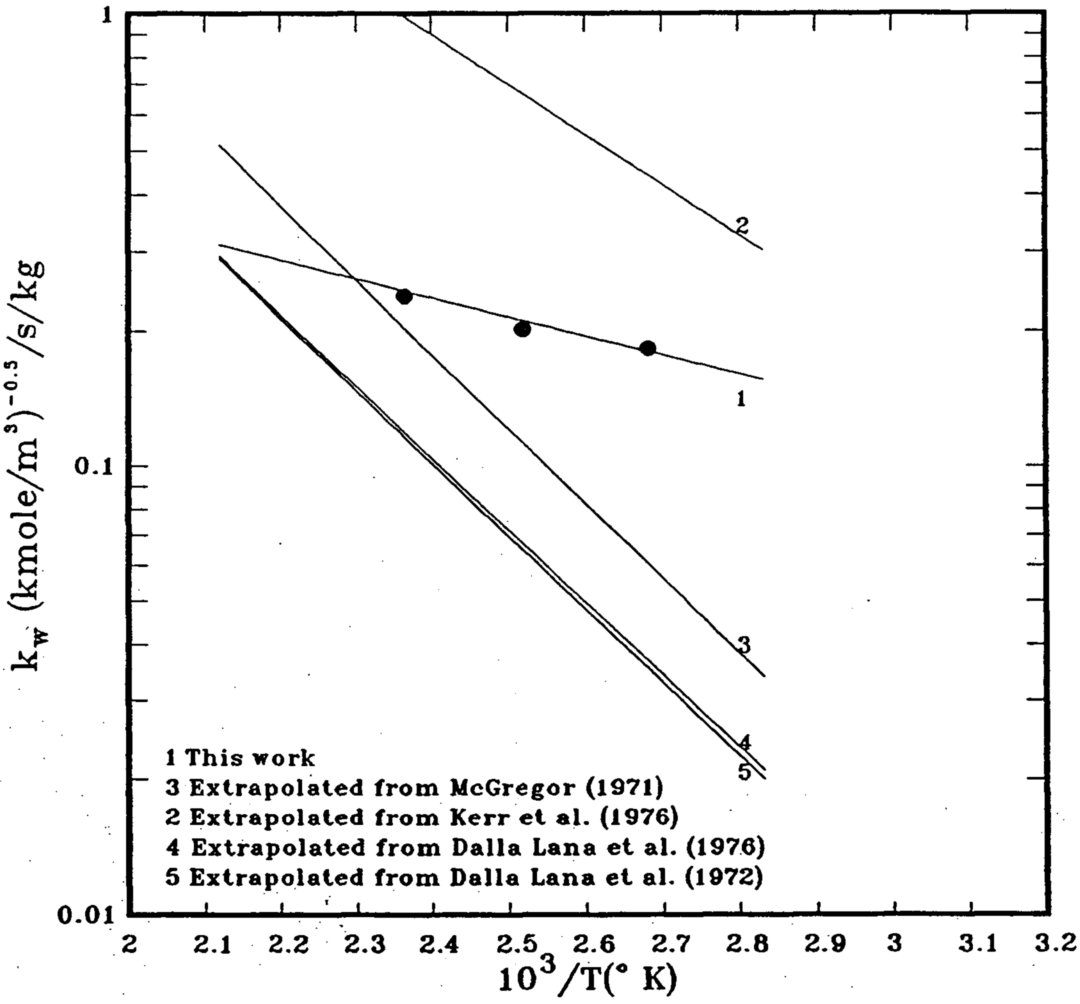

Figure 3.4: Rate constants as a function of temperature for various Claus catalysts

Table 3.3: Activation energies and frequency factors for Claus catalysts

Catalyst	E (kcal/mole)	A_f	Investigator
Bauxite	7.44	807.3	Dalla Lana et al. (1972)
$\gamma-$alumina	7.35	744.1	Dalla Lana et al. (1976)
Cobalt-Molybdate on alumina	5.50	-	George (1974)
Chemisorb-A	25.0	-	George (1975)
Chemisorb-A promoted with 5.0%$NaOH$	15.0	-	George (1975)
Bauxite	5.02	386.4	Kerr et al. (1976)
Bauxite	7.59	1690.8	McGregor (1971)
Alumina S-501	1.93	2.43	This work

Carberry (1976) presented charts for η in terms of the observable quantity, ηDa_0 i.e:

$$\eta Da_0 = \frac{\text{Observed rate}}{C_{H_2S,g} k_g a_p} \tag{3.60}$$

where $C_{H_2S,g}$ denotes the concentration of H_2S in the bulk of the gas phase and Da_0 represents the Damköhler number, i.e the ratio of chemical reaction velocity to the mass transport velocity. k_g denotes a mass transfer coefficient and a_p denotes the interfacial area expressed as the particle surface area per unit particle volume. The mass transfer coefficient in packed beds may be calculated from the correlation reported by Sherwood et al. (1975):

$$k_g = 1.17U(\frac{d_p \rho_g U}{\mu_g})^{-0.42}(\frac{\mu_g}{\rho_g D_g})^{-0.67} \tag{3.61}$$

The observed rate can be calculated from the measured conversion:

$$\begin{aligned} \text{Observed rate} &= \frac{\Delta\chi}{W_{cat}/F_{H_2S,0}} \\ &= \frac{\chi}{W_{cat}/F_{H_2S,0}} \end{aligned} \tag{3.62}$$

Table 3.4: Calculation of external mass transfer effectiveness factor

Temperature (K)	373	397	423
χ	0.93	0.94	0.96
$C_{H_2S,0} \times 10^5$ (kmole/m^3)	1.959	1.841	1.728
$F_{H_2S,0} \times 10^9$ (kmole/s)	3.385	3.181	2.714
Obs. rate $\times 10^9$ (kmole/m^3)/s.kg cat	2.623	2.491	2.16.
Obs. rate $\times 10^6$ (kmole/m^3)/s.m^3	2.086	1.9807	1.717
k_g (m/s)	0.0208	0.0232	0.0281
$\eta Da_0 \times 10^4$	1.664	1.507	1.149
η (from Carberry, 1976)	1	1	1
Effect of mass transfer	Nil	Nil	Nil

where $F_{H_2S,0} = UAC_{H_2S,0}$ (kmole/s) and $C_{H_2S,0}$ =(PPM$\times 10^{-6}$)P/RT (kmole/m^3). The numerical values of the above parameters are presented in Table 3.4.

The pore diffusion effect may be assessed by using the generalized Thiele modulus, Φ. Bischoff (1967) formulated the following criterion for Φ:

$$\Phi = \frac{\text{Observed rate} \times l_c^2 g(C_{H_2S,g})}{2D_e \int_0^{C_{H_2S,g}} g(C_{H_2S}) dC_{H_2S}} \begin{cases} < 1 & \text{Negligible pore diffusion} \\ > 1 & \text{Significant pore diffusion} \end{cases} \tag{3.63}$$

where $g(C_{H_2S})$ denotes the concentration term in the rate expression [i.e. $g(C_{H_2S}) = C_{H_2S}^{1.5}$], D_e denotes the effective diffusivity and l_c is a characteristic length of the catalyst particle. Aris (1957) showed that for a spherical particle, l_c may be taken as $d_p/6$. The effective diffusivity may be estimated from the relation (Sherwood et al., 1975):

$$D_e = \frac{D_g \bar{\theta}}{\zeta} \tag{3.64}$$

where $\bar{\theta}$ denotes the particle voidage and ζ denotes the tortuosity factor. Satterfield (1970) recommended, in the absence of experimental values, that $\bar{\theta} = 0.4$ and $\zeta = 5$. Substituting for $g(C) = C^{1.5}$, equation 3.62 gives:

$$\Phi = \frac{5}{4} \frac{\text{(Observed rate)}(d_p/6)^2}{D_e C_{H_2S,g}} \tag{3.65}$$

Table 3.5: Calculation of Thiele modulus

Temperature (K)	373	397	423
$D_e \times 10^7$ (m^2/s)	7.86	8.9	9.91
$\Phi \times 10^4$	1.789	1.596	1.324
Φ	< 1	< 1	< 1
Effect of pore diffusion	negligible	negligible	negligible

Values of Φ are presented in Table 3.5 and show that the pore diffusion effects are negligible.

Different values of activation energy for a given reaction over a series of catalysts may be attributed to the methods by which such catalysts were prepared. Ashmore (1963) quoted various authors and reported 8 different values of E (for 8 catalysts) for two classical reactions (Methanol synthesis and sulphur dioxide oxidation). For instance the reported activation energy for SO_2 oxidation ranged from 10 to 38 kcal/mole.

It is common to find a relationship between the activation energy, E, and the frequency factor, A_f, for different catalysts promoting a given reaction (Constable, 1925). The form of the relationship is:

$$\ln A_f = a_1 E + a_2 \tag{3.66}$$

This effect was later called the "theta rule" by Schwab (1950) and "the compensation effect" by Cremer (1955). In essence, it states that increases in the activation energy are "compensated for" by increases in A_f. The Compensation effect may arise because catalysts have different energy levels (Cremer, 1955). For example, if the adsorption on catalyst 2 is stronger than that on catalyst 1 (i.e. the desorption energy $E_2^* > E_1^*$ and the activation energy $E_1 > E_2$) then the "activated complex" formed on catalyst 2 possesses less vibrational and rotational freedom than that formed on catalyst 1; in other words the entropy difference between the activated complexes formed on catalyst

1 and the reactants, ΔS_1, is higher than ΔS_2 (the entropy difference between the activated complexes formed on catalyst 2 and reactants). Since A_f is related to the entropy difference, it follows that A_{f_1} must be higher than A_{f_2}. Thomas and Thomas (1967) discussed the importance of lattice imperfections in catalysts and pointed out that the compensation effect may be explained on the basis of lattice defects. The effect has also been observed in other processes such as homogeneous reactions (Fairclough and Hinshelwood, 1937), viscosity of aqueous solutions (Good and Stone, 1972) and conductivity of inorganic (Roberts, 1974) and organic (Eley, 1967) semiconductors. These example are cited to indicate the generality of the compensation behavior. Several mechanistic models have been proposed to explain the compensation phenomena and were discussed in a comprehensive review by Galwey (1977).

George (1975) studied various Claus catalysts and found that the activity of some of the catalysts was improved when they were treated with alkali such as $NaOH$. His study showed that treatment with $NaOH$ resulted in decreased activation energies. Figure 3.5 shows that, for Claus reaction catalysts, the increase in the activation energy is associated with an increase in A_f.

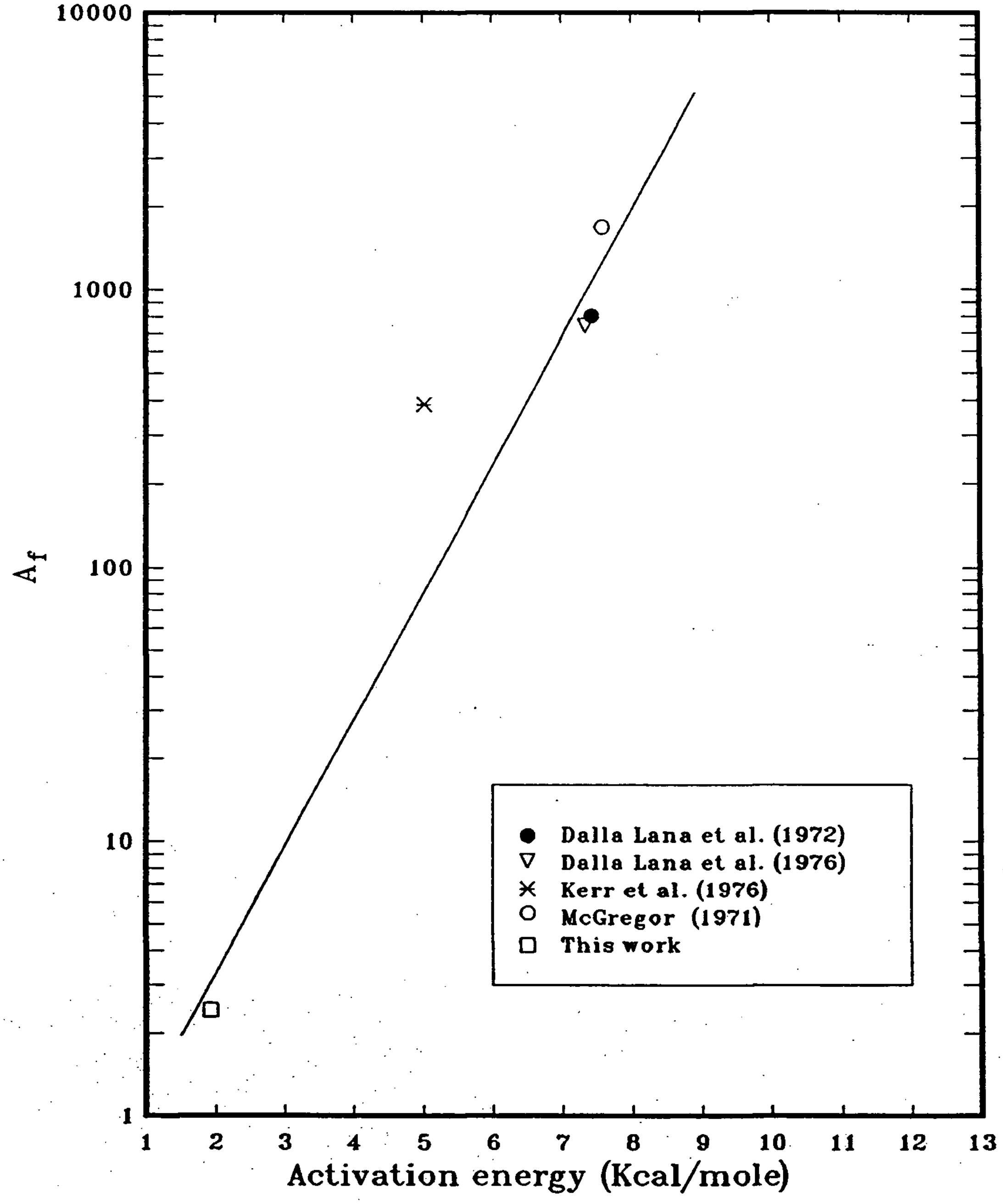

Figure 3.5: Relationship between A_f and E

3.5 MODELS FOR CATALYST FOULING

Several expressions have been suggested for catalyst deactivation (Froment and Bischoff, 1979). Most of these expressions were based on observations of coke deposition on oil cracking catalysts. They contained fitting parameters and need a theoretical justification. A simplified analysis for developing an expression for the deactivation of Claus catalyst is presented in the following paragraphs.

An expression for the deactivation function, Ψ, can be written in terms of the fraction of the sites, ϕ, fouled by sulphur deposits. Such expression may take the form:

$$\Psi = 1 - \phi \tag{3.67}$$

The dependency of ϕ on catalyst sulphur content can be found by considering the deposition of sulphur on the vacant sites, s, to form a mono-sulphur layer:

$$S + s \xrightarrow{k_0} S.s \downarrow$$

Sulphur may also deposit onto fouled sites to form M multilayers i.e:

$$\begin{aligned} S + S.s &\xrightarrow{k_1} 2S.s \downarrow \\ S + 2S.s &\xrightarrow{k_2} 3S.s \downarrow \\ \cdots \quad &\cdots \quad \cdots \\ S + (m-1)S.s &\xrightarrow{k_m} mS.s \downarrow \\ S + mS.s &\xrightarrow{k_{m+1}} (m+1)S.s \downarrow \end{aligned}$$

The net rate of deposition may, in general, be written as:

$$R_{(m-1)S.s} = \frac{dC_{(m-1)S.s}}{dt} = k_{m-1}C_{(m-2)S.s} - k_m C_{(m-1)S.s} \tag{3.68}$$

$$R_{mS.s} = \frac{dC_{mS.s}}{dt} = k_m C_{(m-1)S.s} - k_{m+1} C_{mS.s} \tag{3.69}$$

where $C_{mS.s}$ denotes the surface concentration of sites fouled by m layers of sulphur.

Dividing equation 3.69 by equation 3.68, yields:

$$\frac{dC_{(m-1)S.s}}{dC_{mS.s}} = \frac{k_{m-1}C_{(m-2)S.s} - k_m C_{(m-1)S.s}}{k_m C_{(m-1)S.s} - k_{m+1}C_{mS.s}} \tag{3.70}$$

This expression can be simplified by assuming that all rate constants are equal, i.e:

$$k_0 = k_1 = \cdots = k_m, \tag{3.71}$$

and equation 3.70 reduces to:

$$\frac{dC_{(m-1)S.s}}{dC_{mS.s}} = \frac{C_{(m-2)S.s} - C_{(m-1)S.s}}{C_{(m-1)S.s} - C_{mS.s}} \tag{3.72}$$

Solution of equation 3.72 may be obtained by introducing a distribution ratio, r:

$$r = \frac{C_{mS.s}}{C_{(m-1)S.s}} \tag{3.73}$$

The distribution ratio relates the surface concentration of the (m-1) layer of sulphur to that of the m layer. The ratio may be regarded as constant over short time intervals. The surface concentration of a mono-layer (i.e. when $m = 1$) is:

$$C_{S.s} = C_v r \tag{3.74}$$

and that of the m-layer:

$$C_{mS.s} = C_v r^m \tag{3.75}$$

where C_v denotes the concentration of vacant sites.

A balance on the total sites leads to:

$$C_t \phi = \sum_{m=1}^{M} C_{mS.s} \tag{3.76}$$

$$C_t(1-\phi) = C_v + [C_{H_2S.s} + C_{SO_2.s} + C_{H_2O.s}] \tag{3.77}$$

where C_t denotes the concentration of total sites and the terms between the square brackets counts for the sites occupied with H_2S, SO_2 and H_2O, respectively. Substituting equations 3.74 and 3.73 into equation 3.76, gives:

$$\begin{aligned}\frac{C_t}{C_v} &= \frac{r}{\phi}\left[1+\sum_{m=2}^{M} r^{m-1}\right] \\ &= \frac{r}{\phi}\left(\frac{1-r^M}{1-r}\right).\end{aligned} \tag{3.78}$$

The sites occupied by H_2S, SO_2 and H_2O are a small fraction of the total sites and may be neglected compared with those occupied by sulphur and those which are still vacant. Equation 3.77 therefore becomes:

$$\frac{C_t}{C_v} \cong \frac{1}{1-\phi}. \tag{3.79}$$

Combining equations 3.78 and 3.79 gives:

$$\frac{\phi}{1-\phi} = r\left(\frac{1-r^M}{1-r}\right). \tag{3.80}$$

Alternatively, the distribution ratio may be expressed in terms of sulphur content. Let λ_0 denote the weight of sulphur per site per unit weight of catalyst due to monolayer deposition. The catalyst sulphur content, denoted by λ, can readily be obtained:

$$\lambda = \lambda_0 \sum_{m=1}^{M} mC_{mS.s} \tag{3.81}$$

Substituting equations 3.74 and 3.75 into equation 3.81 yields:

$$\begin{aligned}\lambda &= (\lambda_0 C_v)\sum_{m=1}^{M} mr^m \\ &= (\lambda_0 C_v) r\left[\frac{(1-r^M) - Mr^M(1-r)}{(1-r)^2}\right].\end{aligned} \tag{3.82}$$

Eliminating C_v by substituting equation 3.78 into equation 3.82 leads to:

$$\frac{\lambda}{\lambda_0 C_t} = \phi\left[\frac{1}{1-r} - \frac{Mr^M}{1-r^M}\right]. \tag{3.83}$$

Equations 3.80 and 3.83 can be used to eliminate r and to express ϕ in terms of λ. For the case when $M = 1$, equation 3.80 reduces to:

$$\frac{\phi}{1+\phi} = r \tag{3.84}$$

and equation 3.83 becomes:

$$\frac{\lambda}{\lambda_0 C_t} = \phi. \tag{3.85}$$

Substituting equation 3.84 into equation 3.67 gives:

$$\Psi = 1 - K_s\lambda \tag{3.86}$$

where $K_s = 1/\lambda_0 C_t$.

For the case when $M \longrightarrow \infty$, equations 3.80 and 3.83 become:

$$\phi = \begin{cases} 1 & \text{for} \quad r \geq 1 \\ r & \text{for} \quad r < 1 \end{cases} \tag{3.87}$$

and

$$\frac{\lambda}{\lambda_0 C_t} = \begin{cases} \infty & \text{for} \quad r \geq 1 \\ \frac{\phi}{1-r} & \text{for} \quad r < 1 \end{cases} \tag{3.88}$$

Since the maximum value of ϕ equals 1 and since λ is finite, it follows that the distribution ratio, r, must be less than 1. Equations 3.87 and 3.88 may be combined to eliminate r and to express the fraction of fouled sites, ϕ, in terms of the catalyst sulphur content, λ. Hence for $M \longrightarrow \infty$, equation 3.87 becomes (since $r < 1$):

$$r = \phi \tag{3.89}$$

and equation 3.88 gives:

$$\frac{\lambda}{\lambda_0 C_t} = \frac{\phi}{1-r}. \tag{3.90}$$

Substituting equation 3.89 into equation 3.90 and rearranging yields:

$$1 - \phi = \frac{1}{1 + K_s\lambda}. \tag{3.91}$$

Using equations 3.91 and 3.67, the deactivation function takes the form:

$$\Psi = \frac{1}{1 + K_s\lambda} \tag{3.92}$$

Froment and Bischoff (1979) suggested, without theoretical proof, expressions similar to equations 3.86 and 3.92. The mono-layer model (i.e equation 3.86) was also suggested by Masamune and Smith (1966). The multi-layer model was used in this work to predict the performance of a fluidized bed Claus reactor operating under sulphur condensing conditions (see Section 6.2).

3.6 THERMODYNAMIC CONVERSION

Prediction of the Claus equilibrium conversion can be quite complicated due to the number of species that might be present and consequently the number of chemical reactions that take place. However, simplification results when exploring conditions of a specific mixture. Under the conditions used in this study (see Table 5.1), it is reasonable to assume that elemental sulphur is predominantly present as S_8. The formed sulphur condenses and its mole fraction in the gas phase is negligible. For instance the sulphur vapour pressure at 423 K is 0.026 kPa (Meisen and Bennett, 1979). For a feed mixture containing SO_2, H_2S and N_2, material balances are formulated and presented in Table 3.6 for the reaction:

$$2H_2S + SO_2 \rightleftharpoons \frac{3}{8}S_8 \downarrow +2H_2O \tag{3.93}$$

Table 3.6: Analysis of equilibrium Claus reaction

Component	Molar flow rate into reactor	Equilibrium molar rate of gaseous component	Equilibrium mole fraction
SO_2	f_1	$f_1 - \nu$	$(f_1 - \nu)/(f - \nu)$
H_2S	$2f_1$	$2(f_1 - \nu)$	$2(f_1 - \nu)/(f - \nu)$
N_2	f_2	f_2	$f_2/(f - \nu)$
H_2O	0	2ν	$2\nu/(f - \nu)$
total	$f = 3f_1 + f_2$	$f - \nu$	1.0

The equilibrium constant for the above reaction may be related to the partial pressures of the gaseous components by:

$$K_e = \frac{P^2_{H_2O}}{P^2_{H_2S} P_{SO_2}} \tag{3.94}$$

It is also given by the change in free energy of the reacting system i.e:

$$\ln K_e = \frac{1}{RT}(2\Delta G_{H_2O} + \frac{3}{8}\Delta G_{S_8} - 2\Delta G_{H_2S} - \Delta G_{SO_2}) \tag{3.95}$$

The partial pressures of the gaseous components may be calculated from Table 3.6, thus:

$$P_{H_2O} = (\frac{2\nu}{f-\nu})P \tag{3.96}$$

$$P_{SO_2} = (\frac{f_1-\nu}{f-\nu})P \tag{3.97}$$

$$P_{H_2S} = 2P_{SO_2} \tag{3.98}$$

where ν denotes the extent of reaction under equilibrium condition, f_1 and f denote the molar flow rate of SO_2 and the total molar flow rate into the reaction system, respectively. It is easy to show that:

$$\nu = \frac{f_1 P - f P_{SO_2}}{P - P_{SO_2}} \tag{3.99}$$

and

$$P_{H_2O} = 2(\frac{f_1 P - f P_{SO_2}}{f - f_1}) \tag{3.100}$$

Substituting for P_{H_2S} from equation 3.98 and for P_{H_2O} from equation 3.100 into equation 3.94 and rearranging yields:

$$K_e P^3_{SO_2} - (\frac{f_1 P - f P_{SO_2}}{2f_1 + f_2})^2 = 0 \tag{3.101}$$

where f_2 denotes the molar flow rate of N_2.

The above equation was solved numerically for P_{SO_2} (see Appendix F). The equilibrium conversion may be calculated from the relation:

$$\begin{aligned} \chi &= 1 - \frac{\text{partial pressure of } SO_2 \text{ at equilibrium}}{\text{partial pressure of } SO_2 \text{ in feed}} \\ &= 1 - \frac{P_{SO_2}}{(f_1/f)P} \end{aligned} \tag{3.102}$$

Selected values of equilibrium conversion are presented in Table 3.7 and are shown in Figure 6.3.

Table 3.7: Equilibrium conversion (%)

Temperature (K)	SO_2 concentration in feed	
	300 ppm	650 ppm
373	98.49	98.81
378	98.24	98.19
383	97.97	98.42
388	97.66	98.19
393	97.31	97.92
398	96.94	97.62
403	96.52	97.26
408	96.06	96.93
413	95.54	96.53
418	94.99	96.09
423	94.37	95.61

Chapter 4

EXPERIMENTAL APPARATUS AND MATERIALS

4.1 REACTION EQUIPMENT

The experimental apparatus used in this work (shown schematically in Figure 4.1) was basically designed by Bonsu (1981). It consisted of a fluidized bed reactor and supporting facilities for nitrogen regeneration, gas analysis and operational safety.

4.1.1 Fluidized Bed Reactor

The reactor was a stainless steel tube (0.86m high x 0.1m ID) with a freeboard section (0.3m high x 0.2m ID). The gas distributor was made from a wire mesh laminate (Dynapore, Type 401420, made by Michigan Dynamics Inc., Garden City, Mich.). A similar mesh was installed at the top of the reactor to prevent catalyst elutriation (see Figure 4.2). External heating of the reactor was accomplished with shielded nichrome wires (type D/R19S2, made by Pyrotennax Inc., Trenton, Ont.). The total power supplied by the heater was 2 kW. Cooling was provided by passing water in a coil wound outside of the reactor. Insulation consisted of a 0.025m thick thermal blanket (made by Carborundum Inc., Niagara Falls, NY). The temperature inside the reactor was monitored by four Iron-Constantan thermocouples located 0.05m below and 0.075, 0.56, and 1.1m above the distributor. The desired temperature was maintained within $\pm 3°C$ by the use of two proportional controllers (model 49 made by Omega Engineering Inc., Stamford, Conn.) connected to the second and fourth thermocouples.

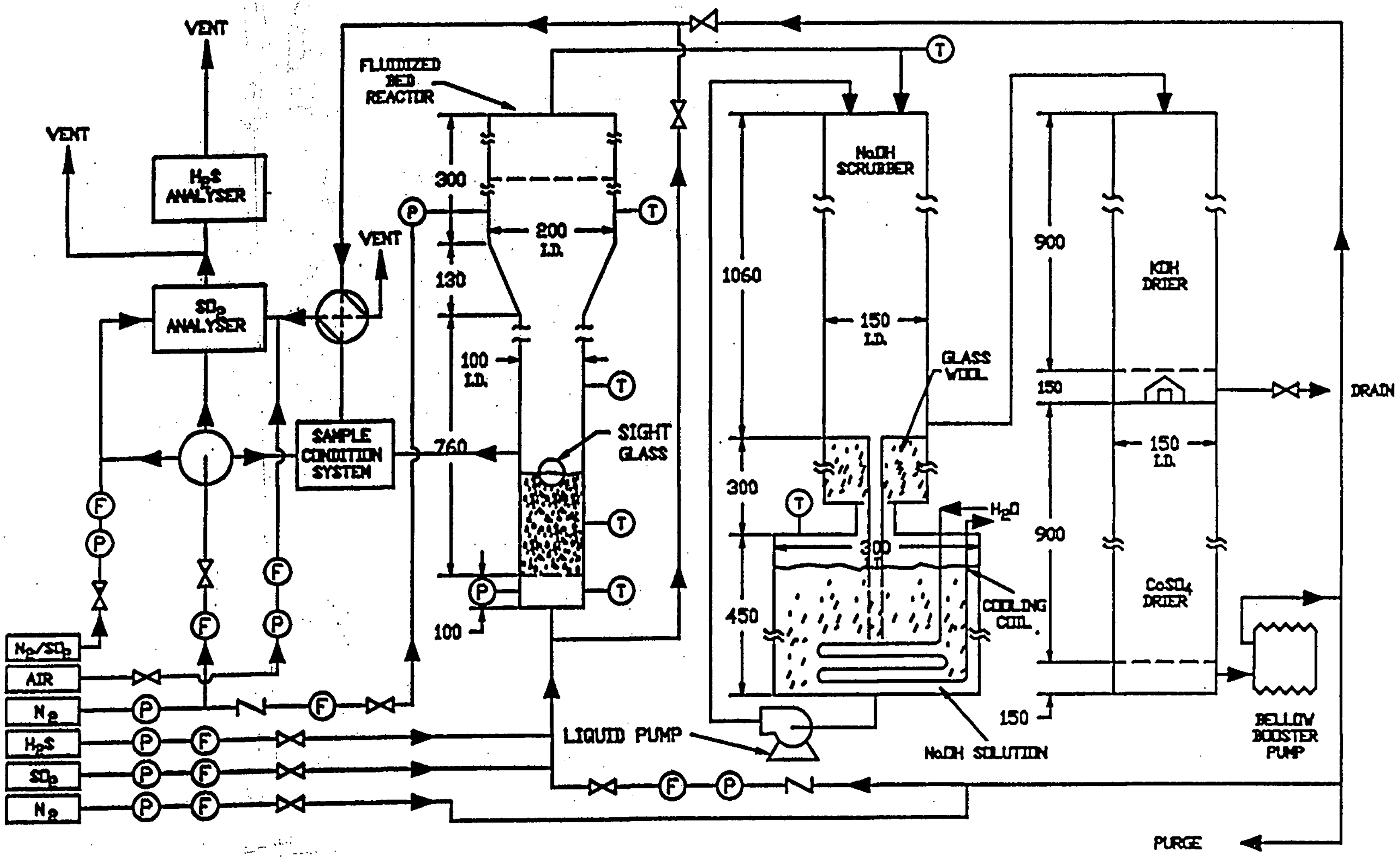

Figure 4.1: Flow diagram of the equipment (All dimensions in mm) from Bonsu (1981)

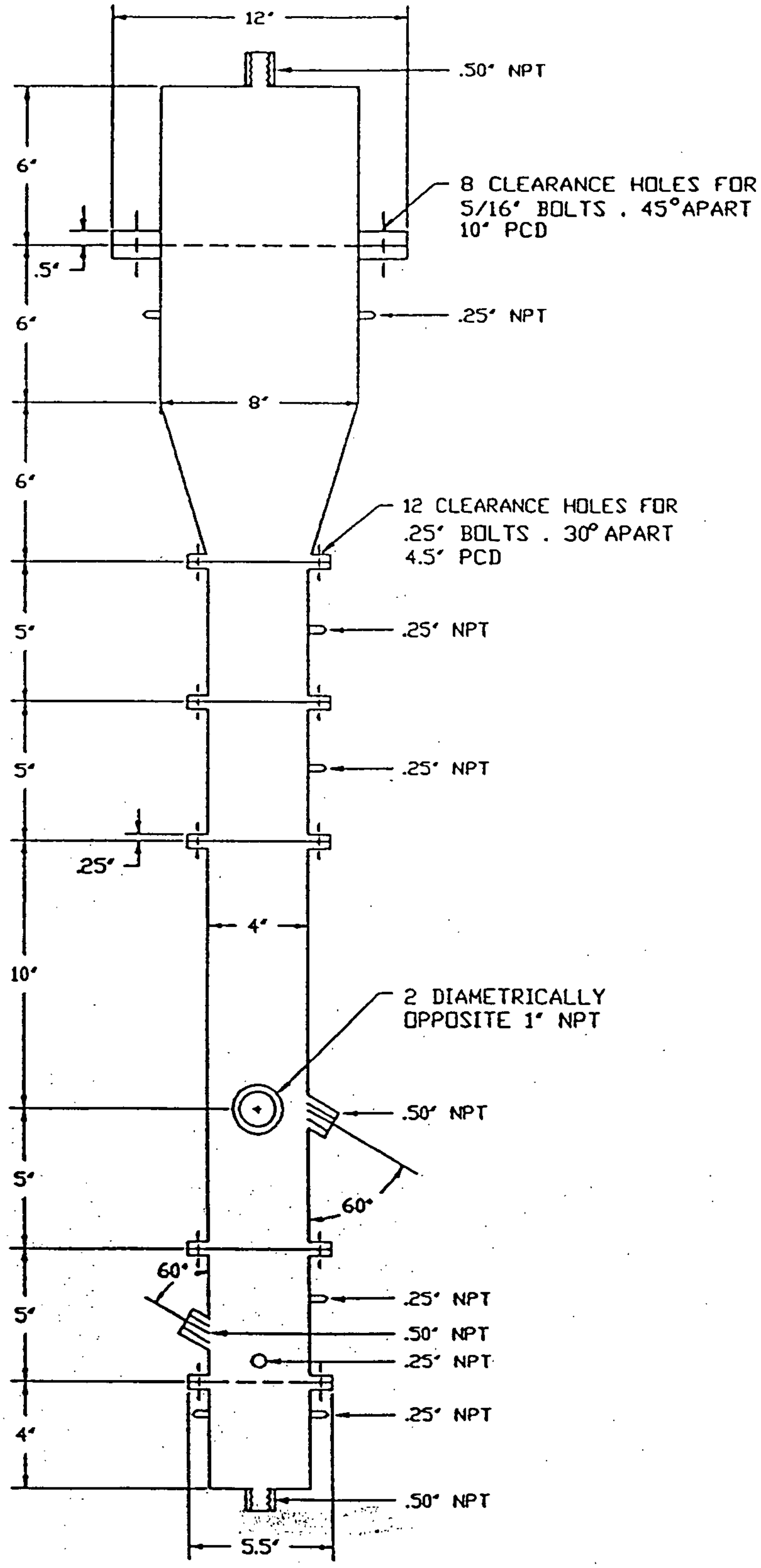

Figure 4.2: Fluidized bed reactor

Two mercury-in-glass manometers were installed just below the gas distributor and in the freeboard section to monitor the pressure inside the reactor. The reactor was equipped with a spring loaded relief valve to avoid excessive pressure build-up. This valve, which was connected to the ventilation system, was designed to open slightly at 7.5 psig and open fully at 10 psig. Rotameters were used to measure the flow rates of pure N_2 as well as mixtures of H_2S and SO_2 in N_2 to the reactor.

The nitrogen and sulphur dioxide feed streams were preheated electrically upstream of the reactor with nichrome wires which were heavily insulated with fiberglass. To avoid sulphur condensation, the line between the reactor and scrubber was similarly heated. The power supplied by the preheater and the exhaust heater was 1.2 and 0.4 kW, respectively. The temperature of these lines were measured by two Iron-Constantan thermocouples and regulated by two proportional temperature controllers.

The quality of fluidization was observed through two identical sight glasses located 0.34m above the distributor. The sight glasses were installed diametrically opposite each other with one behind and the other in front of the reactor. The one-inch NPT ports for accepting the sight glasses were inclined at 60° to the reactor axis. Illumination was provided by a 60 w light bulb mounted on the top of the sight glass located behind the reactor.

4.1.2 Nitrogen Regeneration System

Reactor effluent gas consisted mostly of nitrogen and traces of H_2S, SO_2 and H_2O. It also contained sulphur vapour during catalyst regeneration. It was therefore essential to remove extraneous components before recycling the nitrogen.

The cleaning was accomplished by passing the reactor outlet gas through an aqueous $NaOH$ scrubber as well as glass columns packed with KOH and $CaSO_4$ pellets.

The $NaOH$ scrubber (see Figures 4.1 and 4.3) consisted of a QVF column packed with 1/4″ ceramic Berl Saddles. A solution containing 50wt% $NaOH$ was pumped (at 2 L/min) continuously and concurrently with the reactor gas through the scrubber. the gas was then bubbled through the $NaOH$ solution in the reservoir with a sparger to ensure almost complete removal of H_2S and SO_2. The temperature of the $NaOH$ solution was maintained at about 15°C by passing water through a cooling coil located in the reservoir. A glass wool filter was placed at the bottom of the reservoir to prevent entrainment of spray and mist.

Two glass columns filled with KOH and $CaSO_4$ pellets were used to remove moisture from the gas. Each drier had a stainless steel bottom section. The pellets were supported by a wire mesh installed between the bottom section and the glass column (see Figures 4.1 and 4.4).

The KOH also acted as an absorption medium for water and any residual traces of H_2S and SO_2. The $CaSO_4$, on the other hand, removed moisture with very high efficiency.

Potassium hydroxide is deliquescent; therefore, a saturated solution was formed after absorbing the moisture. This solution was collected in the stainless steel section and was discharged through a drainage valve at the bottom of the drier.

A bellows pump (model MB-302, manufactured by Metal Bellows Corp., Sharon, Mass.) was installed upstream of the reactor. It had a maximum capacity of 85 L/min at 1 atm. A regulating valve and a rotameter were used to control and measure the flow rate of the recycled nitrogen, respectively.

When a sample of the regenerated nitrogen was tested, the H_2S and SO_2 concentrations were below detectable limits of 2 and 1 ppm, respectively. Therefore, the regeneration system was more than 99.99% efficient.

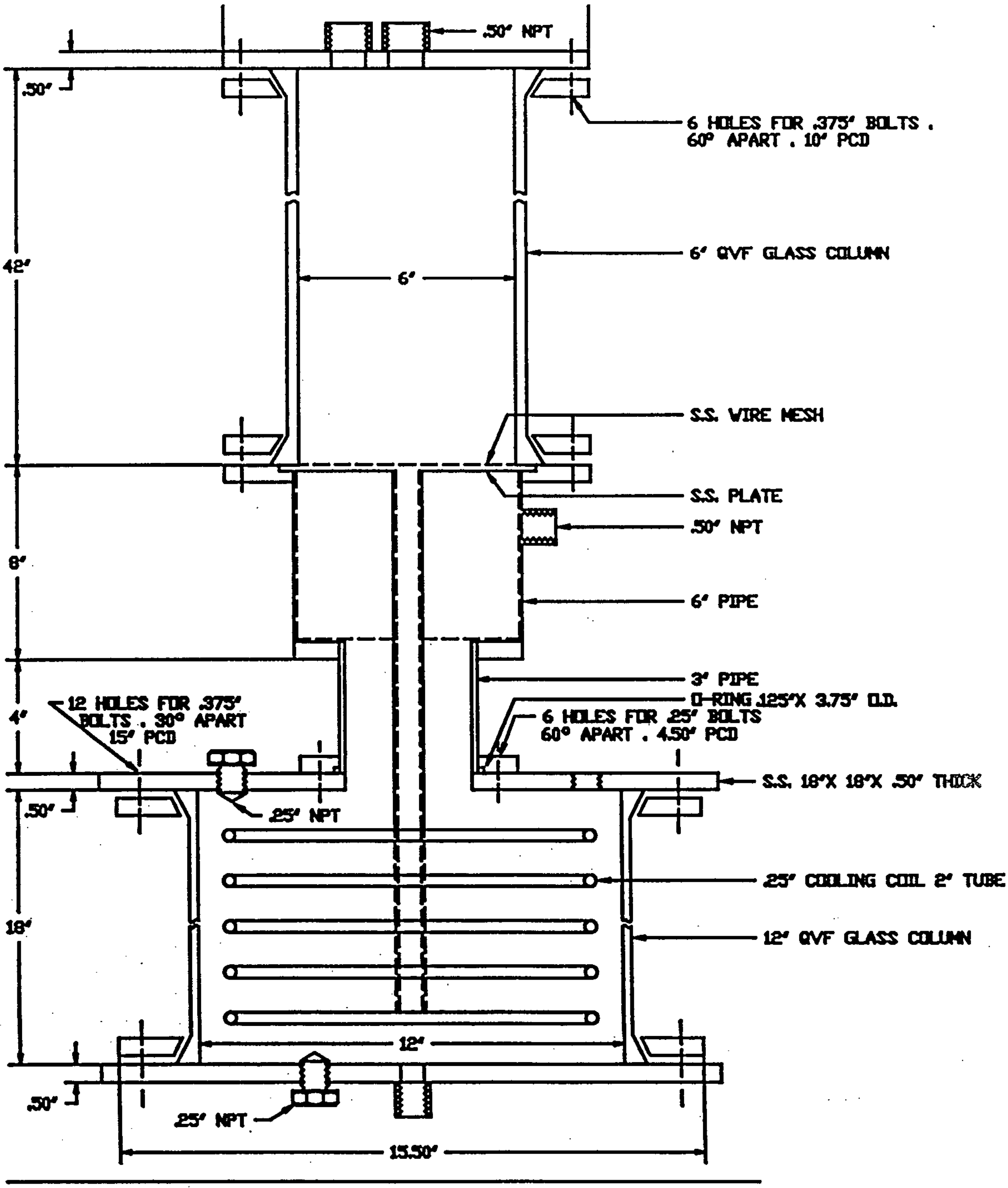

Figure 4.3: $NaOH$ Scrubber and reservoir

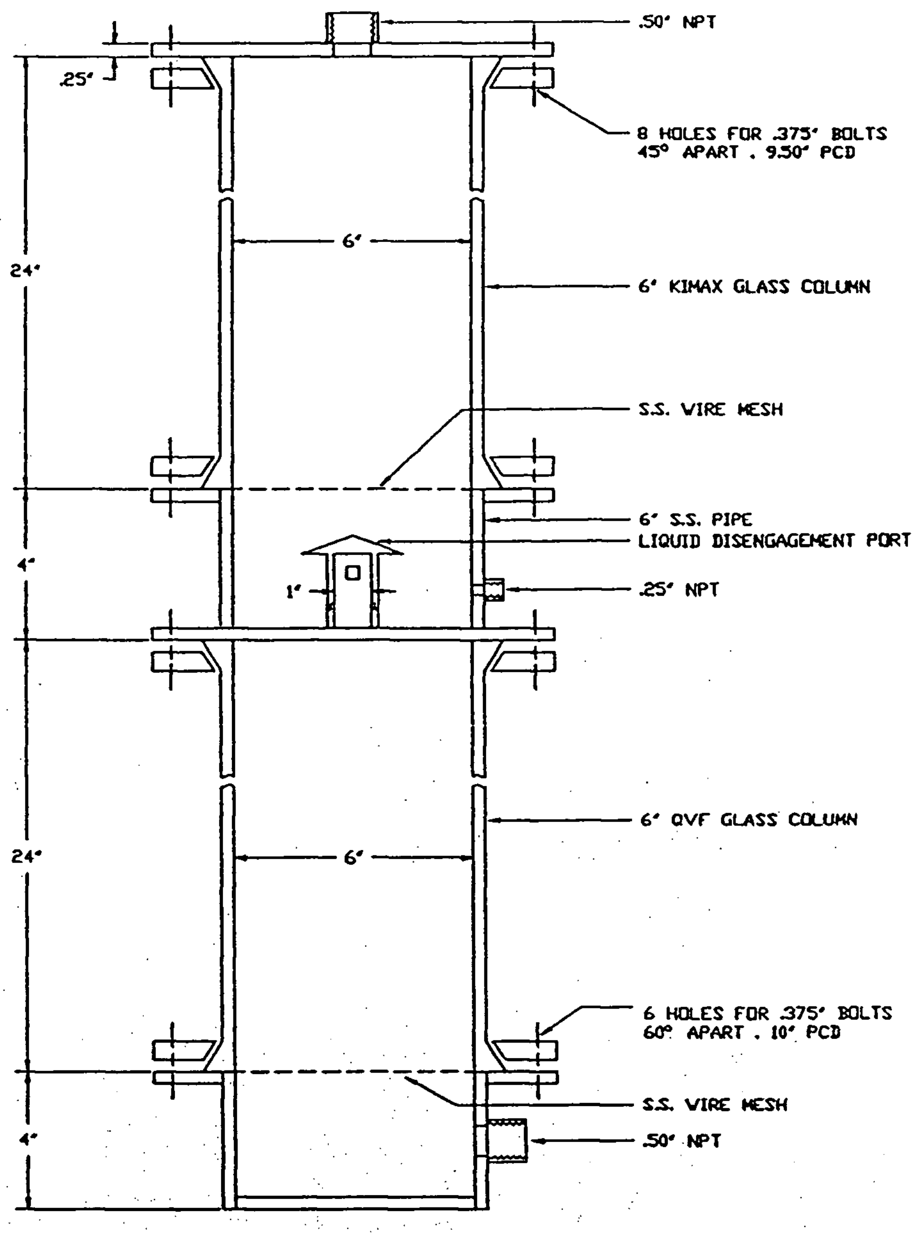

Figure 4.4: Driers

4.1.3 Gas Analysis System

To ensure proper operation of the H_2S and SO_2 analysers, gas samples had to be conditioned prior to analysis. Separation of sulphur particulates was accomplished in a sulphur condenser which contained $CaCl_2$ and glass wool. To obtain dry samples, two driers containing $CaCl_2$ and glass wool were installed downstream of the sulphur condenser. The first drier was equipped with a water cooling coil. Further conditioning was accomplished by a fine filter which removed particulates larger than 0.3 μm in diameter.

A diaphragm pump (Air Codet, model 7530-40, supplied by Cole-Parmer Instrument Co., Chicago, Ill.) which had a maximum capacity of 14.75 L/min at 1 atm, was used as the sampling pump. A sample (flow rate of 4.8 L/min) was introduced to two on-line gas analysers. The latter instruments were a Pulsed Fluorescence SO_2 Analyser (model 40, made by Thermo Electron Corp., Hopkinton, Mass.) and a Photoionization H_2S analyser (model PI 201, made by HNU Systems Inc., Newton, Mass.). These gas analysers were calibrated as described in section 5.2.2. Signals from these instruments and the thermocouples were fed into an analog digital convertor (model ADC-1, supplied by Remote Measurement Systems Inc., Seattle, Wa.) which was capable of scanning 16 channels and contained a built-in temperature compensator in the reference junction. A Commodore computer (model C64, supplied by Commodore Business Machines, Inc., West Chester, Pa.) was used to record and/or display the data on a monitor (A BASIC programme for data logging is included in Appendix D).

4.1.4 Safety Devices

Being aware of the extreme toxicity of H_2S and SO_2 (see Tables 1.1 and 1.2), strict precautions were exercised to ensure the safe operation of the equipment. All joints and fittings were tested by applying soap solution to make sure that they were leak-proof.

To ensure the safe operation of the equipment further, an enclosure was built around the entire equipment including the gas cylinders. A fan capable of creating a small vacuum (approximately 30 mm H_2O) was also provided. The exhaust from this fan was connected to the building ventilation system. A pressure switch was installed on the control panel. In case of vacuum loss due to fan failure or other reasons, the pressure switch shuts-down the entire equipment including the solenoid valves on the H_2S/N_2 and SO_2/N_2 cylinders. A complete equipment shut-down was accomplished by switching off the main power supply to the equipment (see Figure 4.5). The H_2S concentration in the suction line between the fan and the enclosure was frequently checked with the H_2S analyser. When the concentration exceeded approximately 10 ppm, an alarm, which is a built-in feature of the H_2S analyser, would sound. A gas mask with H_2S absorbing canister (model 457069, made by Mine Safety Appliances Co. of Canada Ltd., Downsview, Ont.) was provided in case the operator had to work in an atmosphere containing high levels of H_2S. The allowable H_2S limit for 8-hour exposure is 10 ppm (Archibald, 1977).

4.2 MATERIALS USED

The catalyst used in this study was activated alumina designated commercially as Kaiser S-501. It was supplied by Kaiser Aluminum and Chemical Corporation, Baton Rouge, Louisiana. The catalyst contains mostly aluminum oxide promoted with some lithium oxide (see Table 4.2). It is available as small spheres with a size range -3 +6 mesh. To use the S-501 in the fluidized bed, it was ground and sieved to -42 +150 mesh. The mean particle diameter for the particle size distribution shown in Table 4.3 was calculated from the relation recommended by Kunii and Levenspiel (1969):

$$d_p = 1/\sum_i (w_i/d_{p_i}) \tag{4.1}$$

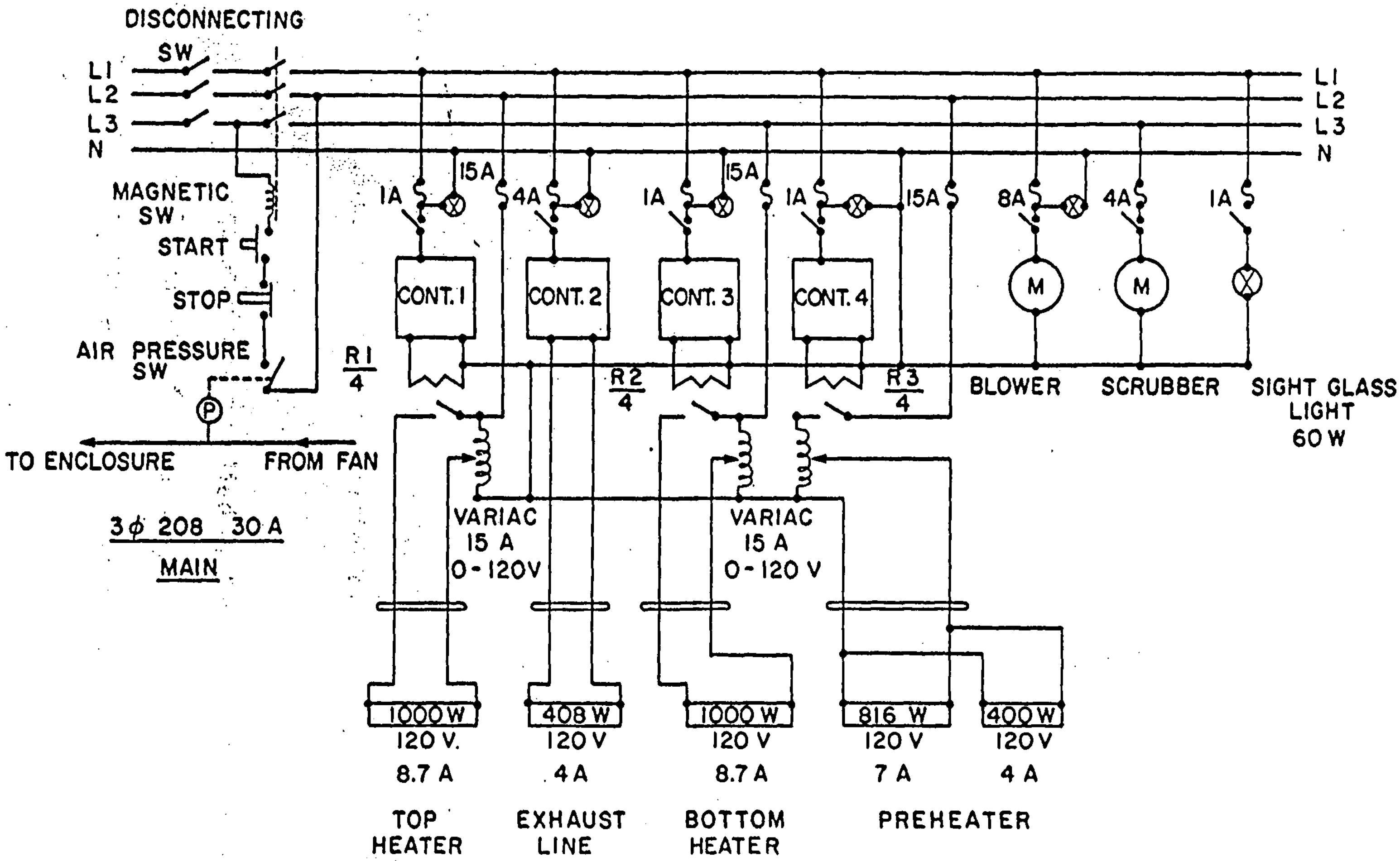

Figure 4.5: Electric circuit of the equipment

where w_i denotes the weight fraction of material in size interval i and d_{p_i} denotes the arithmetic mean diameter in interval i.

The gases used were mixtures of 10% H_2S in 90% N_2 and 5% SO_2 in 95% N_2 by volume. These mixtures were supplied by Canadian Liquid Air Ltd., Vancouver, B.C. The gases were diluted to the desired concentration with pure N_2.

Table 4.1: Physical properties of Kaiser S-501 catalyst.

Average particle diameter (d_p)	195 μm
Particle density (ρ_p)	1843 kg/m^3
Particle bulk density	795 kg/m^3
True density (Bonsu, 1981)	3160 kg/m^3

Table 4.2: Chemical properties of S-501 catalyst on a dry basis.

Al_2O_3 and inorganic promoters	93.5
Loss on ignition	6.0
Na_2O	0.45
Fe_2O_3	0.02
SiO_2	0.02

Table 4.3: Particle size distribution of catalyst used in this study.

Diameter range (μm)	d_{p_i} (μm)	Weight fraction w_i
125 - 149	137	0.094
149 - 177	163	0.354
177 - 210	194	0.156
210 - 250	230	0.115
250 - 295	273	0.187
295 - 354	325	0.094

Chapter 5

EXPERIMENTAL PROCEDURE

5.1 REACTION PROCEDURE

The Claus reaction was carried out in the fluidized bed and the supporting equipment described in section 4.1. Because H_2S and SO_2 are toxic compounds and due to the fact that O_2 may cause catalyst sulphation, it was necessary to avoid any possible leaks. This requirement was accomplished by ensuring that all joints were leakproofed. It was also essential to remove all oxygen from the system prior to each run to avoid catalyst deactivation. Catalyst fouling was a consequence of sulphur deposition on the catalyst within the temperature range shown in Table 5.1; hence it was important to regenerate the catalyst to keep its activity at high levels. To ensure proper operation and achieve accurate and meaningful results, the following procedures similar to those described by Bonsu (1981) were adopted for this work.

5.1.1 Equipment Start-up

To meet safety standards and to ensure the smooth operation of the equipment, the following steps were followed:

1. Remove the fluorocarbon panel in the front of the reactor.

2. Dismount the freeboard section.

3. Introduce the required weight of catalyst to give the desired static bed height.

4. Check the gasket and remount the freeboard section.

5. Test for leaks by pressurizing the reactor and associated equipment with nitrogen from the N_2 cylinder. The pressure in the reactor was maintained at about 10 psig for about 12 hours. Should a drop in pressure occur, leaks where located by applying soap solution to the flanges and joints.

6. Replace the fluorocarbon panel and seal all the edges of the enclosure with 100 mm wide, duct tape.

7. Create a vacuum of about 200 mm Hg by switching on the sampling pump. Maintain the pressure in the reactor at about 560 mm Hg absolute for about 30 min.

8. Introduce nitrogen into the system until the pressure in the reactor returns to atmospheric levels.

9. Switch on the bellows booster pump to fluidize the bed.

10. Purge about 10% of the total gas flow rate through the reactor for about 24 hours with the sampling pump to ensure that virtually all oxygen is removed from the system (see Appendix E).

11. Switch on the caustic solution circulation pump, gas analysers, C64 Commodore computer and heaters for the sight glass, preheaters, reactor, and reactor-scrubber line.

12. Circulate cold water through the cooling coils in the caustic reservoir.

13. Monitor all thermocouples by watching the displayed readings on the TV screen until the desired steady state temperatures are reached (this procedure usually requires about 1 hour).

14. Eliminate the last traces of oxygen and regenerate the catalyst by admitting a small stream of H_2S (20 mL/min) into the reactor for about 30 min.

5.1.2 Reaction Process

Since it had been decided to perform all experiments at atmospheric pressure, two flow rates were adjusted to achieve a reactor pressure of 1 atm at the desired superficial gas velocity.

To ensure proper performance of the gas analysers, their electronic zeros were always checked according to the instruction manuals. Using a sample of known composition from the feed to the reactor, the calibration curves for the analysers were also validated at the beginning of each run. If significant differences were detected, a new calibration curve was generated as described in section 5.2.2. The SO_2 analyser performed exceptionally well. The performance of the H_2S analyser was excellent provided that the optical windows of this analyser were cleaned with acetone every 8 working hours.

It was important to maintain the H_2S and SO_2 concentrations in the feed at a ratio of 2/1. This ratio had been proved to give maximum sulphur conversions (Bennett and Meisen, 1973). To achieve this ratio, the following procedure was adopted:

1. Choose the flow rate of N_2 to give the desired superficial velocity (see Appendix C).

2. Select the desired concentrations of H_2S and SO_2 and calculate the corresponding flow rates of H_2S and SO_2 according to the equations:

$$Q_{H_2S} + Q_{SO_2} + Q_{N_2} = Y_{H_2S} Q_{H_2S} \times 10^6 / P_{(H_2S)f} \tag{5.1}$$

$$Y_{H_2S} Q_{H_2S} / Y_{SO_2} Q_{SO_2} = 2 \tag{5.2}$$

$$P_{(SO_2)f} = 0.5 P_{(H_2S)f} \tag{5.3}$$

where Y_{H_2S} and Y_{SO_2} denote the volume fractions of H_2S and SO_2 in the cylinders containing a mixture of H_2S/N_2 and SO_2/N_2, respectively.

Q_{H_2S}, Q_{SO_2} and Q_{N_2} denote the flow rates to the reactor of mixtures of H_2S in N_2, SO_2 N_2 and pure N_2, respectively.

$P_{(H_2S)f}$ denotes the selected H_2S feed concentration in parts per million and $P_{(SO_2)f}$ denotes the concentration of SO_2 in the feed.

3. Turn on the switch to open the solenoid valves on the H_2S/N_2 and SO_2/N_2 cylinders.

4. Open the H_2S/N_2 and SO_2/N_2 cylinders and set the line pressures to 15 psig using the valves on the regulators.

5. Adjust the flow rates (calculated in step 2) using the rotameters located upstream of the reactor.

6. Withdraw a sample of the feed gas to the reactor and use it to check the calibration curves of the gas analysers.

7. Monitor the concentrations of H_2S and SO_2 in the feed sample as they are being displayed on the TV screen and compare with the desired ones. If the differences are within ± 10 ppm, set the H_2S and SO_2 flow rates precisely. If the difference exceeds ± 10 ppm, validate the calibration curves.

8. Record the feed concentrations and the thermocouple readings for about 10 min using the Commodore computer.

9. Analyze a sample from the reactor outlet and monitor the readings on the TV screen.

10. Check the the concentrations of SO_2 and H_2S in the recycled nitrogen stream.

11. When steady state readings are established, record the H_2S and SO_2 reactor outlet concentrations and the temperatures for about 10 min.

12. Record the flow rates of the H_2S/N_2, SO_2/N_2 and N_2 streams.

5.1.3 Catalyst Regeneration

When sulphur condenses on the catalyst, several types of deactivation may arise (Pearson, 1973). Among these mechanisms are the accumulation of sulphur in the pores of the catalyst and also the formation of sulphates. To keep the catalyst activity at high levels, it was essential to vapourize the sulphur. Although it is unlikely that sulphation took place under the temperature conditions shown in Table 5.1, appropriate catalyst regeneration eliminates sulphates. Pearson (1977) and Grancher (1978) recommended a regeneration temperature of $300°C$ in the presence of H_2S to restore catalyst activity. Their technique was used in this work:

1. At the end of step 12 of section 5.1.2 and before equipment shut-down, close the SO_2/N_2 gas cylinder.

2. Switch off the solenoid valves on the SO_2/N_2 cylinder.

3. Close the regulating valves located downstream of the H_2S and SO_2 rotameters.

4. Switch off the caustic pump.

5. Set the temperature controllers to 300°C.

6. Circulate only nitrogen through the reactor for about 4 hours.

7. Admit a small rate of H_2S (20 mL/min) into the nitrogen stream entering the reactor.

8. Allow the equipment to run under this condition for about 4 hours to regenerate the catalyst. The catalyst sulphur content was tested by heating a sample of the regenerated catalyst at $400°C$ for 24 hours; the results indicated that no traces of sulphur were present

5.1.4 Equipment Shut-down

The main problem likely to occur during equipment shut-down is the sudden loss of pressure in the reactor when the booster pump is switched off. The loss in pressure might cause air to leak into the the reactor and, if there are any sulphur compounds present, sulphation of the catalyst could occur. To avoid this problem, the following procedure was adopted:

1. Close the H_2S/N_2 cylinder.
2. Switch off the solenoid valve on the H_2S/N_2 cylinder.
3. Close the regulating valve located down-stream of the H_2S rotameter.
4. Switch off the heaters
5. Turn off the cold water for the cooling coils in the caustic reservoir.
6. Turn on the cold water for the cooling coils around the reactor.
7. Circulate only nitrogen until the reactor temperature drops to about $80°C$.
8. Increase the N_2 flow rate into the reactor to raise its pressure to about 7 psig.
9. Switch off the booster pump
10. Close the N_2 cylinder.

11. In preparation for the next series of runs, clean the sampling system and refill the condenser and driers with $CaCl_2$ and glass wool. Also, inspect the filter cartridge in the sampler and replace it if severely contaminated. Discharge the deliquescent solution formed at the bottom of the KOH drier and check if there is any sulphur condensed at the exit of the reactor-scrubber line. Finally, clean the optical windows of the H_2S analyser.

5.1.5 Scrubber Clean-up

The scrubber temperature was kept at about 10 - 15°C during all experiments by circulating cold water through the cooling coils inside the $NaOH$ tank. After a few catalyst regeneration cycles, a yellow sulphur layer appeared at the top of the scrubber. The formation of salts such as Na_2S, $NaHS$, Na_2SO_3 and $NaHSO_3$ also took place at the scrubber top. Hence, even though the $NaOH$ solution might not be totally spent, it was necessary to clean the scrubber before blockage occurred.

After several runs, the colour of the aqueous sodium hydroxide solution changed to dark red due to the partial solubility of sulphur in the $NaOH$ solution. During washing of the scrubber with water, the solution became diluted and its colour changed to dark green and then to a light green.

In addition to the substances listed above, there were also iron, aluminum and silicon compounds in the scrubber due to the elutriation of very small quantities of the catalyst from the reactor.

To ensure adequate clean-up of the scrubber the following procedure was adopted:

1. Check to make sure the discharge valve at the bottom of the caustic reservoir is connected, through a pump, to the waste disposal tank.

2. Open the discharge valve and switch on the discharge pump.

3. After emptying the tank, close the discharge valve and fill the reservoir with water.

4. Circulate the water through the scrubber for about 30 min.

5. Repeat steps 2 to 4 about four times.

6. Open the top of the scrubber and remove the packing at the top of the column and clean it with a brush to get rid of the condensed sulphur.

7. Clean the inside walls of the top of the column as well as the covering plate to remove condensed sulphur.

8. Replace the top plate of the scrubber and wash the tower again three times using steps 2 to 4. At this stage the solution is very dilute and can be discharged directly into the drain.

5.2 CALIBRATION OF INSTRUMENTS

5.2.1 Calibration Of Rotameters

Accurate calibration of the rotameters was essential since the flow rates of the various gases influence the analyser calibrations and the estimation of the various hydrodynamic parameters in the reactor. It was recognized that the rotameters had to be calibrated (depending on the range of the flow rates) with several standard flowmeters such as a soap bubble meter, electronic mass meter and wet-test meter. The accuracy and ranges of these standard meters has been described by Nelson (1971) and Cosidine (1974). The soap bubble flow meter was used to measure flow rates ranging from 10 to 1000 mL/min. This flowmeter uses the simple principle of determining the time required for the displacement of a soap bubble between two marks on a tube of a known volume. At low flow rates the soap bubbles move slowly and the time measured with an electronic timer (activated by two photocells) is very accurate.

The electronic mass flowmeter (Model 8160, made by Matheson Co., East Rutherford, N.J.) consisted essentially of an electrically heated tube and an arrangement of thermocouples to measure the differential cooling caused by the passing gas through the tube. This flowmeter was used to measure intermediate flow rates ranging from 500 to 2000 mL/min.

For the measurement of flow rates between 1 L/min and 100 L/min, a wet-test flowmeter (Model TS-63111, supplied by Precision Scientific, Chicago, Ill.) was used.

The flow rates at standard state for a given float position in the rotameter were calculated from the equation recommended by Cosidine (1974):

$$Q_{ss} = \frac{Q_{sm} P_{sm}}{T_{sm}} \sqrt{\frac{T_r T_{ss}}{P_r P_{ss}}} \tag{5.4}$$

where P, T and Q denote the pressure, temperature and volumetric flow rate, respectively. The subscripts r, sm and ss refer to conditions inside the rotameter, standard flowmeter and the standard state, respectively.

For safety reasons, air was used to calibrate the rotameters. The actual flow rates of N_2, H_2S and SO_2 were calculated from the equation recommended by Callahan (1974):

$$Q_i = Q_{ss} / \sqrt{\varrho_i} \tag{5.5}$$

where Q_i denotes the volumetric flow rate of gas i at standard conditions and ϱ_i denotes its specific gravity with respect to air. The computer programme for calculating the flow rates together with calibration tables are presented in Appendix C. Typical rotameter calibration curves are shown in Figures 5.1 to 5.3.

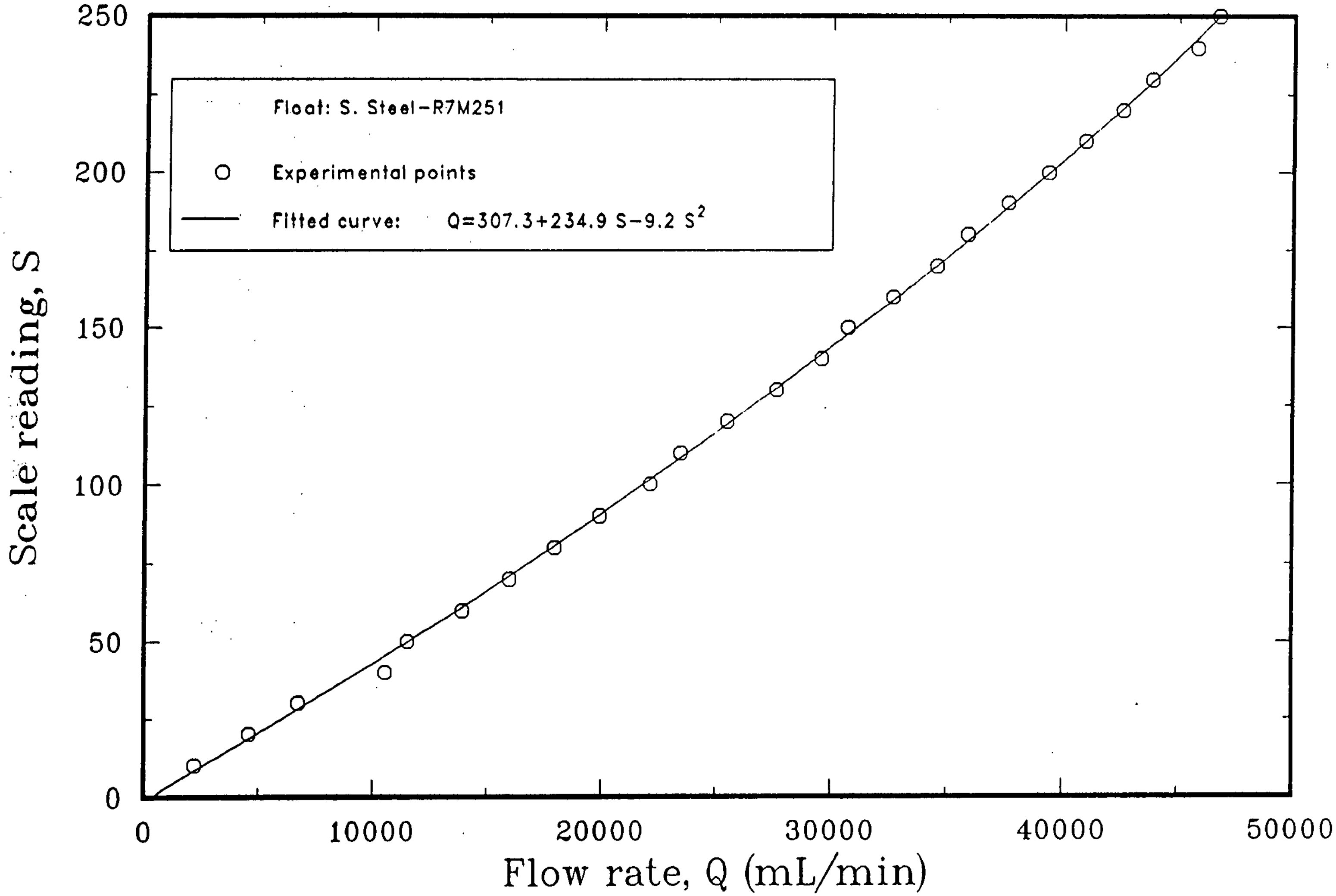

Figure 5.1 Calibration curve for N_2 rotameter

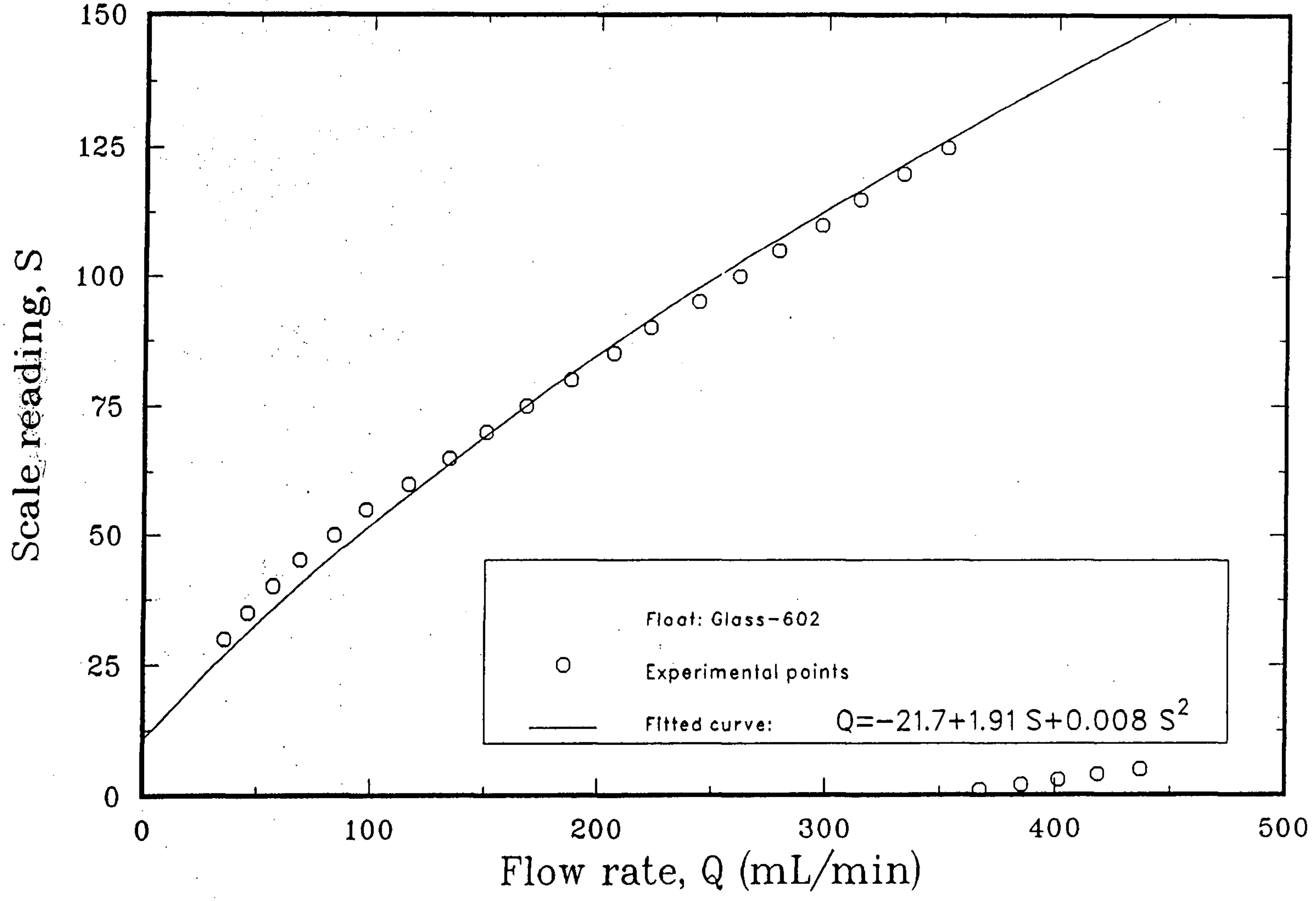

Figure 5.2 Calibration curve for H_2S/N_2 rotameter

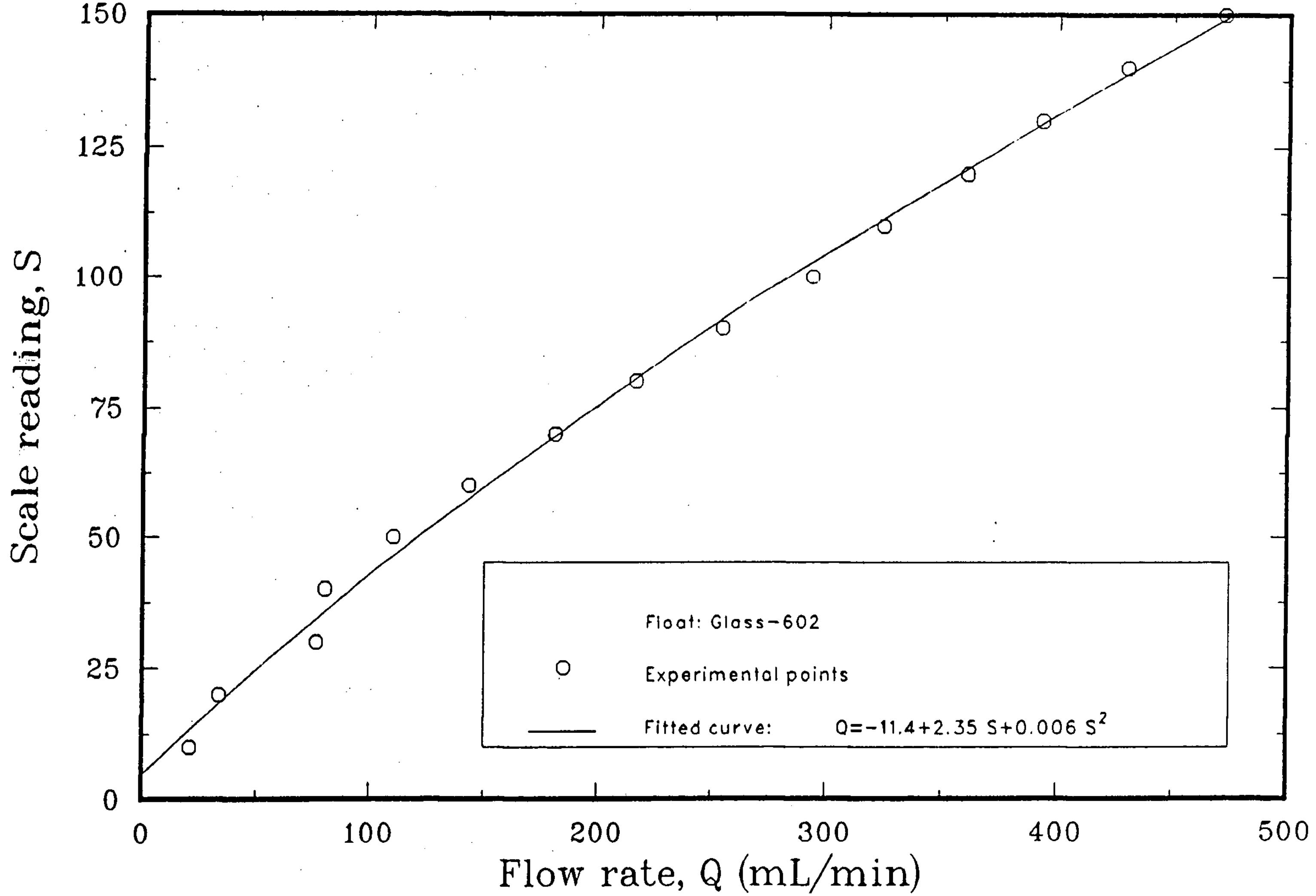

Figure 5.3 Calibration curve for SO_2/N_2 rotameter

5.2.2 Calibration Of Analytical Instruments

The flow rates obtained in the previous section were used to generate, as shown in Figure 5.4, samples of a gas mixture consisting of N_2/H_2S, N_2/SO_2 and $N_2/H_2S/SO_2$. The concentration of H_2S and SO_2 in these samples are calculated from the relations:

$$(ppm)_{H_2S} = Y_{H_2S}Q_{H_2S} \times 10^6/\sum Q_i \qquad (5.6)$$

$$(ppm)_{SO_2} = Y_{SO_2}Q_{SO_2} \times 10^6/\sum Q_i \qquad (5.7)$$

where $\sum Q_i = Q_{H_2S} + Q_{SO_2} + Q_{N_2}$.

Y_{H_2S} and Y_{SO_2} denote the volume fractions of H_2S in H_2S/N_2 cylinder and SO_2 in SO_2/N_2 cylinder, respectively.

The samples were passed through a Photoionization and Pulsed Fluorescent analyser to measure the responses of these instruments, in m.V, due to the presence of the H_2S and SO_2, respectively. The readings from these instruments were recorded as a function of the sample composition.

The Photoionization instrument was built to handle samples with H_2S concentrations between 1 and 1500 ppm. The Pulsed Fluorescent monitor was designed to measure SO_2 concentrations between 1 and 5000 ppm.

It has been observed, however, that the signal from the SO_2 analyser was affected by the presence of the hydrogen sulphide in the sample (Bonsu and Meisen, 1985). The wavelength of the ultraviolet light source for this instrument ranged from 1900 to 2300A°. This wavelength falls into the absorption band of H_2S, i.e 1900 - 2700A° (Watanabe and Jursa, 1964). Bonsu and Meisen (1985) used the Lambert-Beer law to correct for the quenching action of the H_2S, i.e

$$E = E_o exp(-K[H_2S]) \qquad (5.8)$$

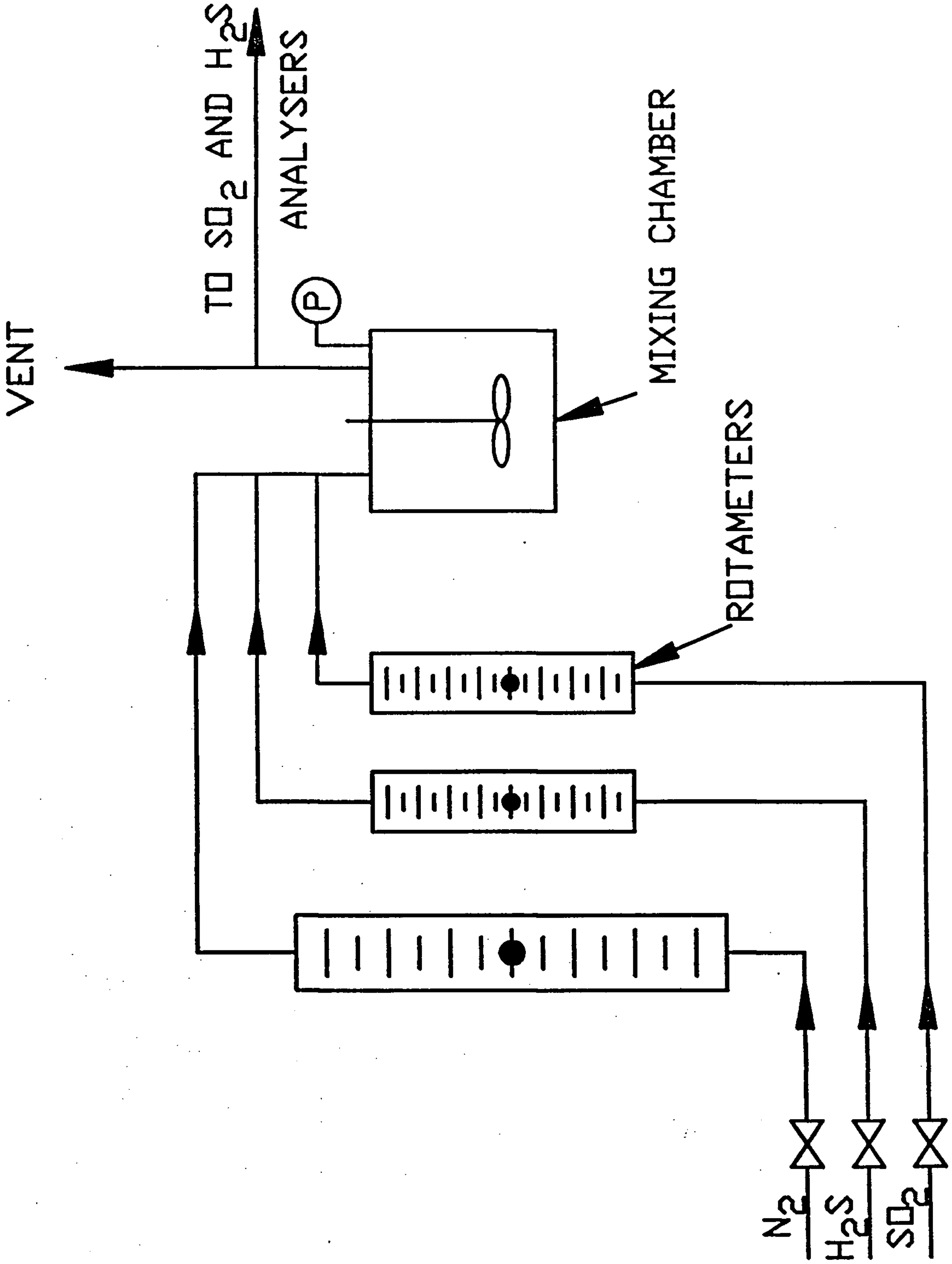

Figure 5.4: Flowsheet for calibrating the analytical instruments

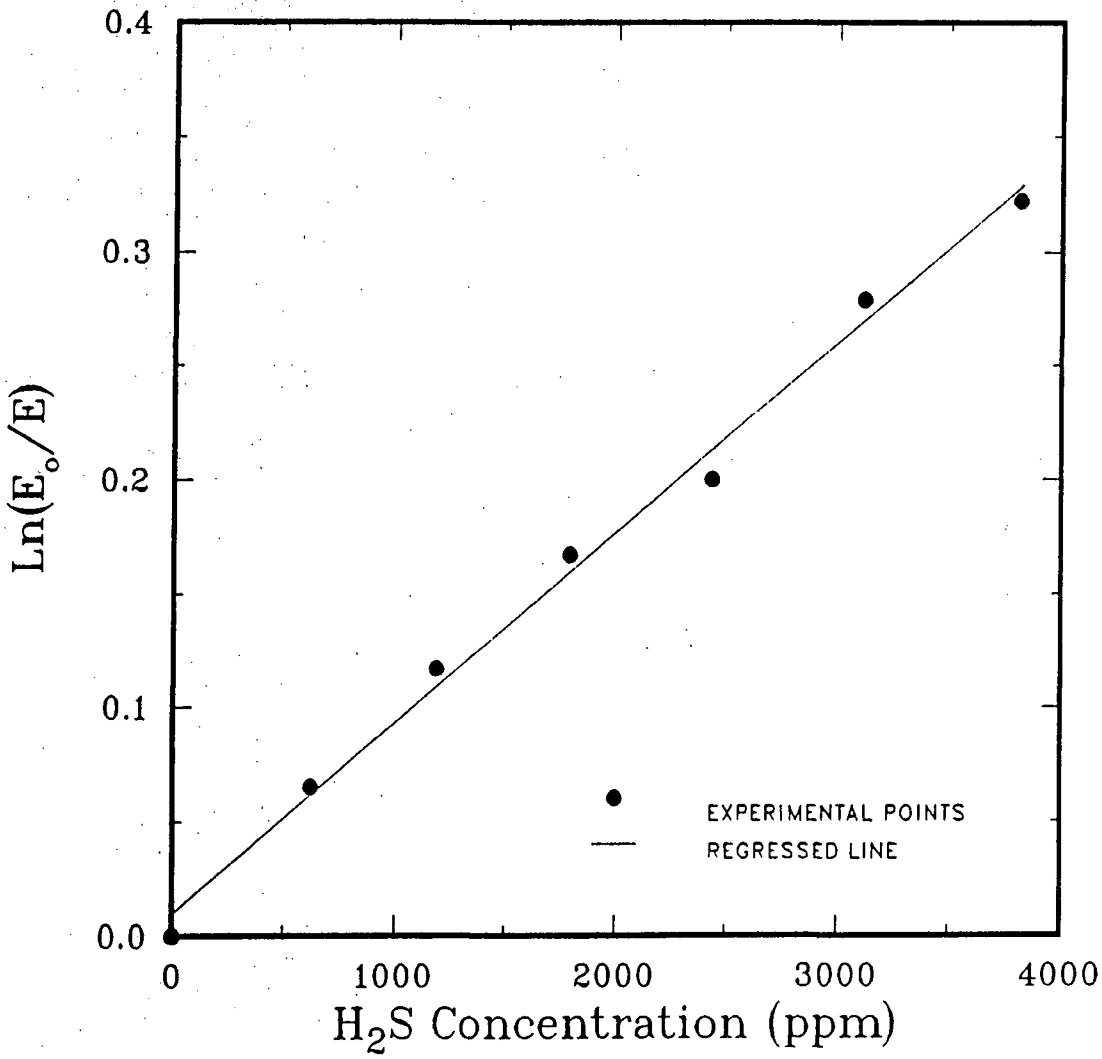

Figure 5.5: Determination of the coefficient, K, due to H_2S

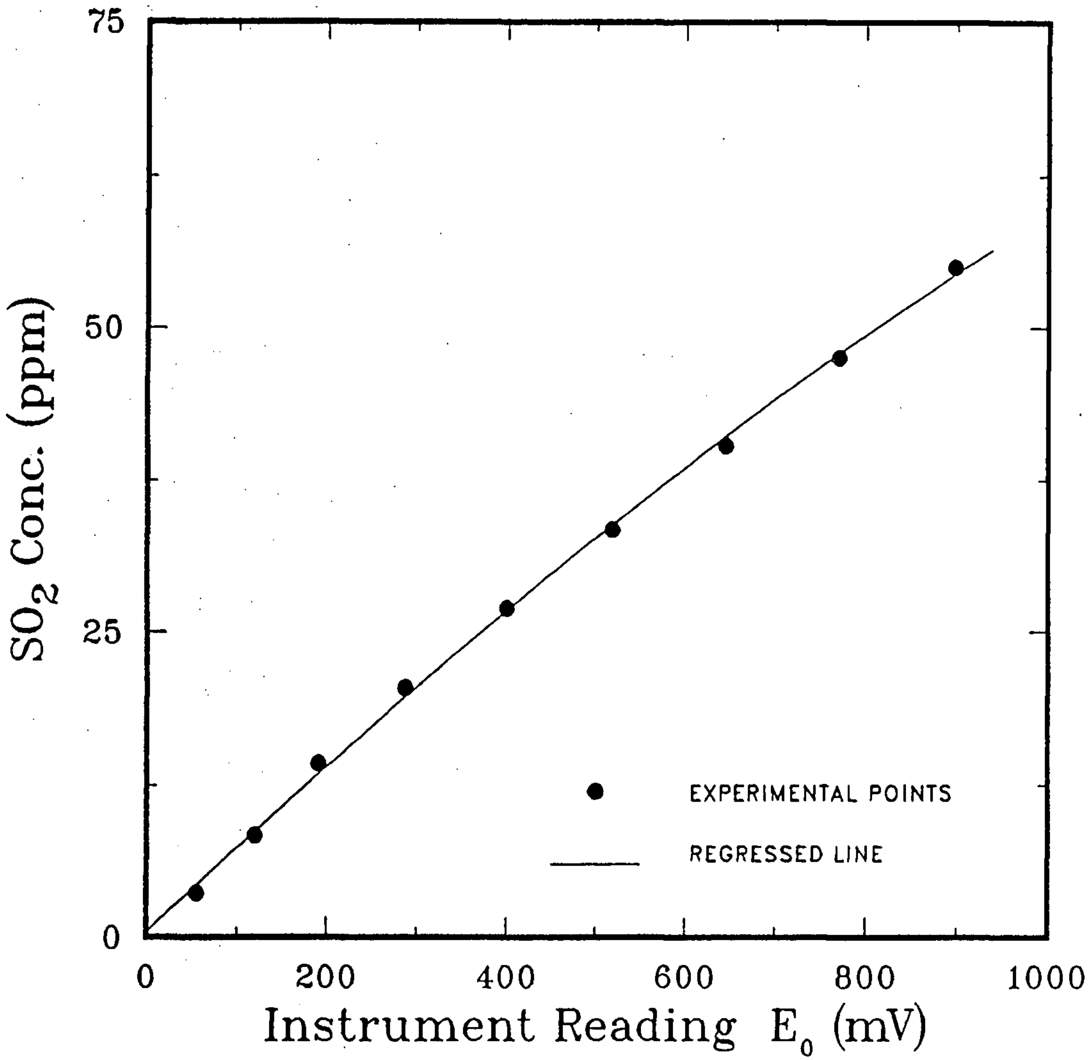

Figure 5.6: Calibration curve for SO_2 analyser (selector marked 0–50 ppm)

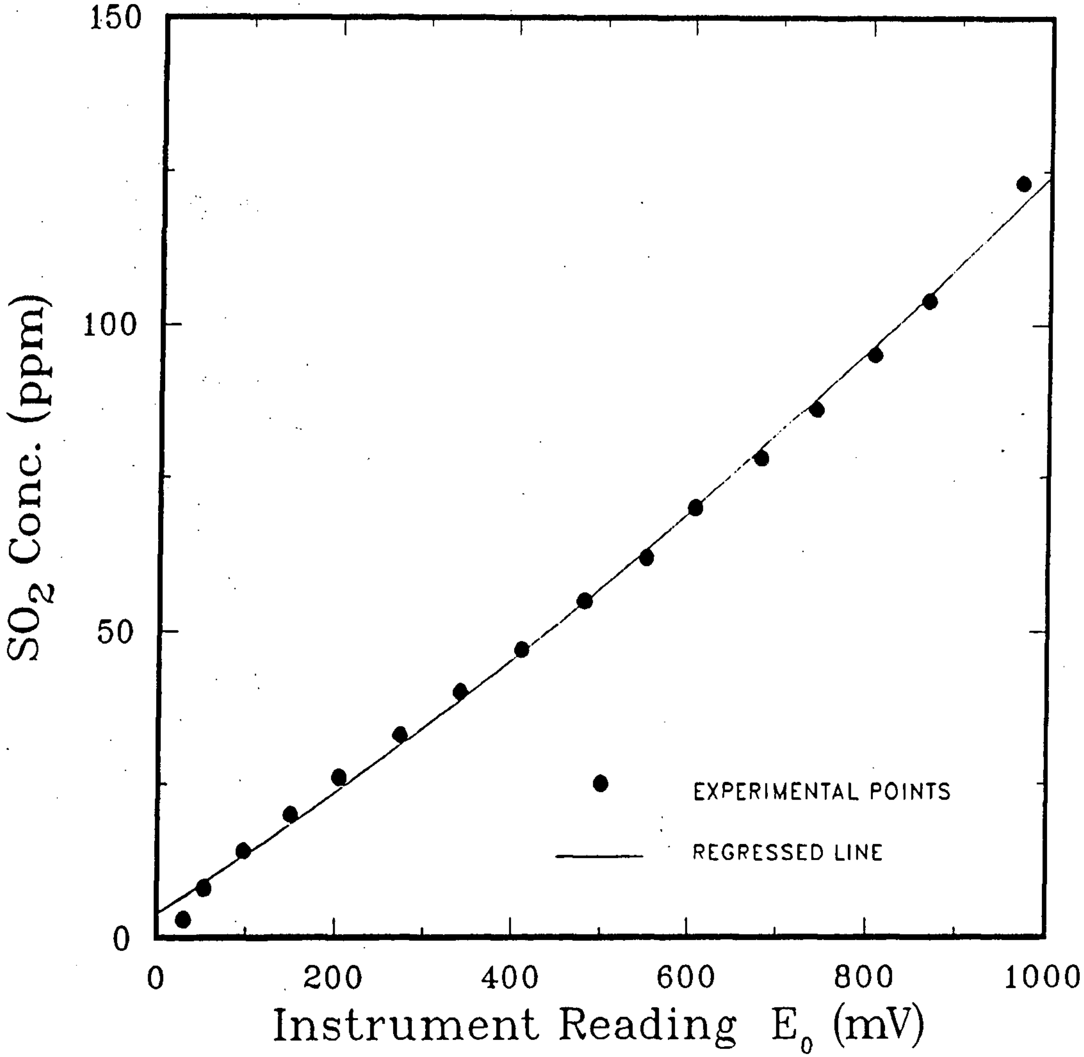

Figure 5.7: Calibration curve for SO_2 analyser (selector marked 0–100 ppm)

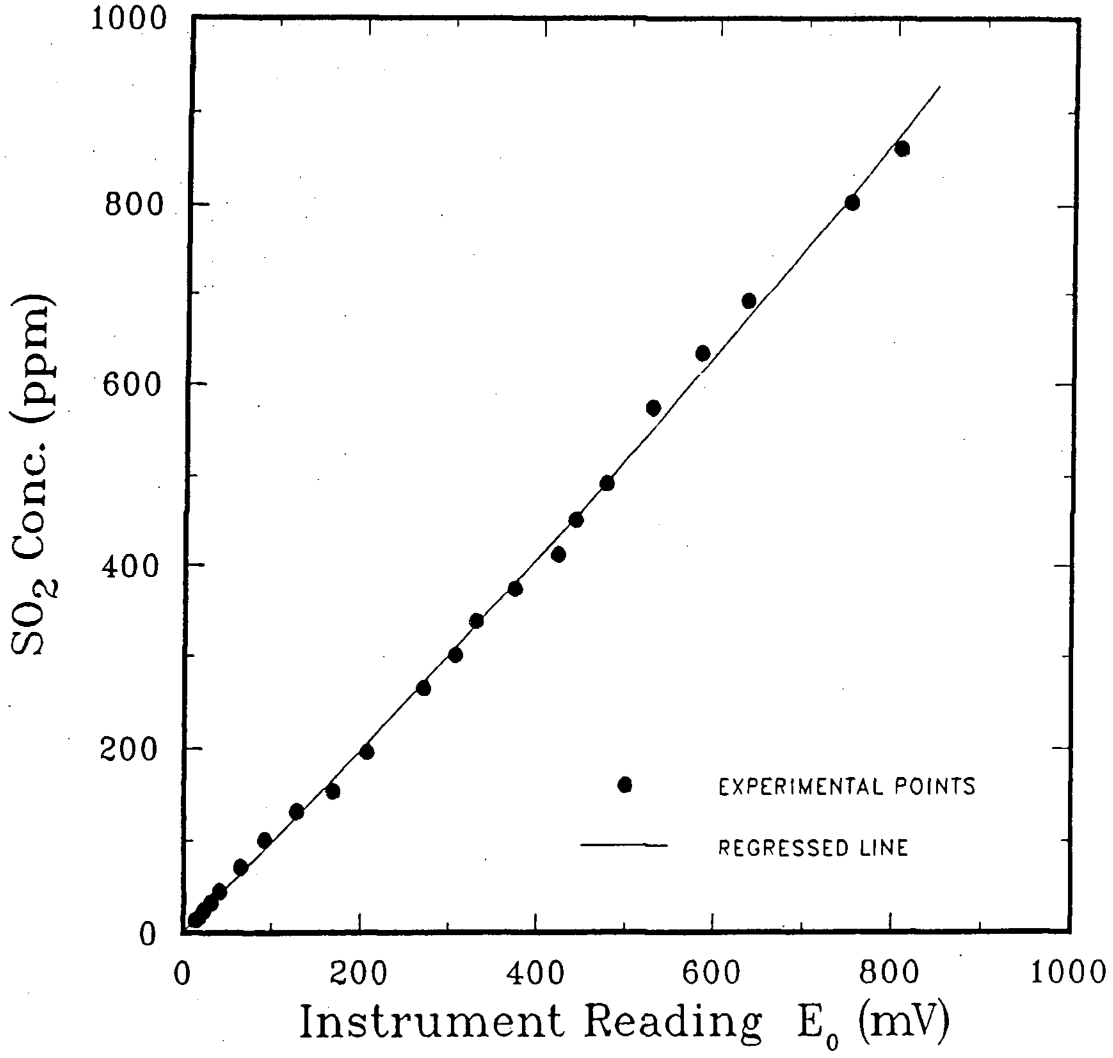

Figure 5.8: Calibration curve for SO_2 analyser (selector marked 0–500 ppm)

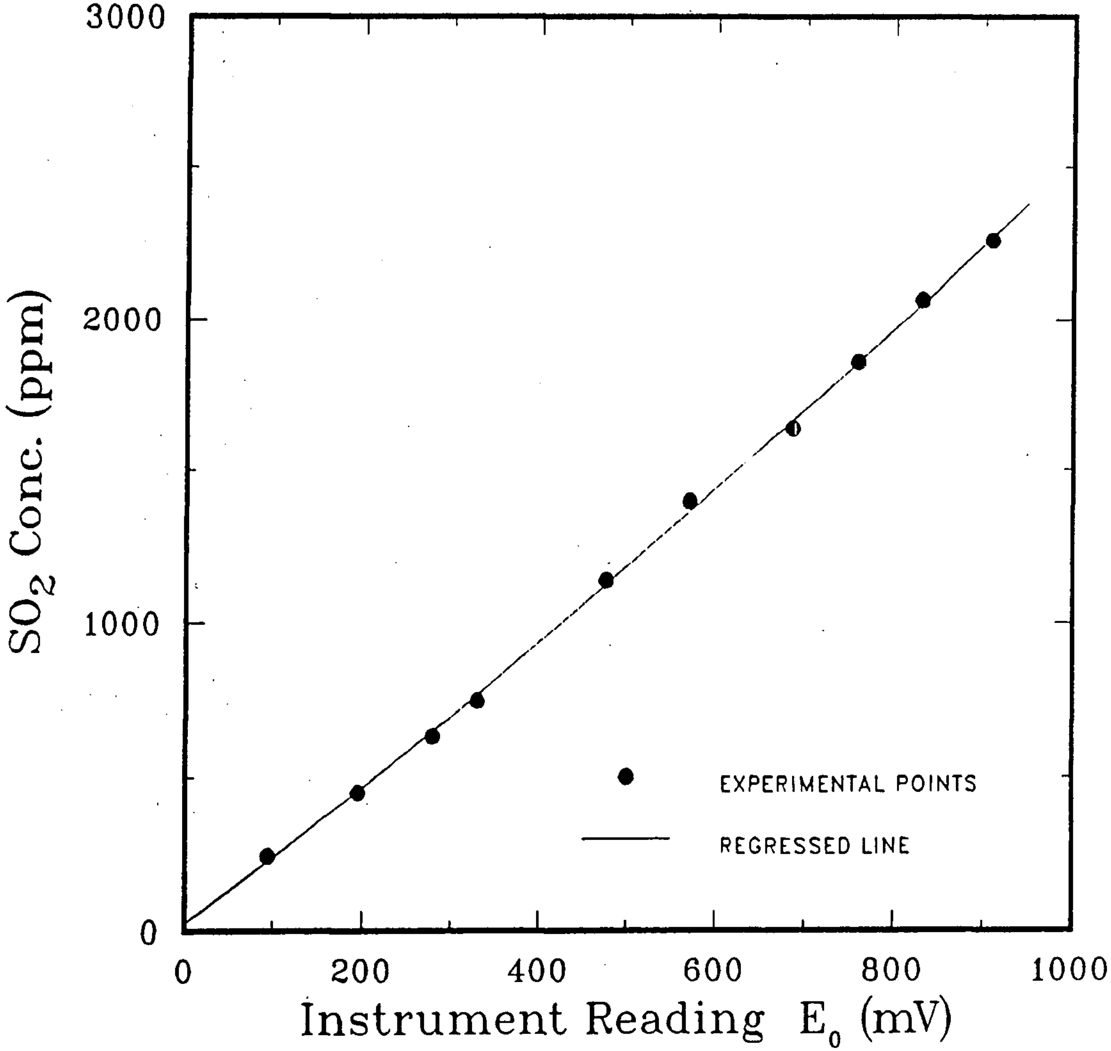

Figure 5.9: Calibration curve for SO_2 analyser (selector marked 0–1000 ppm)

where E and E_o denote the instrument signals for samples with and without H_2S, respectively and $[H_2S]$ denotes the hydrogen sulphide concentration in the sample. The value of the extinction coefficient, K, was obtained from the slope of $\ln E_0/E$ vs. $[H_2S]$ plot. As shown in Figure 5.5, the slope of the straight line was 8.35×10^{-5}/ppm H_2S. Hence, by knowing the H_2S readings produced by the photoionization monitor and E from the SO_2 analyser, E_o was calculated. The concentration of SO_2 in the samples was then obtained from calibration curves shown in Figures. 5.6 to 5.9.

The SO_2 analyser produces fluorescent light of intensity, F, which is related to the SO_2 concentration by the equation (Thermo Electron Corporation, 1976):

$$F = B1\{1 - exp(-B2[SO_2])\} \tag{5.9}$$

$[SO_2]$ denotes the concentration of the sulphur dioxide and B1 and B2 are instrument constants. The exponential nature of the above expression causes a small curvature in the calibration curve, especially at high SO_2 concentrations, as indicated in Figures 5.8 and 5.9. At low SO_2 concentrations, the calibration curve is almost linear (see Figures 5.6 and 5.7) because equation 5.9 can be approximated by:

$$F \cong B[SO_2] \tag{5.10}$$

The H_2S analyser is based on the photoionization principle. For a compound to be detected, its ionization potential must be less than or equal to the energy of the photons emitted by the ultraviolet light source in the instrument. The energy of the light source of this instrument, i.e 10.2 eV, is lower than the ionization potentials of sulphur dioxide and nitrogen (i.e SO_2=12.063 eV and N_2=15.76 eV). Hence, there was no interference from any of these gases. The ionization potential of H_2S is 10.4

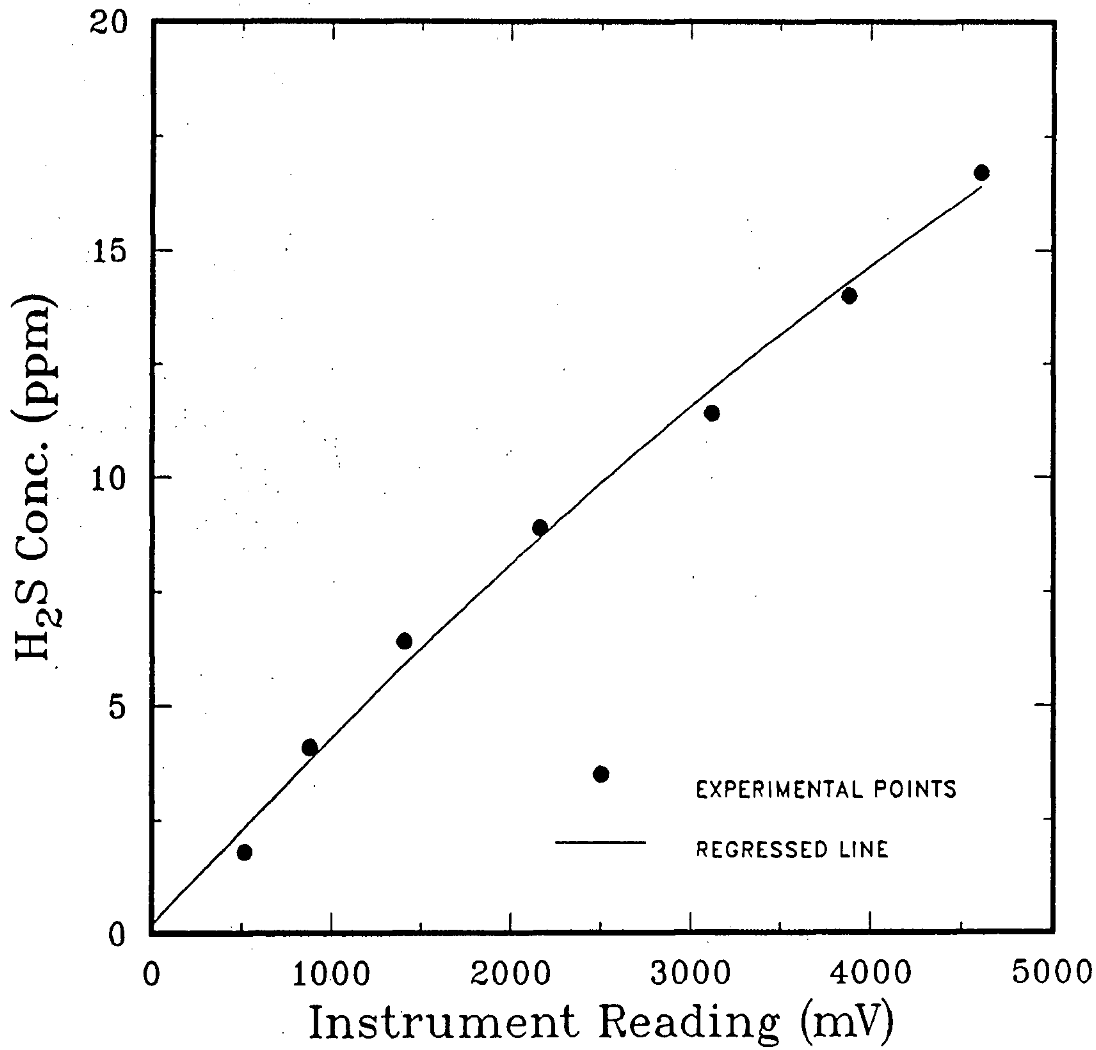

Figure 5.10: Calibration curve for H_2S (selector #1x, range 0–20 ppm)

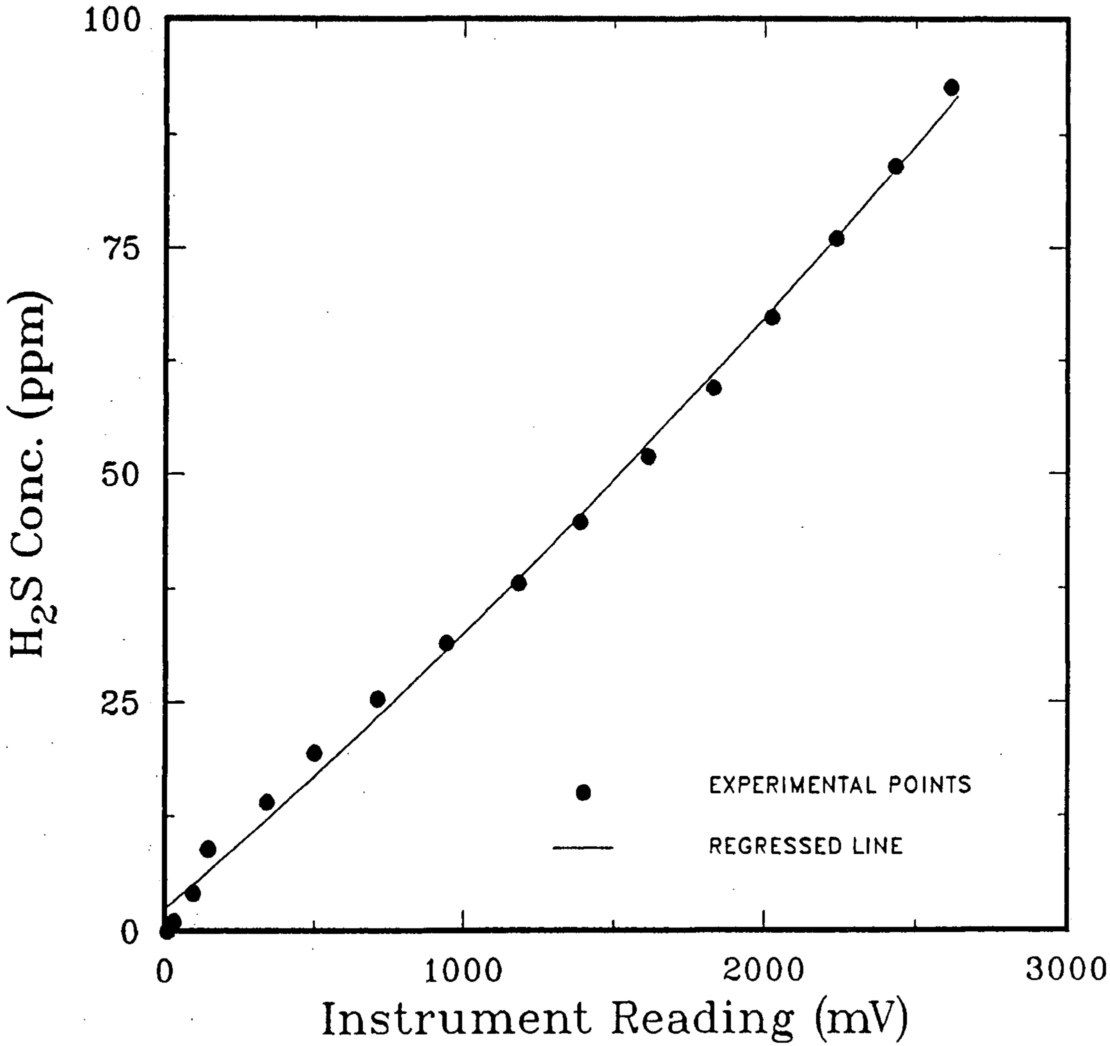

Figure 5.11: Calibration curve for H_2S (selector #10x, range 0–100 ppm)

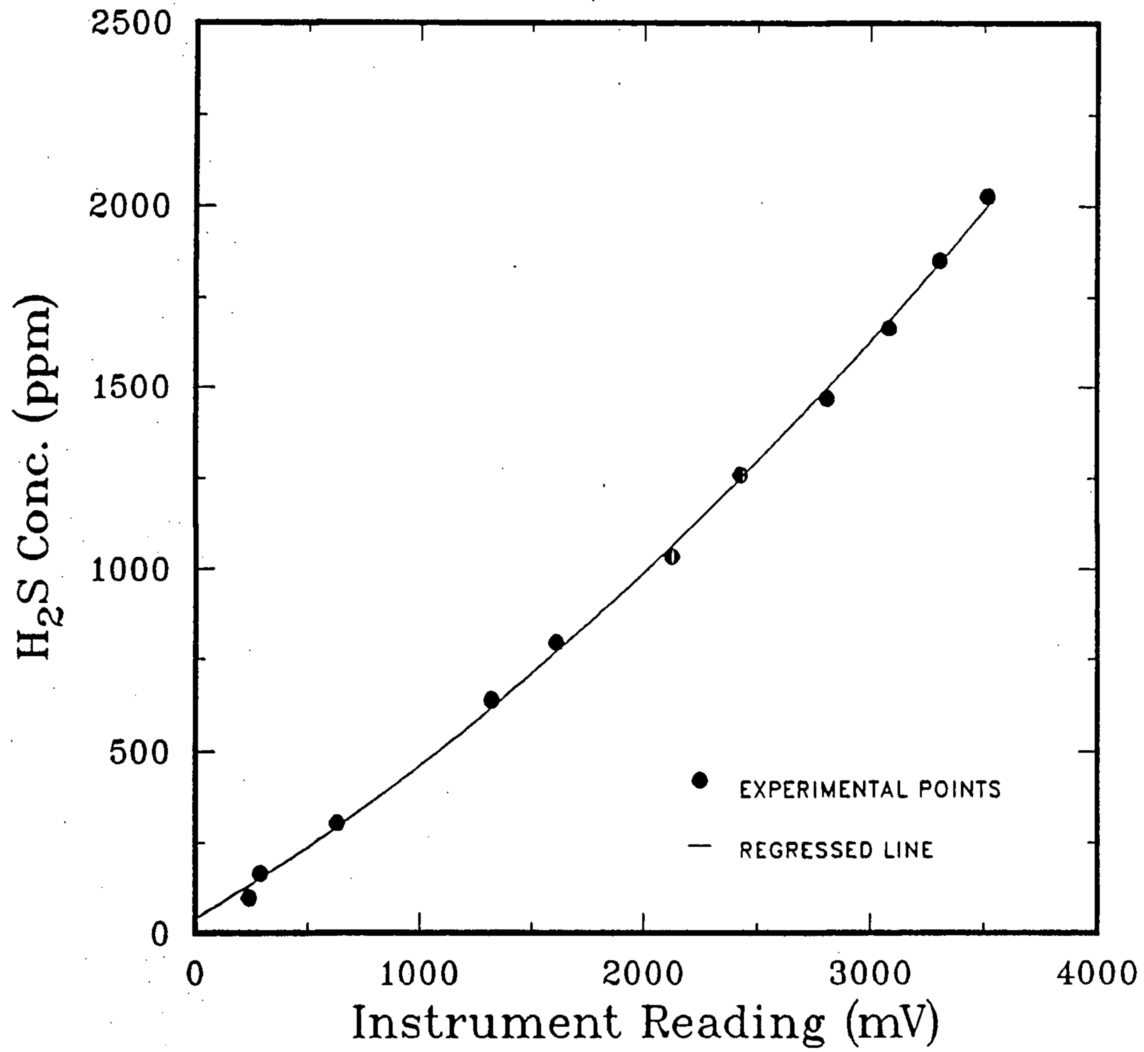

Figure 5.12: Calibration curve for H_2S (selector #100x, range 0–1500 ppm)

eV (Watanabe and Jursa, 1964). The calibration curves for H_2S are presented in Figures 5.10 to 5.12

Bonsu (1981) performed rigorous tests of the conditioning system using dry samples containing H_2S, SO_2 and N_2. He found no change in the sample concentration upon passage through the conditioning system. To explore the effect of moisture on the instrument readings, he passed dry samples over wet $CaCl_2$ and detected a slight decrease in concentration equivalent to an increase in conversion of 0.5 percentage points. This variation falls within the experimental error (see Section 6.3). However, throughout the present experimental runs, great care was exercised to ensure that the surface of the $CaCl_2$ was dry at all times.

Table 5.1: Operating conditions of present experimental equipment

Operating Variable	Range
H_2S feed concentration (ppm)	400 - 1300
SO_2 feed concentration (ppm)	200 - 650
Temperature ($^\circ C$)	100 - 150
U/U_{mf} at reactor conditions	2.24 - 8.88
Static bed height (m)	0.12 - 0.38

Chapter 6

RESULTS AND DISCUSSION

6.1 EXPERIMENTAL RESULTS

6.1.1 Minimum Fluidization Velocity

The minimum fluidization velocity for the catalyst particles was determined from measurements of pressure drop against flow rate of air at ambient conditions (see Figure 6.1). The estimated U_{mf}, based on this plot, is 0.0272 m/s. This result agrees well with value of 0.0266 m/s obtained from equation 2.11. The value of U_{mf} was then corrected to the reactor conditions and was found to be 0.0246 and 0.0225 m/s at 100 and 150°C, respectively.

6.1.2 Sulphur Conversions

The experimental conversion was calculated from material balances on nitrogen and sulphur. Assuming a constant flow rate of N_2 through the reactor, the following expression was derived:

$$\chi = 1 - \frac{y_{out}}{y_{in}} \left[\frac{1 - y_{in}}{1 - y_{out}} \right] \tag{6.1}$$

The conversion of H_2S and SO_2 into elemental sulphur was found to increase (see Figure 6.2) with the reactant concentrations in the feed gas. This result is in general agreement with the previous findings of Bonsu and Meisen (1985). Theoretically,

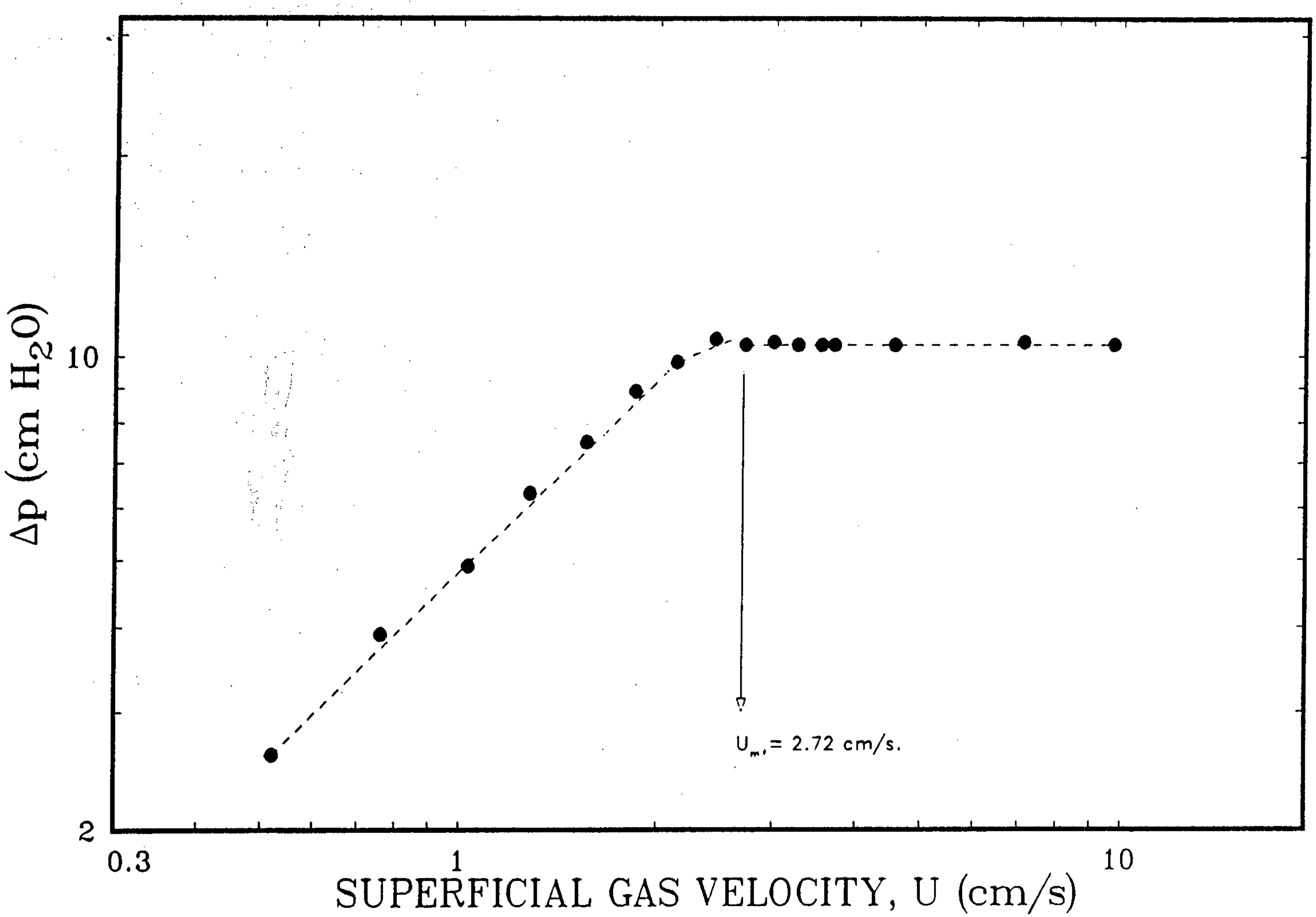

Figure 6.1: Pressure drop versus air velocity for a bed of alumina (Kaiser S-501) at STP

the maximum conversion is dictated by thermodynamic equilibrium. For the temperatures used in this study (100 to 150°C), the Bonsu and Meisen model predicts this maximum to be in excess of 99%. As indicated by Figure 6.2 and columns 2 to 4 of Table 6.1, the experimental conversion for feed compositions of 0 to 1300 ppm H_2S is generally lower than 97%. For instance at 150°C (see column 4 of Table 6.1), the sulphur conversion rose from 75.7 to 97.7% as the H_2S feed concentration increased from 200 to 1300 ppm. The dependency of reaction rate on the reactant concentration is very well known to be first order with respect to H_2S and half order with respect to SO_2 (McGregor et al., 1972; Dalla Lana et al., 1976; Grancher, 1978). For low concentrations of H_2S and SO_2 in the feed, the concentrations of the reactants in the reactor are also small, and the lower the concentrations of these components, the greater the reduction in reaction rate. Consequently, a decline in conversion is plausible. The drastic fall in experimental conversion with decreasing H_2S and SO_2 feed concentrations suggests the likelihood of kinetic limitations on the Claus reaction. These limitations, which are significant as the feed concentrations approach zero, may be noticed by the sharp decrease in the experimental conversion accompanying the decrease in feed concentration from 800 to 200 ppm. Above 800 ppm, the fall in conversion was very gradual suggesting a lower degree of kinetic limitation at higher H_2S feed concentrations.

Closely associated with the effect of the feed concentration on conversion is the role of reaction temperature. Thermodynamic principles suggest that, for the present exothermic reaction, the conversions should rise as the reaction temperature is lowered. Experimental results indicate the opposite trend. Figure 6.3 shows an increase in conversion with increasing temperature. As indicated by Table 6.2, sulphur conversions at H_2S feed concentration increased from 79.4 to 82.0% when

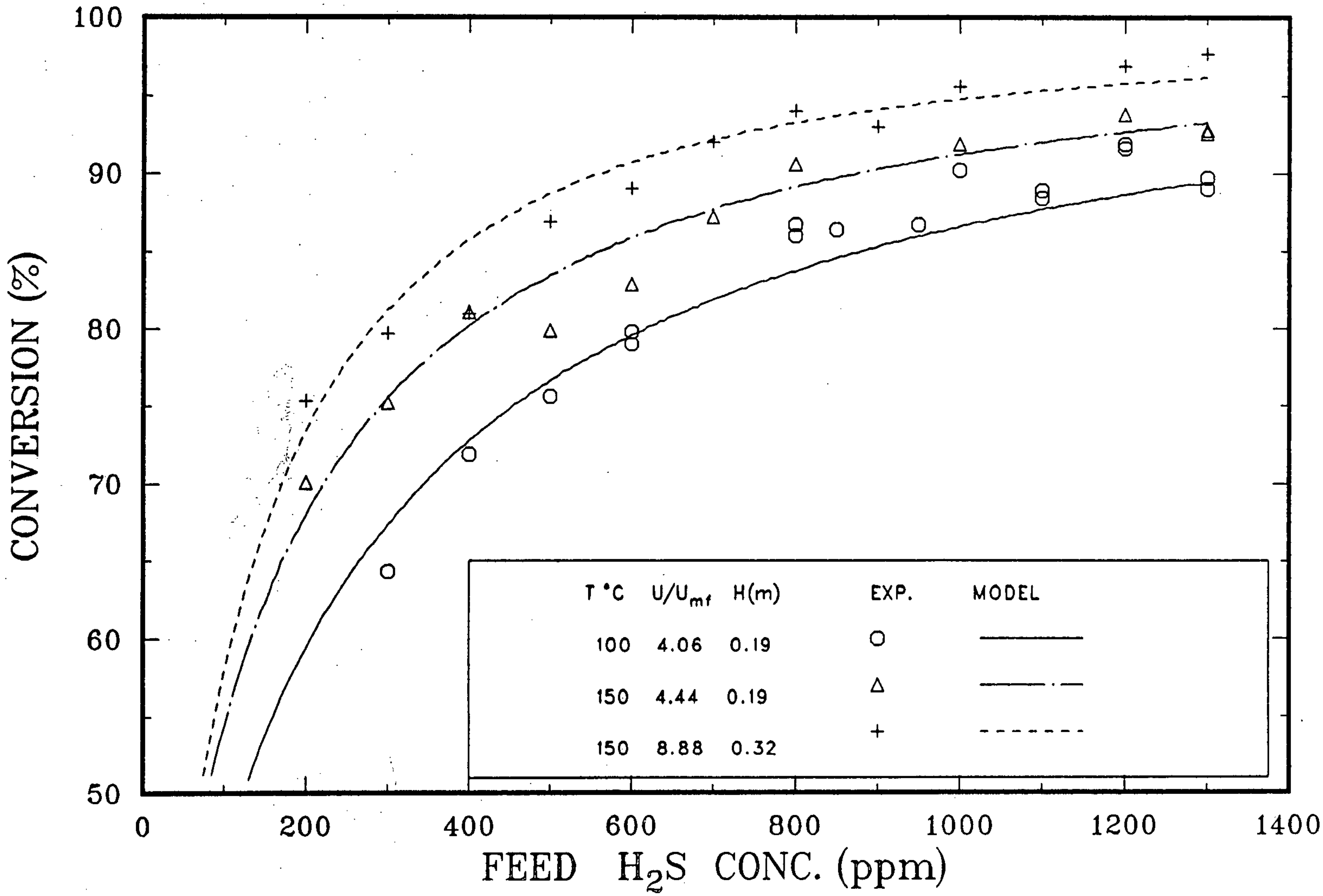

Figure 6.2: Sulphur conversion as a function of H_2S concentration in feed

Table 6.1: Sulphur conversion as a function of H_2S in feed gas

H_2S in feed (ppm)	Experimental conversion (%)			Predicted conversion (%)			%dev		
	a	b	c	a	b	c	a	b	c
200	-	70.1	75.3	59.4	68.0	73.4	-	-2.99	-2.52
300	64.3	75.2	79.7	67.4	75.5	81.3	+4.82	+0.39	+2.01
400	71.9	81.1	81.0	72.8	80.2	85.8	+1.25	-1.11	+5.93
500	75.6	79.9	86.9	76.6	83.5	88.7	+1.32	+4.51	+2.07
600	79.4	82.9	89.0	79.6	85.9	90.7	+0.25	+3.62	+1.91
700	-	87.2	92.1	81.9	87.7	92.2	-	+0.57	+0.11
800	86.3	90.6	93.9	83.7	89.1	93.3	-3.01	-1.66	-0.64
850	86.4	-	-	84.6	89.7	93.7	-2.08	-	-
900	-	-	93.1	85.3	90.3	94.1	-	-	+1.07
950	86.7	-	-	86.0	90.8	94.5	-0.81	-	-
1000	90.2	91.9	95.6	86.6	91.2	94.8	-3.99	-5.77	-0.84
1100	88.9	-	-	87.7	92.0	95.4	-1.35	-	-
1200	91.9	93.8	96.9	88.6	92.7	95.8	-3.59	-1.17	-1.14
1300	89.4	92.8	97.7	89.4	93.3	96.2	0.0	+0.54	-1.54

a: T= 100°C; U/U_{mf} = 4.44; H_s = 0.19m; $RMS\%E$=2.55
b: T= 150°C; U/U_{mf} = 4.44; H_s = 0.19m; $RMS\%E$=2.86
c: T= 150°C; U/U_{mf} = 8.88; H_s = 0.32m; $RMS\%E$=2.32

the temperature increased from 100 to 150 °C. A similar increase in conversion (for H_2S= 1300 ppm) occurred for the same increase in temperature (i.e. 100 to 150°C). This observation was already reported by Bonsu and Meisen for reactor temperatures below 200°C. They found conversions at 150°C to be generally lower than those obtained at 200°C. It is conceivable that the reaction rate is adversely affected by the combination of low temperature and reactant concentrations.

An additional important variable which effects the performance of the fluidized bed reactor is the gas flow rate. This fact is illustrated in Figure 6.4 where a drop in conversion with increasing U/U_{mf} is evident (see also Table 6.3). Bonsu and Meisen found that the performance of their fluidized bed Claus reactor suffered only slightly from the by-passing of gas in the form of bubbles. The simulation of Birkholz et al. (1987) showed that the performance of such reactors is 4.7% less than that of fixed bed reactors. It therefore seems that the effect of gas by-passing is more severe in the case of low reactant concentrations.

The measured conversions of H_2S and SO_2 were found to drop gradually as the catalyst sulphur content increased thereby indicating a fall in catalyst activity due to fouling. Figure 6.5 shows the experimental conversion as a function of the sulphur loading, λ, defined as the weight of sulphur per unit weight of catalyst. There was no change in colour of the catalyst up to a sulphur loading of approximately 50%. At this value, the conversion had fallen to 55% suggesting that deposition of sulphur had deactivated the catalyst significantly. Beyond sulphur loadings of approximately 50%, a yellow film started to appear on the surface of the catalyst (see Figure 6.6) and the particles agglomerated. It was intended to extend the experiments to higher sulphur loadings to explore whether the fall in conversion continued. However, at 60% sulphur loadings, where the conversion had declined to

Table 6.2: Conversion as a function of temperature (U/U_{mf}=4.44, H_s= 0.19m)

Temperature °C	Experimental conversion (%)		Predicted conversion (%)		%dev	
	I	II	I	II	I	II
100	79.4	89.7	79.6	89.4	+0.25	-0.33
110	-	90.7	-	-	-	-0.44
120	81.2	-	-	-	+0.86	-
124	-	-	82.3	91.5	-	-
130	81.4	92.6	-	-	+1.81	-0.65
150	82.9	92.7	84.4	93.3	+1.81	+0.65

I : H_2S feed concentration= 600 ppm ; $RMS\%E$=1.37
II: H_2S feed concentration= 1300 ppm ; $RMS\%E$=0.54

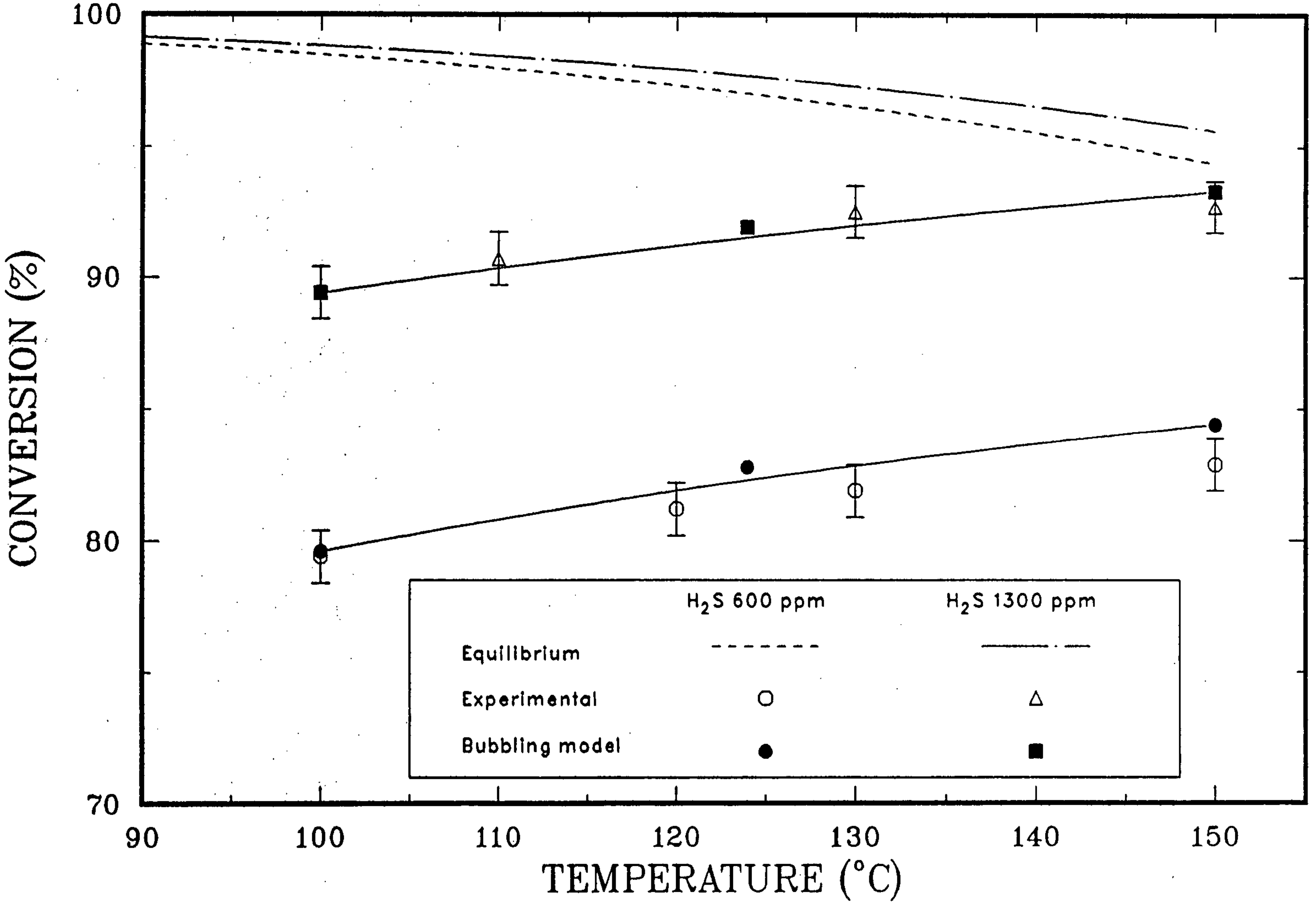

Figure 6.3: Effect of temperature on conversion (U/U_{mf}=4.44, H_s=0.19 m)

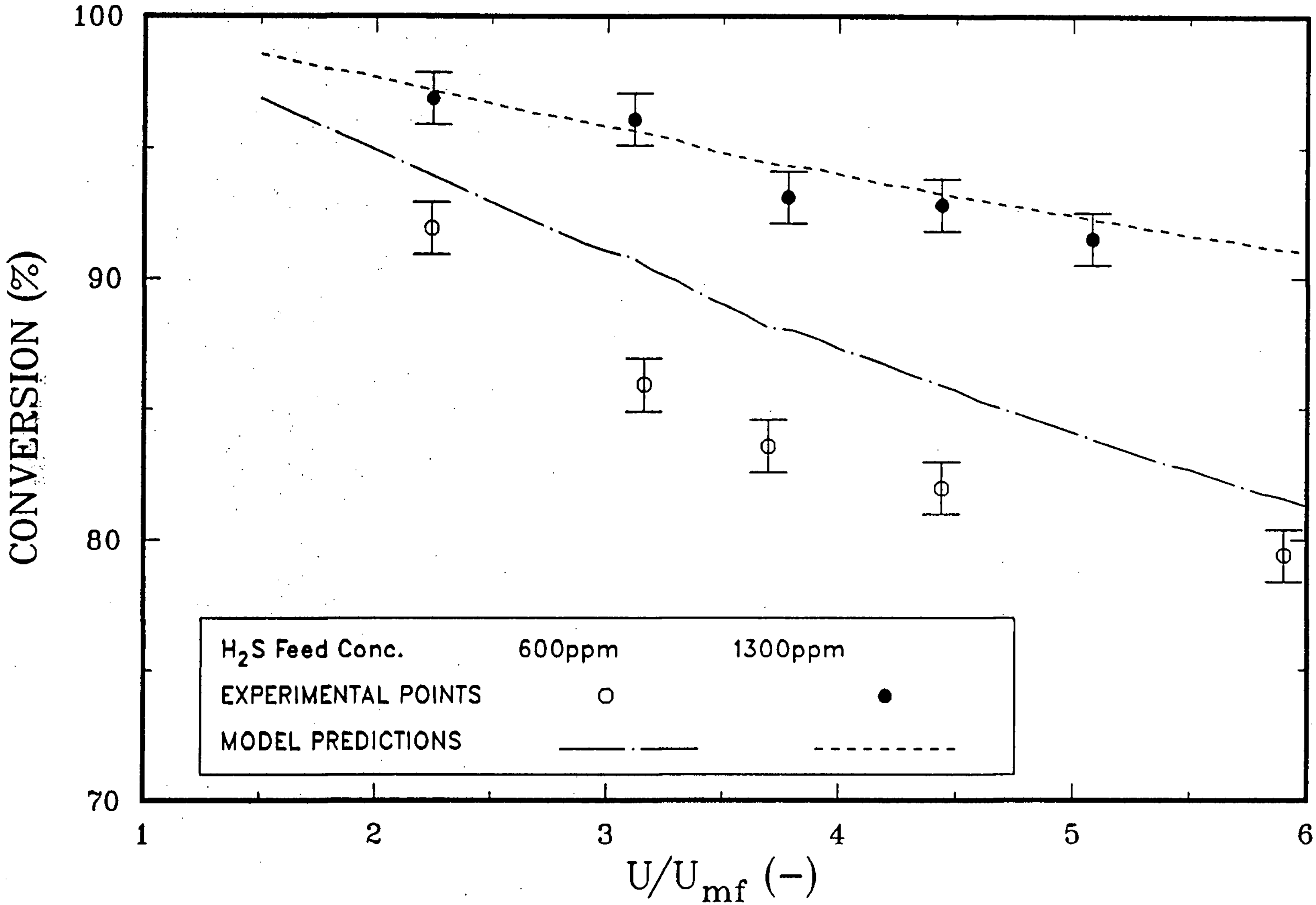

Figure 6.4: Effect of U/U_{mf} on conversion (H_s: 0.19 m, T: 150°C)

Table 6.3: Conversion as a function of U/U_{mf} ($T = 150°C$, H_s= 0.19m)

U/U_{mf}	Experimental conversion (%)		Predicted conversion (%)		$\%dev$	
	I	II	I	II	I	II
2.2	96.9	91.9	97.2	93.9	+0.31	+2.18
3.1	96.1	85.9	95.6	90.6	-0.52	+5.47
3.7	93.1	83.6	94.3	87.0	+1.29	+4.07
4.4	92.7	82.9	93.3	86.0	+0.65	+3.74
5.1	91.5	-	92.4	83.8	+0.98	-
5.9	-	79.4	91.1	81.6	-	+2.77

I : H_2S feed concentration=1300 ppm; RMS%E=0.83
II: H_2S feed concentration 600 ppm; RMS%E=3.82

38%, fluidizing the catalyst became extremely difficult due to particle agglomeration and stickiness. In addition, uniform temperatures could not be maintained as a result of the poor quality of fluidization. No attempt was made to investigate fouling at temperatures above the sulphur melting point ($\sim$ 120°C) where the stickiness would be even more serious.

Experimental conversions are shown as functions of time in Figure 6.7 and Table 6.4. For the first few days, the fall in conversion was rather minor. During this period, the rate of sulphur deposition from the dilute gas is very small and the fresh catalyst has a large active surface available for reaction. As time progressed, the sulphur loading increased as indicated by Figure 6.8 resulting in a reduction of active surface; a gradual decrease in conversion followed.

To investigate the effect of bed height on conversion, experiments were carried out at several static bed heights. Figure 6.9 demonstrates a substantial increase in conversion as the static bed height increased from 0.19 to 0.32m; only slight improvements in the reactor performance were obtained above this height (see Table 6.5). At the elevated reactor temperatures and feed concentrations examined by Bonsu and Meisen (1985), the effect of static bed height on conversion was hardly noticeable. This suggests an optimum bed height generally exists for each set of conditions.

Table 6.4: Conversion as a function of time and sulphur loading (T = 100°C, H_2S= 1000ppm, H_s=0.32m)

Time (h)	S. loading (%)	Conversion (%) Exp.	Conversion (%) Model	Time (h)	S. loading (%)	Conversion (%) Exp.	Conversion (%) Model
2.0	0.01	93.5	95.4	117.0	14.21	79.7	79.6
4.0	0.13	93.5	95.3	125.0	15.13	78.7	78.5
6.0	0.36	93.8	95.1	135.0	16.27	77.4	77.2
9.0	0.53	93.8	95.0	140.8	16.93	76.0	75.2
12.0	0.55	93.9	95.0	151.0	17.90	74.8	75.1
15.0	0.59	93.0	94.9	162.0	18.76	73.8	74.2
18.0	0.72	92.9	94.9	170.0	22.79	73.1	69.6
21.0	0.73	92.9	94.8	178.0	24.99	72.3	67.2
24.0	0.84	92.8	94.7	186.0	25.24	68.9	66.9
27.0	0.89	92.8	94.7	196.0	27.06	68.3	65.1
32.0	1.26	91.6	94.4	207.0	25.22	64.0	66.9
37.0	1.49	92.1	94.1	219.0	29.08	63.4	63.1
42.3	1.52	92.1	94.1	231.0	27.08	61.2	65.1
48.3	1.84	92.4	93.9	243.0	31.97	59.1	60.5
55.0	2.59	90.9	93.1	255.0	37.71	58.1	55.3
60.0	3.51	91.4	92.4	265.0	42.35	57.3	51.9
68.0	4.14	91.7	91.5	277.0	44.44	56.3	50.4
72.0	4.16	90.3	91.5	288.5	45.13	54.2	49.9
80.0	7.05	88.4	88.3	301.0	47.17	52.2	48.6
86.0	6.95	88.0	88.3	313.0	50.81	47.2	46.4
95.0	9.15	81.3	85.8	335.0	54.92	43.0	43.9
99.3	12.02	81.7	82.1	347.0	60.05	39.0	41.3
109.0	13.05	78.8	81.1				

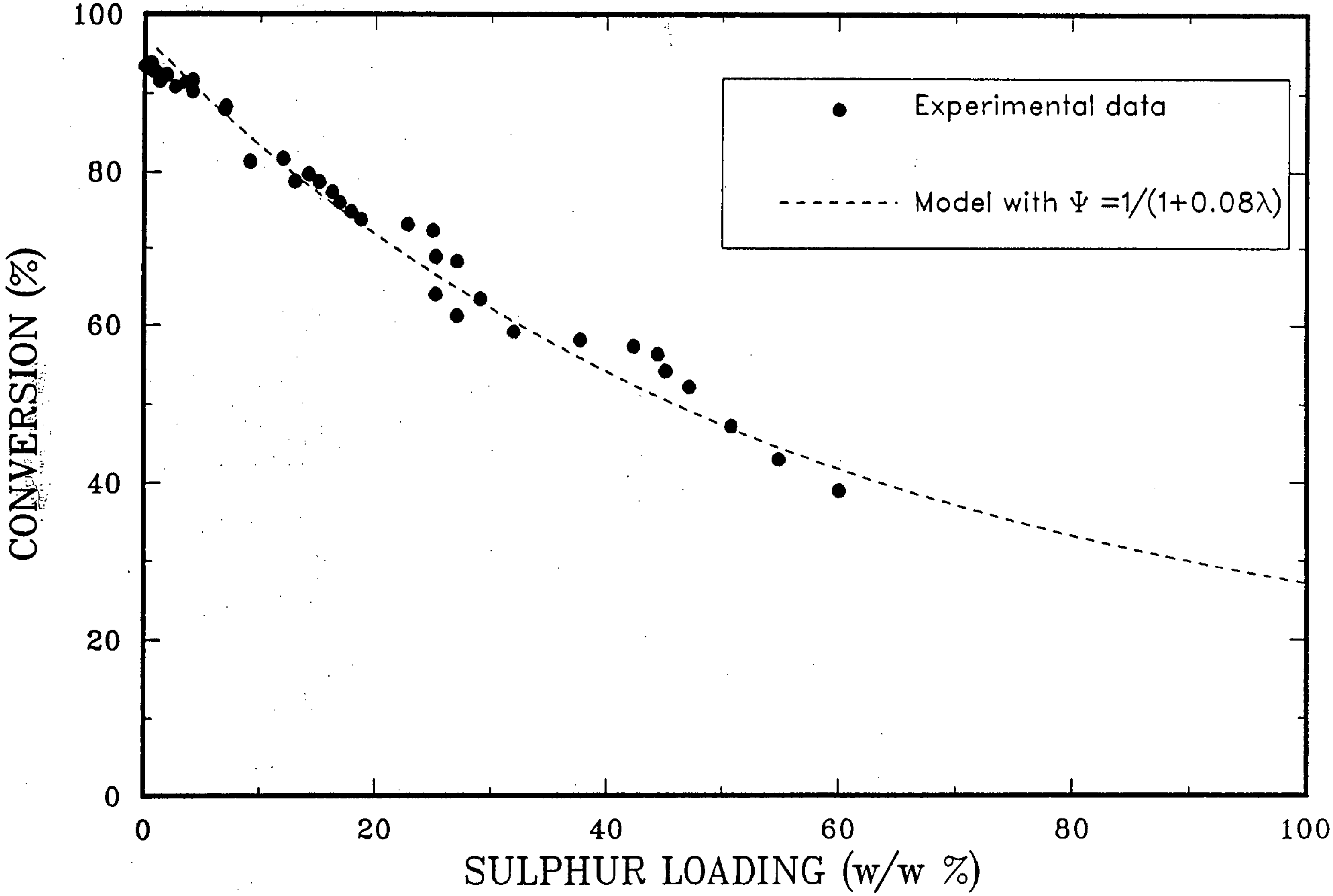

Fig. 6.5: Effect of sulphur condensation on conversion (H_2S=1000ppm, T=100°C, U/U_{mf}=4.44, H_s=0.32m)

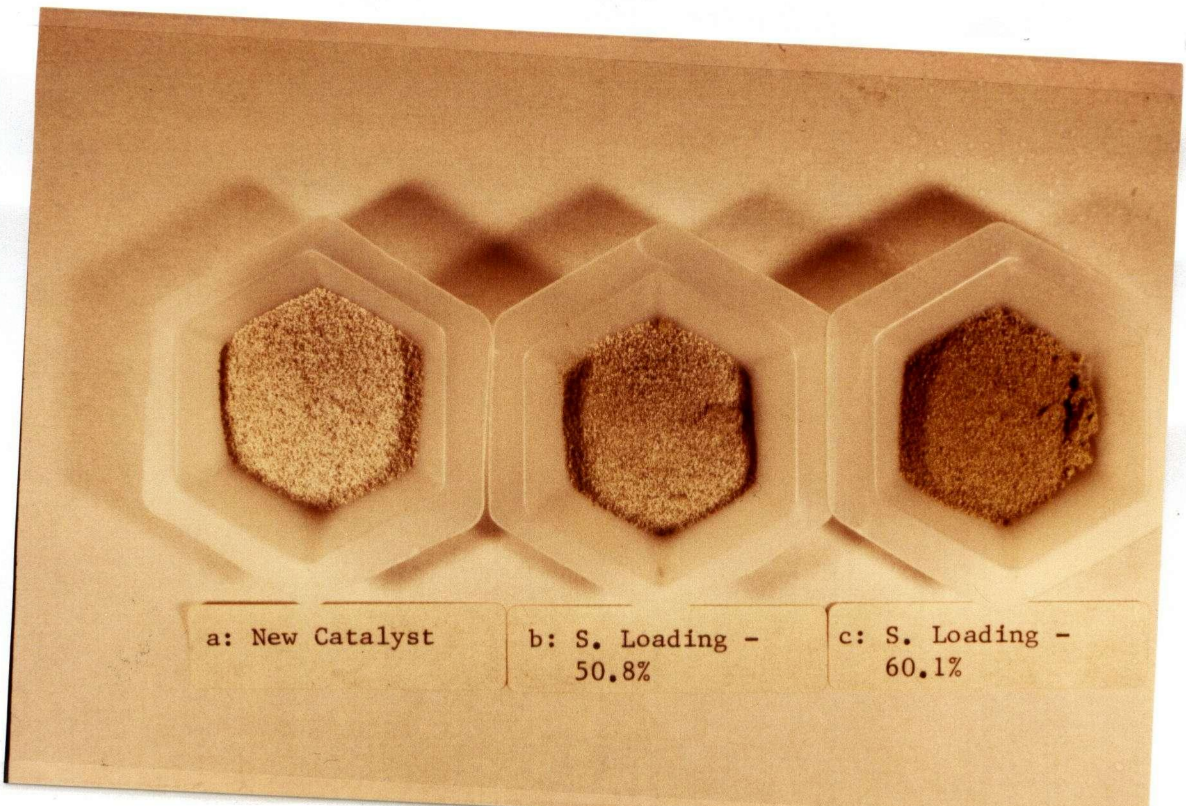

Figure 6.6: External colour of catalyst as a function of sulphur loading

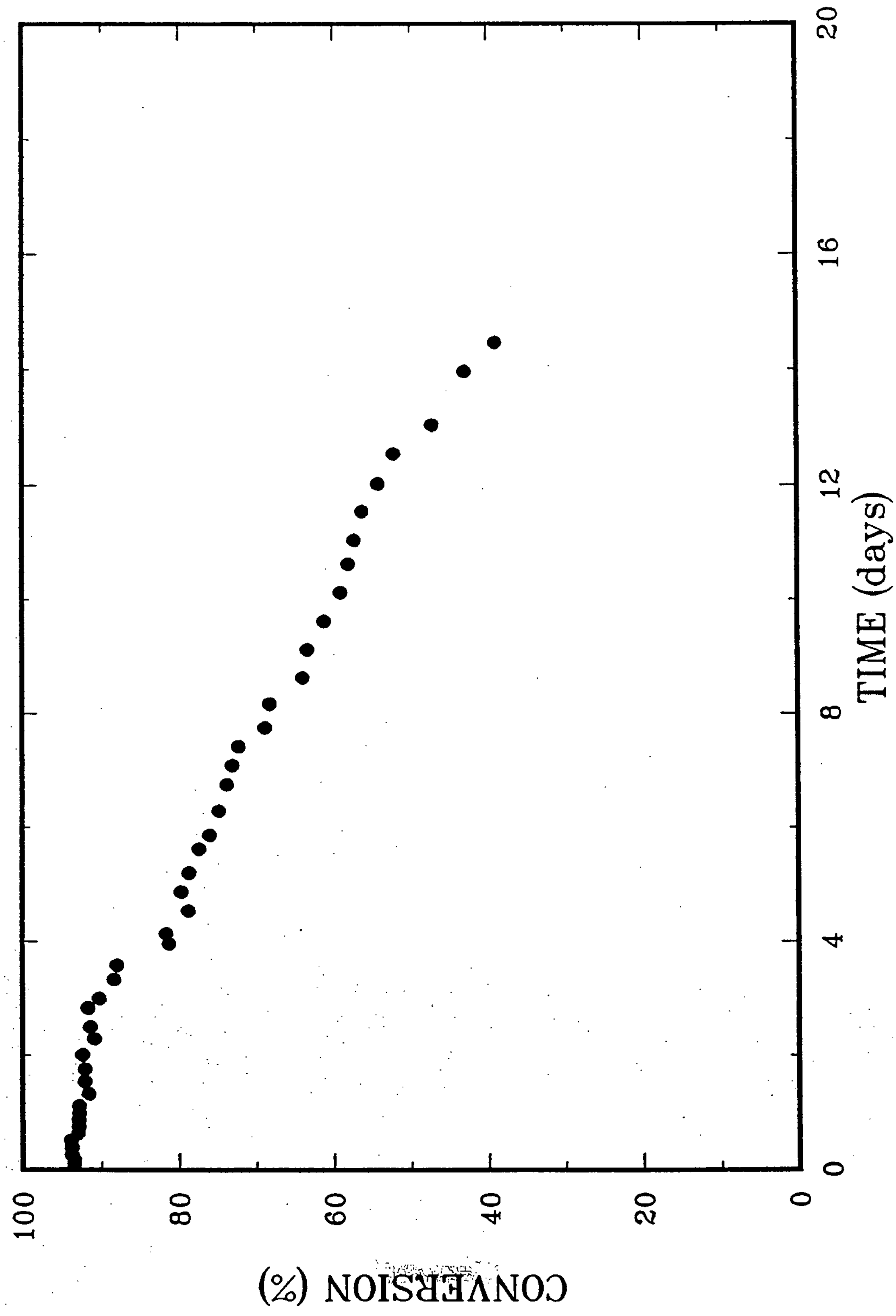

Figure 6.7: Conversion as a function of time (H_2S=1000ppm, U/U_{mf}=4.44, H_s=0.32m, T=100°C)

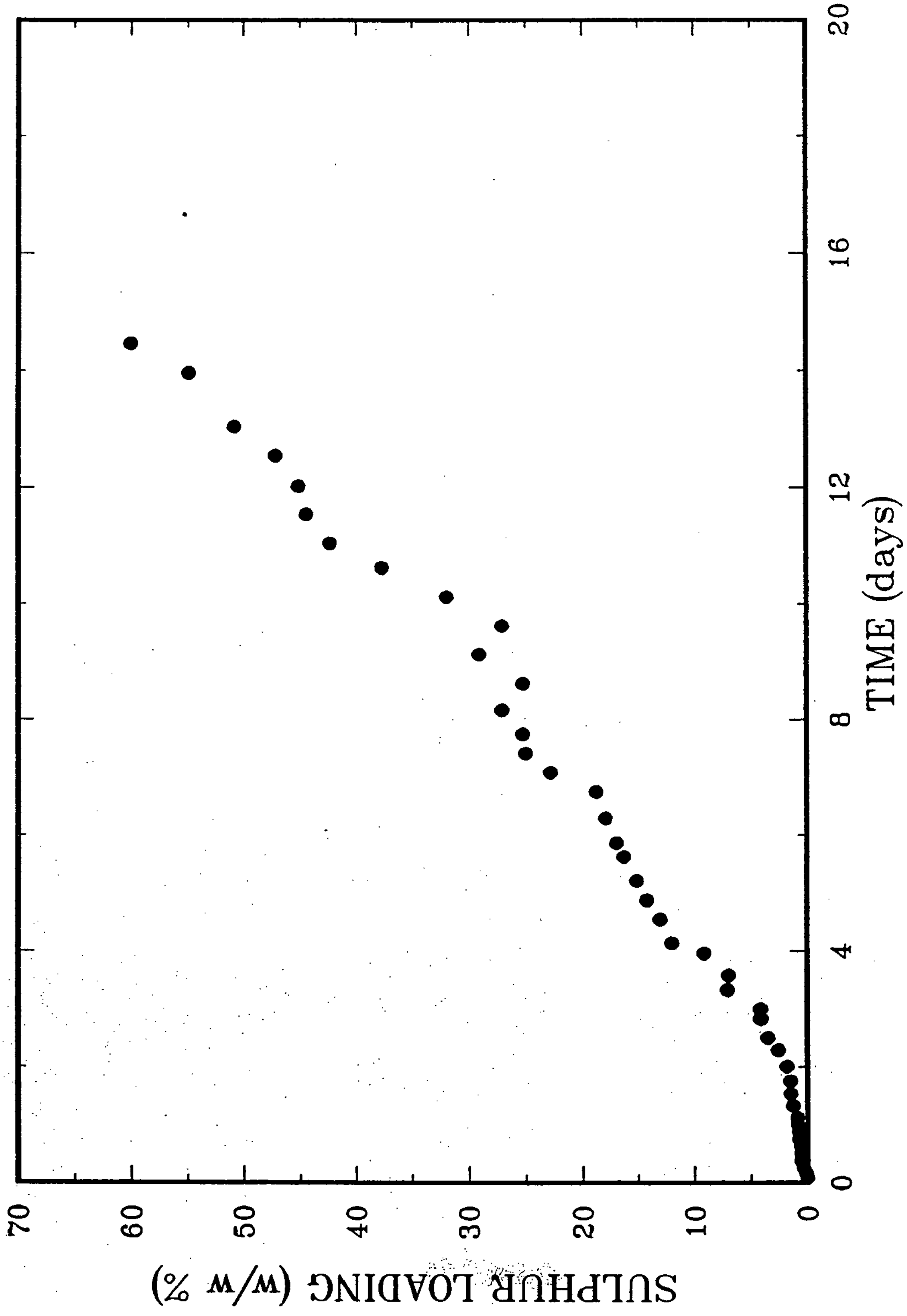

Figure 6.8: Sulphur loading as a function of time (H_2S=500ppm, U/U_{mf}=4.44, H_s=0.32m, T=100°C)

Table 6.5: Conversion at several static bed heights (T = 100°C; U/U_{mf} = 4.44; H_2S= 600ppm; SO_2 = 300 ppm)

Height (m)	Experimental conversion (%)	Predicted conversion (%)
0.12	62.9	63.9
0.19	79.7	79.6
0.25	86.9	87.9
0.32	92.2	92.2
0.38	95.2	94.8

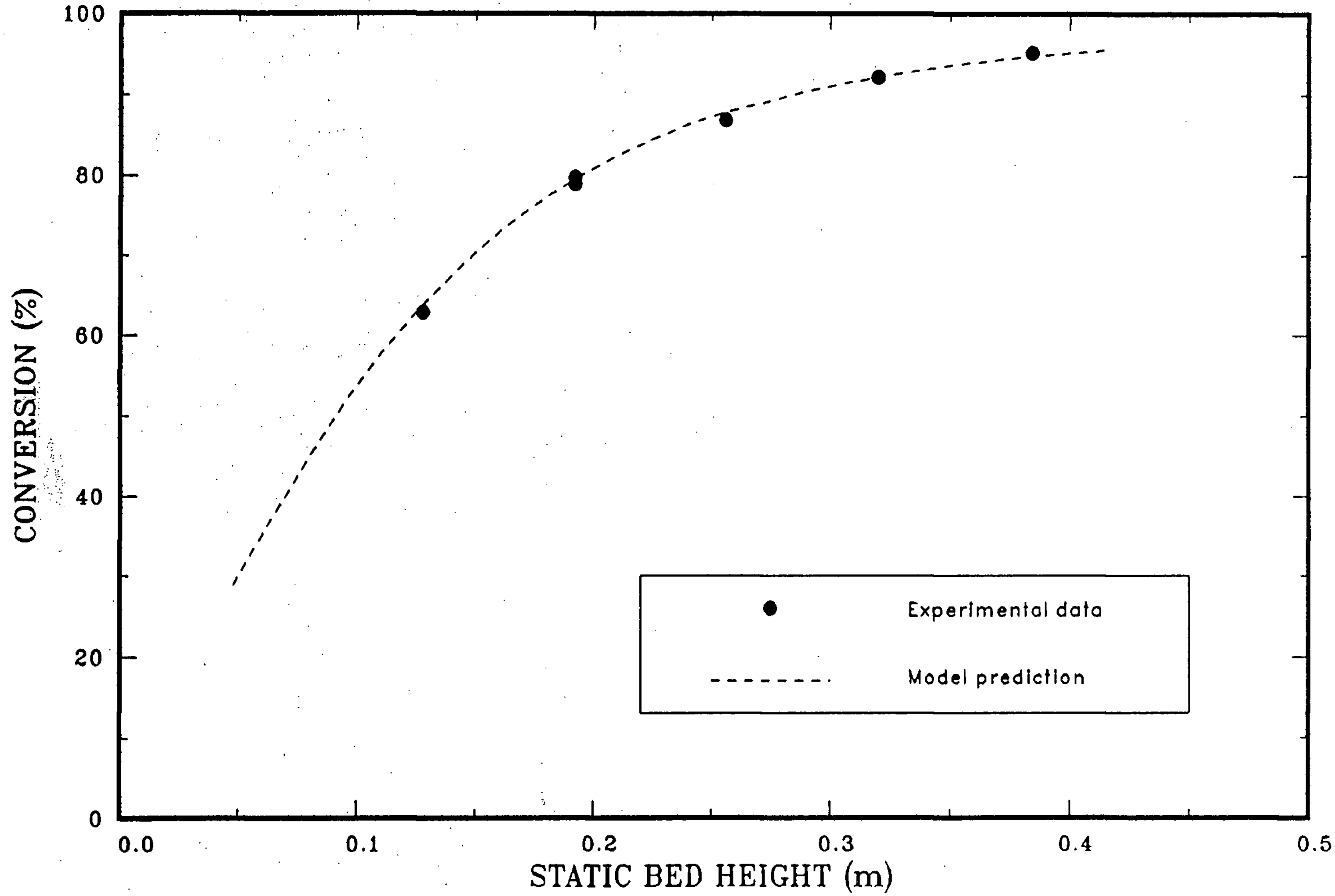

Figure 6.9: Effect of static bed height on conversion (H_2S=600ppm, U/U_{mf}=4.44, T=100° C)

6.1.3 Catalyst Attrition

Large spheres of alumina catalyst (Kaiser S-501) were ground and sieved to the desired particle size range. A representative sample (W_0= 0.508 kg) of the sieved catalyst was then loaded into the reactor. The sample contained no particles smaller than 125 μm. An air flow rate of 3.98 m^3/h (STP) was maintained through the reactor for 1/2 h. The air flow rate corresponded to U/U_{mf}=5.2. Fluidization of the particles was carried out at room temperature and atmospheric pressure. Following the test period the catalyst was recovered, as completely as possible, from the reactor. The collected sample was sieved in a series of screens for 1/2 h. An electronic balance was used to weigh the contents of each screen. The weight of particles smaller than 125 μm was also determined. There was about 0.02% loss of fines. To investigate the effect of fluidization for longer time, particles with $d_p < 125\mu m$ were discarded and the remaining catalyst mass was returned to the reactor. The catalyst was again fluidized with air for increasing time intervals. The process was repeated up to a total time of 303h.

The cumulative mass of particles smaller than 125 μm plus the loss of fines was considered to be the amount of catalyst formed by attrition. The loss of fines occurred only during the first 1/2 h. This loss is probably due to the presence of dust in the newly ground catalyst. The extent of attrition was defined as the mass of particles with $d_p <$ 125 μm divided by the total original mass, i.e:

$$\mathcal{A} = \frac{W_f}{W_0} \tag{6.2}$$

The maximum rate of attrition occurred in the first few hours (see Figures 6.11 and 6.12). These figures show that $\mathcal{A}$ increased from 0 to 2 % in about 5 hours. During this period, the fresh ground particles had irregular shapes with sharp edges and protruding corners. Such particles may easily undergo attrition due to the colliding and rubbing actions. As time passed, the particles became more rounded and developed smooth surfaces. Rounded particles have high attrition resistance and therefore the extent of attrition levels off. As indicated by Figure 6.11, the extent of attrition reached a constant value of about 2.6% within a short period of time. The constant value of $\mathcal{A}$ suggests that the total attrition of the Kaiser S-501 catalyst was quite small. The attrition tendency of this catalyst is also reflected in the sample mean particle diameter (see Figure 6.13). Using equation 4.1, The calculated d_p decreased from 199.68 to an almost constant value of 196.20 μm in about 2 hours.

6.2 MODEL PREDICTIONS

Conversions predicted by the two phase bubbling model are plotted in Figures 6.2 to 6.5 and in Figure 6.14. Model predictions as a function of H_2S feed concentration are presented in columns 5 to 7 of Table 6.1. These predictions may be compared with the experimental values which are included in columns 2 to 4 of the table. For instance, at 100°C as the feed concentration increased from 300 to 1300 ppm both experimental and model conversions increased from 64.3 and 67.4 to 89.4 and 89.4%, respectively. Similarly good agreement between experimental and model conversions can be seen for the second and third sets in Table 6.1 (i.e columns 3 and 4 vs 6 and 7). The three sets of experimental data in this table indicate that a slight deviation from experimental conversions occurs at very low H_2S feed concentration. To quantify this deviation, the following definitions may be used:

$$\%dev = \frac{Pre - Exp}{Exp} \times 100 \tag{6.3}$$

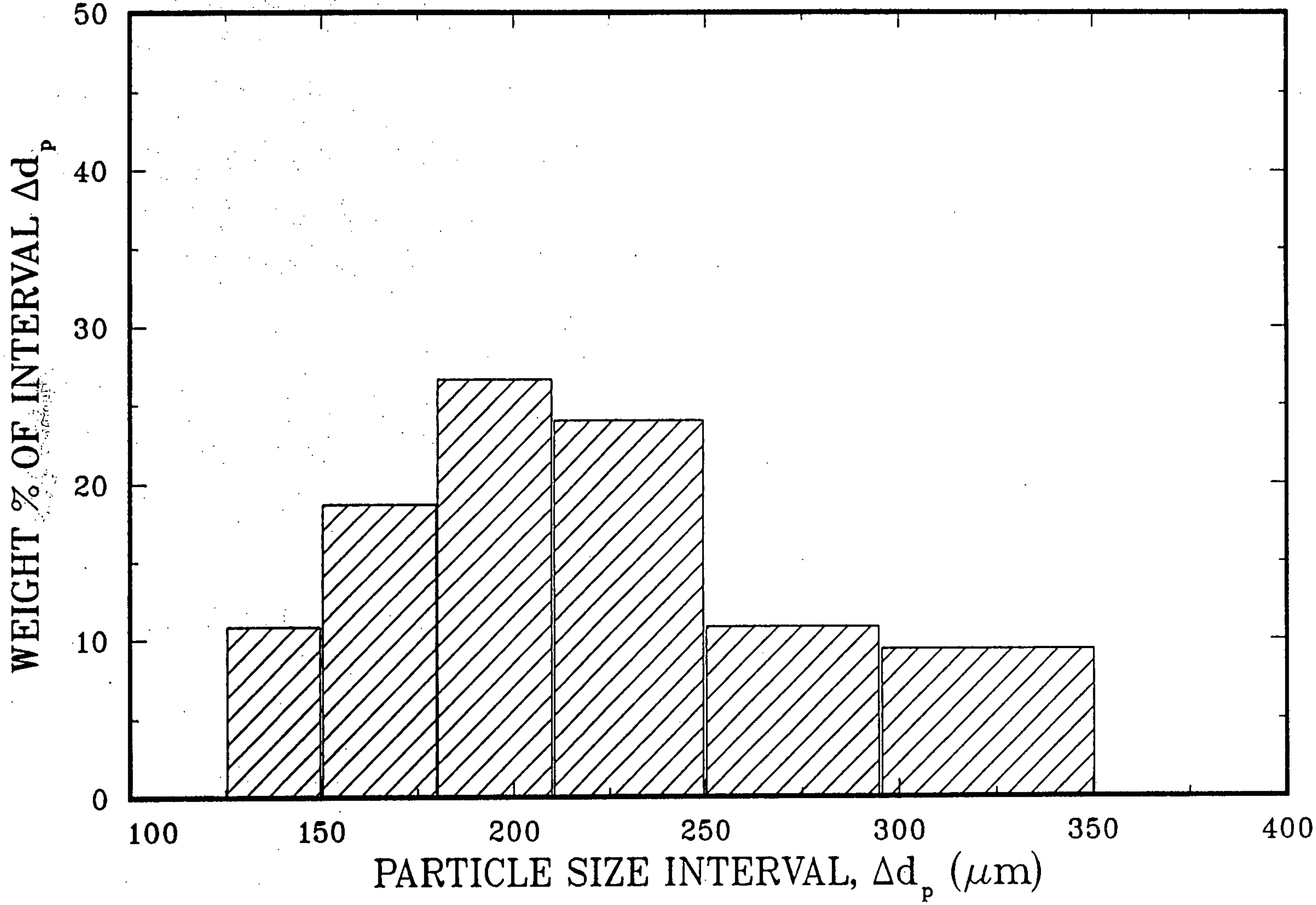

Figure 6.10: Particle size distribution

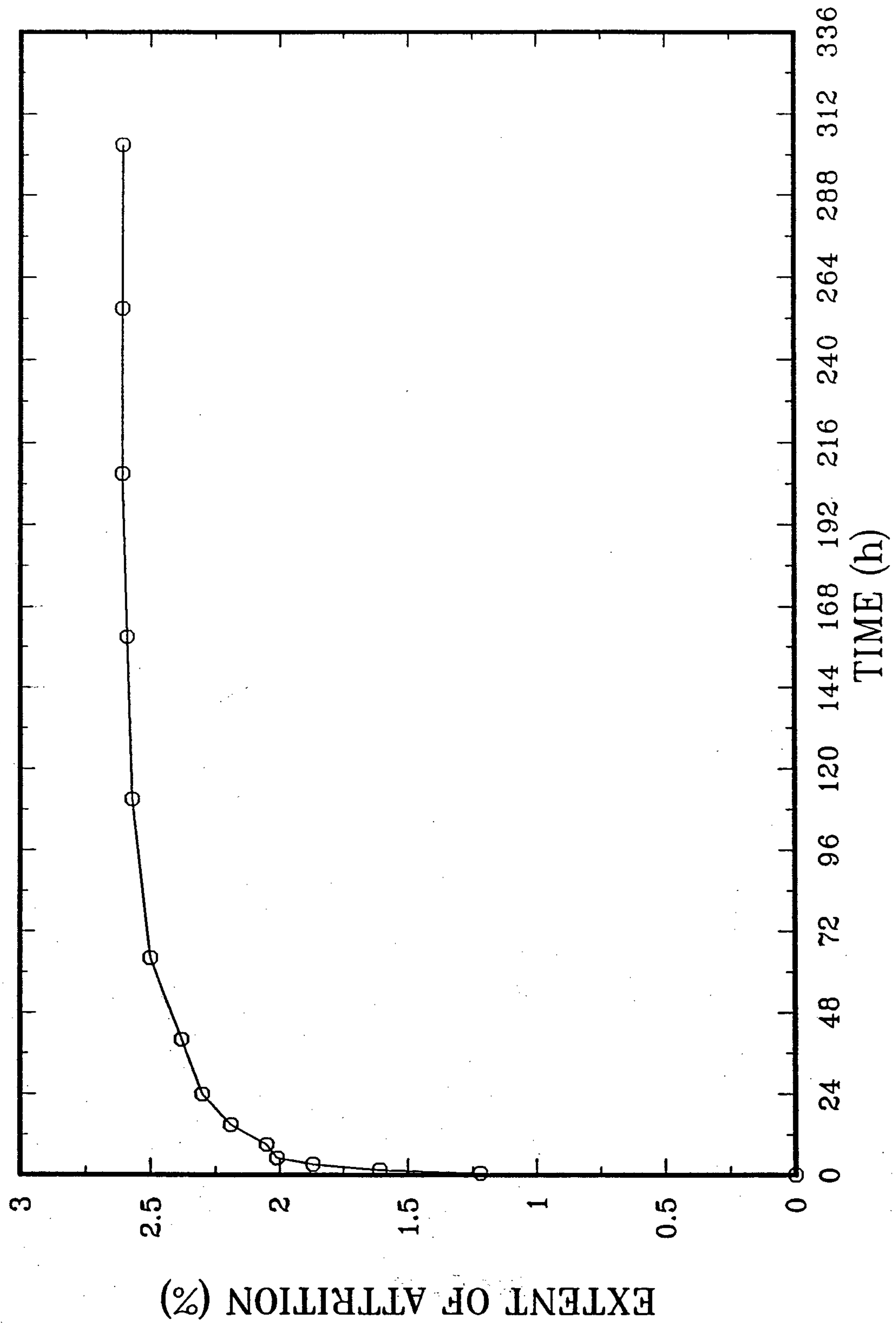

Figure 6.11: Extent of attrition as a function of time

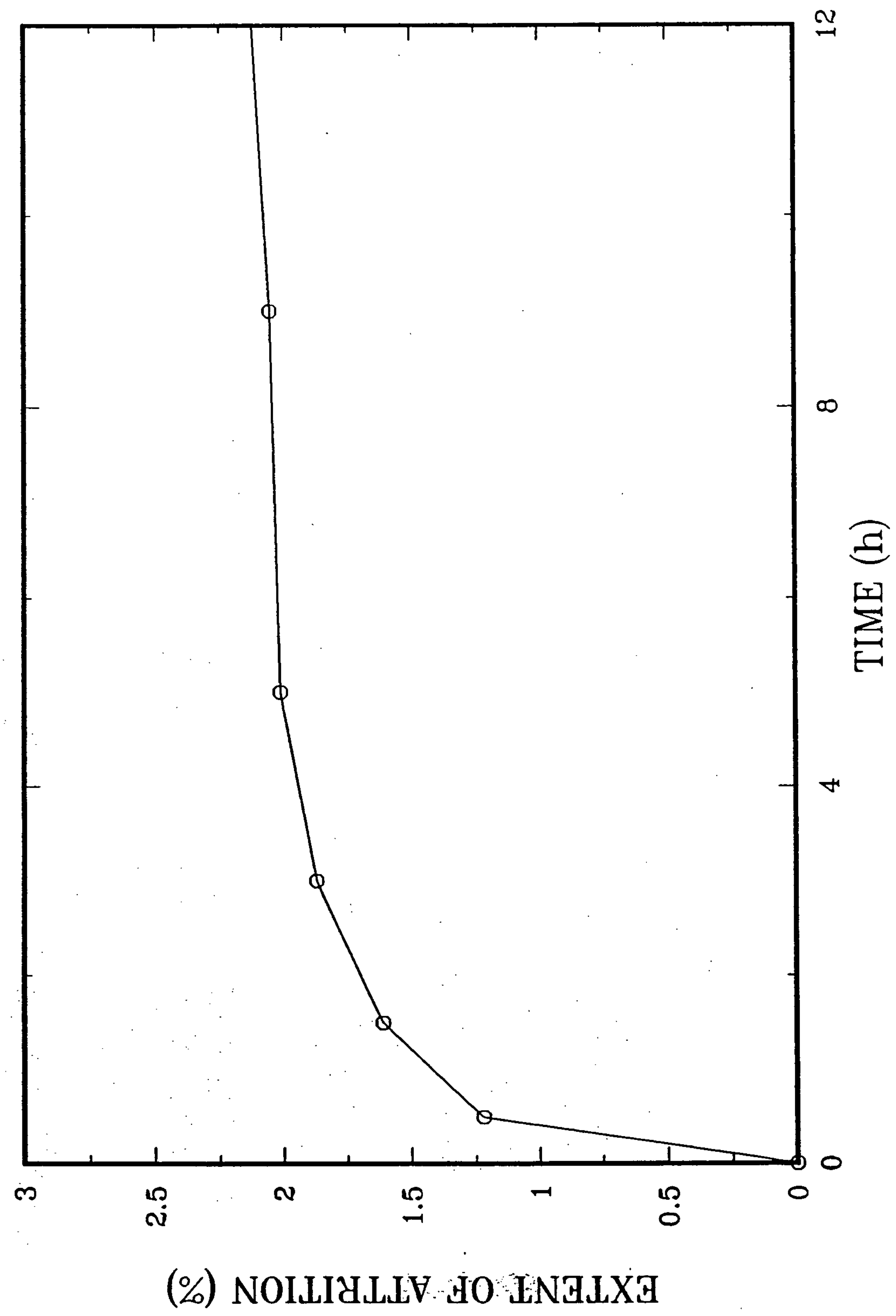

Figure 6.12: Initial extent of attrition (expanded scale)

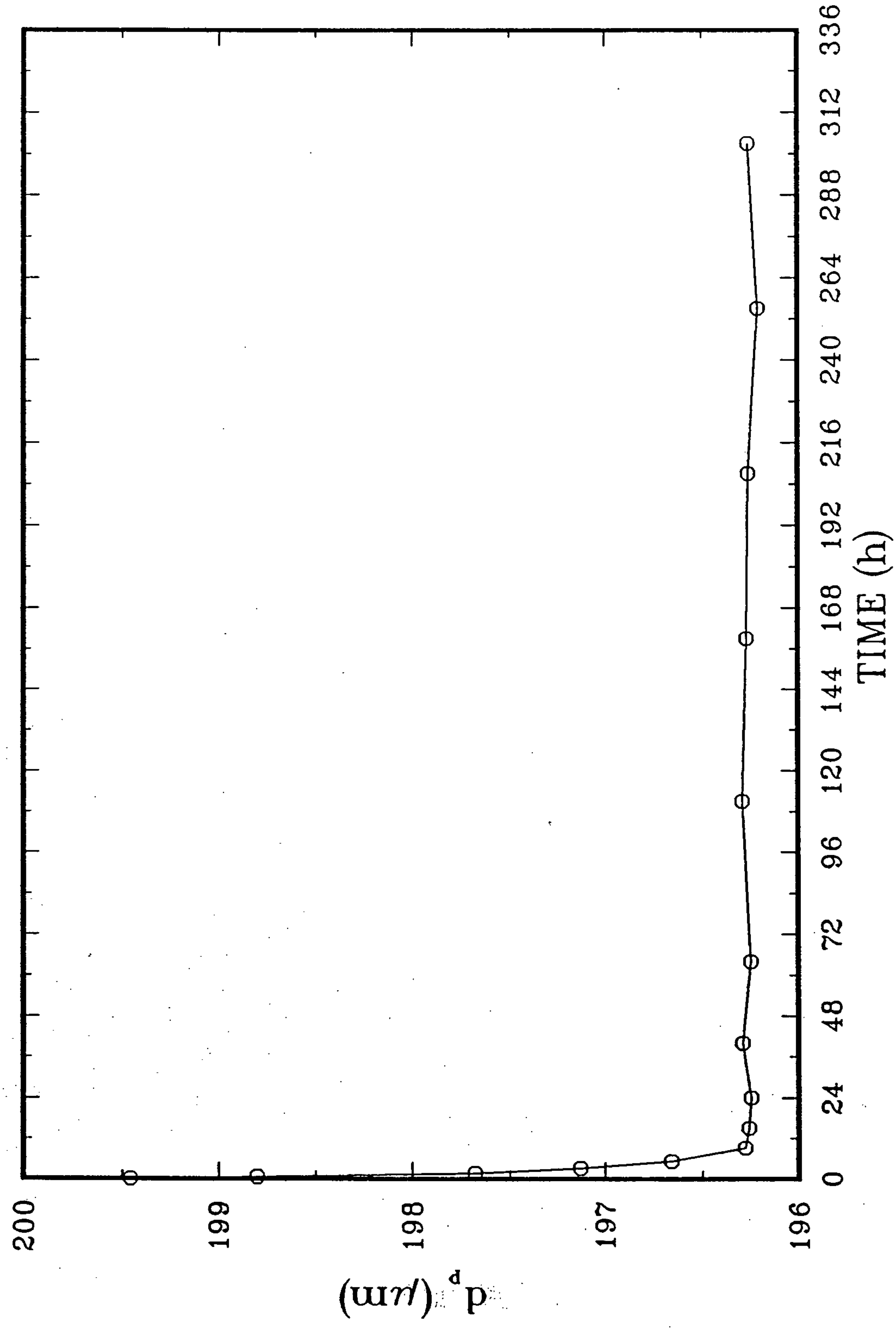

Figure 6.13: Effect of attrition on particle mean diameter

$$RMS\%E = \sqrt{\frac{\sum(dev)^2}{N}} \tag{6.4}$$

where Pre denotes the predicted conversion and Exp denotes the corresponding experimental conversion. N denotes the number of points, $\%dev$ denotes the relative deviation and $RMS\%E$ denotes the root mean square % error. An $RMS\%E$ value of 0 means excellent agreement between model predictions and experimental values whereas $RMS\%E$=100 corresponds to extremely poor predictions. The $\%dev$ and $RMS\%$ errors are included in Table 6.1 for the three sets of data. Values of $RMS\%E$ of less than 3% suggest very good agreement between experimental and predicted conversions. The three sets of data are also plotted in Figure 6.2 which shows good agreement between model predictions and experimental results. In particular, the model clearly follows the sharp fall in conversion in the vicinity of H_2S feed concentration of 800 ppm.

Model predictions as a function of U/U_{mf} are compared with experimental data in Figure 6.4. The experimental conversions are somewhat less than those predicted by the model at low values of feed concentrations. The $RMS\%E$ value of 3.82 for 600 ppm H_2S in the feed is slightly higher than that (i.e. $RMS\%E$=0.83) for 1300 ppm H_2S, but the overall trends are the same and the agreement between model predictions and experimental data is quite reasonable. A better agreement may be noticed for the two sets of data shown in Table 6.2 and plotted in Figure 6.3 where both experimental and predicted conversions increased with increasing temperature. The $RMS\%$ errors for these two sets of data are lower than 1.4%. Typical equilibrium conversions are generally higher than 96% (see Figure 6.3 and Table 3.7). It is obvious that predictions by the two phase bubbling model are far superior to predictions based on equilibrium assumptions.

To predict the performance of the reactor under fouling conditions, a deactivation function was introduced into the rate equation. A deactivation function with hyperbolic dependency on the sulphur content was found to lead to the best model predictions. The theoretical justification for such a function was presented in section 3.5 (i.e. equation 3.92). Values of K_s in equation 3.92 were adjusted to give the model predictions shown in Figure 6.5. A value of K_s=0.08 was found adequate for predicting the sulphur conversions shown in Figure 6.5 and Table 6.4. Hence equation 3.92 may be rewritten as:

$$\Psi = \frac{1}{1 + 0.08\lambda} \tag{6.5}$$

The form of this deactivation function suggests that deposition of sulphur on the catalyst has a retarding effect on the Claus reaction. Unfortunately, the experiments had to be terminated sooner than desired due to the difficulties mentioned earlier and equation 6.5 could not be tested for catalyst sulphur loading higher than 60%.

A final evaluation of model predictions is shown in Figure 6.14. In this graph, conversions predicted by the present bubbling bed model are plotted against the corresponding experimental conversions. The 45° line represents the perfect match between predicted and experimentally determined conversions. Although some of the points deviate, their scatter is close to the 45° line and the agreement is quite reasonable.

6.3 Applicability of the two phase model

The two phase model provides a relationship between the reactor conversion, feed concentration, gas velocity and bed height. A knowldege of any three of these

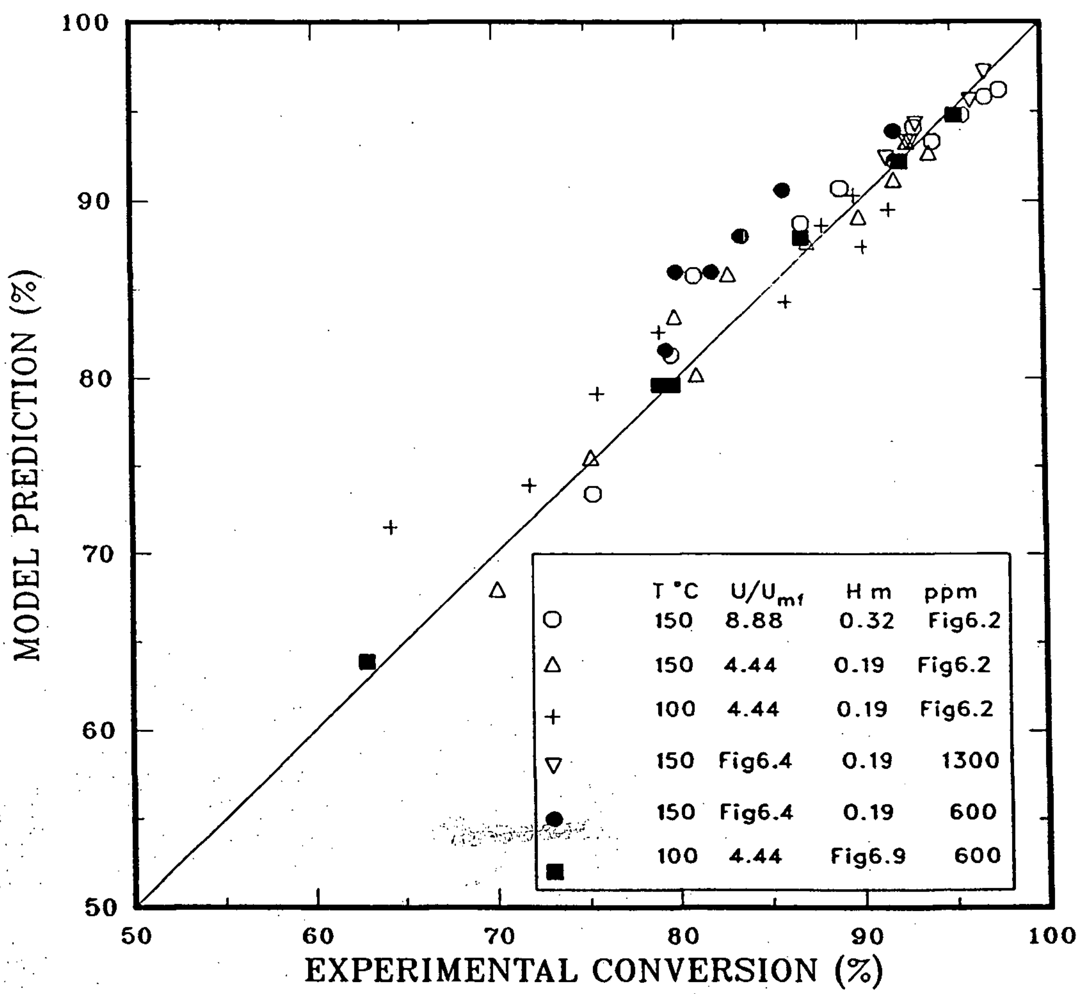

Figure 6.14: Model Prediction vs Experimental conversion

quantities permits the fourth to be calculated, provided the physco-chemical characteristics of all phases and the reaction rates are specified. For scale-up purposes, this model can be applied to solve two primary problems, i.e:

(a) To determine the size of reactor needed to achieve a specific conversion under specified operating conditions.

(b) To calculate, for a given reactor, either the conversion for a specified flow rate and feed concentration or the quantity of gas that can be processed to achieve a given conversion.

Since the number of variables which enter scale-up calculations is large, it is not possible to present several design charts. The following procedure shows how the two phase model may be applied for the design of industrial units and how to predict the consequences of changes in variables.

6.3.1 Use of Two Phase Model in Reactor Design:

(a) For a given gas flow rate, Q, the superficial gas velocity is selected such that $U_{mf} < U < U_t$, where U_t denotes the terminal velocity of the smallest catalyst particles which should be retained in the bed. U_t can be determined from equations available in the literature (see Kunii and Levenspiel, 1969). Other criteria are needed to avoid gas channeling and catalyst slugging. These criteria are presented in section (e) below.

(b) The diameter of the cylindrical reactor is calculated from: $D^2 = 4Q/\pi U$.

(c) Using the two phase model (Equations 3.22, 3.42, 3.44 and 3.45), Figure 6.15 can be obtained. The calculation is staightforward and a computer programme with input variables H_s, U, U_{mf}, d_p, etc. is presented in Appendix B.

Figure 6.15 and Table 6.6 show that the conversion decreases with increasing bed diameter. This trend to is due the increased bubble diameter in large beds and hence increased gas by-passing. The Mori and Wen (1975) equation is used in this work to predict the bubble diameter. It should be noted that this equation is based on more than 400 experimental points and that it should only be applied for $D < 1.3$m, $60 < d_p < 450\mu$m, $0.005 < U_{mf} < 0.2$ m/s and $U - U_{mf} \leq 0.48$m/s.

(d) Once the conversion versus bed diameter plots are available, the static and expanded bed heights required to achieve the desired conversion can be looked up.

(e) The final choice of U, D and H should satisfy the following criteria:

(*i*) U should not exceed the minimum slugging velocity defined as:

$$U_{ms} = U_{mf} + 0.07\sqrt{gD}.$$

(*ii*) The aspect ratio H/D should not exceed 3.5 to avoid slugging.

6.3.2 Choice of particle size

The choice of catalyst particle size affects not only the reactor conversion but also catalyst entrainment. The effect of particle size on conversion may be deduced by examining the relationship between U_{mf} and d_p and the two phase theory. Equation 2.11 shows that increasing the mean particle diameter raises the minimum fluidization velocity which, in turn, increases the gas flow from the dilute into the dense phase. Since the dense phase gas is in intimate contact with the catalyst particles, it follows that increasing the particle size should also increases reactor conversion. However; increasing d_p reduces the bed expansion (see Section 2.2.5),

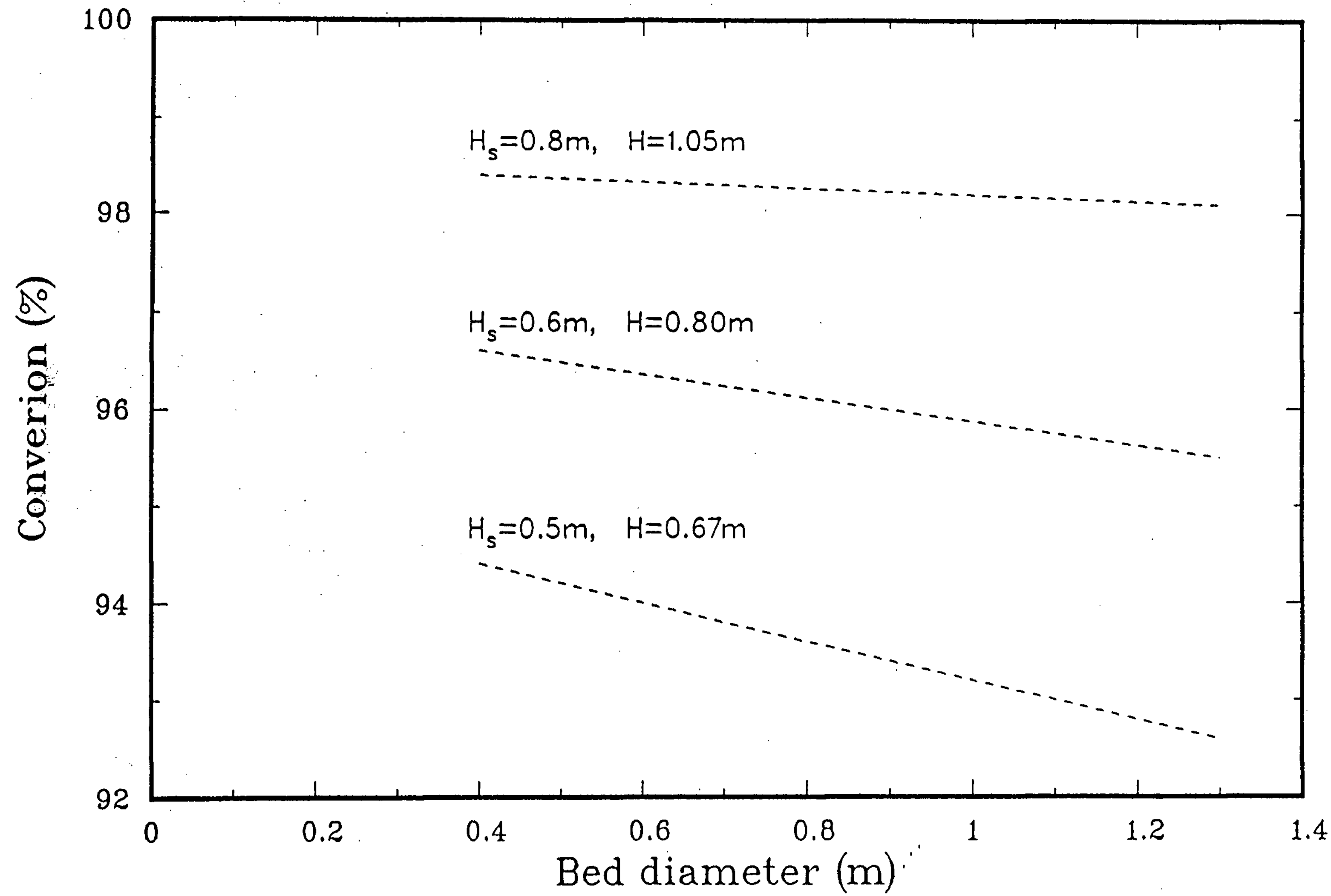

Figure 6.15: Model predictions for large reactors (U=0.25m, d_p=195μm, t=100° C,H_2S=600ppm, catalyst: s-501

lowers the gas residence time and thus causes a fall in conversion. Section 2.2.5 and Equation 2.8 show that the particle size affects the interrelated hydrodynamic parameters in a complex manner.

The primary advantage of using large particle size is that their terminal velocity is high and the likelihood of particle entrainment is reduced as the terminal velocity is increased. The loss of valuable catalyst is minimized and the cost of gas cleaning equipment to reduce pollution is reduced.

However, large particles suffer from the disadvantage that the diffusional resistance encountered by the reacting species in the pores of the catalyst particles is increased which, in turn, lowers the conversion. However, calculations presented in Section 3.5, indicate that diffusion resistance was negligible in this work.

Since the present two phase model yielded results which agreed well with experimental measurements, the model may be used to explore the effect of changing particle size. The results should be reliable, even though corresponding experiments were not performed except for $d_p = 195\mu m$. The model predictions for various particle sizes are presented in Figure 6.16 and Table 6.7. It is clear that in all cases (a to f) that the predicted conversion improves with decreasing particle diameter. The improvement is attributed to the increased residence time which results from the expanded bed height, i.e. H/U rises as shown by Figure 6.17. Curves d, e and f in Figure 6.16 show increases in conversion for $d_p > 320\mu m$. These increases occur because U_{mf} increases with increasing particle size and ultimately U/U_{mf} approaches unity and the bed approaches fixed bed conditions. Hence conversions are high even though H/U is low. On the other hand; for $d_p < 160\mu m$, the increase in the predicted conversion with deacreasing particle diameter is very gradual despite the increasing H/U. U_{mf} decreases substantially with decreasing d_p for particles less than about $160\mu m$ in diameter. This results in dramatic increases in U/U_{mf} as shown by Figure 6.18 and consequently, the effect of increasing H/U is counter balanced by the effect of increasing U/U_{mf}.

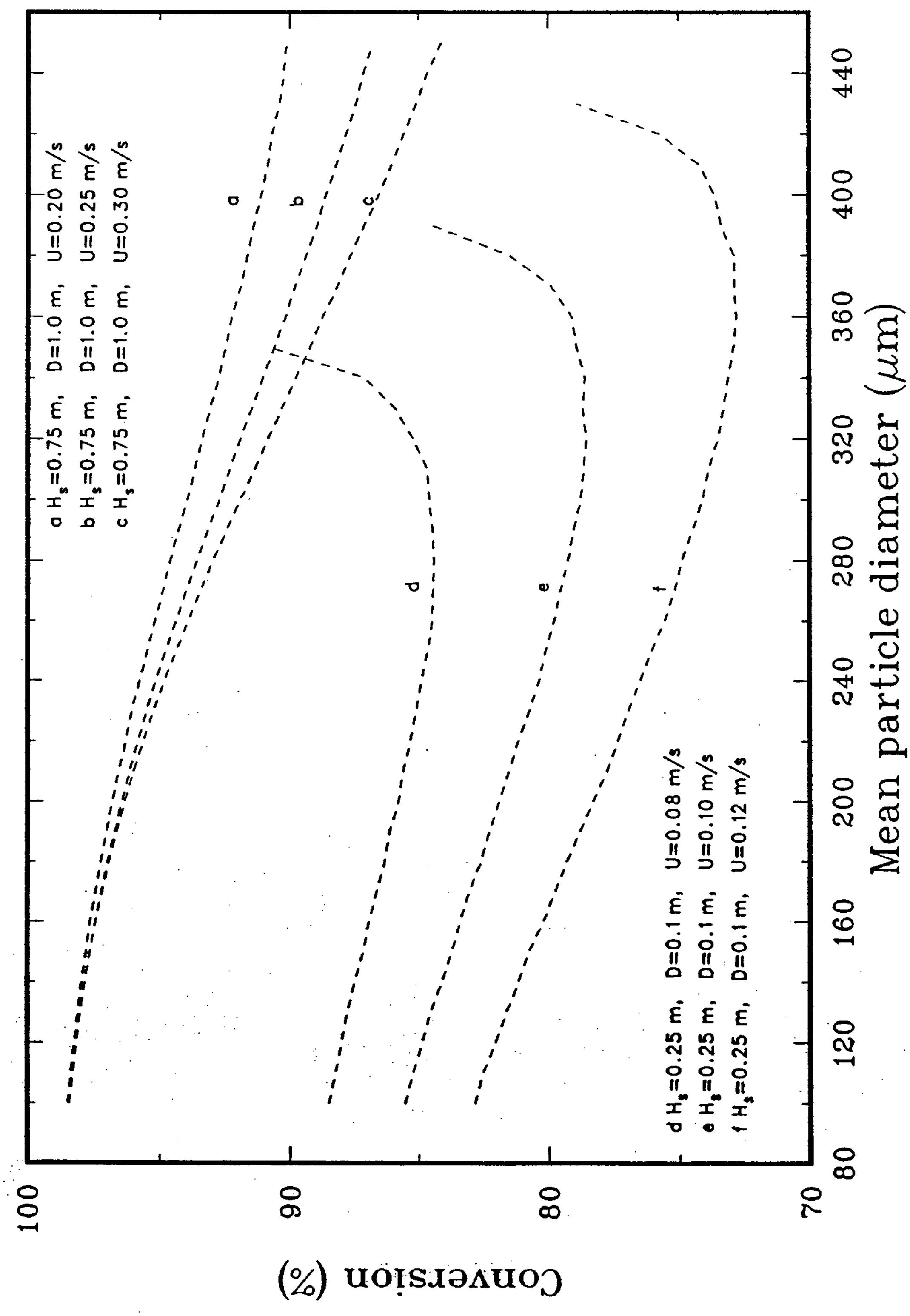

Figure 6.16: Effect of particle size as predicted by the two phase model (T=100° C, H_2S=400 ppm)

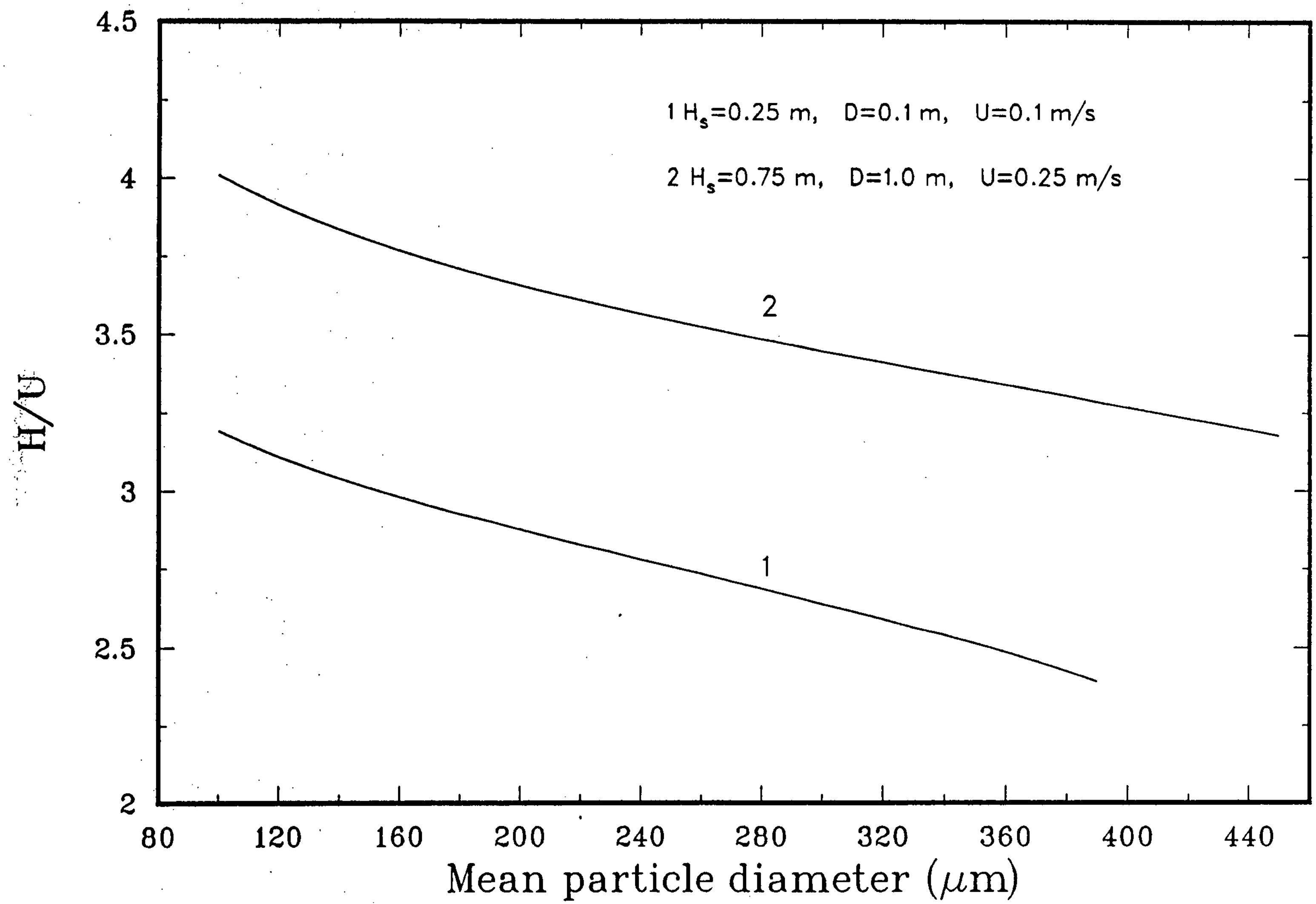

Figure 6.17: Predicted residence time of gas as a function of mean particle diameter

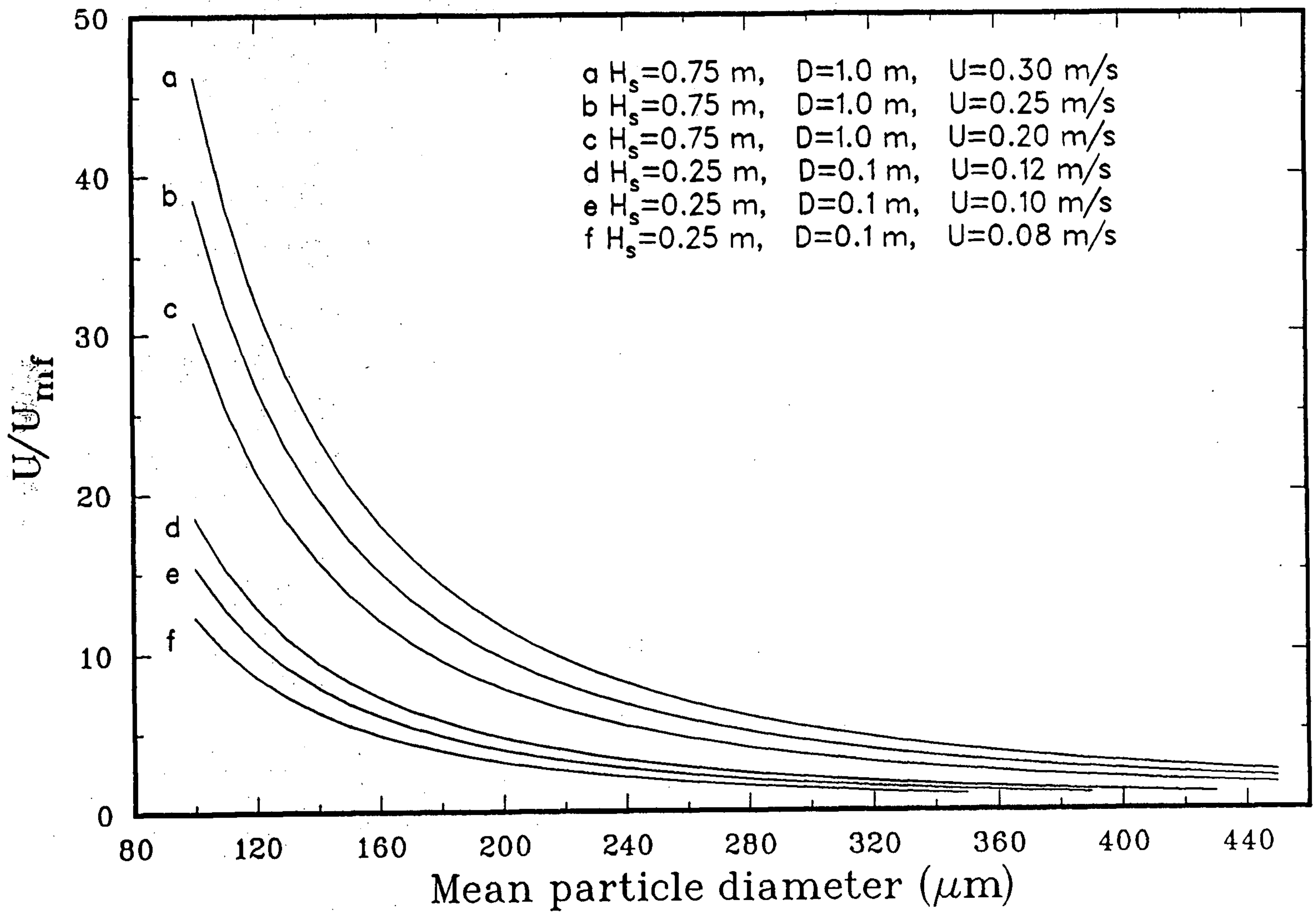

Figure 6.18: Predicted U/U_{mf} as a function of mean particle diameter

Table 6.6: Model predictions as a function of bed dimensions

$U = 0.25m$, $T = 100°C$, $H_2S = 600ppm$

Q	(m^3/h)	108	180	252	360	468	576	720	864	1008	1188
D	(m)	0.40	0.50	0.60	0.70	0.80	0.90	1.00	1.10	1.20	1.30
H_s (m)	H (m)					χ (%)					
0.1	0.15	33.1	32.7	32.5	32.3	32.1	31.9	31.7	31.5	31.4	31.4
0.2	0.28	62.6	62.1	61.3	60.8	60.3	60.0	59.5	59.1	58.8	58.6
0.3	0.42	81.0	80.5	79.9	79.4	78.8	78.4	78.0	77.6	77.2	76.9
0.4	0.55	90.1	89.7	89.3	89.0	88.6	88.3	88.0	87.8	87.4	87.3
0.5	0.67	94.4	94.2	94.0	93.8	93.6	93.4	93.2	93.0	92.8	92.6
0.6	0.80	96.6	96.5	96.4	96.2	96.1	96.0	95.9	95.7	95.6	95.5
0.7	0.92	97.8	97.7	97.6	97.6	97.5	97.4	97.3	97.3	97.2	97.1
0.8	1.05	98.4	98.4	98.4	98.4	98.3	98.3	98.2	98.1	98.1	98.1
0.9	1.17	98.9	98.9	98.9	98.8	98.8	98.8	98.7	98.7	98.7	98.6

D: bed diameter, H_s: static bed height, H: expanded bed height, Q: gas flow rate, U: superficial velocity, χ: conversion.

Table 6.7: Effect of particle diameter on conversion as predicted by the two phase model

d_p (μm)	Conversion (%)					
	(a)	(b)	(c)	(d)	(e)	(f)
100.	88.48	85.53	82.82	98.46	98.40	98.44
110.	88.23	85.22	82.53	98.36	98.28	98.33
120.	87.99	84.86	82.05	98.23	98.15	98.18
130.	87.77	84.56	81.64	98.09	98.00	98.03
140.	87.47	84.11	81.17	97.96	97.83	97.86
150.	87.15	83.73	80.79	97.79	97.64	97.65
160.	86.92	83.40	80.22	97.63	97.44	97.43
170.	86.63	83.05	79.77	97.43	97.22	97.18
180.	86.31	82.60	79.29	97.23	96.97	96.91
190.	86.12	82.27	78.80	97.01	96.70	96.63
200.	85.78	81.89	78.29	96.79	96.43	96.32
210.	85.59	81.52	77.77	96.56	96.13	95.98
220.	85.31	81.16	77.36	96.28	95.80	95.60
230.	85.07	80.74	76.96	96.04	95.48	95.22
240.	84.89	80.36	76.49	95.75	95.13	94.80
250.	84.63	80.11	76.06	95.45	94.76	94.35
260.	84.47	79.77	75.56	95.16	94.36	93.90
270.	84.43	79.53	75.16	94.86	93.98	93.90
280.	84.39	79.23	74.88	94.59	93.57	93.43
290.	84.45	79.03	74.45	94.27	93.15	92.96
300.	84.58	78.75	74.10	93.94	92.71	92.42
310.	84.64	78.64	73.86	93.65	92.30	91.90
320.	85.21	78.53	73.50	93.36	91.89	91.35
330.	85.89	78.67	73.28	93.07	91.46	90.84
340.	87.07	78.58	73.10	92.73	91.03	90.30
350.	90.86	78.90	72.88	92.45	90.59	89.76
360.		79.08	72.78	92.20	90.15	89.20
370.		79.87	72.87	91.87	89.79	88.70
380.		81.47	72.86	91.62	89.35	88.12
390.		84.50	73.38	91.38	88.92	87.62
400.			73.62	91.10	88.59	87.07
410.			74.20	90.83	88.18	86.52
420.			75.73	90.69	87.79	86.03

(a): $U = 0.08 m/s$, $H_s = 0.25 m$, $D = 0.1 m$. (b): $U = 0.10 m/s$, $H_s = 0.25 m$, $D = 0.1 m$. (c): $U = 0.12 m/s$, $H_s = 0.25 m$, $D = 0.1 m$. (d): $U = 0.20 m/s$, $H_s = 0.75 m$, $D = 1.0 m$. (e): $U = 0.25 m/s$, $H_s = 0.75 m$, $D = 1.0 m$. (f): $U = 0.30 m/s$, $H_s = 0.75 m$, $D = 1.0 m$.

6.4 ERROR ANALYSIS

The experimental sulphur conversion, χ, was calculated from the readings of the analytical instruments according to equation 6.1. For every run, a set of instrument readings was recorded as explained in section 6.1.2. These measurements may contain instrument errors which could lead to some error in the experimental conversion. This error can be estimated from the following relation:

$$\Delta\chi = \sum_{i=1}^{i=4}\left(\frac{\partial\chi}{\partial y_i}\right)_{y_j}\Delta y_i \tag{6.6}$$

where y_1, y_2 denote the volume fraction of H_2S and SO_2 in the reactor effluent stream and y_3, y_4 denote the corresponding fractions in the feed. The partial derivatives in equation 6.6 can be obtained by differentiating equation 6.1 i.e:

$$\frac{\partial\chi}{\partial y_1} = \frac{\partial\chi}{\partial y_2} = -\frac{(1-y_3-y_4)}{(y_3+y_4)(1-y_1-y_2)^2}$$

$$\frac{\partial\chi}{\partial y_3} = \frac{\partial\chi}{\partial y_4} = \frac{y_1+y_2}{(1-y_1-y_2)(y_3+y_4)^2}$$

Assuming $\Delta y_1 = -\delta_1$, $\Delta y_2 = -\delta_2$, $\Delta y_3 = +\delta_1$ and $\Delta y_4 = +\delta_2$ leads to the estimation of the maximum error in conversion. Dividing equation 6.6 by equation 6.1 and substituting for Δy_i's gives an expression for the relative error denoted by δ (i.e $\delta = \Delta\chi/\chi$):

$$\delta = \frac{[(y_1+y_2)+(y_3+y_4)] - [(y_1+y_2)^2+(y_3+y_4)^2]}{(y_3+y_4)[1-(y_1+y_2)][(y_3+y_4)-(y_1+y_2)]}(\delta_1+\delta_2) \tag{6.7}$$

Values for δ_1 and δ_2 are chosen as the reliability of the instruments reported by the manufacturers. The manual for the SO_2 analyser states that the instrument reading is reliable to within ±0.5 ppm. The H_2S analyser was designed to detect concentration ranges between 1 to 1500 ppm with a sensitivity of 3 ppm. Hence δ_1 and δ_2 can be assumed as (volume fraction units) 3×10^{-6} and 0.5×10^{-6}, respectively.

The relative error estimated from equation 6.7 is presented in Table 6.8 as a function of feed concentration. The relative error for the runs at $100°C$ ranged from ±0.23 to $\pm1.63\%$. Although the error values are small, Table 6.8 shows that the smaller the feed concentration, the larger the relative error. This trend may be expected since small fluctuations in instrument responses to dilute samples were noticed. The fluctuations in the H_2S and SO_2 outlet concentrations were within ±4 ppm (see Figure 6.19). The fluctuations in the total outlet concentrations (i.e. outlet concentration of H_2S + SO_2) were within ±2 ppm. The fluctuation in conversion ranged from $\pm0.44\%$ (for feed containing 300 ppm H_2S and 150 ppm SO_2) to $\pm0.1\%$ (for feed containing 1300 ppm H_2S and 650 ppm SO_2). Minimization of these fluctuations were achieved by rigorously calibrating each instrument with gas samples of various degrees of dilution (see Section 5.2.2). Bonsu (1981) used these instruments to measure concentrations from samples rich in H_2S and SO_2. He reported an error ranging from ±0.5 to $\pm1.0\%$. Hence a conservative value of the error in this work can be taken as $\pm1.6\%$ (see Table 6.8). The reliability of the results may be tested statistically. As shown in Appendix A, runs for H_2S feed concentrations of 600 and 1300 ppm were duplicated at three temperatures (i.e. 100, 130 and $150°C$) and were examined by the t and F tests. The t-test at 95% level showed that confidence limits of ±1.61 may be assigned to the conversion. This value agrees with the error estimated from equation 6.5. Analysis of the variance for these runs are also presented in Appendix A. The F-test showed, for an increase in the H_2S feed concentration (e.g. from 600 to 1300 ppm, see column 1 of Table A.2) that there is more than a 999 in 1000 chance that the associated increase in conversion (e.g. at $100°C$, see column 2 of Table A.2) from 79.4 to 89.4 is possible. For the increase in temperature from 100 to $150°C$ (row 1 of Table A.2), this test showed there is only a 1 in 100 chance that the increase in conversion (e.g. at 1300 ppm H_2S from 89.4 to 93.1, see row 4 of Table A.2) may be explained on the basis of scatter in data.

6.5 PRACTICAL IMPLICATIONS OF FLUIDIZED BED CLAUS REACTORS

Based on the model predictions and experimental findings, it is evident that thermodynamic conversion efficiencies were not achieved in the present fluidized bed reactor. Furthermore, sulphur condensation led to a substantial decline in reactor performance. Operational problems were encountered when catalyst sulphur loadings exceeded about 50%. Because experimental tests were performed in batch mode, regeneration of the catalyst in this study was carried out in situ. Heating the bed at $300°C$ in the presence of H_2S allowed keeping the catalyst activity at high levels. Samples of the regenerated catalyst were further tested for sulphur content in an oven at $400°C$. The test results indicated no traces of sulphur. In an industrial unit, the catalyst must be regenerated continuously to keep high levels of conversion and to prevent defluidization. Circulation of the catalyst between the reactor and a regenerating unit was tested by Bonsu (1981) who reported the smooth operation of the small scale apparatus.

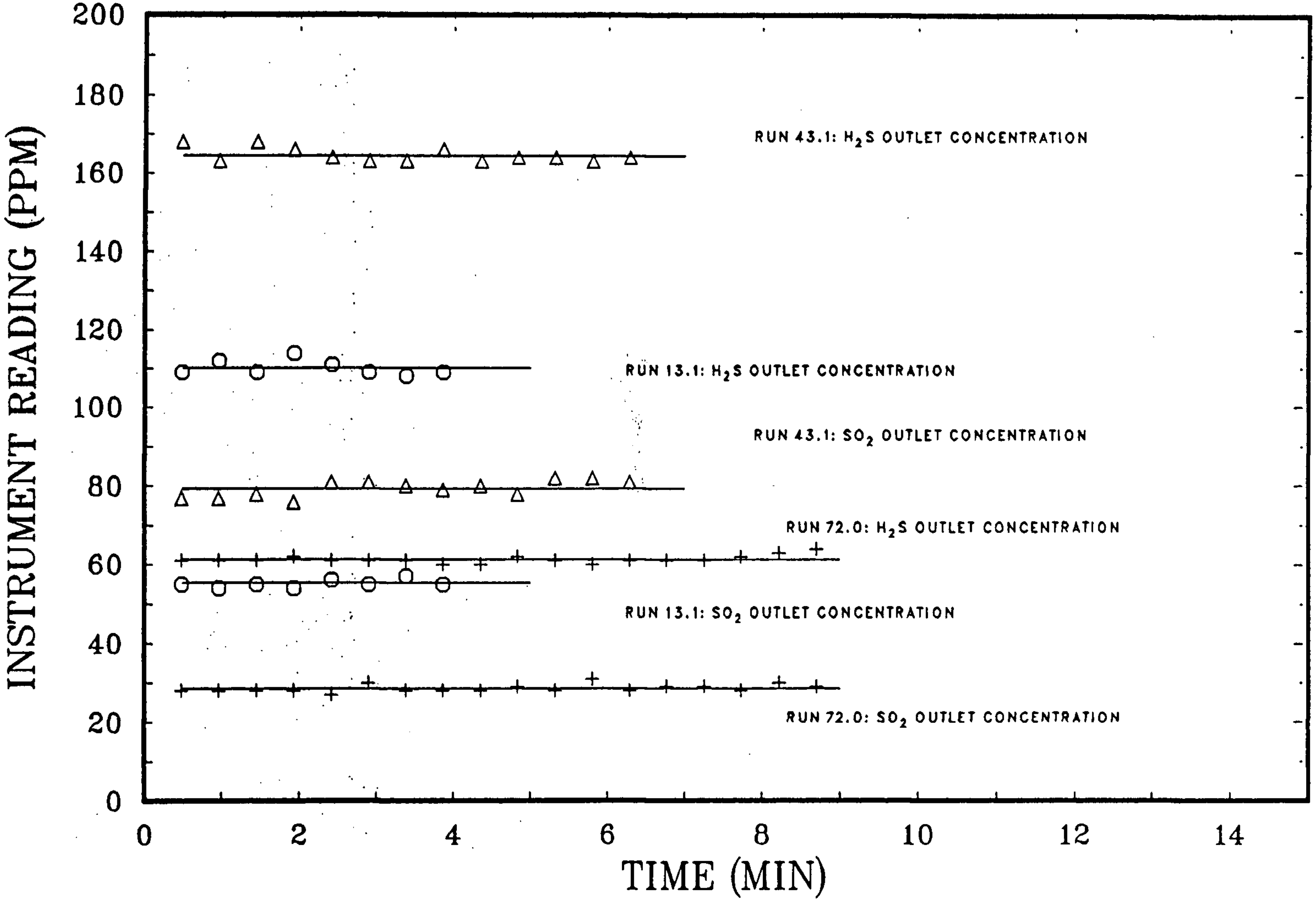

Figure 6.19: Concentrations of hydrogen sulphide and sulphur dioxide in the effluent gas as a function of time

Table 6.8: Relative error as a function of H_2S concentration in the feed

$T = 100°C$, $U/U_{mf} = 4.44$, H_s=0.19m

y_1 (ppm)	300	400	500	600	800	1000	1100	1300
χ (%)	64.3	71.9	75.6	79.4	86.3	90.2	88.9	89.7
δ (%)	1.63	1.06	0.79	0.61	0.40	0.28	0.27	0.23

Chapter 7

CONCLUSIONS AND RECOMMENDATIONS

7.1 CONCLUSIONS

The conversion of hydrogen sulphide and sulphur dioxide into elemental sulphur has been studied in a bubbling fluidized bed reactor. This study has shown that equilibrium conversions could not be achieved within the ranges of the concentration, temperatures and bed heights investigated. The performance of the equipment and associated safety devices was very good.

From the experimental and analytical results presented in chapter 6, the following specific conclusions may be drawn:

(a) At the low temperatures and feed concentrations studied in this work, the sulphur conversions are appreciably lower than the thermodynamic conversions on account of kinetic limitations.

(b) Sulphur conversions in fluidized beds are reduced by decreasing the feed concentration and temperature and increasing the superficial gas velocity.

(c) Conversions are substantially improved with bed height. However, there exist bed heights beyond which only a slight increase in conversion is possible.

(d) Sulphur condensation occurs inside the pores of the catalyst. This condensation causes catalyst deactivation which leads to significant reductions in conversion. The activity of the catalyst can be restored by vapourizing the condensed sulphur. Heating the fluidized bed to $300°C$ in the presence of H_2S was a successful method to return the activity of the catalyst to high levels.

(e) Appreciable amounts of condensed sulphur result in the agglomeration of the catalyst particles. Defluidization of the bed may be avoided by continuous catalyst regeneration.

(f) The performance of the fluidized bed Claus reactor under kinetically limiting conditions can be predicted using a two phase bubbling model.

(g) Catalyst attrition is negligibly small thereby indicating the suitability of the Kaiser S-501 alumina for fluidized bed operation.

7.2 RECOMMENDATIONS

(a) Runs should be undertaken to investigate the effect of moisture in the feed on the performance of fluidized bed Claus reactors. Results from such runs would simulate industrial Claus plants where water vapour formed in the furnace off-gas enters the catalytic stages.

(b) Additional runs are recommended to obtain data using continuous catalyst circulation through the reactor. Results from such studies would be useful in the design of industrial units.

(c) Ghosh and tollefson (1985) studied the direct oxidation of dilute H_2S bearing gas streams over activated carbon. They found that conversion decreased due to catalyst fouling. Exploratory studies should therefore be conducted using a continuously operating fluidized bed. If successful, such an arrangement could be of importance for sulphur recovery from gas streams with very low H_2S concentration.

(d) Pilot plant studies should be carried on fluidized bed Claus reactors to obtain data useful in the scale-up and design of full-scale industrial reactors. The pilot plant should have a diameter larger than 1 m and the effects of feed gas compositon, high gas flow rate and particle size should be studied.

Nomenclature

A	Reactor cross sectional area, m^2.
$\mathcal{A}$	Extent of attrition, $kg/kg\%$.
A_f	Arrhenius pre-exponential factor.
a_b	Bubble interfacial area, m^2/m^3.
a_p	Particle interfacial area, m^2/m^3.
A_1 to A_7	Constants defined by equations 3.24 to 3.28 and 3.38 to 3.39.
a_1	constant defined by equation 3.65, $(kmole/kcal)$.
a_2	constant defined by equation 3.65.
B, $B1$, $B2$	Instrument constants
C_{Ab}	H_2S dilute phase concentration, $kmol/m^3$.
C_{Ad}	H_2S dense phase concentration, $kmol/m^3$.
$C_{Ab,0}$	H_2S dilute phase concentration at $z = 0$, $kmol/m^3$.
$C_{Ad,0}$	H_2S dense phase concentration at $z = 0$, $kmol/m^3$.
C_{H_2S}	H_2S concentration, $kmole/m^3$.
$C_{H_2S,g}$	H_2S bulk concentration, $kmole/m^3$.
$C_{H_2S,0}$	H_2S concentration in feed gas, $kmole/m^3$.
$C_{mS.s}$	Surface concentration of active sites fouled by m. layers of sulphur, *# of active sites fouled/kgcat.*
C_t	Surface concentration of active sites, *# of active sites/kgcat.*

C_v	Surface concentration of active sites completly free of sulphur, *# of active sites/kgcat.*
C_0	Dimensionless feed concentration.
C_1	Dimensionless concentration of H_2S in dilute phase.
C_2	Dimensionless concentration of H_2S in dense phase.
$C_{2,0}$	Dimensionless initial dense phase concentration.
D	Bed diameter, m.
Da_0	Damköhler number.
d_b	Bubble diameter, m.
d_{bm}	Maximum bubble diameter, m.
d_{bo}	Initial bubble diameter, m.
D_e	Effective diffusivity, m^2/s.
D_g	Diffusivity, m^2/s.
D_L	Axial dispersion coefficient, m^2/s.
d_p	Particle diameter, m.
d_{p_i}	Particle diameter in size interval i, m.
D_r	Radial dispersion coefficient, m^2/s.
E	Activation energy, $kcal/mole$.
E^*	Desorption energy, $kcal/mole$.
F	Instrument flourescence.
f	Total molar flow rate, $kmole/s$.
$F_{H_2S,0}$	Molar flow rate of H_2S into reactor, $kmole/s$.
f_1	Molar flow rate of SO_2 into reactor, $kmole/s$.
f_2	Molar flow rate of N_2 into reactor, $kmole/s$.
g	Gravitational constant, m/s^2.

H	Expanded bed height, m.
H_{mf}	Bed height at minimum fluidization, m.
H_s	Static bed height, m.
K	Instrument Extenection coefficient.
K_e	Equilibrium constant, $(atm)^{-1}$.
K_s	Catalyst to sulphur ratio, *kgcat/kgS*.
k_g	Mass transfer coefficient in packed bed, m/s.
k_m	Rate constant governing catalyst fouling, s^{-1}
k_q	Interphase mass transfer coefficient, $m/s/m^2$.
k_v	Reaction rate constant per unit volume of catalyst, $(kmol/m^3)^{-0.5}/s/m^3cat$.
k_w	Reaction rate constant per unit mass of catalyst, $(kmol/m^3)^{-0.5}/s/kgcat$.
n	Order of reaction.
M	Number of sulphur layers on active sites.
m	Layer index.
Pe_L	Peclet number based on axial dispersion.
Pe_r	Peclet number based on radial dispersion.
P_{H_2O}	H_2O partial pressure, $mm\ Hg$.
P_{H_2S}	H_2S partial pressure, $mm\ Hg$.
$P_{(H_2S)f}$	Concentration of H_2S, *ppm*.
P_{SO_2}	SO_2 partial pressure, $mm\ Hg$.
P_{sr}	Pressure inside rotameter, *psia*.
P_{ss}	Standard state pressure, *psia*
R	Gas constant, $kcal./kmol/K$.
$R_{mS.s}$	Rate of formation of active sites fouled by m layers of sulphur, *# of active sites fouled/kgcat.*

r	Ratio of surface concentrations.
r_b	Bubble radius, m
r_c	Cloud radius, m
r_{H_2S}	Disappearance rate of hydrogen sulphide, $(kmol/m^3)/s/kgcat$.
q	Bubble through flow, m^3/s.
Q_b	Volumetric flow rate of dilute phase gas, (m^3/s).
Q_{N_2}	N_2 flow rate, mL/min.
Q_{H_2S}	flow rate of mixture H_2S/N_2, mL/min.
Q_i	Volumetric flow rate of gas i, $\mathrm{m}^3/\mathrm{min}$.
Q_{SO_2}	flow rate of SO_2/N_2 mixture, mL/min.
Q_{sr}	Volumetric flow rate inside rotameter, mL/min.
Q_{ss}	Volumetric flow rate at standard state, mL/min.
T	Temperature, K.
T_r	Temperature inside rotameter, K.
T_{ss}	Temperature at standard state, K.
U	Superficial gas velocity, m/s.
u_b	Bubble velocity, m/s.
U_e	Interstitial superficial gas velocity in dense phase, m/s.
U_{mf}	Superficial gas velocity at minimum fluidization, m/s.
V_b	Volume of bubble. m^3.
V_w	Volume of bubble wake, m^3.
x	Variable defined by equation 3.16.
x_0	Value of x at reactor inlet.
x_1	value of x at reactor outlet.
Y_{H_2S}	Volume fraction of H_2S in the H_2S/N_2 cylinder.

Y_{SO_2}	Volume fraction of SO_2 in the SO_2/N_2 cylinder.
y_{in}	Volume fraction of $H_2S + SO_2$ in feed stream.
y_{out}	Volume fraction of $H_2S + SO_2$ in effluent gas.
z	Height from distributor, m.

Greek letters

α	Dimensionless interphase transfer coefficient.
$\bar{\alpha}$	Ratio of bubble velocity to minimum fluidizatoin velocity.
β_1, β_2	Modified dimensionless rate constants (defined by Eq's 3.12 and 3.13).
γ	Constant, $\gamma = (\beta_2/\beta_1)^{\frac{1}{3}}$.
ΔG	Free energy difference, $kcal/kmol$.
ΔS	Entropy difference, $kcal/kmol/K$.
δ	Relative error in experimental conversion
δ_1, δ_2	Errors in the readings of the H_2S and SO_2 analysers, respectively, ($vol.\%$)
ϵ_b	Bed volume fraction occupied by dilute phase, m^3/m^3.
ϵ_{mf}	Voidage at minimum fluidization, m^3/m^3.
ζ	Tortuosity factor.
η	External effectiveness factor
θ	Angle in spherical coordinates.
$\bar{\theta}$	Particle fractional porosity.
λ	Catalyst sulphur content, $kgS/kgcat\,\%$.

λ_0	Mass of sulphur monolayer per active site, $kgS/active\ site$.
Λ	Function defined by equations 3.30 and 3.31.
Λ_r	Real part of Λ.
Λ_i	Imaginary part of Λ.
μ_g	Gas viscosity, Ns/m^2.
ν	Extent of reaction, $kmole/s$.
ξ	Dimensionless height .
ρ_g	Gas density, kg/m^3.
ρ_p	Particle density, kg/m^3.
ϱ_i	Specific density of gas i relative to air density.
Φ	Thiele modulus.
ϕ	Fraction of sites fouled by sulphur.
ϕ_b	Volume of solids in dilute phase per unit volume of bed, m^3/m^3.
ϕ_d	Solids volume fraction associated with dense phase, m^3/m^3.
χ	Sulphur conversion.
ψ	Sphericity.
Ψ	Fouling function.
ω_i	Mass fraction of catalyst with diameter d_{p_i}.

References

Archibald, R.G., (1977),"Process Sour Gas Safety", *Hydro. Proc.*, 56(3), p.219.

Aris, R., (1957), " On Shape factors for Irregular Particles-I The Steady State Problem: Diffusion and Reaction", *Chem. Eng. Sci.*, 6, p.262.

Ashmore, P.G., (1963), "Catalysis and Inhibition of Chemical Reactions", Butterworths, London.

Bennett, A. and Meisen, A., (1973), "Hydrogen Sulphide-Air Equilibria Under Claus Furnace Conditions", *Can. J. Chem. Eng.*, 51, p.720.

Bennett, H.A. and Meisen, A., (1981),"Experimental Determination of Air-H_2S Equilibria Under Claus Furnace Conditions", *Can. J. Chem. Eng.*, 59, p.532.

Birkholz, R.K.O., Behie, L.A., Dalla Lana, I.G., (1987),"Kinetic Modelling of a Fluidized Bed Claus Plant", *Can. J. Chem. Eng.*, 65, p.778.

Bischoff, K.B., (1967), "An Extension of the General Criterion for Importance of Pore Diffusion with Chemical Reactions", *Chem. Eng. Sci.*, 22, p.525.

Bischoff, K.B. and O., Levenspiel, (1962), "Fluid Dispersion- Generalization and Comparision of Mathematical Models", *Chem. Eng. Sci.*, 17, p.245

Bonsu, A.K., (1981), "Fluidized Bed Claus Reactor Studies", *Ph.D Thesis*, Univ. Of British Columbia, Vancouver, B.C.

Bonsu, A.K. and Meisen, A., (1985),"Fluidized Bed Claus Reactor Studies ", *Chem. Eng. Sci.*, 40, p.27.

Box, G.E.P, Hunter, W.G, Hunter, S.S, (1978), "Statistics for Experimenters: An Introduction to Design, Data, and Model Building", John Wiley & Sons, New York, p633.

Bragg, J.R., (1976), "A Computer Model of the Modified Claus Sulfur Recovery Process", *AIChE Symp. Series,*, 72(156), p.48.

Broadhurst, T.E. and Becker, H.A., (1976), "Onset of Fluidization and Slugging in Beds of Uniform Particles", *AIChE J*, 21, p.238.

Bywater, R.J., (1978), "Fluidized Bed Catalytic Reactor According to a Statstical Fluid Mechanic Model", *AIChE Symp. Series*, 74(176), p.126.

Calderbank, P.H., Pereira, J., Burgess, J.M., (1975), " The Physical and Mass Transfer Properties of Bubbles in Fluidized Beds of Electrically Conducting Particles", *in Fluidization Technology Vol.1*, ed. Keairns, D., Hemisphere Publ. Corp., Washington D.C., p.111.

Callahan, F.J.,Jr., (1974), *Swadgelok Tube Fitting and Installation Manual*, Markad Service Co., Cleveland, Ohio.

Cameron, L.C., (1974), "Aquitain Improves Sulfreen Process for More H_2S Recovery", *Oil and Gas J.*, 72, p.110(June 24).

Carberry, J.J., (1976), "Chemical and Catalytic Reaction Engineering", Chapter 5, p.194, McGraw-Hill book Co., New York, N.Y.

Chavarie, C. and Grace, J.R., (1975), "Performance Analysis of a Fluidized Bed Reactor", *Ind. Eng. Chem. Fundam.*, 14, p.75.

Chavarie, C. and Grace, J.R., (1976), "Interphase Mass Transfer in a Gas-Fluidized Bed", *Chem. Eng. Sci.*, 31, p.741.

Chiba, T. and Kobayashi, H., (1970), "Gas Exchange Between the Bubble and Emulsion Phases in Gas-Solid Fluidized Beds", *Chem. Eng. Sci.*, 25, p.1375.

Clift, R. and Grace, J.R., (1970), "Bubble Interaction in Fluidized Beds", *Chem. Eng. Prog. Symp. Series*, 66(105), p.14.

Clift, R. and Grace, J.R., (1972), "Coalescence of Bubbles in Fluidized Beds", *Trans. Inst. Chem. Engrs*, 50, p.364.

Constable, F.H., (1925), "The Mechanism of Catalytic Decomposition", *Proc., Royal Soc. A*, 108, p355.

Cosidine, D.M., (1974), " Process Instruments and Controls Handbook", McGraw-Hill Book Co., New York.

Cremer, E., (1955), "The Compensation Effect in Heterogeneous Catalysis", *Advances in Catalysis*, 7, Ed. Frankenburg, W.G, V.I., Komarewsky and E.K., Rideal, p.75, Acad. Press Inc., New York, N.Y.

Dalla Lana, I.G., (1978), "Catalysis Research on the Modified Claus process", *Energy Proc. Canada*, 70, p.34.

Dalla Lana, I.G., Liu, C.L. and Cho, B.K., (1976), "The Development of a Kinetic Model for Rational Design of Catalytic Reactors in Modified Claus Process", *Proc. 6th Euro./4th Int. Symp. Chem. Reaction Eng.*,DECHEMA, p.V196.

Darton, R.C., (1979), "A Bubble Growth Theory of Fluidized Bed Reactors", *AIChE Symp. Series*, 74(176), p.126.

Darton, R.C., Lanauze, R.D, Davidson, J.F., Harrison, D., (1977),"Bubble Growth Due to Coalescence in Fluidised Beds ", *Trans. Inst. Chem. Engrs.*, 55, p274.

Davidson, J.F and Harrison, D., (1963), "Fluidised Particles", Cambridge Univ. Press, Cambridge.

Drinkenburg, A.A.H. and Rietema, K., (1972), "Gas Transfer from Bubbles in a Fluidized Bed to the Dense Phase", *Chem. Eng. Sci.*, 27, p.1765, also, 28, p.259(1973)

Eley, D.D., (1967), "Energy Gap and Pre-Exponential Factor in Dark Conduction by Organic Semiconductors", *J. Polym. Sci.*, 7, p.73.

Fairclough, R.A. and Hinshelwood, C.N., (1937), "The Functional Relation Between the Constants of the Arrhenius Equation", *J. Chem. Soc.*, p. 538, also p.573.

Fan, L.T., Fan, L.S., Miyanami, K., (1977), "Reactant Dynamics of Catalytic Fluidized Bed Reactors Characterized by a Transient Axial Dispersion Model With Varying Physical Quantities", *Proc. Pachec Conference*, p.1379.

Fisher, R.A., (1947), " Statistical Methods for Research Workers", Hafner Pupl., Co., New York.

Forsythe, W.L. and Hertwig, W.R., (1949), " Attrition Characteristics of Fluid Cracking Catalysts: Laboratory Studies", *Ind. & Eng. Chem.*, 1(6), p.1200.

Froment, G.F. and Bischoff, K.B., (1961), "Non-Steady State Behaviour of Fixed Reactors Due to Catalyst Fouling", *Chem. Eng. Sci.*, 16, p.189.

Froment, G.F. and Bischoff, K.B., (1979), "Chemical Reactor Analysis and Design", Wily, New York.

Fryer, C. and Potter O.E, (1972), "Counter Current Back Mixing Model for Fluidized Bed Catalytic Reactors; Applicability of Simplified Solutions", *Ind. Eng. Chem. Fundam.*, 11, p.338.

Galwey, A.K., (1977), "Compensation Effect in Heterogeneous Catalysis", *dvances in Catalysis*, 26, Ed. Eley, D.D., Pines, H. and P.B., Weisz., Acad. Press, NY, p.247.

Gamson, B.W. and Elkins, R.H., (1953), "Sulfur from Hydrogen Sulfide", *Chem. Eng. Prog.*, 49, p.203.

George, Z.M., (1974), "Kinetics of Cobalt-Molybdate Catalyzed Reaction of SO_2 with H_2S and COS and the Hydrolysis of COS", *J. Cat.*, 32, p.261.

George, Z.M., (1975). "Effect of Basicity of the Catalyst on Claus Reaction", in Sulphur Removal and Recovery from Industrial Process, *Adv. Chem. Series*, 139, Ed. Pfeirffer, J.B., Amer. Chem. Soc., Washington, D.C., p.75.

Ghosh, T.K, (1985), "Catalytic Oxidation of Low Concentrations of Hydrogen Sulphide", *Energy Proc. Canada* 77, p.16.

Goar, B.G., (1977), "Chemical Reactors as a Means of Separation: Sulfur Removal, Chapter 5", ed. Crynes, B.L., Marcell Dekker Inc., New York.

Goddin, G.S., Hunt, E.B., Palm, J.W, (1974), "CBA Process Ups Claus Recovery", *Hydro. Proc.*, 53(10), p.122.

Good, W. and J. Stone, (1972), "Enthalpy-Entropy Relationships in the Fluid Kinetics of Aqueous Electrolyte Solution Containing only Negatively Hydrated Ions", *Electrochimica Acta*, 17, p.1813.

Grace, J.R., (1986), "Fluidized Beds as Chemical Reactors", in Gas Fluidization Technology, ed. Geldart, D., John Wiley & Sons, New York, Chapter 11.

Grace, J.R., (1971), "An Evaluation of Models for Fluidized-Bed Reactors", *AIChE Symp. Series*, 67(116), p.159.

Grace, J.R, (1981), "Fluidized Bed Reactor Modeling: An Overview", *ACS Symp. Series*, 168, ed. Fogler, H.S., Wasington D.C., p.3.

Grace, J.R., (1982), "Fluidized Bed Hydrodynamics, Chapter 8", Handbook of Multiphase Systems, Ed. Hetsroni, G., Hemisphere Publ. Co., Washington D.C.

Grace, J.R., (1984), "Generalized Models for Isothermal Fluidized Bed Reactors", *in Recent Advances in Engineering Analysis of Chemical Reacting Systems*, ed. Doraiswamy, L.K, Wiley Eastern, New Delhi.

Grace, J.R. and Clift, R., (1974), "On The Two-Phase Theory in Fluidization", *Chem. Eng. Sci.*, 29, p327.

Grancher, P. (1978), "Advances in Claus Technology", *Hydroc. Proc.*, 57(7), p.155.

Guenther, W.C., (1964), " Analysis of Variance", Prentice Hall, Inc, NJ, Chapter 5, p99.

HNU Systems, (1976), "Instruction Manual for PI 201 Photoionization Monitor", HNU Systems, Inc., Newton, Mass.

Hovmand, S., Freedman, W., Davidson, J.F, (1971), "Chemical Conversion in a Pilot-Scale Fluidized Bed", *Trans., Instn. Chem., Engrs.*, 49, p.149.

Horio, M. and Wen, C.Y, (1977), "An Assessment of Fluidized Bed Modeling", *AIChE Symp. Series*, 73(161), p9.

Kato, K. and Wen, C.Y., (1969), "Bubble Assemblage Model for Fluidized Catalytic Reactors", *Chem. Eng. Sci.*, 24, p.1351.

Kelly, K.K., (1937), "Contribution to the Data on Theoretical Metallurgy: VII Thermodynamic Properties of Sulphur and its Inorganic compounds", *U.S.*

Bur Mines Bull., 406, p.1.

Kellog, H.H., (1971), "Equilibria in the Systems C-O-S and C-O-S-H as Related to Sulfur Recovery from Sulfur Dioxide", *Met. Trans.*, 2, p.2161.

Kerr, R.K., H.G. Paskall, and M. Ballash, (1976), "Claus Process: Catalytic Kinetics Part I-Modified Claus Reaction", *Energy Proc./Canada*, p.66, (September-October).

Kohl, A., Riesenfeld, F.C., (1985), "Dry Oxidation Process", Chapter 8 in Gas Purification, 4th. Ed., Gulf Pub. Co., Houston.

Kono, H., (1981), "Attrition Rates of Relatively Coarse Solid Particles in Various Types of Fluidized Beds", *AIChE Symp. Series*, 77(205), p.96.

Kunii, D., Yoshida, K., Hiraki, I., (1967), "The Behaviour of Freely Bubbling Fluidized Beds", *Proc. Inter. Symp. on Fluidization*, Netherlands Univ. Press., Amesterdam, p243.

Kunii, D. and Levenspiel, O., (1969), " Fluidization Engineering", Wiley, New York.

Laundau, M., Molyneax, A., Houghton, R., (1968), "Laboratory and Plant Evaluation of Catalysts for Sulphur Recovery from Lean H_2S Gas Streams", *Inst. Chem. Engrs. Symps. Series*, 27, p.228.

Lewis, W.K., Gilliland, E.R., Glass, W., (1959), "Solid Catalysed Reaction in a Fluidized Bed", *AIChE J.*, 5, p.419.

Levenspiel, O., (1972), "Chemical Reaction Engineering", John Wiley & Sons, New York, NY.

Maadah, A.G. and Maddox, R.N., (1978), "Predict Claus Products", *Hydro. Proc.*, 57(8), p.143.

Martin, J.E. and G., Guyot, (1971), "The Sulfreen Process", Paper presented at the Canadian Natural Gas Processors Association meeting, Edmonton (June).

Masamune, S. and Smith, J.M., (1966), "Performance of Fouled Catalyst Pellets", *AIChE J.*, 12, p.384.

May, W.G., (1959), "Fluidized-Bed Reactor Studies", *Chem. Eng. Prog.*, 55(12), p.49.

McBride, B.J., Hermel, S., Elders, J.G., Gordon, S., (1963), "Thermodynamic Properties to 6000°K for 210 Substances Involving the First 18 Elements", NASA SP-3001, Washington, D.C.

McGregor, D.E., (1971), "Rate Studies of the Catalytic Reaction of H_2S and SO_2", *Ph.D Thesis*, University of Alberta, Edmonton, Alberta.

Meisen, A., (1977), "A Novel Fluidized Bed Claus Process", *27th Can. Chem. Eng. Conf.*, Calgary Alberta, 23-27 October.

Meisen, A. and H.A. , Bennett, (1979), "Predict Liquid Sulfur Vapor Pressure", *Hydro. Proc.*, 58(12), p.131.

Mickley, R.S., Sherwood, T.K., Reed, C.E., (1957), "Applied Mathematics in Chemical Engineering", McGraw Hill Book Company, Inc., N.Y., Chapter 2, p53.

Mireur, J.P. and Bischoff, K.B., (1967), "Mixing and Contacting Models for Fluidized Beds", *AIChE J.*, 13, p.839.

Miwa, K., Mori, S., Kato, T. and Muchi, I., (1972), "Behaviour of Bubbles in Gaseous Fluidized Beds", *Int. Chem. Eng.*, 12, p.1187.

Mori, S. and Wen, C.Y., (1975), "Estimation of Bubble Diameter in Gaseous Fluidized Beds", *AIChE J.*, 21, p.109.

Murray, J.D, (1965), " On the Mathematics of Fluidization", *J. Fluid Mech.*, 21, p.465, also, 22, 57(1966).

Murthy, A.R, and Roa, S.B., (1951), " Behavior of Sulfur Compounds-III: Kinetics of the Gaseous Reaction Between H_2S and SO_2", *Proc. Ind. Acad. Sci.*, 24A, p.283.

Nelson, G.O., (1971), "Controlled Test Atmospheres: Principles and Techniques", Ann Arbor Science Publ. Inc., Ann Arbor, Mich.

Orcutt, J.C., Davidson, J.F., Pigford, R.L, (1962), "Reaction Time Distributions in Fluidized Catalytic Reactors", *Chem. Eng. Prog. Symp. Series*, 58(38), p.1.

Pachovsky, R.A., Best, D.A. and Wojciechowski, B.W., (1973), "Application of the Time On-Stream Theory of Catalyst Decay", *Ind. Eng. Chem. Proc. Des. Dev.*, 12, p.254.

Partridge, B.A., Rowe, P.N., (1966) " Chemical Reaction in a Bubbling Gas-Fluidised Bed", *Trans. Instn. Chem. Engrs.*, 44, p.T335.

Pearson, M.J., (1973), "Developments in Claus Catalysts", *Hydro. Proc.*, 52(2), p.81.

Pearson, M.J., (1977), " Alumina Catalysts in Low-Temperature Claus Process", *Ind. Eng. Chem. Prod. Res. Dev.*, 16, p.154.

Pereira, J.A.F, (1977), "The Physical and Mass Transfer Properties of Bubbles in a Fluidised Bed", *Ph.D. Thesis*, University of Edinburgh.

Pyle, D.L., (1972), "Fluidized Bed Reactors: A Review", *Adv. in Chem. Series*, 109, Chemical Reaction Engineering, Amer. Chem. Soc., Washington, D.C., p.106.

Razzaghi, M. and Dalla Lana, I.G., (1984), "A Model for Predicting Deactivation of a Catalytic Claus Reactor by Adsorption of Sulphur", *Catalysis on the Energy Scene*, Ed., Kaliaguine, S. and Mahay, A., Elsevier Science Publ., Amsterdam, p221.

oberts, G.G., (1974), " Activation Energy for Electronic Conduction in Crystalline Solids", in Transfer and Storage of Energy by Molecules-The Solid State, Chapter 3, Vol. 4, Ed. Burnett, G.M, North, A.M. and J.N., Sherwood, Wilel & Sons, NY, p.153.

Rowe, P.N. and Partridge, B.A., (1962), "The Interaction Between Fluids and Particles", Proc. Symp. On Interaction Between Fluids and Particles, *Inst. Chem. Engrs.*, p.135.

Rowe, P.N. and Partridge, B.A., (1966), " Chemical Reaction in a Bubbling Gas-Fluidised Bed", *Trans. Instn. Chem. Engrs.*, 44, p.T335.

Rowe, P.N. and Partridge, B.A., (1965), "An X-Ray Study of Bubbles in Fluidised Beds", *Trans. Inst. Chem. Engrs.* , 43, p.T157.

Rowe, P.N., Partridge, B.A., Lyall, E., (1964), "Cloud Formation Around Bubbles in Gas Fluidized Beds", *Chem. Eng. Sci.*, 19, p.973.

Sadana, A. and Doraiswamy, L.K., (1971), "Effect of Catalyst Fouling in Fixed, Moving and Fluidized Bed Reactors", *J. Cat.*, 23, p.147.

Satterfield, C.N, (1970), "Mass Transfer in Heterogeneous Catalysis", Chapter 1, p.1, M.I.T. press, Cambridge, Mass.

Schwab, G.M., (1950), "About the Mechanism of Contact Catalysis", *Advances in Catalysis*, 2, Ed. Frankenburg, W.G, V.I., Komarewsky and E.K., Rideal, p.251, Acad. Press Inc., New York, N.Y.

Shen, C.Y. and Johnstone, H.F., (1955), " Gas-Solid Contact in Fluidized Beds", *AIChE J.*, 1, p.349.

Sherwood, T.K., R.L., Pigford, and C.R., Wilke, (1975), "Mass Transfer", MacGraw-Hill book Co., New York, N.Y.

Thomas, J.M. and W.J., Thomas, (1967), "Introdoction to the Principles of Heterogeneous Catalysts", Chapter 5, p.241, Academic Press, London.

Sit, S.P. and Grace, J.R., (1978), "Interphase Mass Transfer in an Aggregative Fluidized Bed", *Chem. Eng. Sci.*, 33, p.115.

Sit, S.P and Grace, J.R., (1981), "Effect of Bubble Interaction on Interphase Mass Transfer in Gas Fluidized Beds", *Chem. Eng. Sci.*, 36, p.327.

Tayler, H.A. and Wessly W.A., (1927), "The Gaseous Reaction Between Hydrogen Sulphide and Sulphur Dioxide", *J. Phys. Chem.*, 31, p.216.

Thermo Electron Corportion, (1976), "Instruction Manual for Model HO Pulsed Fluorescent SO_2 Analyser", TE540-30-76, Thermo Electron Corporation, Hopkintin, Mass.

Toei, R. and Matsuno, R., (1967), "The Coalescence of Bubbles in the Gas-Solid Fluidized Bed", *Proc. Int. Symp. On Fluidization*, Ed. Drinkenburg, A.A.H., Netherland Univ. Press, Amsterdam, p.271.

Toei, R., Matsuno, R., Miyagawa, H., Nishitani, K., Komagawa, Y., (1969), "Gas Transfer Between a Bubble and the Continuous Phase in a Gas-Solid Fluidized Bed", *Int. Chem. Eng.*, 9, p.358.

Toomey, R.D. and Johnstone, H.F., (1952), "Gaseous Fluidization of Solid Particles", *Chem. Eng. Prog.* 48, p.220.

Valenzuela, J.A. and Glicksman, L.R.,(1985), "Gas Flow Distribution in a Bubbling Fluidized Bed", *Powder Tech.*, 44, p103.

Van Deemter, J.J., (1961), "Mixing and Contacting in Gas-Solid Fluidized Beds", *Chem. Eng. Sci.*, 13, p.143.

Vaux, W.G. and Fellers, A.W., (1981), "Measurement of Attrition Tendency in Fluidization", *AIChE Symp. Series*, 77(205), p.107.

Vaux, W.G. and Keairns, D.L., (1980), " Particle Attrition in Fluidized Bed Processes", *in Fluidization*, Eds Grace, J.R. and Matsen, J.M., Plenum Press, New York, p.437.

Vaux, W.G. and Schruben, J.S., (1983), "Kinetics of Attrition in the Bubbling Zone of a Fluidized Bed", *AIChE Symp. Series*, 79(222), p.97.

Venables, W.N., 1989, "Report on Pollution Control objectives for the Chemical and Petroleum Industries of British Columbia as a Result of a Public Inquiry Held by the Director of the Pollution Control Branch", Table VII, p.33, Ministry of Environment, B.C

Walker, B.V., (1975), "The Effective Rate of Gas Exchange in a Bubbling Fluidized Bed", *Trans. Instn. Chem. Engrs*, 53, p.255.

Watanabe, K. and A.S., Jursa, (1964), "Absorption and Photoionization Cross Sections of H_2O and H_2S", *J. Chem. Phys.*, 41, p.1650.

White, W.B., Johnson, S.M., Dantzing, G.B., (1958), "Chemical Equilibrium in Complex Mixtures", *J. Chem Phys.*, 28, p.751.

Werther, J., (1980), "Mathematical Modeling of Fluidized Bed Reactors", *Int. Chem. Eng.*, 20, p.529.

Yates, J.G., (1973), "Fluidised Bed Reactors", *Chem. Engr.*, (London), p.671.

Zenz, F.A., (1979), "Studies of Attrition in Fluid- Particle Systems", *Proc. NSF Workshop on Fluidization and Fluid-Particles Systems*, Ed. Littman, H., Torry NY, p.162.

Appendix A

STATISTICAL ANALYSIS

A.1 ANALYSIS OF VARIANCE

To study the significance of the feed concentration and the reactor temperature on conversion statistically, a variance analysis is presented in the following section (keeping U/U_{mf} and H_s fixed). It should be noted that the term "significance" does not mean "scientific significance". Instead, it means that a hypotheses may be accepted or rejected. A statistically significant effect may or may not be scientifically significant.

According to the so called fixed effect model (Box et al., 1978; Guenther, 1964), the observed conversion, in a given run, may be considered as the sum of four effects i.e:

$$\chi_{tcr} = \Gamma_c + \Gamma_t + \Gamma_{tc} + e_{tcr} \tag{A.1}$$

where Γ_c, denotes the pure concentration effect:

$$\Gamma_c = f_1(C) \tag{A.2}$$

and Γ_t, denotes the pure temperature effect:

$$\Gamma_t = f_2(T) \tag{A.3}$$

Γ_{tc} denotes the interaction effect due to the combined action of the feed concentration and reactor temperature:

$$\Gamma_{tc} = f_3(C,T) \tag{A.4}$$

The term e_{tcr} denotes the experimental error which is assumed to be normally distributed. The subscript c refers to the concentration level and the subscript t denotes the temperature level. The number of replications is indicated by the subscript r.

Four variances are associated with these effects and they may be denoted by: σ_c^2, σ_t^2, σ_I^2, and σ_e^2 which are measures of concentration, temperature, interaction and error effects, respectively. According to Mickley et al. (1957), the corresponding mathematical expressions are given by:

Concentration variance:

$$\sigma_c^2 = \sum^{n_c}(\Gamma_c - \bar{\Gamma}_c)^2/n_c \tag{A.5}$$

where $\bar{\Gamma}_c$ denotes the mean concentration effect and n_c is the number of concentrations levels.

Temperature variance:

$$\sigma_t^2 = \sum^{n_t}(\Gamma_t - \bar{\Gamma}_t)^2/n_t \tag{A.6}$$

Interaction variance:

$$\sigma_I^2 = \sum^{n_t}\sum^{n_c}(\Gamma_{tc} - \bar{\Gamma})^2/n_t n_c \tag{A.7}$$

where $\bar{\Gamma}$ denotes the grand mean.

Error variance:

$$\sigma_e^2 = \sum^{n_t}\sum^{n_c}\sum^{n_r}(e_{tcr} - e_{tc\bar{r}})^2/n_t n_c n_r \tag{A.8}$$

where $e_{tc\bar{r}}$ denotes the mean error averaged over n_r at fixed concentration, C, and temperature level, T.

Once these variances are calculated from experimental data, the F test may be used to determine the significance of each of the effects (i.e $F_i = \sigma_i^2/\sigma_e^2$). Since it is not possible to isolate each variance completely (see Table A.1), an estimate of the population variances, $(s_p^2)_i$, may be used in the F test [i.e $F_i = s_p^2)_i/s_e^2$]. Mickley et al. (1957) recommended that, when the interaction effect is not significant, the F test should be based on a pooled estimate of error variance i.e:

$$(s_e^2)_{bv} = \frac{f_e s_e^2 + f_I (s_p^2)_I}{f_e + f_I} \tag{A.9}$$

where f_e and f_I denote the degrees of freedom associated with the error and interaction variances.

The general calculation technique used in variance analysis is cumbersome. The rest of the discussion will therefore be presented by means of the experimental data shown in Figure A.1. The details of the following procedure are comprehensively covered by Guenther (1964) and are summarized in Table A.1.

Let S_T denotes the sum of squares for the totals and f_T denotes the degrees of freedom for S_T, i.e:

$$S_T = \sum^{n_t}\sum^{n_c}\sum^{n_r} \chi_{tcr}^2 - (\sum^{n_t}\sum^{n_c}\sum^{n_r} \chi_{tcr})^2/n_t n_c n_r \tag{A.10}$$

and the degrees of freedom associated with S_T is:

$$f_T = n_t n_c n_r - 1 \tag{A.11}$$

Referring to Figure A.1, the first term on the right handside of equation A.10 is:

$$\begin{aligned} \sum^{n_t}\sum^{n_c}\sum^{n_r} \chi_{tcr}^2 &= 79.8^2 + 79.9^2 + 83.3^2 + \cdots + 93.3^2 \\ &= 89967.2 \end{aligned}$$

and the second term is given by:

$$\begin{aligned}(\sum^{n_t}\sum^{n_c}\sum^{n_r}\chi_{tcr})^2/n_t n_c n_r &= (79.8+79.9+83.3+\cdots+93.3)^2/(3\times 2\times 2)\\ &= 89596.8\end{aligned}$$

Hence

$$\begin{aligned}S_T &= 89967.2-89596.8\\ &= 370.4\end{aligned}$$

The degrees of freedom for S_T is (equation A.11):

$$\begin{aligned}f_T &= 3\times 2\times 2-1\\ &= 11\end{aligned}$$

For convenience, define the subtotal G_{tc} as

$$G_{tc}=\sum^{n_r}\chi_{tcr} \tag{A.12}$$

Using equation A.10 leads to a new block as shown in Figure A.2. By analogy to equation A.10, the sum of squares for the subtotals may be defined as:

$$S_s=\sum^{n_t}\sum^{n_c}(G_{tc})^2/n_r-(\sum^{n_t}\sum^{n_c}\sum^{n_r}\chi_{tcr})^2/n_c n_t n_r \tag{A.13}$$

The degrees of freedom for S_s is

$$f_s=n_t n_c-1 \tag{A.14}$$

From Figure A.2 it follows that

$$\begin{aligned}\sum^{n_t}\sum^{n_c}(G_{tc})^2/n_r &= (158.8^2+162.8^2+\cdots+186.1^2)/2.\\ &= 89957.7\end{aligned}$$

Hence

$$
\begin{aligned}
S_s &= 89957.7 - 89596.8 \\
&= 360.9
\end{aligned}
$$

and

$$
\begin{aligned}
f_s &= 6 - 1 \\
&= 5
\end{aligned}
$$

Subtracting equation A.13 from equation A.10 gives an equation similar to equation A.8:

$$
\begin{aligned}
S_T - S_s &= \sum^{n_t}\sum^{n_c}\sum^{n_r}\chi^2_{tcr} - \sum^{n_t}\sum^{n_c}(\sum^{n_r}\chi_{tcr})^2/n_r \\
&= \sum^{n_t}\sum^{n_c}[\sum^{n_r}(\chi_{tcr} - \chi_{tc\bar{r}})^2] \\
&= S_e \qquad (A.15)
\end{aligned}
$$

Also from equations A.11 and A.14 it follows that

$$
\begin{aligned}
f_e &= f_T - f_s \\
&= n_t n_c(n_r - 1) \qquad (A.16)
\end{aligned}
$$

where S_e is the error sum of squares and f_e denotes the degrees of freedom for S_e. Substituting for S_T and S_s gives:

$$
\begin{aligned}
S_e &= 370.4 - 360.9 \\
&= 9.5
\end{aligned}
$$

Also

$$
\begin{aligned}
f_e &= 11 - 5 \\
&= 6
\end{aligned}
$$

Using these values for S_e and f_e, the estimate of the population error variance (also called the error mean square) is given by

$$\begin{aligned} s_e &= S_e/f_e \qquad \text{(A.17)} \\ &= 9.56/6 \\ &= 1.58 \end{aligned}$$

Now consider the effect of temperature alone. Referring to Figure A.2, define the sum of squares for the temperature ("columns" in Figure A.2) as:

$$S_t = \sum^{n_t}(\sum^{n_c} G_{tc})^2/n_c n_r - (\sum^{n_t}\sum^{n_c}\sum^{n_r} \chi_{tcr})^2/n_t n_c n_r \qquad \text{(A.18)}$$

and the associated degrees of freedom as:

$$f_t = n_t - 1 \qquad \text{(A.19)}$$

Then from Figure A.2,

$$\begin{aligned} \sum^{n_t}(\sum^{n_c} G_{tc})^2 &= \{(158.8 + 178.7)^2 + (167.8 + 185.3)^2 + (165.2 + 186.1)^2\}/(2 \times 2) \\ &= 89622.9 \end{aligned}$$

Hence:

$$\begin{aligned} S_t &= 89622.9 - 89596.8 \\ &= 26.1 \end{aligned}$$

and the degrees of freedom for S_t is:

$$\begin{aligned} f_t &= 3 - 1 \\ &= 2 \end{aligned}$$

The temperature estimate of population variance (or temperature "column" mean squares) is obtained from:

$$\begin{aligned} (s_p^2)_t &= S_t/f_t \\ &= 26.1/2 \\ &= 13.1 \end{aligned} \tag{A.20}$$

Similarly, the effect of concentration on conversion is investigated by defining the sum of squares for concentration (concentration " row" mean square in Figure A.2) as:

$$S_c = \sum^{n_c}(\sum^{n_t} G_{tc})^2/n_t n_r - (\sum^{n_t}\sum^{n_c}\sum^{n_r} \chi_{tcr})^2/n_t n_c n_r \tag{A.21}$$

and the degrees of freedom for S_c as:

$$f_c = n_c - 1 \tag{A.22}$$

Hence from Figure A.2, the first term on the right handside of equation a.23 is therefore:

$$\begin{aligned} \sum^{n_c}(\sum^{n_t} G_{tc})^2/n_t n_r &= \{(158.8 + 162.8 + 165.2)^2 + (178.7 + 185.3 + 186.1)^2\}/3 \times 2 \\ &= 89930.7 \end{aligned}$$

Hence

$$\begin{aligned} S_c &= 89930.7 - 89596.8 \\ &= 333.9 \end{aligned}$$

with degrees of freedom:

$$\begin{aligned} f_c &= 2 - 1 \\ &= 1 \end{aligned}$$

The concentration estimate of population variance is calculated from the values of S_c and f_c as:

$$\begin{aligned}(s_p^2)_c &= S_c/f_c \qquad \text{(A.23)}\\ &= 333.9\end{aligned}$$

The interaction sum of squares is given by (Guenther, 1964):

$$S_I = S_s - S_t - S_c \qquad \text{(A.24)}$$

The interaction degrees of freedom are given by

$$\begin{aligned}f_I &= f_s - f_t - f_c\\ &= (n_t - 1)(n_c - 1) \qquad \text{(A.25)}\end{aligned}$$

Substituting for the various terms yield:

$$\begin{aligned}S_I &= 360.9 - 26.1 - 333.9\\ &= 0.9\end{aligned}$$

and

$$\begin{aligned}f_I &= (3 - 1)(2 - 1)\\ &= 2\end{aligned}$$

These values of S_I and f_I are used to calculate the interaction estimate of population variance (interaction mean square):

$$\begin{aligned}(s_p^2)_I &= S_I/f_I \qquad \text{(A.26)}\\ &= 0.9/2\\ &= 0.45\end{aligned}$$

$$\text{(A.27)}$$

The interaction hypotheses may be tested by the F test:

$$\begin{aligned} F_I &= (s_p^2)_I / s_e^2 \\ &= 0.45/1.58 \\ &= 0.28 \end{aligned} \tag{A.28}$$

This value indicates that the interaction effect is not significant. The value of F at 50% limit (with 6 and 2 degrees of freedom) is 0.78 which means that 50% of the time the interaction assumption is rejected. It also means the effect of a change in concentration is most probably independent of the temperature level and vice versa. With reference to Table A.1, $\sigma_I^2 \cong 0$. Hence the interaction estimate of the population variance, $(s_p^2)_I$, provides an independent estimation of s_e^2. To form a better estimate of the error variance, s_e^2 and $(s_p^2)_I$ may be pooled in accordance with equation A.9; thus:

$$\begin{aligned} (s^2)_{bv} &= \frac{6 \times 1.58 + 2 \times 0.45}{6 + 2} \\ &= 0.865 \end{aligned}$$

Using this pooled estimate of the error variance, two F tests may be carried out to find the significance of the feed concentration and reactor temperature. For the concentration effect, the F test is:

$$\begin{aligned} F_c &= \frac{(s_p^2)_c}{(s_e^2)_{bv}} \\ &= \frac{333.9}{0.865} \\ &= 386 \end{aligned} \tag{A.29}$$

For 8 and 1 degrees of freedom, the values of F at 0.1 and 1% limits are (Box et al. 1978):

$$F = 25.42 \text{ at } 0.1\% \text{ limit}$$

$$F = 11.26 \text{ at } 1\% \text{ limit}$$

It is clear that the value of F_c falls far below the 0.1% level, therefore, the concentration effect is highly significant. In other words, there is less than 1 in 1000 chance that the observed differences in conversions may be explained on the basis of a scatter in data. Thus it is concluded that the conversion at the different concentration levels are actually different.

The pure temperature effect is treated in the same way, i.e:

$$\begin{aligned} F_t &= \frac{(s_p^2)_t}{(s_e^2)_{bv}} \\ &= \frac{13.1}{0.865} \\ &= 15.14 \end{aligned} \tag{A.30}$$

With 8 and 2 degrees of freedom, the values of F at the 1 and 5% levels are F=8.65 and 5.32, respectively. Thus the temperature effect is also significant.

A.2 CONFIDENCE LIMITS ON CONVERSION

To assign confidence limits to the experimental conversion χ, the Student's t test is used. In this test, the dimensionless quantity, t, is defined as the difference between the measured sample "conversion" mean, $\bar{\chi}$, and the hypothesized "true" (but generally unknown) population mean, $\bar{\bar{\chi}}$, divided by the sample estimate of the standard deviation i.e:

$$t = (\bar{\chi} - \bar{\bar{\chi}})/s_m \tag{A.31}$$

Ordinary t is not known. However, the distribution function for t was derived by Fisher (1946) and this permits probability limits to be assigned to t intervals.

Table A.1: Analysis of variance for a Two-Factor block experiment

Source	Sum of squares	Degrees of freedom	Mean square	Estimate of	F
T-means	S_t [Eq. A.18]	$f_t = n_t - 1$	$(s_p^2)_t = S_t/f_t$	$\sigma_e^2 + n_r\sigma_I^2 + n_r n_c \sigma_t^2$	$(s_p^2)_t/s_e^2$
C-means	S_c [Eq. A.20]	$f_c = n_c - 1$	$(s_p^2)_c = S_c/f_c$	$\sigma_e^2 + n_r\sigma_I^2 + n_r n_t \sigma_c^2$	$(s_p^2)_c/s_e^2$
Interaction	S_I [Eq. A.24]	$f_I = (n_c - 1)(n_t - 1)$	$(s_p^2)_I = S_I/f_I$	$\sigma_e^2 + n_r\sigma_I^2$	$(s_p^2)_I/s_e^2$
Subtotals	S_s [Eq. A.15]	$f_s = n_t n_c - 1$			
Error	$S_T - S_s$	$f_e = n_t n_c (n_r - 1)$	$s_e^2 = S_e/f_e$	σ_e^2	
Totals	S_T [Eq. A.10]	$f_T = n_t n_c n_r - 1$			

Figure A.1: Experimental Block ($U/U_{mf} = 4.44$, $H_s = 0.19m$)

	$100°C$	$130°C$	$150°C$
600 ppm	79.8	83.3	82.9
H_2S	79.0	79.5	82.3
1300 ppm	89.0	93.5	92.8
H_2S	89.7	91.8	93.3

Consequently most statistic books report tables for the probability that the true value lies inside the limits -t and +t (see Box et al., 1978).

To apply the t test to the experimental results shown in Figure A.2, a sample calculation is presented in the following paragraphs and the rest of the calculation is presented in Figure A.3.

Consider the C_1T_1 level (600 ppm,100°C). The average conversion is calculated from Figure A.2 for n_r=2:

$$\chi_{11\bar{r}} = 158.8/2 = 79.4$$

where the bar above the r means that the conversion is averaged over the number of replicates at fixed C and T levels. The estimate of the standard diviation, s_m, can be calculated from the pooled estimate of the error variance, $(s_e^2)_{bv}$, as recommended by Mickley et al. (1964):

$$s_m = \sqrt{(s_e^2)_{bv}/n_r} \tag{A.32}$$

From the previous section $(s_e^2)_{bv}$ was found to be 0.865 with 6 degrees of freedom. Hence

$$\begin{aligned} s_m &= \sqrt{0.865/2} \\ &= 0.658 \end{aligned}$$

From the t-tables (Box et al., 1978) and for 95% confidence limit, $t = \pm 2.447$. Substituting in equation A.31 gives:

$$\begin{aligned} \chi_{11\bar{r}} - \bar{\bar{\chi}}_{11} &= \pm 2.447 \times 0.658 \\ &= \pm 1.61 \end{aligned}$$

Thus for $\chi_{11\bar{r}}$=79.4:

$$77.8 \leq \bar{\bar{\chi}}_{11} \leq 81$$

Figure A.2: Experimental block for the subtotals defined by equation A.12

	$100°C$	$130°C$	$150°C$
600 ppm	158.8	162.8	165.2
1300 ppm	178.7	185.3	186.1

Figure A.3: Confidence limits on χ

		$100°C$	$130°C$	$150°C$
600 ppm H_2S	$\chi_{ct\bar{r}}$	79.4	81.4	82.6
	Upper limit	81.0	83.0	84.2
	Lower limit	77.8	79.8	81.0
1300 ppm H_2S	$\chi_{ct\bar{r}}$	89.4	92.7	93.1
	Upper limit	91.0	94.3	94.7
	Lower limit	87.7	91.0	92.0

Appendix B

COMPUTER PROGRAMME FOR THE MODEL PREDICTIONS

The performance of the fluidized bed Claus reactor was predicted by the two phase bubbling model described in chapter 3. The following computer programme was written in Fortran IV to compute the conversion as a function of the operating conditions listed in Table 5.1. It is divided into a main programme and five subprogrammes: BISECT, CONSTAN, FUN, GUN and HYDRO.

The subprogramme BISECT is a root finding subroutine which uses an incremental search to bracket the roots of a given function. Then it uses the bisection method to converge on each root with a prespecified tolerance (in this case TOL=10^{-6}). It also recognizes function discontinouities.

The subroutine CONSTN is a dummy subprogramme in which the constants α, β_1, β_2 and A_1 to A_7 are computed.

The subprogrammes FUN and GUN are functions whose roots are sought. FUN represents equation 3.10 whose root gives $C_{2,0}$. GUN represents equation 3.40 whose root gives x_1.

The subroutine HYDRO computes the bed hydrodynamic parameters. It uses the iteration procedure described in section 2.2.5 to calculate d_b, H and ϵ_b. It also calculates k_q.

The various parameters appearing explicitly in the model equations were calculated using expressions found in the literature and cited in chapter 2. They are summarized in Table B.1. Other parameters, which did not appear in the model equations but were indirectly needed in the conversion computation, are also shown in Table B.1. Constants defined in chapter 3 are also included in the table.

Table B.1: Parameters calculated in the programme for model predictions

Parameter	Equation	Reference
A_1 to A_7	3.24-3.28, 3.38-3.39	Chapter 3
d_b	2.17	Mori and Wen, (1975)
H	2.16	Grace, (1982)
k_q	2.8	Sit and Grace, (1981)
u_b	1.15	Grace (1982)
U_{mf}	2.11	Grace (1982)
α	3.11	Chapter 3
β_1	3.12	Chapter 3
β_2	3.13	Chapter 3
γ	3.18	Chapter 3
ϵ_b	2.20	Grace, (1982)
ϵ_{mf}	2.12	Broadhurst and Becker, (1975)
ϕ_b	2.21	Grace, (1984)
ϕ_d	2.22	Grace, (1984)

```
      IMPLICIT REAL*8(A-H,O-Z)
      EXTERNAL GUN,FUN
      DIMENSION ROOT(1)
      COMMON/BLK1/BOAL
      COMMON/BLK3/EQ,AB,EB,H,FIB,FID,DB
      COMMON/BLK4/YO
      COMMON/BLK5/HS

C MODEL PREDICTIONS.
C SYMBOLES
C A    : CROSS SECTIONAL AREA OF THE BED
C AB   : INTERFACIAL BUBBLE SURFACE AREA/BUBBLE VOLUME
C AG   : GRAVITATIONAL CONSTANT
C ARN  : ARCHIMEDES NUMBER
C BOAL: BETA2 OVER ALPHA
C C1E  : DIMENSIONLESS CONCENTRATION IN DILUTE PHASE
C C2E  : DIMENSIONLESS CONCENTRATION IN DENSE PHASE
C CE   : EXIT DIMENSIONLESS CONCENTRATION
C CF   : ACTUAL FEED CONCENTRATION
C CONV: CONVERSION %
C DB   : BUBBLE DIAMETER
C DG   : GAS DIFFUSIVITY
C DP   : PARTICLE DIAMETER
C EB   : VOLUME FRACTION OF BED OCCUPIED BY DILUTE PHASE
C EMF  : BED VOIDAGE AT MINIMUM FLUIDIZATION
C EQ   : GAS EXCHANGE COEFFICIENT
```

```
C FIB : FRACTION OF DILUTE PHASE OCCUPIED BY PARTICLES
C FID : FRACTION OF DENSE PHASE  OCCUPIED BY PARTICLES
C GD  : GAS DENSITY
C GV  : GAS VISCOSITY
C H   : EXPANDED BED HEIGHT
C HS  : STATIC  BED  HEIGHT
C PPM : CONCENTRATION  IN PARTS PER MILLION
C REMF: REYNOLD'S NUMBER
C RGAS: GAS CONSTANT
C RK  : REACTION RATE CONSTANT
C T   : ABSOLUTE TEMPERATURE
C U   : SUPERFICIAL  GAS VELOCITY
C UMF : SUPERFICIAL  GAS VELOCITY AT MINIMUM FLUIDIZATION
C URATIO: U/UMF
C W   : CATALYST WEIGHT IN BED
C IF INDEX=-1 THEN CALCULATE CONVERSION AS FUNCTION OF
C FEED CONCENTRATION
C IF INDEX=0  THEN CALCULATE CONVERSION AS FUNCTION OF
C U/Umf
C IF INDEX=1  THEN CALCULATE CONVERSION AS FUNCTION OF
C STATIC BED HEIGHT
C IF INDIX=2 THEN CALCULATE CONVERSION AS FUNCTION OF
C SULPHUR LOADING

      READ(5,2) GD,GV
 2    FORMAT(1X,F6.4,1X,F12.10)
```

```
      AG=9.8D0
      DP=195.0D-6
      RP=1843.0D0
      RGAS=62.4D0
C CALCULATE MINIMUM FLUIDIZATION VELOCITY: UMF
      ARN=GD*(RP-GD)*AG*DP*DP*DP/GV/GV
      REMF=DSQRT(27.2D0*27.2D0+0.0408D0*ARN)-27.2D0
      UMF=REMF*GV/DP/GD
C CALCULATE BED VOIDAGE AT MINIMUM FLUIDIZATION: EMF
      EMF=0.586*(GV*GV/GD/AG/DP/DP/DP/(RP-GD))**(0.029)
     $*(GD/RP)**(0.021)/(0.6D0)**(0.6D))
      READ(5,8) INDEX
  8   FORMAT(I2)
      IF(INDEX.GE.2) GO TO 70
      IF(INDEX)10,30,50
 10   WRITE(6,13)
 13   FORMAT('1',////)
      WRITE(6,12)
 12   FORMAT(10X,'Conversion as a function of feed
     $concentration')
      READ(5,14)T,U,W,DG,RK
      WRITE(6,260) T
 14   FORMAT(1X,F5.1,1X,F5.3,1X,F3.1,1X,F11.9,1X,F6.2)
C     CALCULATE BED HYDRODYAMICS
      URATIO=U/UMF
      CALL HYDRO(UMF,U,W,EMF,DG)
```

```
      WRITE(6,150)
      WRITE(6,160)DB
      WRITE(6,170)H
      WRITE(6,180)EB
      WRITE(6,190)FIB
      WRITE(6,200)FID
      WRITE(6,210)EQ
      WRITE(6,220)UMF
      WRITE(6,230)HS
      WRITE(6,240)EMF
      WRITE(6,250)URATIO
150   FORMAT(/,10X,'Hydrodynamic  parameters')
160   FORMAT(/,10X,'Bubble  diameter'
     $,2X,F5.3)
170   FORMAT(/,10X,'Expanded  bed height'
     $,2X,F4.2)
180   FORMAT(/,10X,'Fraction  of bed occupied by
     $dilute phase',2X,F4.2)
190   FORMAT(/,10X,'Fraction  of catalyst  associated
     $with dilute phase',2X,F6.4)
200   FORMAT(/,10X,'Fraction  of catalyst  associated'
     $with dense phase',2X,F6.4)
210   FORMAT(/,10X,'Interphase  mass transfer
     $coefficient',2X,F6.4)
220   FORMAT(/,10X,'Minimum  fluidizing gas
     $velocity',2X,F7.5)
```

```
230  FORMAT(/,10X,'Static  bed height'
    $,2X,F4.2)
240  FORMAT(/,10X,'Voidage  at minimum
    $fluidization',2X,F5.3)
250  FORMAT(/,10X,'U/Umf'
    $, 2X,F4.2,////)
260  FORMAT(/,10X,'Reactor  temperature  K',2X,F5.1)
     WRITE(6,11)
11   FORMAT(35X,'PPM',4X,'CONVERSION',/)
     PPM=100.0D0
20   PPM=PPM+100.0D0
     CF=PPM*1.0D-6*760.0D0/RGAS/T
C    CALCULATE COSTANTS IN MODEL EQUATION
     CALL CONSTN(CF,U,RK)
C    FIND DENSE PHASE INITIAL CONCETRATION
     CALL BISECT(FUN,0.0D0,1.0D0,1,ROOT,0.01D0,
    $1.0D-5,NR)
     Y0=DSQRT(1.0D0+BOAL*DSQRT(ROOT(1)))
     CALL BISECT(GUN,1.001D0,Y0,1,ROOT,0.01D0,
    $1.0D-5,NR)
     C2E=(ROOT(1)*ROOT(1)-1.0D0)*(ROOT(1)*ROOT(1)
    $-1.0D0)/BOAL/BOAL
     C1E=C2E+(BOAL)*C2E**1.5D0
     CE=C1E
     CONV=100.D0*(1.0D0-CE)
```

```
      WRITE(6,25) PPM,CONV
      IF(PPM.GE.1300) GO TO 999
      GO TO 20
25    FORMAT(34X,F6.1,5X,F5.1,/)
30    WRITE(6,35)
35    FORMAT('1',//////,10X,'Conversion  as a
     $function of U/Umf',/)
      READ(5,32)PPM,W,T,DG,RK
      WRITE(6,31)T
31    FORMAT(/,10X,'Reactor  temperature  K',2X,F5.1)
      WRITE(6,33)PPM
      WRITE(6,37)UMF
      WRITE(6,38)EMF
32    FORMAT(1X,F6.1,1X,F3.1,1X,F5.1,1X,F11.9,1X,F6.2)
33    FORMAT(/,10X,'H2S FEED concentration in ppm  '
     $,2X,F6.1)
      WRITE(6,36)
36    FORMAT(10X,'U/Umf   CONV   Db    H    Eb    Kq
     $phi-b  Phi-d')
37    FORMAT(/,10X,'Minimum  fluidizing velocity    '
     $,2X,F7.5)
38    FORMAT(/,10X,'Voidage  at minimum fluidization'
     $,2X,F5.3,/)
      CF=PPM*1.0D-6*760.0D0/RGAS/T
      URATIO=1.0D0
40    URATIO=URATIO+0.5D0
```

```
      U=UMF*URATIO
      CALL HYDRO(UMF,U,W,EMF,DG)
C     CALCULATE COSTANTS IN MODEL EQUATION
      CALL CONSTN(CF,U,RK)
C     FIND DENSE PHASE INITIAL CONCENTRATION
      CALL BISECT(FUN,0.0D0,1.0D0,1,ROOT,0.01D0,
     $1.0D0-5,NR)
      Y0=DSQRT(1.0D0+BOAL*DSQRT(ROOT(1)))
      CALL BISECT(GUN,1.001D0,Y0,1,ROOT,0.01D0,
     $1.05D-5,NR)
      C2E=(ROOT(1)*ROOT(1)-1.0D0)*(ROOT(1)*ROOT(1)
     $-1.0D0)/BOAL/BOAL
      C1E=C2E+(BOAL)*C2E**1.5D0
      CE=C1E
      CONV=100.D0*(1.0D0-CE)
      WRITE(6,45) URATIO,CONV,DB,H,EB,EQ,FIB,FID
   45 FORMAT(/,10X,F3.1,2X,F5.1,2X,F5.3,2X,F4.2,2X,
     $F4.2,2X,F5.3,2X,F6.4,2X,F6.4)
      IF(URATIO.LT.6.0D0) GO TO 40
      WRITE(6,46)HS
   46 FORMAT(/,10X,'Static bed height',2X,F4.2)
      GO TO 999
   50 WRITE(6,51)
   51 FORMAT('1',//////)
      WRITE(6,52)
   52 FORMAT(10X,'Conversion as a function
```

```
     $of static bed height')
      READ(5,55)PPM,U,T,DG,RK
 55   FORMAT(1X,F6.1,1X,F5.3,1X,F5.1,1X,
     $F11.9,1X,F6.2)
      URATIO=U/UMF
      CF=PPM*1.0D-6*760.0D0/RGAS/T
      WRITE(6,57)
 57   FORMAT(/)
      WRITE(6,31)T
      WRITE(6,33)PPM
      WRITE(6,37)UMF
      WRITE(6,59)URATIO
      WRITE(6,38)EMF
      WRITE(6,57)
      WRITE(6,300)
 59   FORMAT(/,10X,'U/Umf',2X,F4.2)
      W=0.4D0
 60   W=W+0.4D0
      CALL HYDRO(UMF,U,W,EMF,DG)
C     CALCULATE CONSTANTS IN MODEL EQUATION
      CALL CONSTN(CF,U,RK)
C     FIND DENSE PHASE INITIAL CONCENTRATION
      CALL BISECT(FUN,0.0D0,1.0D0,1,ROOT,0.01D0,
     $1.0D-5,NR)
      Y0=DSQRT(1.0D0+B0AL*DSQRT(ROOT(1)))
      CALL BISECT(GUN,1.001D0,Y0,1,ROOT,0.01D0,
```

```
     $1.0D-5,NR)
      C2E=(ROOT(1)*ROOT(1)-1.0D0)*(ROOT(1)*ROOT(1)
     $-1.0D0/BOAL/BOAL
      C1E=C2E+(BOAL)*C2E**1.5D0
      CE=C1E
      CONV=100.D0*(1.0D0-CE)
      WRITE(6,65) HS,CONV,DB,H,EB,EQ,FIB,FID
65    FORMAT(/,10X,F4.2,2X,F5.1,2X,F5.3,2X,F4.2,
     $2X,F4.2,2X,F5.3,2X,F6.4,2X,F6.4)
      IF(W.GE.2.4D0) GO TO 999
      GO TO 60
300   FORMAT(11X,'HS    CONV  Db  H   Eb  Kq
     $Phi-b  Phi-d')
70    WRITE(6,80)
      WRITE(6,85)
      READ(5,83)PPM,T,U,W,DG,RK
      CF=PPM*1.0D-6*760.0D0/RGAS/T
      URATIO=U/UMF
      CALL HYDRO(UMF,U,W,EMF,DG)
      WRITE(6,31)T
      WRITE(6,33)PPM
      WRITE(6,150)
      WRITE(6,160)DB
      WRITE(6,170)H
      WRITE(6,180)EB
      WRITE(6,190)FIB
```

```
      WRITE(6,200)FID
      WRITE(6,210)EQ
      WRITE(6,220)UMF
      WRITE(6,230)HS
      WRITE(6,240)EMF
      WRITE(6,250)URATIO
80    FORMAT('1',//////)
83    FORMAT(1X,F6.1,1X,F5.1,1X,F5.3,1X,F3.1,1X,
     $F11.9,1X,F6.2)
85    FORMAT(10X,'Conversion  as a function of
     $sulphur loading')
      WRITE(6,102)
      SL=0.000D0
90    SLOAD=1.0D0+SL*0.085D0
      FRK=RK/SLOAD
      SL=SL+5.0D0
      CALL CONSTN(CF,U,FRK)
C     FIND DENSE PHASE INITIAL CONCENTRATION
      CALL BISECT(FUN,0.0D0,1.0D0,1,ROOT,0.01D0,
     $1.0D-5,NR)
      Y0=DSQRT(1.0D0+BOAL*DSQRT(ROOT(1)))
      CALL BISECT(GUN,1.001D0,Y0,1,ROOT,0.01D0,
     $1.0D-5,NR)
      C2E=(ROOT(1)*ROOT(1)-1.0D0)*(ROOT(1)
     $-1.0D0)/BOAL/BOAL
      C1E=C2E+(BOAL)*C2E**1.5D0
```

```
      CE=C1E
      CONV=100.D0*(1.0D0-CE)
      WRITE(6,101) SL,CONV
      IF(SL.GE.60.0D0) GO TO 999
      GO TO 90
101   FORMAT(/,33X,F5.1,10X,F5.1)
102   FORMAT(//,28X,'Sulphur loading  conversion')
999   CONTINUE
      STOP
      END

      DOUBLE PRECISION FUNCTION FUN(X)
      IMPLICIT REAL*8(A-H,O-Z)
      COMMON/BLK1/A
      FUN=A*X**1.5D0+X-1.0D0
      RETURN
      END

      DOUBLE PRECISION FUNCTION GUN(X)
      IMPLICIT REAL*8(A-H,O-Z)
      COMMON/BLK2/AL,S1,S2,S3,A1,A2,A3,A4,A5,A6,A7
      COMMON/BLK4/YO
      FACT=(2.0D0*A7+S1*A6)/S1/DSQRT(3.0D0)
      T1=A1*DLOG((1.0D0+X)/(1.0D0+YO))
      T2=-A3*DLOG(DABS((1.0D0-X)/(1.0D0-YO)))
      T3=A5*DLOG((S1+X)/(S1+YO))
```

```
      T4=0.5D0*A6*DLOG((X*X-S1*X+S2)/(Y0*Y0-S1*Y0+S2))
      T5=-A2*((1.0D0/(1.0D0+X))-(1.0D0/(1.0D0+Y0)))
      T6=A4*((1.0D0/(1.0D0-X))-(1.0D0/(1.0D0-Y0)))
      T7=FACT*DATAN((2.0D0*X-S1)/S1/DSQRT(3.0D0))
      T8=-FACT*DATAN((2.0D0*Y0-S1)/S1/DSQRT(3.0D0))
      G1=T1+T2+T3+T4+T5+T6+T7+T8+AL/S3/2.0D0
      GUN=G1
      RETURN
      END

      SUBROUTINE HYDRO(UMF,U,W,EMF,DG)
      IMPLICIT REAL*8(A-H,O-Z)
      COMMON/BLK3/Q,AB,EB,H,FIB,FID,DB
      COMMON/BLK5/HS
      Y=0.7D0
      RP=1843.0D0
      RB=795.0D0
      A=0.007854D0
      D=0.1D0
      AG=9.8D0
      URATIO=U/UMF
      HS=W/A/RB
      EP=1-RB/RP
C CALCULATION OF BED HYDRODYNAMICS:
C ESTIMATE  FLOW RATE, VB,IN BUBBLE PHASE (CORRECTED
C TWO PHASE THEORY)
```

```
      UDIFF=U-UMF
      VBOA=Y*UDIFF
C ESTIMATE MAXIMUM STABLE BUBBLE DIAMETER USING
C MORI & WEN CORRELATION FOR POROUS PLATE
C DISTRIBUTOR
      DBM=1.64D0*(A*UDIFF)**0.4D0
      DBO=0.376D0*UDIFF*UDIFF
      HMF=HS*(1.0D0-EP)/(1.0D0-EMF)
C GUESS FRACTION OF BED  OCCUPIED BY BUBBLES, EB
      EB=0.1D0
C START ITERATION TO FIND CORRECT EB BY CALCULATING
C BED HEIGHT (H)
   10 H=HMF/(1.D0-EB)
C ESTIMATE BUBBLE DIAMETER, DB, AT HALF BED HEIGHT
      DBDIFF=DBM-DBO
      DB=DBM-DBDIFF*DEXP(-0.3D0*H/2.D0/D)
C ALSO ESTIMATE BUBBLE VELOCITY (UB) USING DB
C AT 1/2 BED HEIGHT
      UB=0.711D0*(AG*DB)**0.5D0+Y*UDIFF
C     CALCULATE NEW EB  USING NEW  (UB)
      EBOLD=EB
      EB=VBOA/UB
C CHECK DIFFERENCE BETWEEN THE NEW AND OLD EB'S.
C IF THIS DIFFERENCE IS >0.001 GO BACK AND GUESS
C AGAIN OTHERWISE ESTIMATE THE REQUIRED PARAMETERS.
```

```
      IF(DABS(EBOLD-EB).GT.1.0D-3)  GO TO 10
C ESTIMATE GAS EXCHANGE BETWEEN PHASES
      Q=UMF/3.D0+(4.D0*DG*EMF*UB/DB/3.1459D0)
     $**0.5D0
C CALCULATE RATIO OF BUBBLE SURFACE AREA
C TO ITS VOLUME
      AB=6.0D0/DB
C CALCULATE FRACTION OF SOLIDS IN DENSE PHASE
      FID=(1.D0-EMF)*(1.0D0-EB)
C CALCULATE FRACTION OF SOLIDS IN DILUTE PHASE
      FIB=0.010D0*EB
      RETURN
      END

      SUBROUTINE CONSTN(CF,U,RK)
      IMPLICIT REAL*8(A-H,O-Z)
      COMMON/BLK3/Q,AB,EB,H,FIB,FID,DB
      COMMON/BLK2/ALFA,S1,S2,S3,A1,A2,A3,
     $A4,A5,A6,A7
      COMMON/BLK1/BOAL
      RGAS=62.358D0
C DEFINE CONSTANTS NEEDED TO FIND THE
C ROOT OF THE MODEL EQUATION
      ALFA=Q*AB*EB*H/U
      DLK=RK*H*CF**0.5D0/U
```

```
      B1=DLK*FIB
      B2=DLK*FID
      S1=(B2/B1)**(1.0D0/3.0D0)
      S2=S1*S1
      S3=S1*S2
      S4=S1*S3
      S5=S1*S4
      S6=S5*S1
      S7=S6*S1
      S8=S1*S7
      A1=1.5D0*S3/(S3-1.0D0)/(S3-1.0D0)
      A2=-0.5D0/(S3-1.0D0)
      A3=1.5D0*S3/(S3+1.0D0)/(S3+1.0D0)
      A4=0.5D0/(S3+1.0D0)
      A5=-(3.0D0*S2-1.0D0)/(S2-1.0D0)/(S2-1.0D0)
     $/S1/3.0D0
      A6=-(6.0D0*S6+7.0D0*S4+S2+1.0D0)/(S4+S2+1.0D0
     $)/(S4+S2+1.0D0)/S1/3.0D0
      A7=(3.0D0*S6-4.0D0*S4-4.0D0*S2-1.0D0)/(S4+S2
     $+1.0D))/(S4+S2+1.0D0)/3.0D0
      BOAL=B2/ALFA
      RETURN
      END

        SUBROUTINE BISECT(F,XI,XF,NROOT,R,DXI,TOL,NR)
C SOLVES EQUATION F(X)=0
```

```
C USES INCREMENTAL SEARCH TO BRACKET NR ROOTS OF THE
C FUNCTION F(X) IN INTERVAL (XI,XF) USING INITIAL
C INCREMENT DXI
C BISECTION METHOD IS APPLIED TO CONVERGE ON EACH ROOT.
C THE ROOTS ARE RETURNED IN THE ARRAY R(NROOT).
C TOL IS THE ERROR TOLERANCE ON F(X): F(X) .LT.TOL
C NROOT= NO. OF ROOTS SOUGHT
C NR=NO. OF ROOTS FOUND
C METHOD AVOIDS DISCONTINUITIES
      IMPLICIT REAL*8(A-H,O-Z),INTEGER(I-N)
      DIMENSION R(NROOT)
      NR=0
      X=XI
    4 DX=DXI
    1 X2=0.0D0
      E2=0.0D0
    2 IF(X.GT.XF) RETURN
      E=F(X)
      E1=E2
      E2=E
      X1=X2
      X2=X
      IF(DABS(E).LT.TOL) GO TO 9
      IF(E1*E2.LT.0.D0.AND.DX.EQ.DXI) GO TO 5
      IF(E1*E2.LT.0.D0.AND.DX.NE.DXI) GO TO 6
      X=X+DX
```

```
      GO TO 2
 5    DY1=DABS(E2-E1)
      X=X-DX
      DX=DX/10.D0
      GO TO 1
 6    DY2=DABS(E2-E1)
      IF(DY2.LT.DY1) GO TO 7
      WRITE(6,12)X

12    FORMAT(10X,'THE FUNCTION IS DISCONTINOUS
     $At X=',F10.5)
      X=X2
      GO TO 4
 7    ICOUNT=0
11    IF(ICOUNT.GE.100) GO TO 8
      X=(X1+X2)/2.D0
      E=F(X)
      ICOUNT=ICOUNT+1
      IF(DABS(E).LT.TOL) GO TO 9
      IF(E1*E.LT.0.D0) GO TO 3
      X1=X
      E1=E
      GO TO 11
 3    X2=X
      E2=E
      GO TO 11
```

```
8   X=X2
    GO TO 4
9   NR=NR+1
    R(NR)=X
    IF(NR.EQ.NROOT) RETURN
    X=X+DX
    GO TO 4
    END
```

Table B.2: Model predictions

Table B.2.1: Conversion as a function of H_2S feed concentration for T=423.0 $°K$, U/U_{mf} = 4.44, H_s=0.19m

a: Hydrodynamic parameters:

Bubble diameter, d_b	0.028
Expanded bed height, H	0.25
Fraction of bed occupied by dilute phase, ϵ_b	0.13
Fraction of catalyst associated with dilute phase, ϕ_b	0.0013
Fraction of catalyst associated with dense phase, ϕ_d	0.3347
Interphase mass transfer coefficient, k_q	0.0241
Minimum fluidizing gas velocity, U_{mf}	0.0224
Voidage at minimum fluidization, ϵ_{mf}	0.616
α	1.68
γ	6.36

Table B.2.1: Conversion as a function of H_2S feed concentration for T=423.0 °K, U/U_{mf} = 4.44, H_s=0.19m (cont.)

b: Conversion

H_2S Concentration in feed (ppm)	Conversion (%)	β_1	β_2
200.0	68.1	0.0034	0.88
300.0	75.5	0.0042	1.08
400.0	80.2	0.0049	1.26
500.0	83.5	0.0054	1.39
600.0	85.9	0.0059	1.52
700.0	87.7	0.0064	1.65
800.0	89.2	0.0069	1.78
900.0	90.3	0.0073	1.88
1000.0	91.2	0.0077	1.98
1100.0	92.0	0.0081	2.09
1200.0	92.7	0.0084	2.16
1300.0	93.3	0.0088	2.25

Table B.2.2: Conversion as a function of H_2S feed concentration for T=423.0 $°K$, U/U_{mf} = 8.88, H_s=0.19m

a: Hydrodynamic parameters:

Bubble diameter, d_b	0.063
Expanded bed height, H	0.44
Fraction of bed occupied by dilute phase, ϵ_b	0.18
Fraction of catalyst associated with dilute phase, ϕ_b	0.0018
Fraction of catalyst associated with dense phase, ϕ_d	0.3140
Interphase mass transfer coefficient, k_q	0.0215
Minimum fluidizing gas velocity, U_{mf}	0.02248
Static bed height, H_s	0.32
Voidage at minimum fluidization, ϵ_{mf}	0.616
U/U_{mf}	8.90
α	1.63
γ	5.59

Table B.2.2: Conversion as a function of H_2S feed concentration for T=423.0 °K, U/U_{mf} = 8.88, H_s=0.19m

b: Conversion

H_2S Concentration in feed (ppm)	Conversion (%)	β_1	β_2
200.0	73.4	0.0084	1.46
300.0	81.3	0.0103	1.79
400.0	85.8	0.0118	2.06
500.0	88.7	0.0132	2.308
600.0	90.7	0.0145	2.53
700.0	92.2	0.0157	2.73
800.0	93.3	0.0168	2.92
900.0	94.1	0.0178	3.11
1000.0	94.8	0.0186	3.29
1100.0	95.4	0.0196	3.43
1200.0	95.8	0.0205	3.58
1300.0	96.2	0.0214	3.73

Table B.2.3: Conversion as a function of H_2S feed concentration for T=373.0 °K, U/U_{mf} = 4.44, H_s=0.19m

a: Hydrodynamic parameters

Bubble diameter, d_b	0.029
Expanded bed height, H	0.25
Fraction of bed occupied by dilute phase, ϵ_b	0.13
Fraction of catalyst associated with dilute phase, ϕ_b	0.0013
Fraction of catalyst associated with dense phase, ϕ_d	0.3353
Interphase mass transfer coefficient, k_q	0.0253
Minimum fluidizing gas velocity, U_{mf}	0.0245
Voidage at minimum fluidization, ϵ_{mf}	0.613
α	1.701
γ	6.36

Table B.2.3: Conversion as a function of H_2S feed concentration for T=373.0 $°K$, U/U_{mf} = 4.44, H_s=0.19m (cont.)

b: Conversion

H_2S Concentration in feed (ppm)	Conversion (%)	β_1	β_2
200.0	57.0	0.0031	0.801
300.0	65.0	0.0038	0.981
400.0	70.6	0.0044	1.132
500.0	74.7	0.0049	1.266
600.0	77.8	0.0054	1.387
700.0	80.2	0.0058	1.498
800.0	82.3	0.0062	1.601
900.0	84.0	0.0066	1.698
1000.0	85.3	0.0069	1.790
1100.0	86.6	0.0073	1.878
1200.0	87.6	0.0076	1.961
1300.0	88.4	0.0079	2.041

Table B.2.4: Conversion as a function of U/U_{mf} for T= 423°K, H_2S in feed= 600ppm, H_s= 0.19m

Minimum fluidizing velocity (m/s) 0.02248

Voidage at minimum fluidization 0.616

U/U_{mf}	χ	d_b	H	ϵ_b	k_q	ϕ_b	ϕ_d	α	β_1	β_2	γ
1.5	96.9	0.011	0.22	0.03	0.027	0.0003	0.3712	2.88	0.0036	4.44	10.72
2.0	94.9	0.015	0.23	0.05	0.026	0.0005	0.3627	2.66	0.0047	3.40	8.98
2.5	92.9	0.018	0.23	0.07	0.025	0.0007	0.3556	2.39	0.0052	2.67	8.01
3.0	91.0	0.021	0.24	0.09	0.025	0.0009	0.3494	2.29	0.0056	2.28	7.30
3.5	89.0	0.023	0.24	0.10	0.025	0.0010	0.3438	1.99	0.0059	1.92	6.99
4.0	87.4	0.026	0.24	0.12	0.024	0.0012	0.3389	1.77	0.0059	1.66	6.54
4.5	85.7	0.028	0.25	0.13	0.024	0.0013	0.3343	1.65	0.0059	1.51	6.33
5.0	84.1	0.030	0.25	0.14	0.024	0.0014	0.3300	1.49	0.0057	1.34	6.17
5.5	82.7	0.033	0.26	0.15	0.024	0.0015	0.3261	1.38	0.0058	1.26	6.02
6.0	81.4	0.035	0.26	0.16	0.024	0.0016	0.3225	1.27	0.0056	1.14	5.88

Table B.2.5: Conversion as a function of U/U_{mf} for T=423°K, H_2S in feed =1300ppm, H_s=0.19m

Minimum fluidizing velocity (m/s) 0.0224

Voidage at minimum fluidization 0.616

U/U_{mf}	χ	d_b	H	ϵ_b	k_q	ϕ_b	ϕ_d	α	β_1	β_2	γ
1.5	98.6	0.011	0.22	0.03	0.027	0.0003	0.3712	2.88	0.0053	6.54	10.72
2.0	97.7	0.015	0.23	0.05	0.026	0.0005	0.3627	2.66	0.0069	5.01	8.98
2.5	96.7	0.018	0.23	0.07	0.025	0.0007	0.3556	2.39	0.0077	3.93	8.01
3.0	95.8	0.021	0.24	0.09	0.025	0.0009	0.3494	2.29	0.0087	3.36	7.30
3.5	94.8	0.023	0.24	0.10	0.025	0.0010	0.3438	1.99	0.0082	2.83	6.99
4.0	94.0	0.026	0.24	0.12	0.024	0.0012	0.3389	1.77	0.0087	2.44	6.54
4.5	93.2	0.028	0.25	0.13	0.024	0.0013	0.3343	1.65	0.0087	2.22	6.33
5.0	92.4	0.030	0.25	0.14	0.024	0.0014	0.3300	1.49	0.0084	1.97	6.17
5.5	91.7	0.033	0.26	0.15	0.024	0.0015	0.3261	1.38	0.0085	1.85	6.02
6.0	91.0	0.035	0.26	0.16	0.024	0.0016	0.3225	1.27	0.0082	1.68	5.88

Table B.2.6: Conversion as a function of sulphur loading

Reactor temperature ($^\circ K$)	373.0
H_2S feed concentration (ppm)	1000.0
<u>Hydrodynamic parameters:</u>	
Bubble diameter, d_b	0.041
Expanded bed height, H	0.40
Fraction of bed occupied by dilute phase, ϵ_b	0.12
Fraction of catalyst associated with dilute phase, ϕ_b	0.0012
Fraction of catalyst associated with dense phase, ϕ_d	0.3427
Interphase mass transfer coefficient, k_q	0.0237
Minimum fluidizing gas velocity, U_{mf}	0.02458
Static bed height, H_s	0.32
Voidage at minimum fluidization, ϵ_{mf}	0.613
U/U_{mf}	4.43
α	1.665
β_1	0.0093
β_2	2.645
γ	6.58

Table B.2.6: Conversion as a function of sulphur loading (cont.)

Sulphur loading (%)	Conversion (%)
5.0	95.0
10.0	89.8
15.0	83.6
20.0	77.1
25.0	70.9
30.0	65.1
35.0	60.0
40.0	55.4
45.0	51.3
50.0	47.8
55.0	44.6
60.0	41.8

Table B.2.7: Conversion as a function of static bed height

Reactor temperature ($^\circ K$)	373.0
H_2S Feed concentration (ppm)	600.0
Minimum fluidizing velocity (m/s)	0.02458
U/U_{mf}	4.44
Voidage at minimum fluidization	0.613

H_s	χ	d_b	H	ϵ_b	k_q	ϕ_b	ϕ_d	α	β_1	β_2	γ
0.13	61.6	0.022	0.17	0.15	0.027	0.0015	0.3283	1.88	0.0038	0.83	6.02
0.19	77.8	0.029	0.25	0.13	0.025	0.0013	0.3353	1.68	0.0049	1.25	6.34
0.26	86.8	0.036	0.33	0.12	0.024	0.0012	0.3396	1.58	0.0059	1.68	6.57
0.32	91.6	0.041	0.40	0.12	0.024	0.0012	0.3427	1.69	0.0072	2.05	6.58
0.38	94.3	0.046	0.48	0.11	0.023	0.0011	0.3449	1.58	0.0079	2.48	6.80
0.45	95.9	0.051	0.55	0.11	0.023	0.0011	0.3466	1.64	0.0090	2.85	6.82

Appendix C

COMPUTER PROGRAMME FOR ROTAMETER CALIBRATION

```
      DIMENSION PR(60),FACTOR(60),QS(50),QR(50,10),SR(50)
      CHARACTER GAS*3
      CHARACTER SFLOAT*10
C THIS PROGRAMME CALCULATES GAS FLOW RATES, INTO THE
C REACTOR AT ATMOSPHERIC PRESSURE AND ROOM TEMPERATURE,
C AS FUNCTION OF PRESSURE AND TEMPERATURE INSIDE THE
C ROTAMETER AND SCALE READINGS FROM GAS FLOW RATES AT
C SATANDARD STATE. THIS RATE WAS LATER CORRECTED TO
C REACTOR TEMPERATURE.
C A,B,C: POLYNOMIAL COEFFICIENTS OBTAINED FROM FLOW
C RATES AT STANDARD CONDITIONS
C NSR NO. OF SCALE READINGS
C GAS: GAS TO BE MEASURED
C FLOAT: TYPE OF FLOAT USED
C I,J: SCALE READING and PRESSURE COUNTERS
C PREACR: REACTOR PRESSURE (=14.7 PSIA)
C PROTR : ROTAMETER PRESSURE
C PS    : STANDARD STATE PRESSURE (=14.7PSIA)
```

```
C  QS    : FLOW RATE AT STANDARD STATE
C  QREACR: FLOW RATE INTO REACTOR AT REACTOR PRESSURE AND
C  AT ROOM TEMPERATURE
C  SG    : GAS SPECIFIC DENSITY
C  TREACR: ROOM TEMPERATURE
C  TROTR : TEMPERATURE INSIDE ROTAMETER=ROOM TEMPERATURE
C  TS    : STANDARD STATE TEMPERATURE=294.15 deg K
      READ(5,351) SFLOAT
      READ(5,350) GAS
 350  FORMAT(A3)
 351  FORMAT(A12)
      WRITE(6,352) SFLOAT
 352  FORMAT(10X,'Float  ',2X,A12,'\\')
      WRITE(6,353) GAS
 353  FORMAT(10X,'Gas measured  ',2X,A3,'\\')
      READ (5,400) NSR,SG
      READ(5,401) A,B,C
      READ(5,402) TR,TM,TS,PM,PS
 400  FORMAT(1X,I3,1X,F5.3)
 401  FORMAT(F8.3,F7.3,F9.6)
 402  FORMAT(1X,F6.2,1X,F6.2,1X,F6.2,1X,F4.1,1X,F4.1)
      FACT=TM*TM*PS/TS/TR/PM/PM/SG
      PR(1)=14.7
      FACTOR(1)=(FACT*PR(1))**0.5
      PP=19.7
```

```
      DO 10 J=2,6
      PR(J)=PP
      FACTOR(J)=(FACT*PP)**0.5
10    PP=PP+5.0
      S=0.0
      DO 20 I=1,NSR
      S=S+10.0
       SR(I)=S
      QS(I)=A+B*S+C*S*S
      QR(I,1)=QS(I)*FACTOR(1)
      DO 20 J=2,6
20    QR(I,J)=QS(I)*FACTOR(J)
      WRITE(6,500) TR
      WRITE(6,490)
490   FORMAT('Scale reading & & & Flow rate & (mL/min)
     $& & \\ \hline')
      WRITE(6,501) (PR(I),I=1,6)
      DO 30 I=1,NSR
      WRITE(6,503)
30    WRITE(6,502)  SR(I),(QR(I,J),J=1,6)
      WRITE(6,504)
500   FORMAT(20X,'Temperature=  ',F7.2,'\\')
501   FORMAT('Pressure  (psia)',6('&',F7.2),'\\  \hline')
502   FORMAT(F4.0,6('&',F8.2),'\\')
503   FORMAT(1X,6('&',1X),1X,'\\')
504   FORMAT(1X,6('&',1X),1X,'\\')
```

```
STOP
END
```

Table C.1: Volumetric flow rates of H_2S/N_2

Tube No: 602
Float: GLASS
Gas measured H_2S/N_2
Temperature= 290.15 (K)

Pressure (psia)	14.70	19.70	24.70	29.70	34.70	39.70
Scale reading			Flow rate	(mL/min)		
10.	10.59	12.26	13.72	15.05	16.69	17.40
20.	19.71	22.81	25.54	28.01	30.28	32.38
30.	42.79	49.53	55.46	60.82	65.74	70.32
40.	67.50	78.14	87.50	95.95	103.71	110.93
50.	93.85	108.65	121.66	133.40	144.20	154.23
60.	121.83	141.04	157.93	173.18	187.19	200.22
70.	151.45	175.32	196.32	215.27	232.69	248.89
80.	182.70	211.50	236.82	259.69	280.70	300.24
90.	215.58	249.56	279.44	306.43	331.22	354.28
100.	250.09	289.52	324.18	355.49	384.25	411.00
110.	286.24	331.36	371.04	406.87	439.78	470.40
120.	324.02	375.10	420.01	460.57	497.83	532.49
130.	363.44	420.73	471.11	516.59	558.39	597.26
140.	404.48	468.25	524.31	574.94	621.45	664.72
150.	447.16	517.66	579.64	635.60	687.03	734.86

Table C.1: Volumetric flow rate of H_2S/N_2 (cont.)
Tube No: 602
Float: Stainless steel
Gas measured H_2S/N_2
Temperature= 290.15 (K)

Pressure (psia)	14.70	19.70	24.70	29.70	34.70	39.70
Scale reading			Flow rate (mL/min)			
10.	18.06	20.90	23.41	25.67	27.74	29.67
20.	86.93	100.63	112.68	123.56	133.56	142.86
30.	155.17	179.63	201.14	220.56	238.40	255.00
40.	222.77	257.88	288.76	316.64	342.26	366.09
50.	289.73	335.40	375.56	411.82	445.14	476.13
60.	356.05	412.18	461.53	506.09	547.04	585.12
70.	421.74	488.22	546.68	599.46	647.96	693.07
80.	486.78	563.52	630.99	691.92	747.90	799.97
90.	551.19	638.08	714.49	783.47	846.86	905.82
100.	614.97	711.91	797.15	874.12	944.84	1010.62
110.	678.10	785.00	878.99	963.86	1041.84	1114.37
120.	740.60	857.35	960.00	1052.70	1137.86	1217.08
130.	802.46	928.96	1040.19	1140.62	1232.90	1318.74
140.	863.68	999.83	1119.55	1227.65	1326.97	1419.35
150.	924.27	1069.97	1198.08	1313.76	1420.05	1518.92

Table C.1: Volumetric flow rate of H_2S/N_2 (cont.)
Tube No: 604
Float Glass
Gas measured H_2S/N_2
Temperature= 290.15 (K)

Pressure (psia)	14.70	19.70	24.70	29.70	34.70	39.70
Scale reading			Flow rate (mL/min)			
10.	564.89	653.94	732.24	802.94	867.90	928.32
20.	1172.15	1356.93	1519.40	1666.11	1800.90	1926.28
30.	1793.84	2076.62	2325.27	2549.78	2756.07	2947.95
40.	2429.95	2813.01	3149.83	3453.96	3733.39	3993.32
50.	3080.49	3566.10	3993.09	4378.64	4732.88	5062.40
60.	3745.45	4335.89	4855.05	5323.82	5754.54	6155.18
70.	4424.83	5122.38	5735.70	6289.50	6798.34	7271.66
80.	5118.65	5925.56	6635.06	7275.70	7864.32	8411.86
90.	5826.88	6745.45	7553.11	8282.39	8952.46	9575.75
100.	6549.55	7582.03	8489.87	9309.60	10062.77	10763.36
110.	7286.64	8435.32	9445.32	10357.30	11195.23	11974.67
120.	8038.15	9305.30	10419.47	11425.51	12349.86	13209.69
130.	8804.09	10191.98	11412.32	12514.22	13526.66	14468.41
140.	9584.45	11095.36	12423.86	13623.43	14725.60	15750.84
150.	10379.23	12015.44	13454.11	14753.15	15946.72	17056.97

Table C.2: Volumetric flow rate of SO_2/N_2

Tube No: 602
Float: Glass
Gas measured SO_2/N_2
Temperature = 290.15 (K)

Pressure (psia)	14.70	19.70	24.70	29.70	34.70	39.70
Scale reading			Flow rate	(mL/min)		
10.	12.61	14.59	16.34	17.92	19.37	20.72
20.	37.73	43.68	48.91	53.63	57.97	62.01
30.	64.04	74.14	83.01	91.03	98.39	105.24
40.	91.53	105.96	118.65	130.11	140.63	150.42
50.	120.21	139.16	155.82	170.87	184.69	197.55
60.	150.07	173.73	194.53	213.31	230.57	246.62
70.	181.12	209.67	234.77	257.44	278.27	297.64
80.	213.34	246.98	276.55	303.25	327.78	350.60
90.	246.76	285.66	319.86	350.74	379.12	405.51
100.	281.35	325.71	364.70	399.92	432.27	462.37
110.	317.13	367.13	411.08	450.78	487.24	521.17
120.	354.10	409.92	459.00	503.32	544.04	581.91
130.	392.24	454.08	508.45	557.54	602.65	644.60
140.	431.58	499.61	559.43	613.45	663.08	709.24
150.	472.09	546.51	611.95	671.04	725.32	775.82

Table C.2: Volumetric flow rate of SO_2/N_2 (cont.)
Tube No: 602
Float: Stainless steel
Gas measured SO_2/N_2
Temperature= 290.15 (K)

Pressure (psia)	14.70	19.70	24.70	29.70	34.70	39.70
Scale reading			Flow rate	(mL/min)		
10.	88.32	102.24	114.48	125.53	135.69	145.14
20.	158.01	182.92	204.82	224.60	242.77	259.67
30.	226.86	262.62	294.06	322.46	348.54	372.81
40.	294.86	341.34	382.21	419.11	453.02	484.56
50.	362.01	419.08	469.26	514.57	556.20	594.92
60.	428.32	495.84	555.21	608.82	658.07	703.89
70.	493.78	571.62	640.07	701.87	758.65	811.47
80.	558.40	646.43	723.83	793.71	857.93	917.66
90.	622.17	720.25	806.49	884.36	955.90	1022.46
100.	685.09	793.09	888.05	973.80	1052.58	1125.86
110.	747.17	864.96	968.52	1062.04	1147.96	1227.88
120.	808.40	935.84	1047.89	1149.07	1242.03	1328.51
130.	868.79	1005.74	1126.17	1234.90	1334.81	1427.74
140.	928.33	1074.67	1203.34	1319.53	1426.28	1525.59
150.	987.02	1142.61	1279.42	1402.96	1516.46	1622.04

Table C.2: Volumetric flow rate of SO_2/N_2 (cont.)
Tube No: 604
Float: Glass
Gas measured: SO_2/N_2
Temperature = 290.15

Pressure (psia)	14.70	19.70	24.70	29.70	34.70	39.70
Scale reading			Flow rate (mL/min)			
10.	528.49	611.80	685.06	751.20	811.97	868.51
20.	1179.25	1365.15	1528.61	1676.20	1811.81	1937.95
30.	1824.43	2112.04	2364.92	2593.27	2803.07	2998.22
40.	2464.03	2852.47	3194.01	3502.40	3785.75	4049.33
50.	3098.05	3586.44	4015.86	4403.60	4759.87	5091.26
60.	3726.49	4313.94	4830.48	5296.88	5725.41	6124.02
70.	4349.35	5034.99	5637.86	6182.21	6682.37	7147.61
80.	4966.63	5749.58	6438.01	7059.62	7630.76	8162.04
90.	5578.33	6457.71	7230.93	7929.10	8570.58	9167.29
100.	6184.45	7159.38	8016.61	8790.64	9501.83	10163.37
110.	6784.99	7854.59	8795.06	9644.26	10424.50	11150.29
120.	7379.95	8543.34	9566.28	10489.94	11338.61	12128.03
130.	7969.33	9225.63	10330.27	11327.69	12244.13	13096.60
140.	8553.13	9901.46	11087.02	12157.51	13141.09	14056.00
150.	9131.36	10570.84	11836.54	12979.41	14029.47	15006.24

Table C.3: Volumetric flow rate of total N_2

Tube No: R7M251
Float: Steel
Gas measured: Total N_2
Temperature= 290.15

Pressure (psia)	14.70	19.70	24.70	29.70	34.70	39.70
Scale reading			Flow rate	(mL/min)		
10.	2618.55	3031.34	3394.30	3722.03	4023.15	4303.25
20.	4892.75	5664.05	6342.24	6954.61	7517.25	8040.63
30.	7127.80	8251.44	9239.43	10131.53	10951.19	11713.64
40.	9323.67	10793.47	12085.83	13252.76	14324.94	15322.28
50.	11480.37	13290.16	14881.46	16318.32	17638.52	18866.55
60.	13597.90	15741.50	17626.31	19328.20	20891.90	22346.45
70.	15676.26	18147.50	20320.39	22282.40	24085.11	25761.97
80.	17715.45	20508.14	22963.70	25180.93	27218.13	29113.12
90.	19715.47	22823.45	25556.23	28023.77	30290.97	32399.90
100.	21676.32	25093.41	28097.98	30810.95	33303.63	35622.31
110.	23597.99	27318.02	30588.96	33542.43	36256.10	38780.34
120.	25480.50	29497.29	33029.16	36218.25	39148.40	41874.00
130.	27323.84	31631.21	35418.59	38838.38	41980.51	44903.29
140.	29128.00	33719.79	37757.24	41402.84	44752.44	47868.21
150.	30893.00	35763.02	40045.12	43911.63	47464.19	50768.76

Table C.3: Volumetric flow rate of total N_2 (cont.)
Float: S. steel-R7M251

160.	32618.82	37760.91	42282.22	46364.73	50115.75	53604.93
170.	34305.47	39713.45	44468.55	48762.15	52707.14	56376.74
180.	35952.95	41620.64	46604.10	51103.89	55238.33	59084.16
190.	37561.26	43482.48	48688.88	53389.96	57709.36	61727.22
200.	39130.40	45298.98	50722.88	55620.35	60120.18	64305.90
210.	40660.37	47070.14	52706.10	57795.07	62470.84	66820.19
220.	42151.16	48795.95	54638.55	59914.10	64761.30	69270.13
230.	43602.79	50476.41	56520.22	61977.46	66991.56	71655.69
240.	45015.25	52111.53	58351.13	63985.14	69161.69	73976.88
250.	46388.53	53701.30	60131.25	65937.13	71271.56	76233.69

Table C.4: Volumetric flow rate of cylinder nitrogen

Tube No: 603
Float: Glass
Gas measured: Make-up N_2
Temperature= 290.15

Pressure (psia)	14.70	19.70	24.70	29.70	34.70	39.70
Scale reading			Flow rate (mL/min)			
10.	238.13	275.67	308.68	338.49	365.87	391.34
20.	443.34	513.23	574.68	630.17	681.15	728.58
30.	640.28	741.21	829.96	910.10	983.73	1052.21
40.	828.94	959.62	1074.52	1178.26	1273.59	1362.26
50.	1009.33	1168.44	1308.35	1434.67	1550.74	1658.71
60.	1181.45	1367.70	1531.46	1679.33	1815.19	1941.57
70.	1345.30	1557.38	1743.85	1912.22	2066.93	2210.83
80.	1500.88	1737.48	1945.52	2133.36	2305.96	2466.50
90.	1648.18	1908.00	2136.46	2342.74	2532.28	2708.58
100.	1787.21	2068.95	2316.68	2540.37	2745.89	2937.06
110.	1917.98	2220.33	2486.18	2726.23	2946.79	3151.95
120.	2040.47	2362.13	2644.96	2900.34	3134.98	3353.25
130.	2154.68	2494.35	2793.01	3062.69	3310.47	3540.95
140.	2260.63	2617.00	2930.35	3213.28	3473.24	3715.06
150.	2358.30	2730.07	3056.96	3352.12	3623.31	3875.58

Table C.4: Volumetric flow rate of cylinder nitrogen (cont.)
Tube No: 603
Float: S steel
Gas measured: Make-up N_2
Temperature = 290.15

Pressure (psia)	14.70	19.70	24.70	29.70	34.70	39.70
Scale reading			Flow rate (mL/min)			
10.	513.47	594.41	665.59	729.85	788.90	843.82
20.	921.11	1066.32	1193.99	1309.28	1415.20	1513.73
30.	1311.31	1518.03	1699.79	1863.91	2014.70	2154.97
40.	1684.06	1949.54	2182.97	2393.74	2587.40	2767.54
50.	2039.37	2360.86	2643.54	2898.78	3133.30	3351.45
60.	2377.23	2751.99	3081.50	3379.02	3652.40	3906.69
70.	2697.65	3122.92	3496.84	3834.47	4144.69	4433.25
80.	3000.63	3473.65	3889.57	4265.12	4610.18	4931.15
90.	3286.16	3804.19	4259.68	4670.97	5048.87	5400.38
100.	3554.24	4114.53	4607.19	5052.03	5460.75	5840.94
110.	3804.88	4404.68	4932.08	5408.29	5845.83	6252.83
120.	4038.07	4674.64	5234.36	5739.75	6204.11	6636.06
130.	4253.82	4924.40	5514.02	6046.42	6535.59	6990.62
140.	4452.12	5153.96	5771.07	6328.29	6840.27	7316.51
150.	4632.98	5363.33	6005.52	6585.37	7118.14	7613.73

Table C.5: Volumetric flow rate of sample

Tube No: 603
Float: Glass
Gas measured: Sample
Temperature = 290.15

Pressure (psia)	14.70	19.70	24.70	29.70	34.70	39.70
Scale reading			Flow rate (mL/min)			
10.	250.79	290.32	325.08	356.47	385.31	412.14
20.	453.19	524.63	587.44	644.16	696.28	744.75
30.	647.88	750.01	839.81	920.90	995.40	1064.71
40.	834.86	966.47	1082.19	1186.68	1282.69	1371.99
50.	1014.14	1174.01	1314.58	1441.51	1558.13	1666.61
60.	1185.71	1372.63	1536.98	1685.38	1821.74	1948.57
70.	1349.58	1562.33	1749.39	1918.30	2073.50	2217.86
80.	1505.73	1743.10	1951.81	2140.27	2313.42	2474.49
90.	1654.18	1914.95	2144.24	2351.27	2541.50	2718.44
100.	1794.93	2077.88	2326.68	2551.33	2757.74	2949.74
110.	1927.96	2231.89	2499.13	2740.43	2962.13	3168.37
120.	2053.29	2376.98	2661.58	2918.57	3154.69	3374.33
130.	2170.91	2513.14	2814.05	3085.76	3335.41	3567.62
140.	2280.83	2640.38	2956.53	3241.99	3504.28	3748.26
150.	2383.04	2758.70	3089.02	3387.27	3661.31	3916.22

Table C.5: Volumetric flow rate of sample (cont.)
Tube No: 603
Float: S. steel
Gas measured: Sample
Temperature= 290.15 (K)

Pressure (psia)	14.70	19.70	24.70	29.70	34.70	39.70
Scale reading			Flow rate	(mL/min)		
10.	572.98	663.31	742.73	814.44	880.33	941.62
20.	971.72	1124.91	1259.60	1381.22	1492.96	1596.90
30.	1354.73	1568.29	1756.07	1925.62	2081.41	2226.32
40.	1721.99	1993.45	2232.14	2447.66	2645.68	2829.88
50.	2073.52	2400.40	2687.81	2947.33	3185.78	3407.58
60.	2409.32	2789.13	3123.08	3424.63	3701.69	3959.41
70.	2729.37	3159.64	3537.96	3879.56	4193.43	4485.38
80.	3033.69	3511.93	3932.43	4312.12	4660.98	4985.49
90.	3322.27	3846.00	4306.50	4722.31	5104.36	5459.74
100.	3595.11	4161.85	4660.18	5110.13	5523.55	5908.12
110.	3852.22	4459.49	4993.45	5475.59	5918.57	6330.64
120.	4093.59	4738.91	5306.32	5818.67	6289.41	6727.30
130.	4319.22	5000.11	5598.80	6139.38	6636.08	7098.10
140.	4529.11	5243.09	5870.88	6437.73	6958.56	7443.03
150.	4723.27	5467.86	6122.55	6713.71	7256.86	7762.11

Appendix D

COMPUTER PROGRAMME FOR DATA LOGGING

```
1000 poke 646,0
1010 rem claus reaction project 1987
1020 rem investigator el. besher
1025 rem program written by van le
1030 rem prog. for data logging
1040 rem with c64, adc-1 & instruments
1050 rem version 1.a (1987)
1060 :
1070 open 2,2,0,chr$(136)+chr$(0):rem        ** open i/o port 2 ' 1200 baud **
1080 poke 53281,12:poke 53280,11:print chr$(14)chr$(8)
1090 te$="":gosub 2570:rem                    ** ml data (te$=input) **
1100 :
1110 rem ** get data from user **
1120 print "|████     CLAUS  REACTION  PROJECT (1987)"
1130 print:print "      Program for Data Logging With"
1140 print "   C64, ADC-1, Thermocouple & Analyzer"
1150 poke 646,0:print:print:print"                MAIN  MENU  "
1160 print:print "          1) record temperatures"
1170 print "          2) display recorded data"
1180 print:print:print:print"         Enter your choice: ";:sys 49152,1:print
1190 if te$="1" then 1220
1200 if te$="2" then 2850
1210 goto 1120
1220 print:print "  Do you wish to write data to disk?  ◥";:sys 49152,1:print
1230 if te$="n" then do$="n":goto 1360
1240 if te$="y" then do$="y":goto 1260
1250 print "███":goto 1220
1260 print "█   Enter filename:                ◥◥◥◥◥◥◥◥◥◥◥◥◥◥◥◥";
1270 sys 49152,16:print
1280 print "█   creating file "te$"...."
1290 close 15:close 7:open 15,8,15:open 7,8,9,te$+",s,w":gosub 2810
1300 if e<>0 then 1220
1310 print "█  enter # of sets of data you wish to"
1320 print "     retrieve before recording the 16"
1330 print "       latest temperatures to disk."
1340 print:print"      enter # of sets of data: ";:sys 49152,3:print:tn=val(te$)
1350 print:print "    Enter run # ";:sys 49152,8:print:da$=te$
1360 print:print "  enter current time (hhmmss):         ◥◥◥◥◥◥";:sys 49152,6
1370 if len(te$)<6 or te$>"240000" then print "██":goto 1360
1380 ti$=te$
```

```
1385 tt$=te$
1390 if do$="y" then print#7,da$
1400 :
1410 dim a(6), b(6) :rem coeff. array
1420 dim tp(16) :rem temporary array
1430 cal=1.0     :rem calib. factor
1440 ag=20       :rem amp gain
1450 :
1460 restore:for i=0 to 5:read a(i):next i
1470 data -0.0489 , 0.01987 , -2.1861e-7 , 1.1569e-11 , -2.6492e-16 , 2.0184e-21
1480 for p=0 to 5:read b(p):next p
1490 data  0.02266, 0.02415,  6.7233e-8 , 2.2103e-12 , -8.6096e-16 , 4.8351e-20
```

```
1500 :
1510 gosub 4000
1511 print:print"■   Enter H2S Range 1,10 or 100:     ▼▼▼";:input r1
1512 print"■     confirming r1= ";:print r1
1513 print:print"■   Enter SO2 Range50,100,500,1000 :    ▼▼▼";:input r2
1514 print"■     confirming r2= ";:printr2:print:print:print:i=0
1515 i=i+1:if i<100 then 1515
1520 gosub 6000
1545 :
1547 print chr$(147)
1548 print "| "
1550 for lo=1 to tn:rem loop x times          before writing data to disk
1560 :
1570 cn=48:gosub 2210:gosub 2210
1580 tb=(z/10)-273.16+cal
1590 :
1600 vc=1019+(tb-20)*51.45:rem                 ** calculate junction voltage **
1610 :
1620 rem print current time at top
1630 poke53281,11:poke53280,12:poke646,1
1640 print "| ■■■"
1650 print spc(13)"Current time ";left$(ti$,2)":";mid$(ti$,3,2)":"right$(ti$,2)
1655 gosub 6200
1660 poke646,1
1670 print "| ":print "    CLAUS  REACTION  PROJECT (1987)":poke 646,0
1680 print "              DATA   LOGGING    "
1681 print:print"■■"
1690 :
```

```
1400 :
1410 dim a(6), b(6) :rem coeff. array
1420 dim tp(16) :rem temporary array
1430 cal=1.0     :rem calib. factor
1440 ag=20       :rem amp gain
1450 :
1460 restore:for i=0 to 5:read a(i):next i
1470 data -0.0489 , 0.01987 , -2.1661e-7 , 1.1569e-11 , -2.6492e-16 , 2.0184e-21
1480 for p=0 to 5:read b(p):next p
1490 data  0.02266, 0.02415,  6.7233e-8 , 2.2103e-12 , -8.6096e-16 , 4.8351e-20
1500 :
1510 gosub 4000
1511 print:print"■   Enter H2S Range 1,10 or 100:     ◥◥◥";:input r1
1512 print"■     confirming r1= ";:print r1
1513 print:print"■   Enter SO2 Range50,100,500,1000 :    ◥◥◥";:input r2
1514 print"■     confirming r2= ";:printr2:print:print:print:i=0
1515 i=i+1:if i<100 then 1515
1520 gosub 6000
1545 :
1547 print chr$(147)
1548 print "| "
1550 for lo=1 to tn:rem loop x times        before writing data to disk
1560 :
1570 cn=48:gosub 2210:gosub 2210
1580 tb=(z/10)-273.16+cal
1590 :
1600 vc=1019+(tb-20)*51.45:rem                ** calculate junction voltage **
1610 :
1620 rem print current time at top
1630 poke53281,11:poke53280,12:poke646,1
```

```
1640 print "|■■■"
1650 print spc(13)"Current time ";left$(ti$,2)":";mid$(ti$,3,2)":"right$(ti$,2)
1655 gosub 6200
1660 poke646,1
1670 print "| ":print "     CLAUS  REACTION  PROJECT (1987)":poke 646,0
1680 print "              DATA   LOGGING   "
1681 print:print"■■"
1690 :
1700 rem print reference temperature,#1
```

```
1710 :
1720 print a$(1);"          ◥◥◥◥◥◥◥◥◥";chr$(5);int(tb);chr$(144)
1730 tp(1)=int(tb)
1740 rem read a/d channel 1 (reference)
1750 :
1760 cn=16:gosub 2210:gosub 2210
1770 :
1780 za=z*(100/ag):rem                           ** convert reading to voltage
1790 :
1800 rem *** read next  10 channels ***
1810 :
1820 for i=2 to 11
1830 :
1840 cn=15+i:gosub 2210:gosub 2210
1850 zt=z*(100/ag)
1860 :
1870 vd=zt-za+vc:rem                             ** calc. corresponding voltage
1880 :
1890 rem calc. corresp. temperature by
1900 rem using the polynomial function
1910 :
1920 t=0
1930 for j=0 to 5
1940 t=t+a(j)*vd^j
1950 if peek(653)=7 then 2530:rem                ** if shift,c=,ctrl down, abort
1960 next j
1970 :
1980 rem print temp. of next 11 chs.
1990 print a$(i);"         ◥◥◥◥◥◥◥◥◥";chr$(5);int(t);chr$(144)
2000 tp(i)=int(t)
2010 next i
2020 rem read chanal 12(k-thermocouple)
2030 cn=27:gosub2210: gosub 2210
2035 vc=813+(tb-20)*40.3
2040 zw= z*(100/ag)
2050 vq=zw-za+vc
2060 t=0
```

```
2070 for p=0 to 5
2080 t=t+b(p)*vq^p
2090 if peek(653)=3 then  2530
2100 next p
2110 :
2120 rem print temp. of channel 12,chan 13 and 14 are not connected
2130 print a$(12);"           ▼▼▼▼▼▼▼▼▼";chr$(5);int(t);chr$(144)
2140 tp(12)=int(t)
2150 rem read h2s channel
2151 cn=30:gosub 2210:gosub2210
2152 zbt=-(z*245.8)/(10*ag):rem convert reading to m.volt
2153 ppm=c(1)+c(2)*zbt+c(3)*zbt*zbt
2154 tp(15)=int(ppm)
2155 if peek(653)=3 then 2530
2156 print"           **"
2157 print a$(15);"           ▼▼▼▼▼▼▼▼▼";chr$(5);int(ppm);chr$(144)
2158 rem read so2 channel
2159 cn=31:gosub2210:gosub2210
2160 e=(51.85*z)/(10*ag):rem con. reading to m.volt
2161 e0=e*exp(k1+k2*ppm):rem  correct for h2s effect
2162 ppm=d(1)+d(2)*e0+d(3)*e0*e0
2163 tp(16)=int(ppm)
2164 if peek(653)=3 then 2530
2165 :
2166 print a$(16);"           ▼▼▼▼▼▼▼▼▼";chr$(5);int(ppm)
2168 next lo
2169 if do$="n" then 1550
2170 gosub 2470:rem                              ** write data to disk **
2180 goto 1550:rem                               ** go back and read more temps
2190 rem subroutine for reading a/d
2200 :
2210 c$=chr$(cn)
2220 gosub 2350
2230 c$=chr$(161)
2240 gosub 2350
2250 hb=ch
2260 if (hb and 128)<>0 then 2230
2270 c$=chr$(145)
2280 gosub 2350
2290 lb=ch
2300 hm=hb and 15
```

```
2310 x=lb+256*hm
2320 if (hb and 16)=0 then x=-x
2330 return
2340 :
2350 fl=0
2360 print#2,c$;
2370 tm=ti
2380 if ti>tm+4 then 2400:rem                    ** delay of 4 milliseconds **
2390 goto 2380
2400 get#2,x$
2410 if peek(168)<10 then fl=1:return
2420 if st=0 then 2370
```

```
2430 ch=peek(170)
2440 return
2450 :
2460 rem ** write data to file **
2470 :
2480 print#7,ti$:for wr=1 to 11:print#7,a$(wr);tp(wr):next wr
2481 print#7,a$(12);tp(12)
2482 print#7,a$(15);tp(15)
2485 print#7,a$(16);tp(16)
2490 for lk=1 to 10:poke 53280,int(rnd(1)*15):next lk:return
2500 :
2510 rem ** abort & go to main menu **
2520 :
2530 close 7:close 15:run
2540 :
2550 rem ** ml code for input **
2560 :
2570 for i=0 to 5:read a:next i:for p=0 to 5:readb:nextp
2580 for i=49152 to 49262:read a:poke i,a:next i:goto 2690
2590 :
2600 data 160,0,140,111,192,132,204,177,122,201,44,240,4,162,1,208,3,32,241,183
2610 data 142,112,192,32,228,255,201,0,240,249,201,13,240,53,201,20,208,10,172
2620 data 111,192,240,236,206,111,192,16,29,170,41,127,201,32,144,224,138,172
2630 data 111,192,204,112,192,176,215,238,111,192,208,5,206,111,192,48,205,153
2640 data 113,192,32,210,255,169,0,133,212,76,23,192,160,2,173,111,192,145,45
2650 data 200,169,113,145,45,200,169,192,145,45,230,204,169,32,76,210,255
```

Table D.1: Principal experimental measurements made in reaction experiments

Reactor temperature:	373.0 K
Static bed height:	0.19 m
Y_{H_2S}:	0.1
Y_{SO_2}:	0.05
Minimum fluidization velocity:	0.0245 m/s

Run #	Flow rate (mL/min)			U/U_{mf} (-)	Inlet conc. (ppm)		Outlet conc. (ppm)	
	N_2	H_2S/N_2	SO_2/N_2		H_2S	SO_2	H_2S	SO_2
13-0	51069	154	77	4.44	300	150	108	53
14-0	50990	205	102	4.44	400	200	113	55
11-0	50915	256	128	4.44	500	250	122	61
18-1	50840	310	155	4.44	600	300	121	61
18-2	50840	310	155	4.44	600	300	127	63
15-0	50685	410	205	4.44	800	400	110	50
15-1	50685	410	205	4.44	800	400	111	57
21-0	50645	435	218	4.44	850	425	116	57
20-0	50770	487	244	4.44	950	475	125	65
12-1	50530	515	255	4.44	1000	500	96	51
42-0	50455	565	282	4.44	1100	550	121	62
42-1	50455	565	282	4.44	1100	550	126	65
41-0	50375	615	308	4.44	1200	600	101	45
41-1	50375	615	308	4.44	1200	600	99	51
43-0	50300	665	335	4.44	1300	650	140	74
43-1	50300	665	335	4.44	1300	650	136	65

Table D.1: Principal experimental measurements made in reaction experiments (cont.)

Reactor temperature: 423.0 K

Static bed height: 0.19 m

Y_{H_2S}: 0.1

Y_{SO_2}: 0.05

Minimum fluidization velocity: 0.0225 m/s

Run #	Flow rate (mL/min)			U/U_{mf} (-)	Inlet conc. (ppm)		Outlet conc. (ppm)	
	N_2	H_2S/N_2	SO_2/N_2		H_2S	SO_2	H_2S	SO_2
24-1	46935	95	47	4.44	200	100	58	32
25-1	46865	140	70	4.44	300	150	72	38
23-1	46795	190	95	4.44	400	200	77	36
26-0	46725	235	118	4.44	500	250	103	58
30-0	46655	280	140	4.44	600	300	104	50
27-0	46580	330	165	4.44	700	350	90	44
40-1	46510	380	190	4.44	800	400	74	39
28-0	46370	470	235	4.44	1000	500	82	40
36-0	46230	565	282	4.44	1200	600	74	36
33-0	46160	610	306	4.44	1300	650	95	49
33-1	46160	610	305	4.44	1300	650	94	46

Table D.1: Principal experimental measurements made in reaction experiments (cont.)

Reactor temperature: 423.0 K

Static bed height: 0.32 m

Y_{H_2S}: 0.1

Y_{SO_2}: 0.05

Minimum fluidization velocity: 0.0224 m/s

Run #	Flow rate (mL/min)			U/U_{mf} (-)	Inlet conc. (ppm)		Outlet conc. (ppm)	
	N_2	H_2S/N_2	SO_2/N_2		H_2S	SO_2	H_2S	SO_2
80-1	93870	190	95	8.88	200	100	49	25
80-0	93730	280	140	8.88	300	150	62	29
78-0	93590	375	188	8.88	400	200	77	37
77-0	93450	470	235	8.88	500	250	66	31
73-0	93310	565	282	8.88	600	300	66	33
76-0	93165	660	330	8.88	700	350	57	27
75-0	93025	755	378	8.88	800	400	47	25
83-0	92880	850	425	8.88	900	450	63	32
74-0	92745	940	470	8.88	1000	500	45	21
79-0	92460	1130	565	8.88	1200	600	37	19
82-0	92320	1225	612	8.88	1300	650	28	17

Table D.1: Principal experimental measurements made in reaction experiments (cont.)

H_2S/SO_2 concentration:	600 ppm
Static bed height:	0.19 m
N_2 flow rate:	48750 mL/min
H_2S/N_2 flow rate:	295 mL/min
SO_2S/N_2 flow rate:	148 mL/min
Y_{H_2S}:	0.1
Y_{SO_2}:	0.05

Run #	Temperature ($°C$)	Outlet conc. (ppm)	
		H_2S	SO_2
18-1	100	121	61
18-2	100	127	63
44-0	120	114	55
45-0	130	102	48
30-0	150	104	50

Table D.1: Principal experimental measurements made in reaction experiments (cont.)

H_2S/SO_2 concentration:	600 ppm
Static bed height:	0.19 m
N_2 flow rate:	48230 mL/min
H_2S/N_2 flow rate:	640 mL/min
SO_2/N_2 flow rate:	320 mL/min
Y_{H_2S}:	0.1
Y_{SO_2}:	0.05

Run #	Temperature ($°C$)	Outlet conc. (ppm)	
		H_2S	SO_2
43-0	100	140	74
43-1	100	135	65
47-0	110	122	59
46-1	130	104	56
33-0	150	95	49
33-1	150	94	46

Table D.1: Principal experimental measurements made in reaction experiments (cont.)

Reactor temperature:	423.0 K
H_2S/SO_2 concentration:	600/300
Static bed height:	0.19 m
Y_{H_2S}:	0.1
Y_{SO_2}:	0.05
Minimum fluidization velocity:	0.0225 m/s

Run #	Flow rate (mL/min)			U/U_{mf} (-)	Outlet conc. (ppm)	
	N_2	H_2S/N_2	SO_2/N_2		H_2S	SO_2
51-0	23585	140	70	2.2	49	24
50-0	33250	200	100	3.1	83	44
49-0	38900	235	118	3.7	99	49
30-0	46655	280	140	4.4	106	56
52-0	61712	375	188	5.9	122	63

Table D.1: Principal experimental measurements made in reaction experiments (cont.)

Reactor temperature: 423.0 K

H_2S/SO_2 concentration: 1300/650

Static bed height: 0.19 m

Y_{H_2S}: 0.1

Y_{SO_2}: 0.05

Minimum fluidization velocity: 0.0225 m/s

Run #	Flow rate (mL/min)			U/U_{mf} (-)	Outlet conc. (ppm)	
	N_2	H_2S/N_2	SO_2/N_2		H_2S	SO_2
55-0	23380	310	155	2.2	39	21
56-0	32525	430	215	3.1	51	25
53-0	39370	520	260	3.7	89	45
33-0	46160	610	306	4.4	95	49
33-1	46160	610	305	4.4	94	46
54-0	52900	700	350	5.1	111	54

Table D.1: Principal experimental measurements made in reaction experiments (cont.)

Reactor temperature:	373 K
Static bed height:	0.32 m
H_2S/SO_2 concentration:	1000/500 ppm
N_2 flow rate:	50530 mL
H_2S/N_2 flow rate:	515 mL
SO_2/N_2 flow rate:	255 mL
Y_{H_2S}:	0.1
Y_{SO_2}:	0.05

Time (h.)	S.Loading (g/g%)	Outlet concentration (ppm)		Time (h.)	S.Loading (g/g%)	Outlet concentration (ppm)	
		H_2S	SO_2			H_2S	SO_2
2.00	0.011	67	31	109.25	13.048	212	106
4.00	0.135	66	31	117.00	14.213	204	100
6.00	0.355	63	30	125.00	15.129	213	106
9.00	0.532	64	29	135.00	16.271	227	112
12.00	0.548	62	30	140.75	16.927	239	121
15.00	0.593	71	34	151.00	17.904	251	126
18.00	0.716	70	36	162.00	18.764	263	130
21.00	0.728	70	37	170.00	22.786	269	134
24.00	0.844	72	35	178.00	24.994	277	138
27.00	0.892	73	36	186.00	25.241	312	154
32.00	1.264	85	39	196.00	27.062	318	157
37.00	1.489	79	39	207.00	25.220	361	179
42.25	1.523	78	41	219.00	29.080	367	181
48.25	1.837	77	37	231.00	27.078	389	192
55.00	2.592	88	48	243.00	31.969	410	203
60.00	3.505	87	42	255.00	37.711	418	210
68.00	4.144	83	41	265.00	42.353	426	214
72.00	4.159	98	47	277.00	44.444	438	217
80.00	7.049	115	59	288.00	45.125	457	230
86.00	6.950	120	60	301.00	47.172	479	237
95.00	9.153	186	94	313.00	50.812	529	263
99.25	12.016	181	93	335.00	54.922	570	284
				347.00	60.055	611	303

Table D.1: Principal experimental measurements made in reaction experiments (cont.)

Reactor temperature:	$100°C$
H_2S/SO_2 concentration:	600/300
N_2 flow rate:	50840 mL/min
H_2S/N_2 flow rate:	310 mL/min
SO_2/N_2 flow rate:	155 mL/min

Run #	Static bed height (m)	Outlet concentration (ppm)	
		H_2S	SO_2
R-5	0.12	224	110
18-1	0.19	121	61
18-2	0.19	127	63
R-2	0.25	79	39
R-4	0.32	48	22
R-3	0.38	28	15

Table D.1: Principal experimental measurements made in reaction experiments (cont.)

H_2S/SO_2 concentration: 600/300 ppm

Y_{SO_2}: 0.05

Y_{H_2S}: 0.1

W_{cat}: 1.2 Kg

Run #	Temperature (K)	Flow rate (mL/min)			Outlet conc. (ppm)	
		N_2	H_2S/N_2	SO_2/N_2	H_2S	SO_2
64-0	373	10275	62	31	44	19
65-0	397	10275	62	31	36	23
63-0	423	9340	57	28	29	12

Appendix E

PURGING-TIME OF REACTOR SYSTEM

The presence of oxygen in the reactor system could adversely affect the catalyst at high temperatures. In addition, since it did not constitute part of the feed gas, it was absolutely necessary to purge it from the reactor as well as the nitrogen recycle loop.

The purging-time, τ, for a system of known volume, V, is given by the equation (Nelson, 1971):

$$\tau = 2.303\frac{V}{Q}\log_{10}\frac{C_i}{C_f} \tag{E.1}$$

Where C_i and C_f denote the initial and final concentration of O_2 and Q denotes the purge rate.

The volume of the system was approximately 90 l. Accordingly, the concentration of oxygen can be reduced from 21% to 1 ppb within a period of about 6 hours at a purge rate of 5 L/min.

Appendix F

PREDICTIONS OF EQUILIBRIUM CONVERSION

```
      IMPLICIT REAL*8(A-H,O-Z),INTEGER(I-N)
      EXTERNAL F
      COMMON/BLK1/EC,FSO2,FN2,FTOTAL
      DIMENSION A(4,7),FRT(4),ROOT(1)
      DATA A/0.322571D+1,0.3916307D+1,0.4156502D+1,
     $ 0.7783897D+1,0.5655121D-2,-0.3513967D-3,-0.1724433D-2,
     $ 0.2509982D-1,-0.2497021D-6,0.4219131D-5,0.5698232D-5,
     $ -0.3714831D-4,-0.4220677D-8,-0.2745366D-8,-0.4593004D-8,
     $ 0.2615731D-7,0.2139273D-11,0.4858364D-12,0.1423365D-11,
     $ -0.7120913D-11,-0.3690448D+5,-0.3609558D+4,-0.3028877D+5,
     $ 0.1011458D+5,0.9817704D+1,0.2366004D+1,-0.6861625D+0,
     $ 0.4762179D+1/

C   A    :Coefficients in free energy expressions
C   TO   :Temperature at which equilibrium conversion
C         is sought
C   PPM  :Concentration of SO2 in parts per milion
C   Q    :Volumeteric flow rate
```

```
C   FRT   :Free energy of any substance/RT
C   DRET  : Delta FRT
C  EC     :Equilibrium constant
C  FTOTAL:Total molar flow rate
C  FSO2   :Molar flow rate of SO2
C  FH2S   :Molar flow rate of H2S
C  FN2    :Molar flow rate of N2
C  XI,XF  :Interval at which root being sought
C  DXI    :Interval increment
C  TOL    :Accuracy in root
C  ROOT   :Root of equilibrium expression
C  CON    :Equilibrium conversion
C  PSO2   :partial pressure of SO2
C         Specify total volumetric flow rate and SO2
C         feed concentration
        Q=49.193D-3
        PPM=300.0D0
C         Specify temperature range
        N=120
        TI=90.0D0+273.0D0
        TF=150.0D0+273.0D0
        TO=TI
        RN=N
        DT=(TF-TI)/RN
C         Calculate: free energy, free energy difference and
C         equilibrium constant at temperature TO
```

```
 20    T1=1.0D0-DLOG(T0)
       T2=T0
       T3=T2*T0
       T4=T3*T0
       T5=T4*T0
       DO 30 K=1,4
       FRT(K)=A(K,1)*T1-A(K,2)*T2/2.0D0-A(K,3)*T3/6.0D0
      $ -A(K,4)*T4/12.0D0-A(K,5)*T5*0.05D0+A(K,6)/T2-A(K,7)
 30    CONTINUE
       DFRT=2.0D0*FRT(3)+3.0D0*FRT(4)/8.0D0-2.0D0*FRT(2)-FRT(1)
       EC=DEXP(-DFRT)
C       Calculate molar flow rates.
       FTOTAL=760.0D0*Q/62.4D0/T0
       FSO2=PPM*1.0D-6*FTOTAL
       FH2S=FSO2*2.0D0
       FN2=FTOTAL-FSO2-FH2S
C       Find the root of the equilibrium equation
       XI=0.0D0
       XF=1.0D-1
       DXI=0.100D-2
       TOL=1.0D-9
       CALL  BISECT(F,XI,XF,1,ROOT,DXI,TOL,NR)
C       Calculate partial pressure of SO2
       PSO2=ROOT(1)
C       Calculate equilibrium conversion
       CON=100.0D0*(1.0D0-FTOTAL*PSO2/FSO2)
```

```
      WRITE(6,200) TO, CON
C     Increase temperature
      TO=TO+DT
C      Check for temperature range
      IF(TO.LE.TF) GO TO 20
 100  FORMAT(7(1X,D15.7))
 200  FORMAT(1X,F5.1,1X,F7.3)
      STOP
      END

      DOUBLE PRECISION FUNCTION F(X)
      IMPLICIT REAL*8(A-H,O-Z)
      COMMON/BLK1/EK,FS,FN,FT
      T=(FS-FT*X)/(2.0D0*FS+FN)
      F=EK*X*X*X-T*T
      RETURN
      END
```